Türkiye Earthquake
Reconnaissance and Research
Alliance

RECONNAISSANCE REPORT
on
February 6, 2023 Kahramanmaraş-Pazarcık (M_w=7.7) and Elbistan (M_w=7.6) Earthquakes

<u>Coordinators</u>

Prof. Dr. Kemal Önder Çetin

Dr. Makbule Ilgaç

March 6, 2023

Preface:

The February 6, 2023, Kahramanmaraş earthquakes struck the city of Kahramanmaraş in Türkiye, affecting a total of eleven provinces leaving behind a trail of destruction and loss. The provinces of Kahramanmaraş, Adıyaman, Hatay, Osmaniye, Gaziantep, Kilis, Şanlıurfa, Diyarbakır, Malatya, Adana, and Elazığ in eastern Turkiye significantly affected due to loss of lives of our people and damage to buildings and infrastructure. As the authors, we are deeply sorry for the loss of lives and injured citizens. We would like to convey our deepest condolences to the relatives of those who lost their lives during these events.

In the aftermath of this tragedy, it is important to conduct a collaborative reconnaissance study to understand the impact of the earthquake and to provide valuable insights that can aid in the recovery and rebuilding efforts. This study brings together experts from different fields, including civil engineering, geology, seismology, social sciences, and disaster management from various universities, institutions, and private companies, to undertake a comprehensive assessment of the earthquake's impact.

The study aims to analyze the structural damage to buildings, the condition of infrastructure systems, geological and geotechnical features, the impacts on the environment, and the social effects of the earthquake. More than 110 researchers from different institutions voluntarily worked together and offered their expertise for this report. I would like to express our gratitude to all the experts who contributed their time, knowledge, and expertise to this study.

We hope that this study will help to provide preliminary reconnaissance findings in the aftermath of the Kahramanmaraş earthquakes and serve as a guide for future earthquake preparedness and response.

On behalf of the members of Türkiye Earthquake Reconnaissance and Research Alliance

Prof. Dr. Kemal Önder Çetin

Table of Contents

Table of Figures

Table of Tables

Chapter 1. Introduction

By:

Kemal Önder Çetin[a], Candan Gökçeoğlu[b], Makbule Ilgaç[c], M. Murat Monkul[d], Erkut Sayın[e], Mesut Gör[e], Arda Özacar[f], Gizem Can[g], Elife Çakır[a]

[a] Middle East Technical University, Civil Engineering Department, Ankara, Türkiye
[b] Hacettepe University, Geological Engineering Department, Ankara, Türkiye
[c] University of California, Civil and Environmental Engineering, Berkeley, USA
[d] Yeditepe University, Department of Civil Engineering, İstanbul, Türkiye
[e] Fırat University, Civil Engineering Department, Elazığ, Türkiye
[f] Middle East Technical University, Geological Engineering Department, Ankara, Türkiye
[g] Royal Haskoning DHV Resilience& Maritime-BL Maritime & Water, Netherlands

1. 1. Introduction

On February 6, 2023, at 04:17 (01:17 GMT), a moment magnitude (M_w) 7.7 (AFAD, Disaster, and Emergency Management Presidency www.afad.gov.tr), earthquake occurred on the East Anatolian Fault. The epicenter of the Pazarcık-Kahramanmaraş-Türkiye Earthquake is located at N37.288°, E37.043° and approximately 40 km north-west of Gaziantep, and 33 km south-east of Kahramanmaraş, with a focal depth of 8.6 km (AFAD).

Following the first event, approximately 9 hours later, at 13:24 (10:24 GMT), an M_w 7.6 earthquake at Elbistan-Kahramanmaraş-Türkiye shook the region again. The epicenter of the second event is located at N38.089°, E37.239°, approximately 98 km north-west of Adıyaman, and 62 km north-east of Kahramanmaraş, with a focal depth of 7.0 km (AFAD). Both events took place on the East Anatolian Fault Zone (EAFZ), one of Türkiye's two major active fault systems. Figure 1.1 presents the locations of the epicenters.

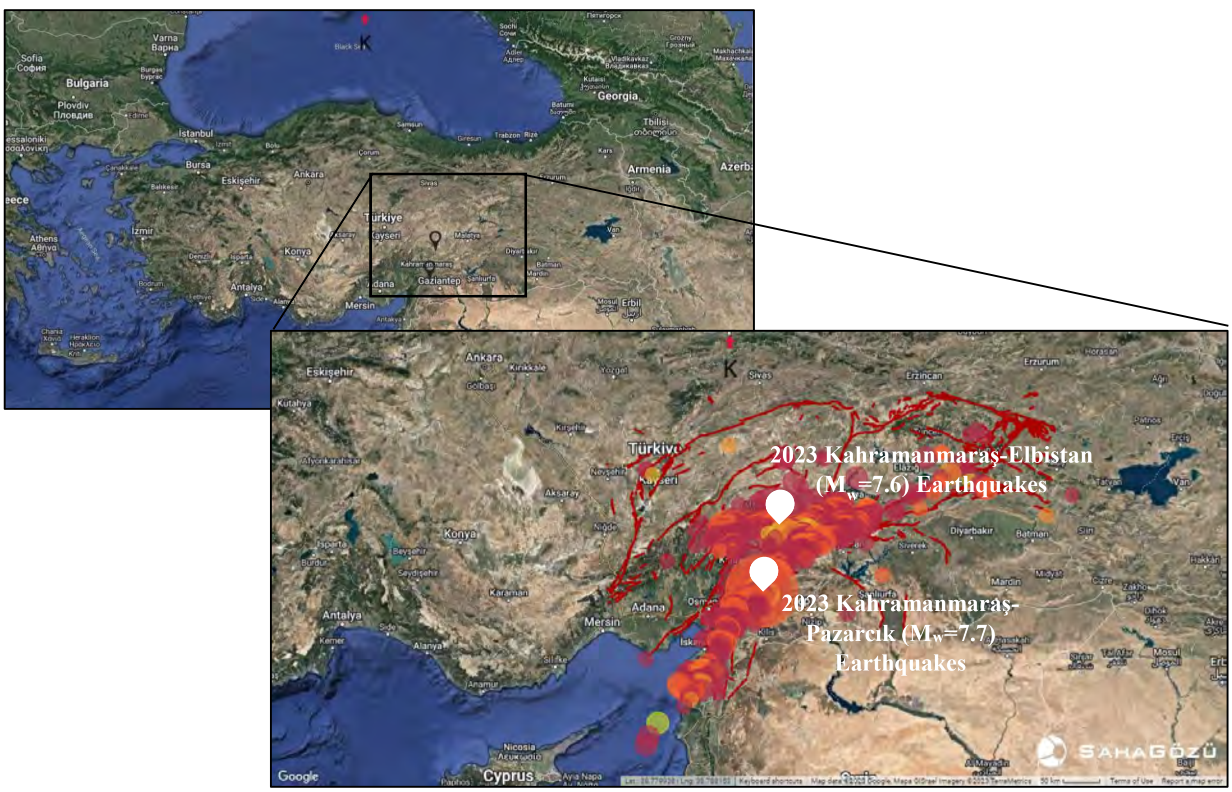

Figure 1.1 Map of Türkiye (Google Maps). The epicenter of the February 6, 2023, Kahramanmaraş-Pazarcık (M_w=7.7) and Kahramanmaraş-Elbistan (M_w=7.6) Earthquakes are shown with white pins.

The magnitude, depth, and source characteristics of February 6, 2023, Kahramanmaraş-Pazarcık (M_w=7.7) and Elbistan (M_w=7.6) Earthquakes events are summarized in Tables 1.1 and 1.2, as reported by different national and international agencies. Consistent with the characteristics of the East Anatolian fault (EAF), the fault mechanism of the earthquakes is left-lateral strike-slip.

Table 1.1 Characteristics of M_w=7.7 Kahramanmaraş-Pazarcık Earthquake

Institution	Focal Mechanism	Depth (km)	M_W
AFAD[1]		8.6	7.7
KOERI[2]	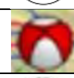	10	7.7
USGS[3]		17.9	7.8
EMSC[4]		10	7.7

[1]Turkish Prime Ministry-Disaster and Emergency Management Presidency
[2]Kandilli Observatory and Earthquake Research Institute
[3]United States Geological Survey
[4]European Mediterranean Seismological Centre

Table 1.2 Characteristics of M_w=7.6 Elbistan Earthquake

Institution	Focal Mechanism	Depth (km)	M_W
AFAD[1]	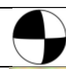	7	7.6
KOERI[2]		10	7.6
USGS[3]	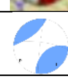	10	7.5
EMSC[4]	NAV	10	7.5

[1]Turkish Prime Ministry-Disaster and Emergency Management Presidency
[2]Kandilli Observatory and Earthquake Research Institute
[3]United States Geological Survey
[4]European Mediterranean Seismological Centre

Both events mostly affected the cities of Kahramanmaraş, Adıyaman, Hatay, Osmaniye, Gaziantep, Kilis, Şanlıurfa, Diyarbakır, Malatya, Adana, and Elazığ with residents of over 15 million. The events caused significant shaking and damage. As of March 1, the approximate number of causalities reached 50,000, and 130,000 were injured. More than 120,000 buildings were collapsed or were heavily damaged.

A total number of 11020 aftershocks were recorded in the region as of March 1, within 200 km epicenter distance. More than 400 of these aftershocks have magnitudes exceeding M_w 5.0. For instance, on February 20, 2023, an M_w 6.4 earthquake occurred in Yayladağı-Hatay, at N 36.037°, E36.021° with a focal depth of 21.73 km (AFAD). This event was mostly classified as an independent event by the scientific community. A total of 280 strong-motion stations, operated by AFAD, within 436 km from the zone of energy release, successfully recorded the February 6, 2023, Pazarcık-Kahramanmaraş (M_W=7.7) earthquake. The maximum peak ground acceleration (PGA) was reported as 1.23 g at Station 3126: Antakya. A total of 244 strong-motion stations, operated by AFAD and located within 445 km from the zone of energy release, recorded the second earthquake shaking. Similarly, the maximum PGA was reported as 0.65 g at station 4612: Kahramanmaraş Göksun. These aftershocks are also shown in Figure 1.1 along with the active fault lines and zones. A more detailed discussion regarding strong ground motion records is available in Chapter 4.

The destructive earthquakes which took place on the EAFZ are listed as follows:

- In May 1971, Bingöl earthquake (M_w 6.9)
- In September 1975, Lice earthquake (M_w 6.7)
- In May 1986, Sürgü earthquake (M_w 6.1)
- In May 2003, Bingöl earthquake (M_w 6.4)
- In March 2010, Elazığ-Kovancılar (M_w 6.1)
- In January 2020 Elazığ-Sivrice (M_w 6.8)

In response to the event, as part of the reconnaissance studies, members from various universities, governmental agencies, academic/private institutions, and firms were mobilized to the region. These ongoing reconnaissance studies have covered an area of approximately 450 km by 100 km, including the mostly affected cities in Türkiye. The objective of this preliminary reconnaissance report is to share the effects of the event on the natural and built environment.

The first team accessed the area on February 7, the next day after the events, to collect and document perishable data in the form of structural damage, fault rupture, ground deformations, liquefaction manifestations, possible failure or non-failure performances of soil and rock slopes, buildings, retaining structures, ports, roads, bridges, airports, lifelines, hydraulic structures, and social impact. More specifically, the subsequent investigative efforts have mostly focused on documenting the followings:

- Background information related to the geology and seismo-tectonics of the region and geological field observations,
- Seismological background and processing of strong ground motions records,
- Detailed field reconnaissance information for all the provinces
- Performance of residential structures,
- Performance of industrial structures,
- Performance of transportation systems including airports, railways, highways,
- Performance of bridges and tunnels,
- Performance of historical structures,
- Foundation performance of buildings,
- Performance of infrastructures,
- Information on soil and rock slopes, seismic soil liquefaction manifestations, rockfalls, earth dams, harbors, lifelines, ports, airports, deep excavations, retaining structures, industrial structures,
- Coastal structures and tsunami effects,
- Emergency response and community impact,

The preliminary reconnaissance findings regarding all these will be presented next.

The opinions and conclusions presented in the report are the responsibility of the individual chapter authors and do not necessarily reflect the views of the entire report or the organization publishing it.

As the authors, we are deeply sorry for the loss of lives and injured citizens. We would like to convey our deepest condolences to the relatives of those who lost their lives during these events.

Acknowledgements

We would like to acknowledge the funding provided for the fieldwork by The Scientific and Technological Research Institution of Turkiye (TÜBİTAK) “1002-C Natural Disasters-Focused Fieldwork Emergency Support Program (Doğal Afetler Odaklı Saha Çalışması Acil Destek Programı)”.

Chapter 2. Digital Data Management for Post-Earthquake Field Studies

By:

Onur Pekcan[a], Ahmet Bahaddin Ersöz[a], Türker Teke[b], Özgür Aydoğmuş[b], Furkan Aydoğan[b], Murat Altun[a], Mehmet Türkezer[a], Ediz Karaali[a], Serhat Erinmez[b], Yunus Eren Kaya[a], Muzaffer Ata Özbilen[a], Görkem Kılıç[a]

[a] Middle East Technical University, Civil Engineering Department, Ankara, Türkiye
[b] i4Works Incorporation, Ankara, Türkiye

2. 1. Introduction

In the aftermath of an earthquake, rapid and accurate assessment of the extent of damage is critical to facilitate practical disaster response efforts. Data collection and management play a crucial role in post-earthquake field studies, as they enable researchers to collect and analyze vast amounts of data effectively. Researchers can gain insights into the nature and extent of damage, evaluate the spatial distribution of vulnerabilities to earthquake(s) and assess the performance of the engineering structures. The lessons learned from the analyses will support the policymakers to update the relevant design codes and guidelines and enhance risk assessment by providing more accurate information on the likelihood and potential impact of future earthquakes.

Numerous researchers from different disciplines of earthquake engineering have visited the affected sites to observe the damage to infrastructure from the point of their expertise. During the visits, a vast amount of data is collected from the site to be analyzed. Therefore, the national or international collaborative efforts both between the researchers of the same field and across different disciplines can enhance the quality of the collected data, leading to a more comprehensive understanding of earthquake impacts through their analyses, and enhancing knowledge and expertise among researchers, practitioners, and policymakers. Hence, a common digital platform developed for data sharing and analysis facilitates these efforts. Moreover, digital data management improves the accuracy of the collected data by avoiding missing data; increases accessibility from anywhere with an offline and online connection; organizes and stores vast amounts of data via search, filter, and categorize features; and provides interactive and shared data visualization.

SiteEye is a cloud-based photogrammetry and visual data management software available via www.siteeye.co. Following the earthquakes that occurred in Türkiye on February 6th, the SiteEye developers worked in collaboration with earthquake engineering experts from the Middle East Technical University to voluntarily create the SiteEye Disaster Plugin, aimed at supporting earthquake research. The plugin provides a data collection add-in that allows for the import of geolocated site data, such as drone footage, ground images, and videos. It seamlessly integrates this data with various earthquake-related map layers, efficiently manages the collected information in an organized manner, and facilitates damage interpretation through data analysis. The details of data management for post-earthquake field studies via SiteEye Disaster Plugin are presented in the following section under the name of data collection, data management, and data analysis.

2. 2. Data Collection

The field data that present the condition of the infrastructure including geo-structures, buildings, and lifelines are collected by the researchers as drone footage, ground images, and videos via either SiteEye mobile application or its web plugin. As the telecommunication infrastructure of the affected provinces was significantly damaged by the earthquakes, which in turn restricted communication with the outside world and access to the internet due to the site conditions in the first days up to its recovery, the data collection methods are adapted to suit the site conditions. During site visits, collecting the site data into the mobile application is more practical compared to the one on the web. Therefore, the data collection in the mobile application is adapted to be compatible with the site conditions. While internet access is available, the researcher can capture images or videos using an application that directly detects the geolocation. Otherwise, the data can be collected offline with its geolocation on the application and uploaded to the server as soon as an online connection is established. Alternatively, the data can be saved in the mobile phone gallery with its geolocation and imported to the application when online access is available. On the other hand, the web application is developed by assuming data entry takes place after the site visit.

Each registered data in the application is tagged with its relevant structure and damage types selected from the list created by experts in the field of geotechnical, structural, and coastal engineering. While it is tagged during or after a data registry in the web application, the registered data is tagged later than its registry in the mobile application for practical reasons. A sample tag of the data registered for the GEO-Reconnaissance project is provided in Figure 2.1.

In the GEO-Reconnaissance project, with the contribution of 32 researchers, the conditions of 3485 geo-structures, 539 buildings, and 111 coastal structures are registered with different damage types. The statistics of substructure and damage types of each structure type are reported in Table 2.1.

Table 2.1. The statistics of substructure and damage types for (a) geo-structure, (b) buildings and (c) coastal structures (SiteEye Disaster Plugin ,2023)

Geo-Structures			
By Substructure Types		**By Damage Types**	
Ground Failure:	2490	Lateral Spread	954
Building Damage (Geotechnical Reasons)	676	Liquefaction/Sand Boils	983
Retaining Structures	97	Landslide/Slope Stability	485
Gravity Wall	13	Rockfall	474
Abutment	17	Settlement/Excessive foundation displacements	1099
MSE Walls	4	Fault Displacement/ Surface Rapture	1030
Deep Excavation	19	Subsidence	206
Earth Dams	2	Ground Cracking	765
Harbors	4	Ground Heave	368
Tunnel Damage	18	Bearing Capacity Failure	653
Highway / Pavement / Asphalt Damage	114	Tilting:	72
Damage to Railways	18	No Damage	276
Damage to Energy Transmission Lines	11		
Damage to (Sewage/Tap/Drinking/Storm) Water Pipelines, Conduits	2		

Buildings			
By Substructure Types		**By Damage Types**	
Reinforced Concrete Building	413	No Damage	21
Masonry Building	11	Light Damage	177
Wood Building/Hmish	1	Medium Damage	255
Historical Buildings	104	Severe Damage	262
Industrial Buildings / Steel Structures	8	Partial or Full Collapse	423
Bridge	2		

Coastal / Ocean Structures			
By Substructure Types		**By Damage Types**	
Seawalls and Revetment	10	Scouring Seaward	2
Breakwater	56	Scouring Leeward	16
Piers/Wharf	10	Sliding Seaward: 48	48
Quay Wall	30	Sliding Leeward: 16	16
Cranes	1	Soil Failure (Sand Boil, Settlement, Seepage, Liquefaction): 42	42
Embankments/Reclamation	4	Core Settlement: 27	27
		Fracture of Concrete: 72	72
		Partial Instability of Breakwater Units: 21	21
		No Damage: 21	21

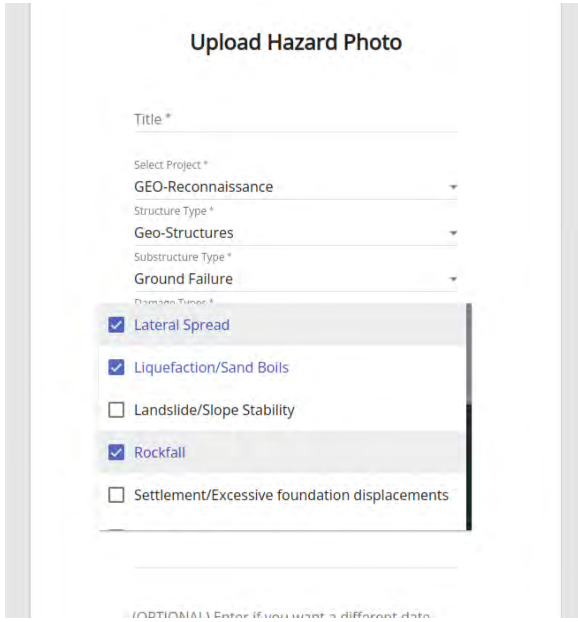

Figure 2.1. A sample registered data with tagging information (SiteEye Disaster Plugin ,2023)

2. 3. Data Management

The first process to manage the collected images and videos is their visualization on a comprehensive map to present their spreading as figured out in Figure 2.2 throughout the affected provinces by matching their geolocation with map coordinates. The data distribution may give an idea for the conditional assessment of the damage and possible locations, for which additional data should be registered.

In addition to collected images and videos, numerous seismological data, such as fault lines, surface ruptures, PGA and PGV distributions, and Mv distributions, can also be incorporated into the map as layers (Figure 2.3). This method displays the data as distinct layers, each of which presents unique information on the map. These layers are arranged vertically to allow for the representation of various information on the map at the same time. Including layer(s) on the map would add value to the conditional assessment of structures.

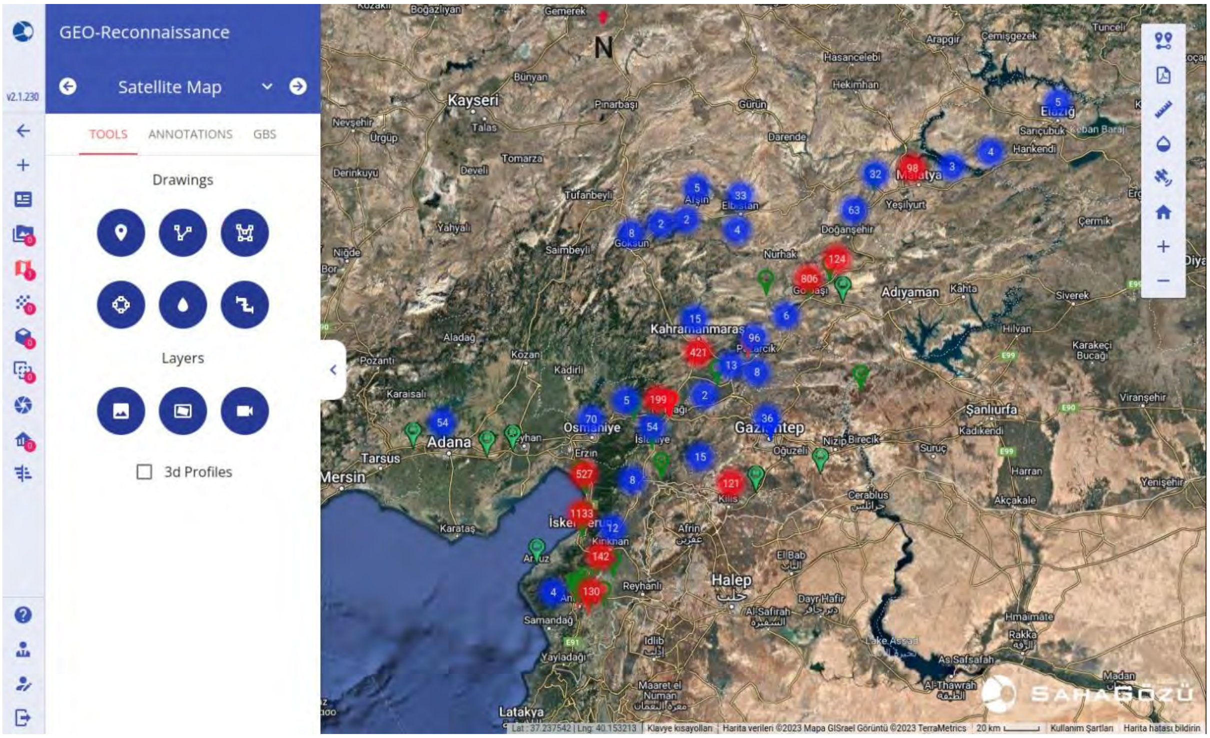

Figure 2.2. The distribution of collected images (SiteEye Disaster Plugin ,2023)

Collecting a huge amount of data decreases its manageability to examine each data one by one. Therefore, they are grouped according to the contribution of the researchers to divide the data into manageable units. Moreover, marker clustering is provided based on the zooming details to improve the performance of the application (Figure 2.2).


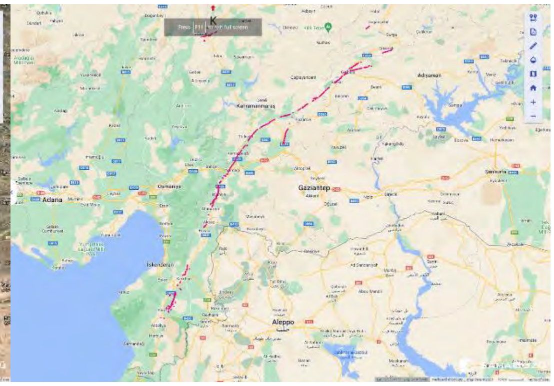

(a) (b)

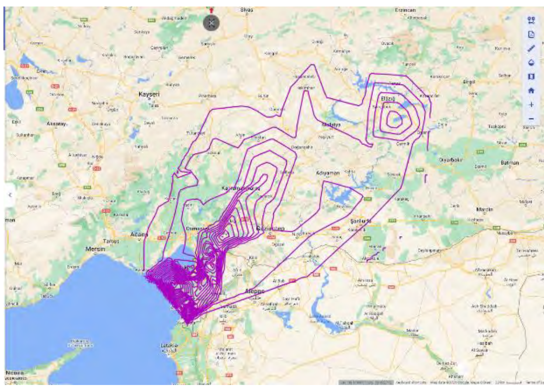
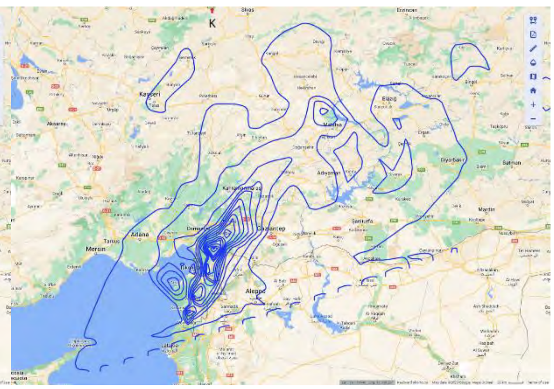

(c) (d)

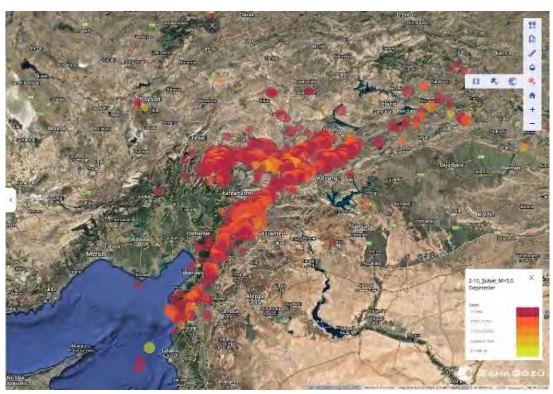

(e)

Figure 2.3. a) Fault lines, b) Surface ruptures, c) PGA distribution, d) PGV distribution, e) M_w distribution (SiteEye Disaster Plugin, 2023)

2. 4. Data Analyses

Collecting several data from the widespread earthquake sites is utterly essential so that meaningful patterns about the destructiveness of events can be extracted. Analyzing and deducing information from these patterns especially help post-earthquake studies to improve and provide insightful approaches for future disasters. These procedures can be conducted by visual inspection via SiteEye Disaster Plugin with varying functions of filtering tagged images according to the different infrastructure and damage types and dates of data acquisition (Figure 2.4).

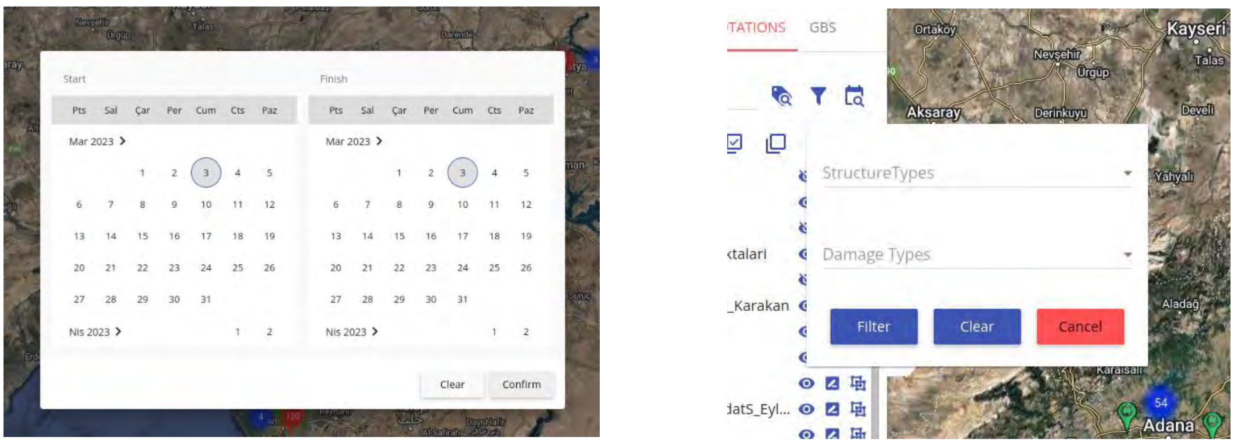

(a) (b)

Figure 2.4. Data filtering according to (a) Infrastructure and damage type, (b) Data acquisition date (SiteEye Disaster Plugin,2023)

Visualization of data on the map by utilizing filtering options enables users to interpret earthquakes' influences on the field. In this way, regions with specific structural or geotechnical damages can be represented in more compact and synthesized illustrations. This representation could be particularly vital when decision-makers are ought to take safety precautions immediately after earthquakes. Moreover, gathering periodical data from the same spots provides an opportunity for observing the occurring changes. SiteEye Disaster Plugin provides an option for filtering images in terms of their acquisition dates and enables the deconstruction and construction process of the fields to be tracked.

In Section 2.2, the importance of geolocated drone footage, ground images, and videos is profoundly emphasized. Besides gathering data after an earthquake, it could be very fruitful to make a pre-post-earthquake analysis of these images and videos from the ones collected before the earthquake. SiteEye is enhanced with a street-view plugin so that structures can be analyzed according to their damage degrees on the same view (Figure 2.5). This can significantly reduce the waste of time for damage detection.

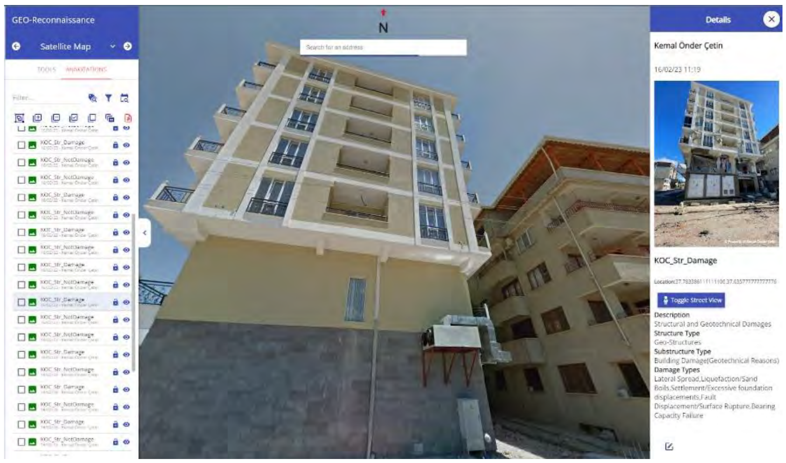

Figure 2.5. Comparison of condition structure before and after the earthquake (SiteEye Disaster Plugin ,2023)

2. 5. Future Studies

Comprehensive data on the conditions of the structures due to the earthquakes that occurred in Türkiye in February have been collected and continuously increasing in the voluntarily developed disaster plugin of SiteEye. In the current version of the Site Eye Web application (version 2.1.229) SiteEye Mobile plugin (version 1.0.28(9)), a visual inspection on the layered map is provided with alternative grouping, structure/substructure, and damage types and time horizon filtering options. In the future, earthquake-related data layers can be reinterpreted to construct a quantitative and qualitative relationships between seismological data and the conditions of the structures. Additionally, using sophisticated computer vision and artificial intelligence approaches, SiteEye models can be constructed to estimate the level and type of damage for different structures to support faster and more accurate damage assessment when possible.

References

i4Works (2023). "SiteEye: Cloud-based Photogrammetry and Project Management", [Computer Software]. Available from: https://siteeye.co

Chapter 3. Active Tectonic Setting and Seismic Source

By:

A. Arda Özacar[a], Bora Uzel[b], Erdin Bozkurt[a], Taylan Sançar[c], Eyüp Sopacı[a,d], Hakan Bora Okay[a], Nuretdin Kaymakçı[a], Bora Rojay[a], Zeynep Gülerce[e,*], Cem Kıncal[b,f], Duygu Köksal[g], Laura Gregory[h]

[a] Middle East Technical University, Geological Engineering Department, Ankara, Türkiye
[b] Dokuz Eylul University, Geological Engineering Department, Izmir, Türkiye
[c] Munzur University, Geography Department, Tunceli, Türkiye
[d] Middle East Technical University, Geodetic, and Geographic Information Technology, Ankara, Türkiye
[e] Middle East Technical University, Civil Engineering Department, Ankara, Türkiye, currently in International Atomic Energy Agency (IAEA, Vienna)
[f] Dokuz Eylul University, The Graduate School of Natural and Applied Sciences, Izmir, Türkiye
[g] Dokuz Eylul University, The Graduate School of Natural and Applied Sciences, Geographical Information Systems Dept., Izmir, Türkiye
[h] University of Leeds, School of Earth and Environment, Leeds, United Kingdom

[*]This is not an IAEA report and views expressed in any signed article do not represent those of the International Atomic Energy Agency and the IAEA accepts no responsibility for them.

3. 1. Active Tectonic Setting

Türkiye is one of the most seismically active regions in the world and has a dramatic history of damaging earthquakes resulting mainly from two intra-continental transform fault zones, namely the dextral North Anatolian (NAFZ), sinistral East Anatolian fault zones (EAFZ). These structures are developed due to the collision of the Arabian Plate into the Eurasian Plate along the Bitlis-Zagros Suture that gave way to the westward escape of the Anatolian block from the zone of high convergent strain in eastern Anatolia. On the other hand, western Anatolia is dominated by extensional structures that also produced devastating earthquakes and is characterized by normal fault-controlled horst-and-graben morphology developed due to extensional strain resulting from southwards migration of the Aegean-Cyprian Trench due to the roll-back of northwards subducting African oceanic lithosphere below Anatolian block Figure 3.1. We refer to Duman et al. (2018) for the full account of active faults and database for major earthquakes in Türkiye.

NAFZ is about 1500 km long, northwards convex, approximately E–W-trending dextral strike-slip fault system. It extends from Karlıova in the east of Türkiye to Greece and is responsible for the largest seismic events in the last century, which occurred multiple earthquakes in a cascading manner starting from the 1939 M_w=7.8 Erzincan earthquake in the east and ending with 1999 M_w= 7.2 Düzce earthquakes in the west.

EAFZ is about 450 km long, a NE-trending left-lateral strike-slip fault system that extends from Karlıova in the NE to the Mediterranean Sea in the SW. Except for a few studies, it has been mostly neglected in the literature due to its long-lasting seismic quiescence. The available studies ascribed this silence to the accumulation of elastic strain that could produce devastating future events (e.g. Duman and Emre, 2013; Yönlü et al., 2013; Mahmoud et al., 2013; Karabacak and Altunel., 2013; Bayrak et al., 2015; Gülerce et al., 2017; Yönlü et al., 2017). The most recent studies, mainly related to recent events such as the Mw=6.8 Elazığ earthquake in 2020, raised attention to its seismic hazard potential (e.g. Pousse-Beltran et al., 2020; Ragon et al., 2020; Tatar et al., 2020; Akgün and İnceöz, 2021; Doğru et al., 2021; Güvercin et al., 2022; Kelam et al., 2022; Akbayram et al., 2022).

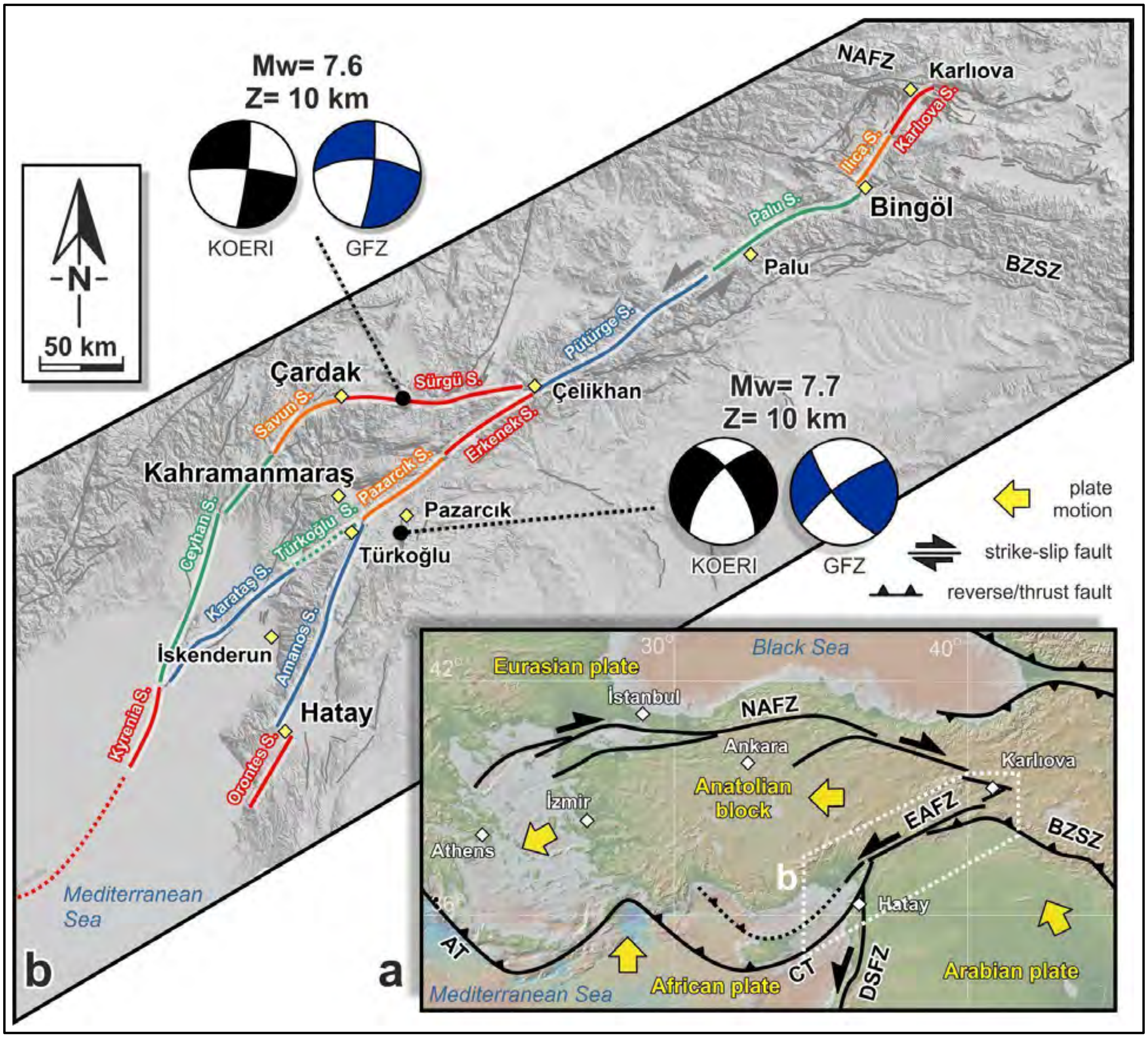

Figure 3.1 a) Simplified tectonic picture of Türkiye. NAFZ: North Anatolian Fault Zone, EAFZ: East Anatolian Fault Zone, DSFZ: Dead Sea Fault Zone, BZSZ: Bitlis-Zagros Suture Zone, AT: Aegean Trench, CT: Cyprian Trench. b) Segments along the EAFZ and DSFZ (after Gülerce et al., 2017) and focal mechanisms of recent events according to different agencies. Active faults (dark gray lines) are after Emre et al. (2018).

The EAFZ is first defined by Arpat and Şaroğlu (1972), then various studies focused on its geometry and fault pattern, morphotectonic features, kinematics, paleoseismology, and seismotectonic characteristics (Duman and Emre, 2013 and references therein). More recent studies are mainly related to monitoring the fault zone using geodetic and various remote sensing techniques as well as assessing its seismic hazard potential. However, there is debate on the western extension of the EAFZ and its relationship with the Dead Sea Fault Zone (DSFZ). Some studies argue that the EAFZ and DSFZ meet around Kahramanmaraş and the EAFZ continues westwards towards Iskenderun following the Türkoğlu segment (Yılmaz et al., 2006; Karabacak et al., 2010; Yönlü et al., 2017; Khalifa et al., 2018). However, others emphasize that EAFZ continues as far as south as Hatay and meets the DSFZ there (Rojay et al., 2001; Tatar et al., 2004; Akyüz et al., 2006; Kaymakci et al., 2010: Emre et al., 2018; Barbot and Weiss, 2021). The recent Mw=7.7 Pazarcık earthquake seems to support the latter claim (Figure 3.1b).

The 6 February 2023 M_w=7.8±0.1 Pazarcık and M_w=7.7±0.1 Elbistan earthquakes, demonstrated that many adjacent faults segments can interact with each other. Therefore, in light of the related literature but mainly after Gülerce et al. (2017), 14 fault segments can be defined for the EAFZ between Karlıova and Hatay. These are from east to west; Karlıova, Ilıca, Palu, Pütürge, Erkenek, Pazarcık, Amanos, Orontes, Türkoğlu, Karataş, Sürgü, Savrun, Ceyhan, and Kyrenia segments (Figure 3.1b). The lengths of these fault segments vary between 30 and 140 km and their slip rates can reach up to 10 mm/yr. The rates might become lower when lateral motion is partitioned between multiple fault segments. However, some of the transverse segments might accommodate the total horizontal strain and transfer it to vertical strain (Mahmoud et al., 2013; Duman and Emre, 2013; Bayrak et al., 2015; Aktuğ et al., 2016; Yönlü et al., 2017; Gülerce et al., 2017; Barbot and Weiss, 2021).

3. 2. Major Earthquake History

The EAFZ is a major transform plate boundary, where the Arabian plate is moving northwards with respect to the Anatolian block at approximately 10-11 mm/yr (Çetin et al., 2003; Reilinger et al., 2006) with a total offset of 15-30 km (Şaroğlu et al., 1992; Westaway, 1994; 2003; Moreno et al., 2011). The EAFZ joins the NAFZ at the Karlıova junction, where the Eurasian Plate moves to the east and the Anatolian plate moves to the west relatively (Figure 3.1a). Both NAFZ and EAFZ are similar in hosting multiple large earthquakes over short time intervals, demonstrating cascading behavior. The historical earthquakes along the EAFZ are partly contemporaneous, such that many of the segments slipped with similar magnitude earthquakes around the 19th century (Figure 3.2).

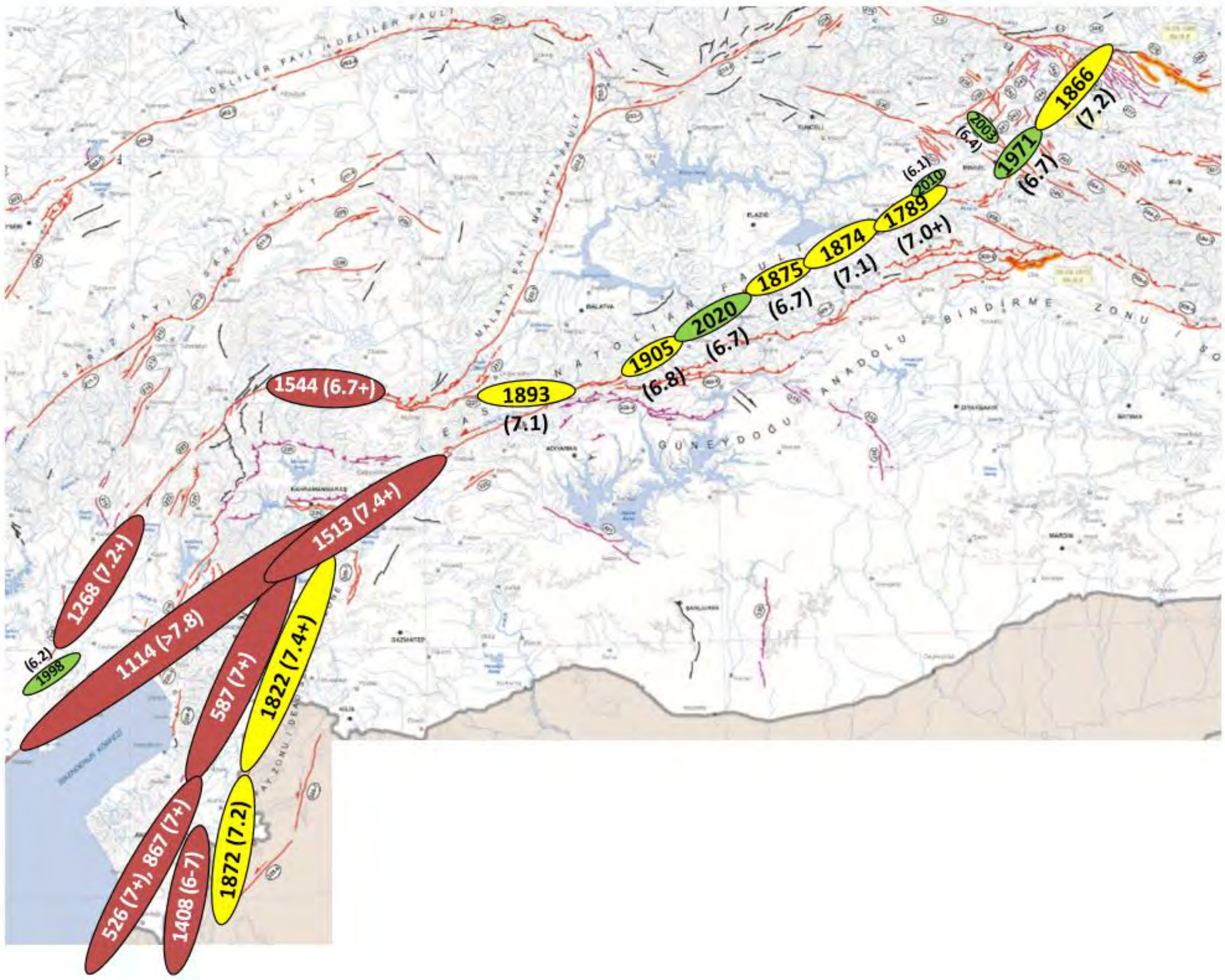

Figure 3.2. Map of the latest known or inferred surface fault ruptures along the East Anatolian Fault Zone (EAFZ) before the current earthquake sequence. Major earthquakes with their estimated rupture area (ellipse) are shown over the active fault map taken from MTA. The earthquake information is compiled from Akyüz et al. 2006, Ambraseys (1989), Ambraseys and Finkel (1995), Ambraseys and Melville (1995), Ambraseys and Jackson (1998), Duman and Emre, (2013), Duman et al. (2016) and historical earthquake catalog of KOERI (2023).

During the 2023 Pazarcık earthquake (M7.8), Amanos, Pazarcık, and Erkenek fault segments are ruptured. Figure 3.2 shows the inferred ruptures of the past large earthquakes. According to compiled historical earthquake records, the Pazarcık segment was ruptured previously with a large earthquake (M7.4+) in 1513 (Ambraseys, 1989). In the south, the historical records that occurred over the last two millennia are more ambiguous and the earthquake in 1822 (M7.4+) is often mistakenly attributed to the Amanos segment. In contrast, this historic event more likely occurred further east on a parallel Yesemek fault segment (Ambraseys, 1989; Ambraseys and Melville, 1995); Duman and Emre, 2013). Similarly, the event in 1872 (M7.2) occurred just south of the 1822 earthquake, likely rupturing the fault segment that controls the Amik basin from the east near Reyhanlı (Ambraseys, 1989). This implies that the Amanos segment ruptured during the 6th century with a sequence of earthquakes in 506, 526, 528, and 587 (Duman et al., 2018). Among them, the deadliest event was 526 (7+) claiming the loss of 250.000 lives, which occurred near Samandağ (KOERI, historical earthquake catalog), most likely rupturing the southwestern side of the Amanos segment. On the other hand, the northeastern side of the Amanos segment possibly ruptured during the 587 (7+) earthquake and caused the loss of approximately 60.000 lives. The earthquake in 867 (7+) is the latest historic event in the region that may have occurred in the Amanos segment (Duman et al., 2018). Hence, the stress has been built up for more than a thousand years on this fault segment (Figure 3.2).

Çardak fault in the western part of the Sürgü fault segment is ruptured during the 2023 Elbistan earthquake (M7.7). The earthquake in 1893 (M7.1), caused damage across Malatya and Adıyaman, previously attributed to the Erkenek segment that ruptured during the 2023 Pazarcık earthquake (Duman and Emre, 2013). Alternatively, the 1893 event may have occurred along the eastern part of the Sürgü segment which would explain why the Erkenek segment, not the eastern part of the Sürgü segment, is ruptured during the recent earthquake sequence (Figure 3.2). According to historical records, an earthquake in 1544 (6.7+) took place along the recently ruptured section of the Sürgü segment, which suggests that elastic strain has accumulated for ~500 years, similar to the Pazarcık segment (Ambraseys, 1989).

The latest known earthquake along the Ceyhan and Savrun fault segments which are located at the western prolongation of the recent Elbistan earthquake rupture took place a long time ago (1268, 7.2+) and thus accumulated elastic strain may lead to a large earthquake in the near future (Figure 3.2). Similarly, the northern tip of the Dead Sea fault did not rupture since 1408 and significant elastic strain might have built up. Karataş and Türkoğlu fault segments located on the SW continuation of the Pazarcık segment also deserve the utmost attention for their seismic potential. Türkoğlu segment is not identified as an active fault by MTA (Duman et al., 2018); however, the proposed left-lateral strike-slip faulting connecting Pazarcık and Karataş segments is kinematically viable (Gülerce et al. 2017). The earthquake in 1114 (>M7.8) caused widespread damage around

Kahramanmaraş including Adıyaman, Ceyhan (Misis), and Antakya (Kesik, 2012). This was one of the largest earthquakes (>7.8) in the region and likely ruptured Erkenek, Pazarcık, Türkoğlu, and Karataş segments together or Erkenek, Pazarcık, and Amanos segments as in the 2023 Pazarcık earthquake (Figure 3.2). After the 2023 earthquake sequence, seismic gaps of EAFZ remain along the Savrun, Ceyhan, Kyrenia, Türkoğlu, Karataş, and Orontes fault segments in the south and on Gökdere push-up located SW of Bingöl in the north (Figures 3.1a and 3.2) (Gülerce et al. 2017).

3. 3. Seismic Source

On February 6, 2023; at 01:47 UTC, a large earthquake with M7.8±0.1 occurred near Pazarcık, Kahramanmaraş. The event epicenter is located south of the EAFZ at 37.1123N, 37.1195E according to KOERI (Figure 3.3). Moment tensor solution revealed almost pure left-lateral strike-slip motion on a nearly vertical NE-SW trending fault. The earthquake was initiated on a smaller Narlı fault in the south, jumped to the north, and ruptured the Pazarcık and Erkenek segments of EAFZ towards NE and the Amanos segment towards SW. The multi-event nature of this earthquake also resulted in distinctly separated codas on some of the strong motion recordings (Figure 3.3). The distribution of aftershocks indicates that the earthquake rupture reached Antakya (Hatay) in the south and terminated in the north at the Pütürge segment close to the 2020 Doğanyol, Elazığ earthquake segment (Figure 3.3). The total rupture length is just over 300 km with a maximum surface displacement exceeding 4 m. Ten minutes after the mainshock, a strong aftershock with M6.8 occurred just west of the mainshock's hypocenter, which may rupture the Salçagöz fault near the epicenter of the Pazarcık earthquake.

Nine hours later, the Elbistan earthquake with M7.7 ±0.1 occurred along the Sürgü fault segment, exhibiting a unique example of short-term earthquake triggering. The event epicenter is located south of Elbistan near Ekinözü at 38.0717N, 37.2063E by KOERI (Figure 3.3). Like the previous event, the moment tensor solution suggested almost pure left-lateral strike-slip motion. Seismic data indicate that the earthquake initially ruptured the ~E-W trending Çardak fault which strike WSW in the west and continued eastward towards Malatya on the NE-SW striking Doğanşehir fault zone. It is also worth noting that aftershocks on the western rupture tip are curving further southwards and imply possible activation of pre-existing faults with different orientations (Figure 3.3). The total rupture length is around 160 km with a maximum surface displacement exceeding 6 m.

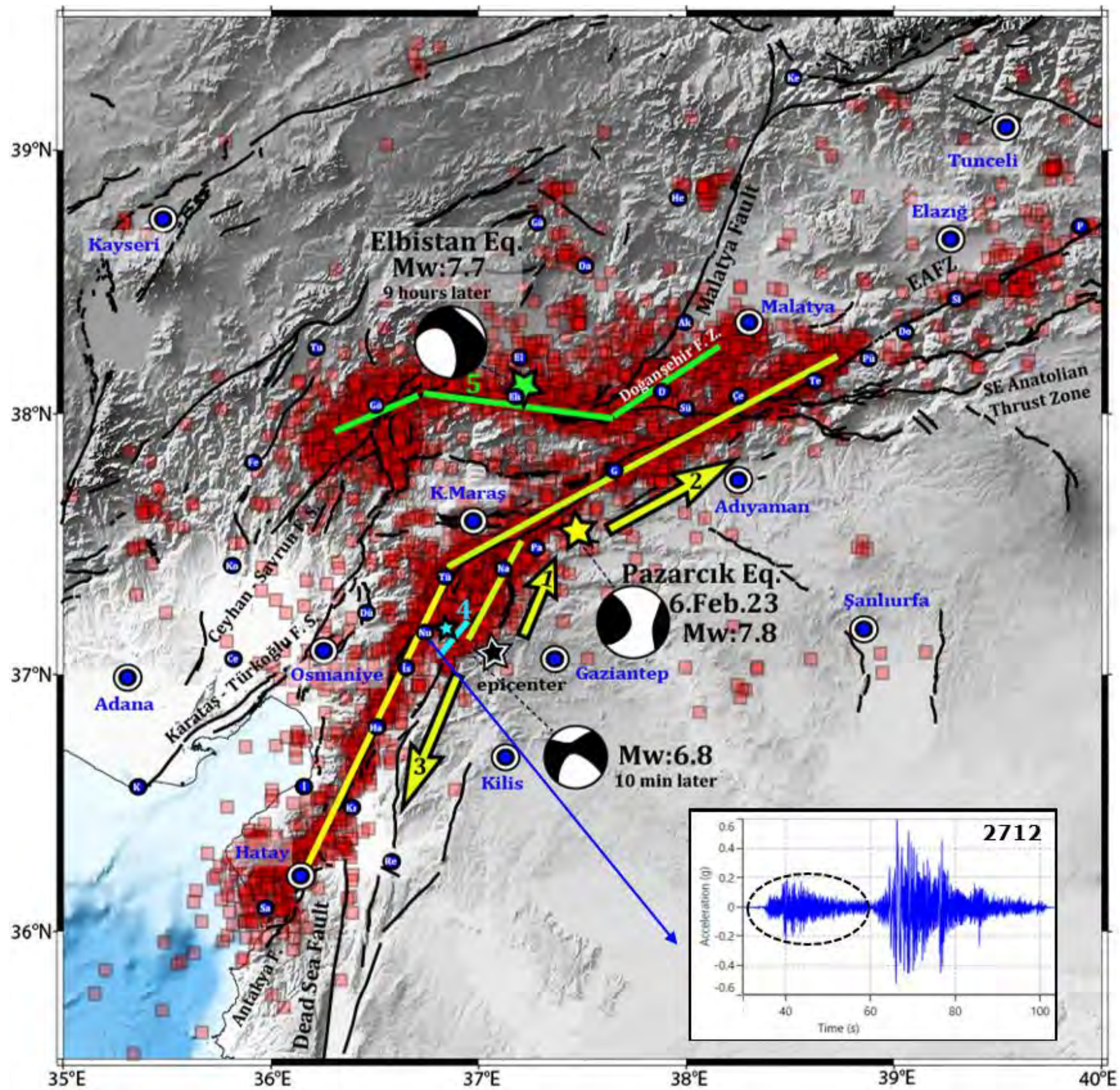

Figure 3.3. Seismotectonic map showing inferred rupture planes and aftershocks taken from AFAD along with Harvard global centroid moment tensor solutions of major earthquakes. Arrows indicate the inferred rupture direction of the initial Kahramanmaraş Pazarcık earthquake. The Inset figure shows an acceleration record of AFAD station 2712 near Nurdağı.

3. 4. Surface Rupture and Geological Field Observations

After the 6 February 2023 M7.8 Pazarcık and M7.7 Elbistan earthquakes, various surface ruptures were observed and mapped along the fault trace (Pazarcık, Amanos, and Sürgü) segments using open-access satellite images provided by institutions such as MAXAR (https://www.maxar.com) and PLANET (https://www.planet.com), aerial photographs provided by the General Directorate of Mapping (Türkiye), and field studies by geoscientists. Considering that we are still in the period dealing with the physical and mental effects of the destruction, especially satellite images proved to be important sources of information for the detection and mapping of these ruptures. Several online repositories of digital mapping became available just after the earthquake to help those working on earthquakes remotely and on-site. One example is geodetic data and satellite imagery from the USGS (Reitman et al., 2023).

For example, surface faulting can be observed in the MAXAR satellite images of the Türkbahçe Village vicinity to the north of İslahiye (Figure 3.4). In this area, man-made features such as stabilized roads, farm borders, and walls are left-laterally displaced, which continues approximately 2 km in a general right-stepping geometry. Here, in this report, comparisons were made at points where the displacements were best observed using Google Earth (https://earth.google.com/) images, and in Figure 3.4. pre-and post-earthquake figures are presented. The measured displacement amount in these images reaches up to 2.5 m.

During the field observations, many deformation zones and offsets features were also documented along with the surface ruptures observed on the satellite images. Some of these are left-lateral offsets observed on the asphalt roads near Güzelyurt and Pazarcık, where the displacement is about 2.4 m (Figure 3.5). In addition, a left lateral displacement on the railway around İslahiye is developed on the Amanos segment after the Pazarcık earthquake (left panel of Figure 3.6). Similar field observations are also documented along the Sürgü segment. The left lateral offset observed on a garden fence reveals the lateral component of the Elbistan earthquake fault. The displacement amount measured at this point reaches up to 6.7 m (right panel of Figure 3.6).

Figure 3.4. Satellite photos downloaded from MAXAR showing surface rupture and estimated displacements associated with the first event (Mw=7.8) between Türkoğlu and İslahiye (https://www.maxar.com).

Figure 3.5. Photos of the surface fault rupture of the Pazarcık earthquake (Mw=7.8) offsetting the roads near Güzelyurt and Pazarcık (taken by M. Tolga Yılmaz and Erdin Bozkurt respectively).

Figure 3.6. The photo on the left (taken by K. Önder Çetin) shows the deformation on the railroad track caused by the surface fault rupture of the Pazarcık earthquake (M_w=7.8) near İslahiye. The photo on the right (taken by Taylan Sançar) shows the 6.7 m fence offset along the Sürgü-Çardak fault that ruptured during the Elbistan earthquake (M_w=7.7).

3. 5. Geodetic observations

Interferogram is generated by cross-multiplying, pixel-by-pixel, the first SAR image with the complex conjugate of the second. When a prior SAR image is acquired before an earthquake, and a coherent interferogram can be produced with a second post-earthquake SAR image, it is possible to study the coseismic deformation of an event even in the most remote regions (Bürgman, 2000; Ferretti et al., 2007). Coseismic deformation maps provide an investigation to determine the location, geometry, and kinematics of the seismic event. Additionally, InSAR studies contribute geological and geophysical applications with low cost and great measurement density monitoring techniques to understanding surface deformation (Békési et al., 2021; Bürgman, 2000; Solari et al., 2016; Lazecky et al., 2020).

The deformation of the ground during the M7.8 Pazarcık and M7.7 Elbistan earthquakes was captured by satellite radar, which reveals a detailed picture of the large-scale motions of the earth's surface as a result of the earthquakes. Figure 3.7 shows the first interferogram, with colored fringes indicating how the ground has moved towards or away from the satellite between two data acquisitions (on the 29th of January and the 10th of February 2023). The range pixel offset tracking in Figure 3.7 (right panel), shows the ground displacement in meters, with greater intensity of color indicating larger displacements.

Preliminary data suggest greater displacement across the NE segments of the EAFZ fault during the M7.8 Pazarcık earthquake on the order of 3 – 7 m and relatively lower displacements on the fault segment directly above the hypocenter. The M7.7 Elbistan earthquake has displacements of 2 – 8 m, greatest in the central section of the Sürgü segment, close to the earthquake hypocenter. These are the preliminary results, and much greater detail can be achieved with future modeling of the data. The geodetic data show that many of the segments identified in Figure 3.1 were active in the two earthquakes and hosted significant displacement over rupture lengths of 300 km and 100 km, respectively (Figure 3.7).

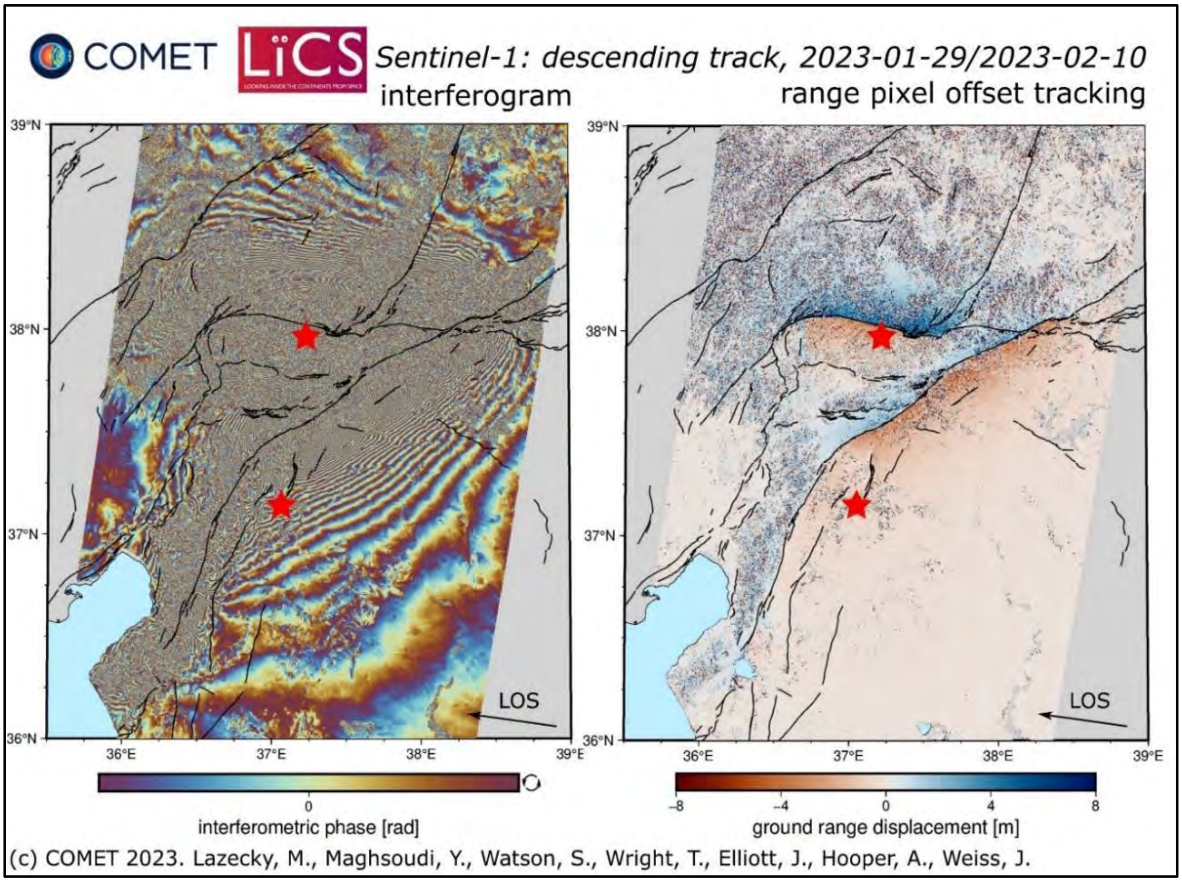

Figure 3.7. Sentinel-1 interferogram and range pixel offset tracking showing the ground deformation that occurred during the M7.8 Pazarcık and M7.7 Elbistan earthquakes (epicenters indicated by red stars). Figure from COMET (Centre for the Observation and Modelling of Earthquakes, Volcanoes, and Tectonics, 2023; courtesy of Lazecky, M., Maghsoudi, Y., Watson, S., Wright, T., Elliott, J., Hooper, A., and Weiss, J; method from Lazecky et al., 2020).

In this report, interferometric analyzes were also carried out using Sentinel-1's SAR dataset. In the analysis, two pairs S1-A descending orbits (Track 21) have been processed for İskenderun and Kahramanmaraş with the Sentinel Application Platform (SNAP, version 8.0) and Standford Method for Persistent scatter interferometry (StaMPS) open-source software tools. A total of four products acquired in TOPSAR Interferometric Wide (IW) SWATH Mode in Single Look Complex (SLC) format, are downloaded freely accessible through the Copernicus Science Hub and Alaska Satellite Facility (ASF) (https://scihub.copernicus.eu/, https://asf.alaska.edu/). Table 3.1 lists the information on the coseismic pairs and the location of data frames is given in Figure 3.8.

Table 3.1 The information of coseismic orbit pairs.

Study area	Orbit Pairs of Interferometric	Orbit Direction	Orbit Pairs
İskenderun -Antakya	S1A_IW_SLC__1SDV_20230129T033452_20230129T033519_046993_05A2FE_BE0B	Descending Track21	29/01/2023 - 10/02/2023
	S1A_IW_SLC__1SDV_20230210T033451_20230210T033518_047168_05A8CD_E5B0		
Kahramanmaraş-Elbistan	S1A_IW_SLC__1SDV_20230129T033427_20230129T033455_046993_05A2FE_6FF2		
	S1A_IW_SLC__1SDV_20230210T033426_20230210T033454_047168_05A8CD_FAA6		

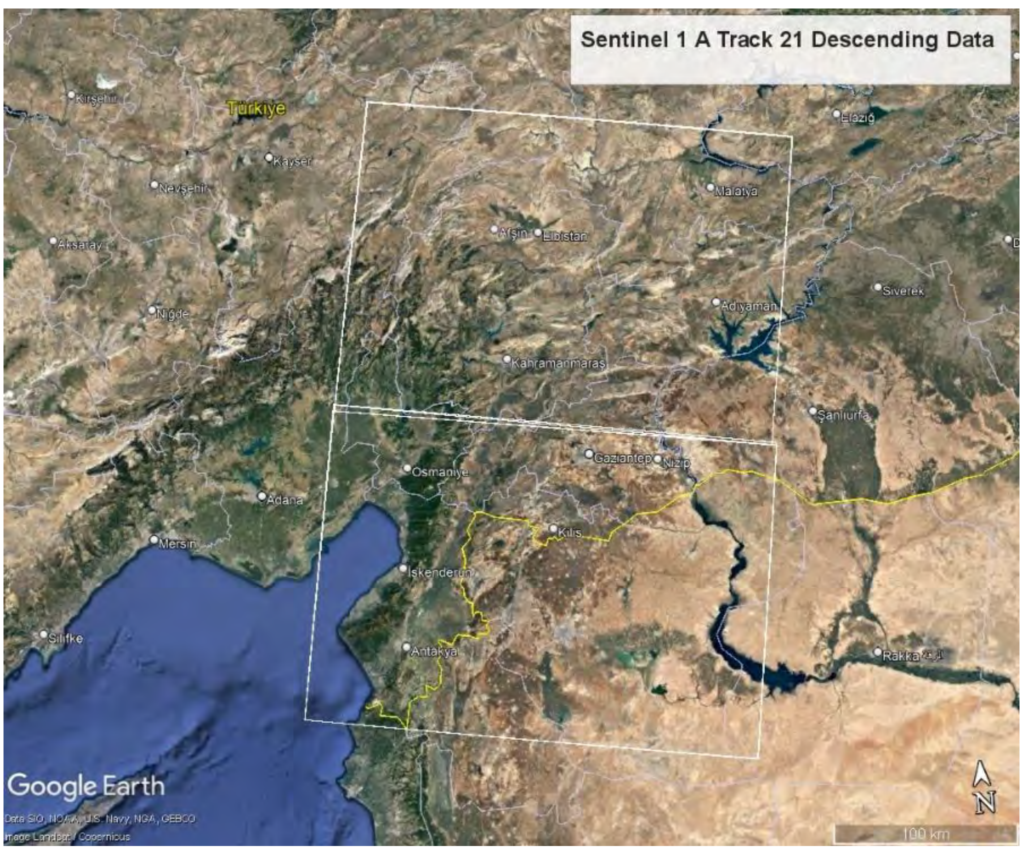

Figure 3.8. Google Earth satellite image shows the image pair Jan. 29-Feb.10, 2023 (Sentinel 1A descending orbit).

Descending data have been analyzed by the SAR interferometry technique (InSAR). Firstly, Sentinel-1 pairs are co-registered to master image with Sentinel-1 Back Geocoding operator with Enhanced spectral diversity. This makes use of image statistics to overlap both products at sub-pixel accuracy. After interferograms are formed, the topographic phase component is removed. Shuttle Radar Topography Mission (SRTM) 1 Arc-Second Digital Elevation Model (DEM) was used to remove the topographic phase. The interferogram should now only contain variations from displacement, atmosphere, and noise. Then the Goldstein phase filtering is applied for decreasing noise from temporal and geometric decorrelation, volume scattering, and other processing errors (Braun &Veci, 2021). Another important processing step is phase unwrapping by using SNAPHU and line of sight (LOS) displacement map is acquired by using phase to displacement tool. This stage provides relative information about deformation (https://web.stanford.edu/group/radar/softwareandlinks/sw/snaphu/).

In the deformation map generated using the scenes acquired 4 days after the event, the displacement signal in the InSAR data showed up to 2 meters of uplift and up to 0.5 meters of subsidence zones indicating where the earthquakes took place. A slight subsidence was observed along the East of Yesemek and Narlı Segments of the Ölüdeniz Fault Zone. In addition, subsidence zones were apparently observed as about -0.8 meters along the fault line of the DAF Amanos Segment. In the north, deformations were also observed above -0.5 meters in the north of the Çardak Fault (Figure 3.9).

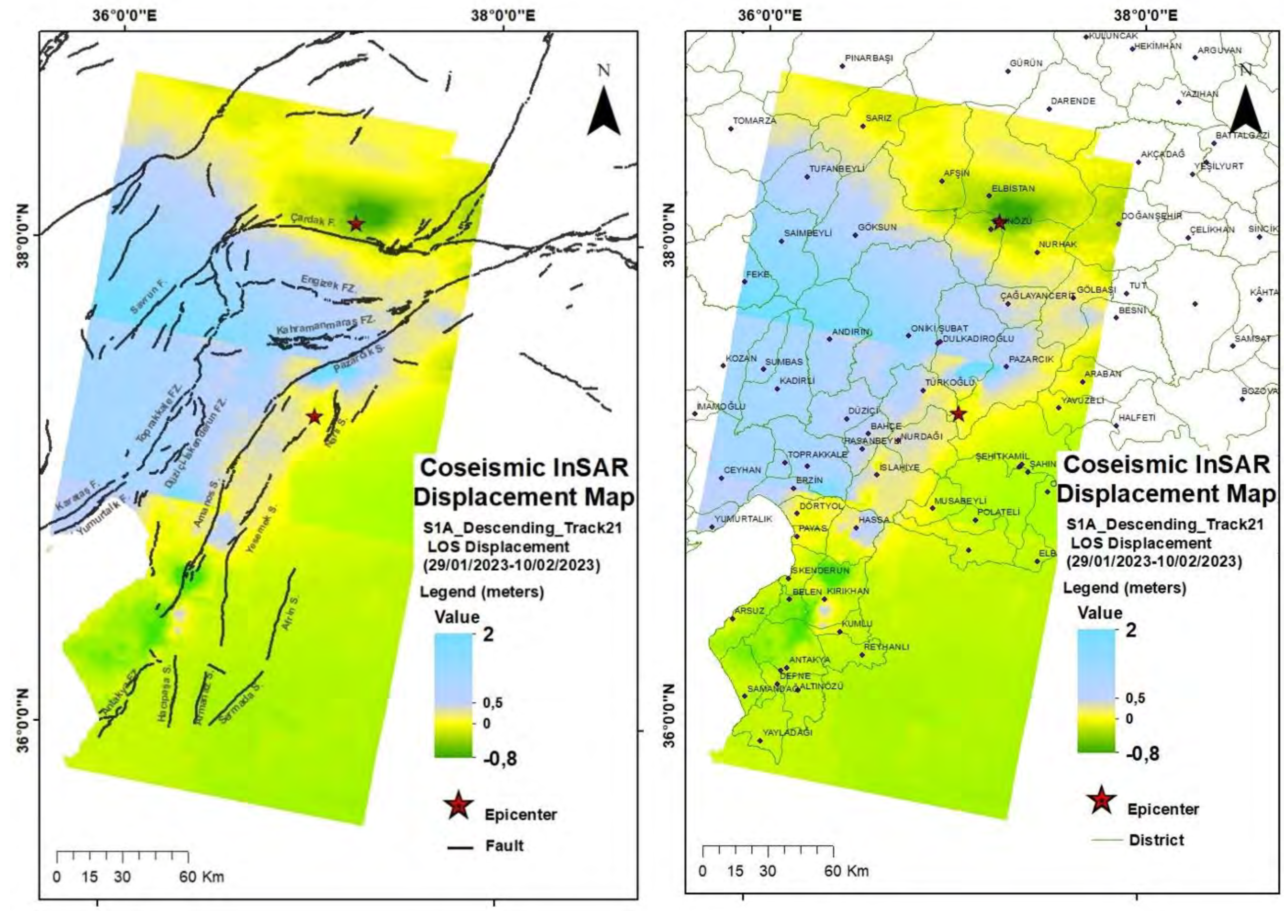

Figure 3.9. On the left panel, Sentinel 1 A Track 21 descending coseismic displacement map between 29/01/2023 -10/02/2023 dates. On the right panel, S1A Track 21 descending coseismic displacement map with district vector data.

3. 6. Preliminary Conclusions and Recommendations

The M7.8 Pazarcık and M7.7 Elbistan earthquake sequence including the M6.8 aftershock, have occurred on EAFZ with left-lateral strike-slip mechanisms and caused devastating effects in the surrounding cities of Kahramanmaraş, Gaziantep, Malatya, Adıyaman, Hatay and Osmaniye (Figure 3.3). Based on historical data, fault segments ruptured during this earthquake sequence were seismic gaps with tectonic stress accumulating for at least 500 years.

Pazarcık earthquake initiated on a nearby, lesser-known fault and then propagated towards NE and SW along EAFZ, rupturing Erkenek,Pazarcık and Amanos fault segments with a total surface rupture length of just over 300 km. This earthquake initiated on a secondary fault and then ruptured the main fault segments of EAFZ bilaterally towards the NE and SW directions. The observed rupture evolution along multiple fault segments is a unique example of complex rupture displaying multi-event nature.

Elbistan earthquake was triggered 9 hours after the first event rupturing the ~W-E trending Çardak fault and the NE-SW trending Doğanşehir fault zone bilaterally with a total surface rupture length reaching up to 160 km. This earthquake sequence displays a great example of short temporal seismic clustering, with two large earthquakes occurring closely in space and time, only 9 hours apart. The estimated static stress changes using Coulomb failure along with historical earthquake records point out the fault segments that are prone to failure. Preliminary static stress change calculations indicate pronounced increases, especially along Malatya, Savrun, Türkoğlu, and Orontes (Antakya) fault segments where tectonic stress has not been released by a large earthquake for a long time (Figure 3.10). Unfortunately, this earthquake sequence resulted in the greatest tragedy in Türkiye and Syria that will linger for several decades. Therefore, meticulous data analysis is very critical for realistic seismic hazard assessment and preparedness in Türkiye and worldwide.

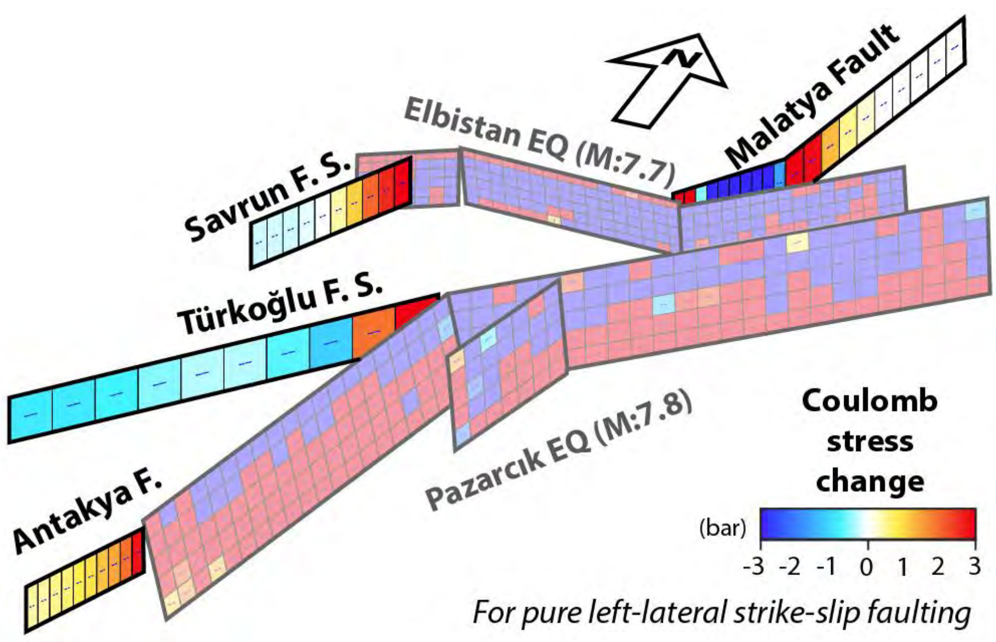

Figure 3.10. Coulomb static stress change on the neighboring fault segments after the recent earthquake sequence. Calculations made for left-lateral strike-slip faults using finite fault solutions computed by USGS.

At the time of writing this text, another earthquake with M6.3 occurred on 20 February 2023 along the Orontes (Antakya) fault segment near Samandağ, Hatay and caused additional panic. As mentioned previously, this event took place along the fault segment where especially M7.8 Pazarcık earthquake transferred up to 3 bar of additional static stress (Figure 3.10).

Acknowledgments

We thank the Disaster and Emergency Management Presidency (AFAD) for sharing strong motion records and aftershock information. Also, thanks to Centre for the Observation and Modelling of Earthquakes, Volcanoes, and Tectonics (COMET) for sharing their initial InSAR findings and MAXAR for providing access to satellite images.

We also thank to Aerospace Information Research Institute (AIR) under the Chinese Academy of Sciences (CAS) for sharing Chinese EO satellite data related to earthquakes in Türkiye under the framework of Collaborated network on Disaster Data Response (CDDR) of the National Remote Sensing Center of China (NRSCC).

References

Akbayram, K., Bayrak, E., Pamuk, E., Özer, Ç., Kıranşan, K., and Varolgüneş, S., 2022. Dynamic sub-surface characteristics and the active faults of the Genç District locating over the Bingöl Seismic Gap of the East Anatolian Fault Zone, Eastern Turkey. Natural Hazards, 114(1), 825-847.

Akgün, E., and İnceöz, M., 2021. Tectonic evolution of the central part of the East Anatolian Fault Zone, Eastern Turkey. Turkish J Earth Science, 30, 928-947, doi:10.3906/yer-2104-15.

Aktuğ, B., Özener, H., Doğru, A., Sabuncu, A., Turgut, B., Halıcıoğlu, K., Yılmaz, O., 2016. Slip rates and seismic potential on the East Anatolian Fault System using an improved GPS velocity field. J. Geodyn., 94–95, 1–12, doi:10.1016/j.jog.2016.01.001.

Akyüz, S.H., Altunel, E., Karabacak, V., and Yalçıner, C.C., 2006. Historical earthquake activity of the northern part of the Dead Sea Fault Zone, southern Turkey. Tectonophysics, 426, 281–293.

Alaska Satellite Facility, https://asf.alaska.edu/.

Ambraseys, N.N., 1989. Temporary seismic quiescence: SE Turkey. Geophysical Journal International, 96(2), 311–331.

Ambraseys, N.N. & Finkel, C., 1995. The seismicity of Turkey and adjacent areas 1500-1800. MS EREN, Istambul.

Ambraseys, N.N., and Melville, C.P., 1995. Historical evidence of faulting in Eastern Anatolia and Northern Syria. Cambridge University Press, 3-4/38.

Arpat, E. and Şaroğlu, F., 1972. The East Anatolian Fault System; Thoughts on its Development. Bull. Miner. Res. Explor., 78.

Barbot, S., and Weiss, J.R., 2021. Connecting subduction, extension, and shear localization across the Aegean Sea and Anatolia. Geophys. J. Int., 226, 422–445.

Bayrak, E., Yılmaz, Ş., Softa, M., Türker, T., and Bayrak, Y., 2015. Earthquake hazard analysis for East Anatolian Fault Zone, Turkey. Natural Hazards, 76, 1063–1077, doi:10.1007/s11069-014-1541-53.

Békési, E., Fokker, P. A., Martins, J. E., Norini, G., & Van Wees, J. D. (2021). Source parameters of the 8 February 2016, Mw= 4.2 Los Humeros earthquake by the inversion of InSAR-based ground deformation. Geothermics, 94, 102133.

Bozkurt, E., 2001. Neotectonics of Turkey—a synthesis, Geodinamica Acta, 14(1–3), 3–30.

Braun, A., & Veci, L. (2021). TOPS Interferometry Tutorial. Sentinel-1 Toolbox.

Bürgmann, R., Rosen, P. A., & Fielding, E. J. (2000). Synthetic aperture radar interferometry to measure Earth's surface topography and its deformation. Annual review of earth and planetary sciences, 28(1), 169-209.

Copernicus Open Access Hub, https://scihub.copernicus.eu/.

Çetin, H., Güneyli, H. &Mayer, L. (2003) Paleoseismology of the Palu-Lake Hazar segment of the East Anatolian Fault Zone,Turkey.Tectonophysics, 374, 163-197.

Doğru, A., Bulut, F., Yaltırak, C., and Aktuğ, B., 2021. Slip distribution of the 2020 Elazığ Earthquake (M w 6.75) and its influence on earthquake hazard in the Eastern Anatolia. Geophysical Journal International, 224(1), 389-400.

Duman, T.Y., Emre, Ö., 2013. The East Anatolian Fault: Geometry, segmentation, and jog characteristics. Geol. Soc. Spec. Publ., 372, 495–529. doi:10.1144/SP372.14.

Duman, T.Y., Çan, T., Emre, Ö., Kadiroğlu, F.T., Baştürk, B.N., Kılıç, T., Arslan, C., Özalp, S., et al., 2016. Seismotectonic Map of Turkey with Explanations. General Directorate of Mineral Research and Exploration (MTA), Special Series-34, Ankara, Türkiye.

Duman, T. Y., Çan, T., Emre, Ö., Kadirioğlu, F. T., Başarır Baştürk, N., Kılıç, T., et al., 2018. Seismotectonic database of Turkey. Bulletin of Earthquake Engineering, 16, 3277-3316.

Emre, O., Duman, T., Özalp, S., Şaroğlu, F., Olgun, C., Elmaci, H., and Can, T., 2018. Active fault database of Turkey. Bull. Earthq. Eng., 16, 3229–3275.

Ferretti, A., Massonnet, D., Monti-Guarnieri, A., Prati, C., & Rocca, F. (2007). Guidelines for SAR Interferometry—Processing and Interpretation. InSAR Principles.

Gülerce, Z., Shah, S.T., Menekşe, A., Özacar, A.A., Kaymakci, N., and Çetin, K.Ö., 2017. Probabilistic seismic-hazard assessment for east Anatolian fault zone using planar fault source models. Bull. Seismol. Soc. Am., 107, 2353–2366, doi:10.1785/0120170009.

Güvercin, S. E., Karabulut, H., Konca, A. Ö., Doğan, U., and Ergintav, S., 2022. Active seismotectonics of the East Anatolian Fault. Geophysical Journal International, 230(1), 50-69.

Karabacak, V., and Altunel, E., 2013. Evolution of the northern Dead Sea Fault Zone in southern Turkey. J. Geodynamics, 65, 282–291. http://dx.doi.org/10.1016/j.jog.2012.04.012.

Karabacak, V., Altunel, E., Meghraoui, M., and Akyüz, H.S., 2010. Field evidences from northern Dead Sea Fault Zone (South Turkey): new findings for the initiation age and slip rate. Tectonophysics, 480, 172–182.

Kelam, A.A., Karimzadeh, S., Yousefibavil, K., Akgün, H., Askan, A., Erberik, M.A., Koçkar, M.K., Pekcan, O., and Ciftci, H., 2022. An evaluation of seismic hazard and potential damage in Gaziantep, Turkey using site-specific models for sources, velocity structure, and building stock. Soil Dynamics and Earthquake Engineering, 154, 107129.

Khalifa, A., Çakır, Z., Owen, L.A., and Kaya, Ş., (2018. Morphotectonic analysis of the East Anatolian Fault, Turkey. Turkish J. Earth Sci., 27, 110–126, doi:10.3906/yer-1707-16.

KOERI, 2023. KOERI, Boğaziçi University Kandilli Observatory and Earthquake Research Institute, http://www.koeri.boun.edu.tr/sismo/2/tr/.

Kuzucuoğlu, C., Şengör, A.M.C., and Çiner, A., 2019. The tectonic control on the geomorphological landscapes of Turkey. Landscapes and landforms of Turkey, pp 17-40.

Lazecky, M., Spaans, K., Gonzalez, P.J., Maghsoudi, Y., Morishita, Y., Albino, F., Elliott, J., Greenall, N., Hatton, E., Hooper, A., Juncu, D., McDougall, A., Walters, R.J., Watson, C.S., Weiss, J.R., and Wright, T.J., 2020. LiCSAR: An automatic InSAR tool for measuring and monitoring tectonic and volcanic activity. Remote Sensing, 12(15), 2430.

Mahmoud, Y., Masson, F., Meghraoui, M., Çakır, Z., Alchalbi, A., Yavasoglu, H., Yönlü, O., et al., 2013. Kinematic study at the junction of the East Anatolian Fault and the dead sea fault from GPS measurements. Journal of Geodynamics, 67, 30–39, doi:10.1016/j.jog.2012.05.006.

Moreno, D.G., Hubert-Ferrari, A., Moernaut, J., Fraser, J.G., Boes, X., Van Daele, M., Avsar, U., Çağatay, N. and De Batist, M. (2011). Structure and recent evolution of the Hazar Basin: a strike-slip basin on the East Anatolian Fault, EasternTurkey. Basin Research 23, 191-207.

Pousse-Beltran, L., Nissen, E., Bergman, E.A., Cambaz, M.D., Gaudreau, É., Karasözen, E., and Tan, F., 2020. The 2020 Mw 6.8 Elazığ (Turkey) Earthquake Reveals Rupture Behavior of the East Anatolian Fault. Geophys. Res. Lett. 47, e2020GL088136, doi:10.1029/2020GL088136.

Ragon, T., Simons, M., Bletery, Q., Cavalié, O., and Fielding, E., 2021. A Stochastic View of the 2020 Elazığ M w 6.8 Earthquake (Turkey). Geophys. Res. Lett., 48, doi:10.1029/2020gl090704.

Reilinger, R., McClusky, S., Vernant, P., Lawrence, S., Ergintav, S., Cakmak, R., et al. (2006) GPS constraints on continental deformation in the Africa-Arabia-Eurasia continental collisional zone and implications for the dynamics of plate interactions. *Journal of Geophysical Research: Solid Earth*, **111**(B5), B05411.

Reitman, Nadine G., Briggs, Richard W., Barnhard, William D., Thompson Jobe, Jessica A., DuRoss, Christopher B., Hatem, Alexandra E., Gold, Ryan D., and Mejstrik, John D., 2023. Preliminary fault rupture mapping of the 2023 M7.8 and M7.5 Türkiye Earthquakes http://doi.org/10.5066/P985I7U2.

Rojay, B., Heimann, A., and Toprak, V., 2001. Neotectonic and volcanic characteristics of the Karasu fault zone (Anatolia, Turkey): the transition zone between the Dead Sea transform and the East Anatolian fault zone. Geodinamica Acta, 14, 197–212.

Şaroğlu, F., Emre, Ö. & Kuşçu, İ. (1992) The East Anatolian Fault zone of Turkey. Ann.Tecton., 6,99-125 (Special Issue-Supplement).

Şengör, A.M.C., Zabcı, C., and Natal'in, B.A., 2019. Continental transform faults: Congruence and incongruence with normal plate kinematics. Transform Plate Boundaries and Fracture Zones. 9, 169-247, doi:10.1016/B978-0-12-812064-4.00009-8.

Solari, L., Ciampalini, A., Raspini, F., Bianchini, S., & Moretti, S. (2016). PSInSAR analysis in the Pisa urban area (Italy): A case study of subsidence related to stratigraphical factors and urbanization. Remote Sensing, 8(2), 120.

Standford University, Radar Remote Sensing Project, https://web.stanford.edu/group/radar/softwareandlinks/sw/snaphu/

Tatar, O., Piper, J.D.A., Gürsoy, H., Heimann, A., and Koçbulut, F., 2004. Neotectonic deformation in the transition zone between the Dead Sea Transform and the East Anatolian Fault Zone, Southern Turkey: a palaeomagnetic study of the Karasu Rift Volcanism. Tectonophysics, 385, 17–43.

Tatar, O., Sözbilir, H., Koçbulut, F., Bozkurt, E., Aksoy, E., Eski, S., Özmen, B., Alan, H., and Metin, Y., 2020. Surface deformations of 24 January 2020 Sivrice (Elazığ)–Doğanyol (Malatya) earthquake (Mw= 6.8) along the Pütürge segment of the East Anatolian Fault Zone and its comparison with Turkey's 100-year-surface ruptures. Mediterranean Geoscience Reviews, 2, 385-410.

Westaway, R. (1994). Present-day kinematics of the Middle East and eastern Mediterranean. J. Geophys. Res., 99, 12071-12090.

Westaway, R. (2003). Kinematics of the Middle East and Eastern Mediterranean Updated. Turkish J. Earth Sci., 12, 5-56.

Yılmaz, H., Över, S., and Özden, S., 2006. Kinematics of the East Anatolian Fault Zone between Türkoğlu (Kahramanmaraş) and Çelikhan (Adıyaman), eastern Turkey. Earth, Planets Sp., 58, 1463–1473, doi:10.1186/BF03352645.

Yönlü, Ö., Altunel, E., Karabacak, V., and Akyüz, S.H., 2013. Evolution of the Gölbaşı basin and its implications for the long-term offset on the East Anatolian Fault Zone, Turkey. Journal of Geodynamics, 65, 272-281.

Yönlü, O., Altunel, E., and Karabacak, V., 2017. Geological and geomorphological evidence for the southwestern extension of the East Anatolian Fault Zone, Turkey. Earth Planet. Sci. Lett., 469, 1–14, doi:10.1016/j.epsl.2017.03.034.

Chapter 4. Preliminary Analysis of Strong Ground Motion Characteristics

By:

Zeynep Gülerce [(a), *], Ayşegül Askan [(b)], Özkan Kale [(c)], Abdullah Sandıkkaya [(d)], Nihat Sinan Işık [(e)], Okan İlhan [(f)], Gizem Can [(g)], Makbule Ilgaç [(h)], A. Arda Ozacar [(b)], Eyüp Sopacı [(b)], Kemal Önder Çetin [(b)]

Burak Akbaş [(b), (i)], Abdullah Altındal [(b)], Baran Guryuva[(d)], Onur Kanun [(b)], Kubilay Albayrak [(b)], Gamze Muratoglu [(b)], Oguz Salih Okcu[(d)], Abdullah Icen[(j)], Mehmet Firat Aydin [(b)]

[(a)] Middle East Technical University, Civil Engineering Department, Ankara, Türkiye, currently in International Atomic Energy Agency (IAEA, Vienna)
[(b)] Middle East Technical University, Civil Engineering Department, Ankara, Türkiye
[(c)] TED University, Civil Engineering Department, Ankara, Türkiye
[(d)] Hacettepe University, Civil Engineering Department, Ankara, Türkiye
[(e)] Gazi University, Civil Engineering Department, Ankara, Türkiye
[(f)] Yildirim Beyazit University, Civil Engineering Department, Ankara, Türkiye
[(g)] Royal Haskoning DHV Resilience & Maritime Netherlands-BL Maritime & Water
[(h)] University of California, Civil and Environmental Engineering, Berkeley, USA
[(i)] Atilim University, Civil Engineering Department, Ankara, Türkiye
[(j)] Munzur Universitesi, Civil Engineering Department, Tunceli, Türkiye

4. 1. Introduction

The mainshocks of February 6, 2023 M_W=7.7 Kahramanmaraş -Pazarcik and M_W=7.6 Elbistan earthquakes and their aftershock sequences were recorded in a large region by the strong motion stations operated by AFAD (Disaster and Emergency Presidency of Türkiye). The recordings and station metadata are disseminated through AFAD's website, soon after both earthquakes (1st event at https://tadas.afad.gov.tr/event-detail/15499 and 2nd event at https://tadas.afad.gov.tr/event-detail/15512, last accessed on February 12, 2023). The reconnaissance team downloaded the raw strong motion data immediately after they were available. However, sharing the responsibility of providing accurate data sets to the scientific and earthquake engineering community, updates in data by AFAD's personnel are being carefully monitored and changes have been implemented in this report as much as possible. It is clear that these recordings are currently evaluated by AFAD and improvements in data quality are expected in near future. The locations of strong ground motion stations in Türkiye are shown in Figure 4.1.

Figure 4.1. The locations of strong ground motion stations in Türkiye (AFAD-TADAS)

For this preliminary report, 292 and 268 three-component recordings from the first and second event, respectively, were compiled, analyzed for data quality, and processed as summarized in Section 4.2. Further assessments, including the analysis of spectral shapes and amplifications, comparisons with design envelopes and mean predictions of current ground motion models were performed by using data that passed the quality check. Therefore, this chapter aims to present only the current state of factual data on the strong motion characteristics of these very important events.

With this report, we state that we have no intention or authorization to disseminate the strong motion data that is owned by the national network.

Our objective is to offer several ground motion intensity measures (GMIMs) that may be used for the analysis of structural and geotechnical performance of structures during the February 6, 2023 earthquakes. Therefore, several amplitude and intensity parameters (peak accelerations, peak and cumulative absolute velocities, Arias and Housner intensities, etc.), significant duration, Fourier Amplitude and response spectrums for 5% damping are provided in this report. Important GMIMs are also disseminated through the Site Eye Software (https://siteeye.co). The metadata for stations, including the shear wave velocity profiles and the extended source-to-site distance metrics, are carefully evaluated with the current state of available information. As the geological reconnaissance efforts progress, the extent of rupture will be more accurately defined. This may change some of the initial interpretations given in this report, especially for the recordings collected from both ends of the rupture.

4. 2. Quality Control and Strong Motion Data Processing

The strong motion database used in this report mainly consists of data disseminated by the AFAD-TADAS website between February 6-10, 2023. However, some recordings were updated in the system on February 12-13, 2023, which were also utilized in this report. The “freezing date” for data compilation was set as February 13, 2023 to ensure timely publication of the report and any changes made after the freezing date were not implemented in the analyses.

4. 2. 1. Visual Checks on the Waveform Data

Collected (raw) waveforms underwent an initial visual screening to identify non-standard errors, as defined by Douglas (2003) and Boore and Bommer (2005). Since the rupture propagation of the first event was bilateral, with directions towards Kahramanmaraş in the northeast and Hatay in the southwest, most waveforms included multiple wave packets. The recorded time series initially included the wave packets from the northeast-oriented rupture of the Pazarcik segment, followed by the southwest-oriented rupture of the Amanos segment, which slightly overlapped with the first. The time lag between these multiple wave packets was sometimes visible, as shown in Figure 4.2(a), but varied significantly depending on the station location. Due to the difficulty of separating these wave packets in most stations without finite fault modelling (e.g., Figure 4.2b); we did not attempt to perform waveform analysis or eliminate these recordings from the database. However, we used the entire time history in the evaluation of ground motion intensity measures.

On the other hand, some recordings do not show a clear shape of a seismic waveform, as shown in Figure 4.3(c). These recordings were eliminated from the database during visual screening. Unfortunately, almost all recordings from the stations in Adıyaman province had an incomplete trace of the main event, as shown in Figure 4.3(a) and were excluded from the dataset for this report. We anticipate that AFAD may recompile these recordings from the equipment at a later stage. In addition to the multiple wave groups and incomplete trace problems, some recordings had significant noise content that standard processing could not eliminate (e.g., Figure 4.3b), while others had spikes or were disconnected during the event (e.g., Figure 4.3d). Many recordings had a combination of these problems and were also excluded from the dataset during visual processing.

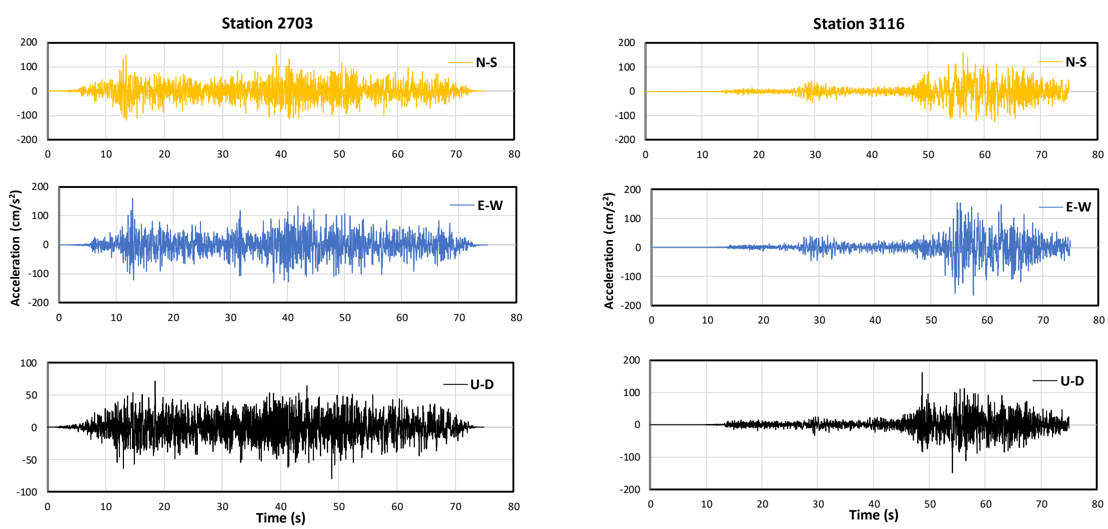

Figure 4.2. A sample acceleration-time history set from Stations ID# 2703 and 3116

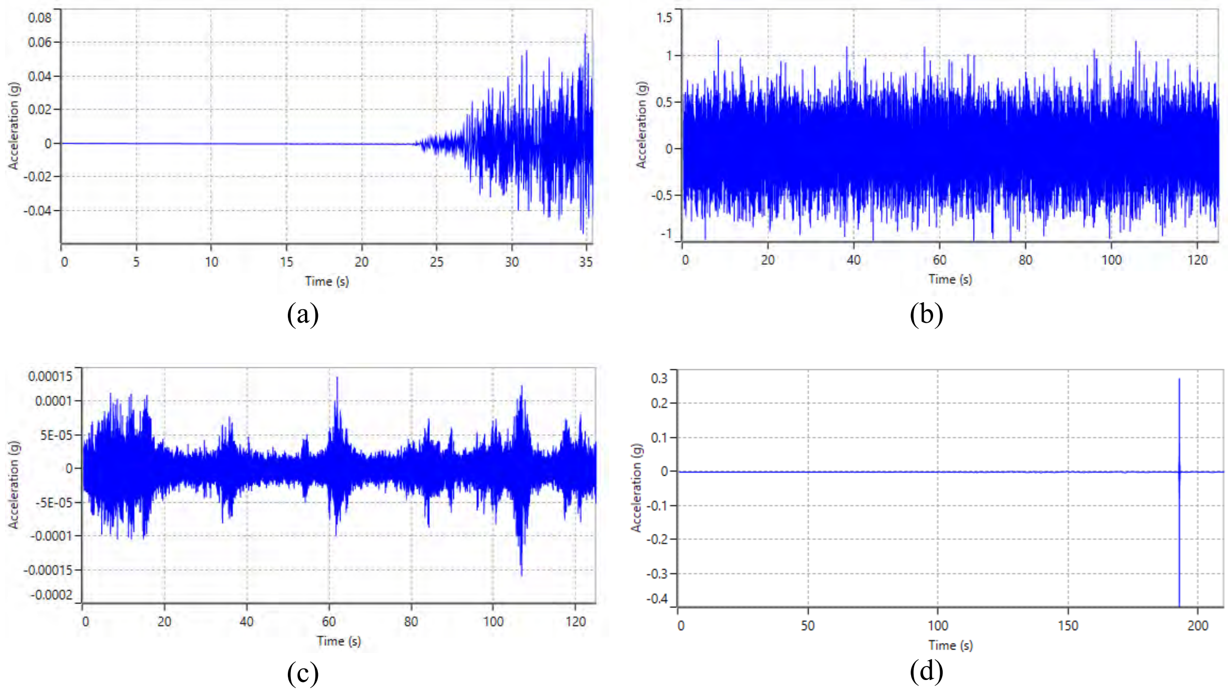

Figure 4.3. Samples for non-standard errors (a) incomplete trace, Station ID# 0210, (b) significant noise content, ID# 3117, (c) unclear trace of event, ID# 3113 and (d) spike, ID# 0719.

4. 2. 2. Data Processing

After the visual screening, the non-standard, error-free records were processed using the procedures defined in Akkar et al. (2014). First, the zero-ordered correction, which removes the mean acceleration value from the entire waveform, was applied. Next, the low- and high-filter cut-off frequencies were determined by visually inspecting the Fourier Amplitude Spectrum (FAS), velocity, and displacement time series of each waveform (Boore and Bommer, 2005; Douglas and Boore, 2011) as shown in Figure 4.4. An acausal 4-pole Butterworth band-pass filter was used to remove any phase distortion in the signal. Finally, the post processing procedure described in Boore et al. (2012) was used to remove zero pads during band-pass filtering. Most of the low-cut values chosen for the records are below the magnitude-dependent corner frequency of the theoretical source spectrum proposed by Atkinson and Silva (2000) to ensure that the low-frequency motions are retained in the waveforms.

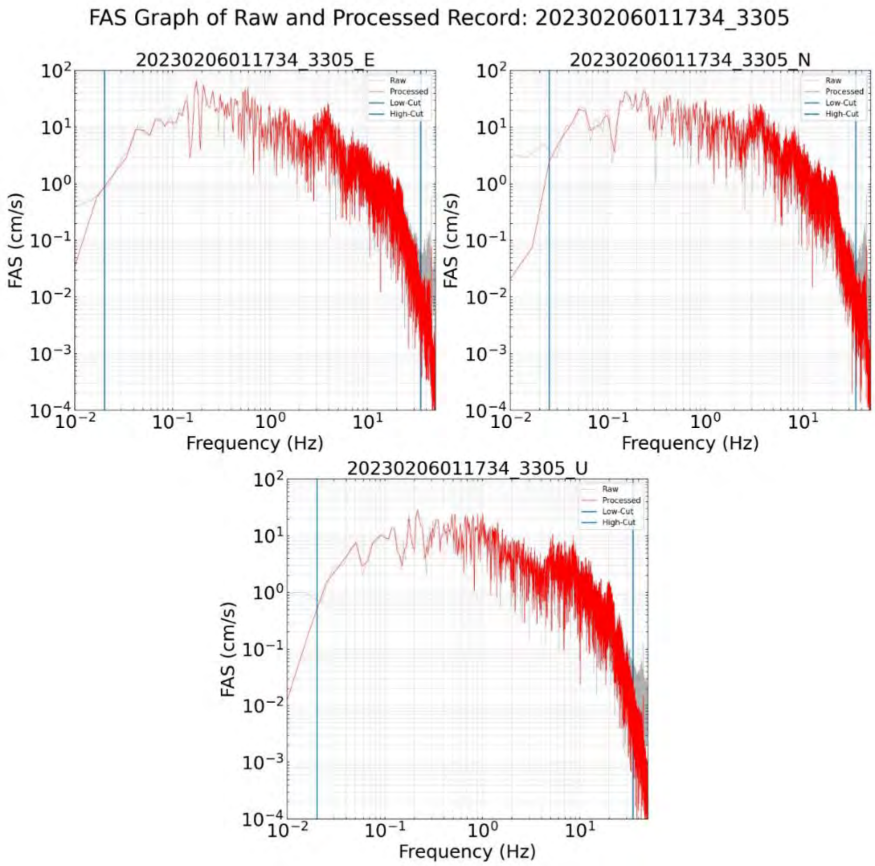

Figure 4.4. FAS of the raw and processed waveforms. The blue solid lines show the low- and high-cut filter frequencies.

4. 2. 3. Ground Motion Intensity Measures

Following visual quality control and data processing, 245 recordings from the first earthquake and 244 recordings from the second earthquake remained in the database. Figures 4.5(a) and (b) display the spatial distribution of these recordings for each event, respectively. Additionally, Figure 4.5 shows epicenters (represented by yellow stars) and the surface projections of the estimated rupture planes for each earthquake (for details, please refer to Chapter 3). The extended source-to-site-distance metrics, including rupture distance R_{RUP} and Joyner-Boore distance, R_{JB} were estimated using the procedure given in Kaklamanos et al. (2011) based on these tentative rupture plane parameters. It is worth noting that the depth to the top of the rupture (Z_{TOR}) is assumed to be zero since the rupture is clearly visible at the surface. The fault plane angles are provided in Chapter 3.

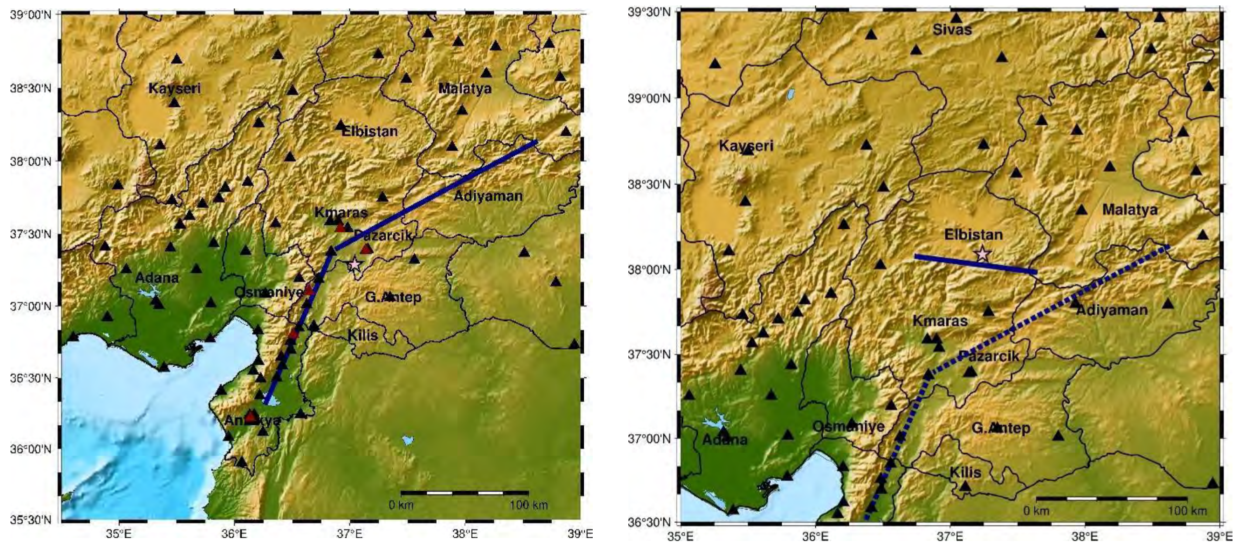

(a) (b)

Figure 4.5. Distribution of the strong motion stations that are located within 200km of the rupture plane for a) M_w=7.7 Kahramanmaraş -Pazarcik and b) M_w=7.6 Elbistan earthquakes.

For the first event, the V_{S30} (time-averaged shear wave velocity in the upper 30m) information is available for 185 stations. Geophysical methods (MASW and ReMi) were used to measure Vs at141 and 111 recording stations, respectively. Herein, the consistency of V_{S30} values available on AFAD-TADAS website was re-evaluated using site characterization reports. For 9 stations (Station ID: 125, 603, 3133, 3144, 4614, 4628, 5804, 6302, and 3113), the V_{S30} computed from Vs profile provided in the report (based on MASW) was adopted instead of the values given on the AFAD-TADAS website. For the remaining 44 stations, V_{S30} values in AFAD's database were estimated using the topographic slope proxy parameter, as site characterization reports were not available.

For the second earthquake, V_{S30} values were reported for 164 stations on the AFAD-TADAS website, with MASW and ReMi measurements available for 143 and 91 stations, respectively. A similar verification of V_{S30} values was performed, and the V_{S30} information from MASW measurements for 6 stations (Station ID: 603, 3144, 4614, 6302, 4628, and 5804) was adopted.

Figure 4.6 and 4.7 shows the R_{RUP} – V_{S30} distributions of the recordings from the first and second events, respectively. For both events, majority of the stations are located on sites with ZC class according to TBEC (2019). Please note that the site classification scheme of TBEC (2019) is quite similar to that of ASCE 7-19. The remaining stations are classified as ZD or ZB, and there are no stations with V_{S30} < 180 m/s (ZE). The number of near-fault stations (R_{RUP} < 10 km) is significant for the first earthquake but limited for the second earthquake. For both events, ~70% of the stations are located at rupture distances greater than 100 km.

Peak ground motion amplitudes, significant duration, and Arias as well as Housner intensity values of these recordings within R_{RUP}<100km are provided in Table 4.1 and 4.2. In these tables, PGA, and PGV are the peak ground acceleration and velocity, and CAV is the cumulative absolute velocity. The significant duration is calculated as the time between 5% and 95% of the cumulative Arias Intensity. Acceleration time histories, Fourier amplitude spectra and the 5%-damped acceleration response spectra of the recorded accelerations at these stations are provided in Appendix A and a few examples are provided in Figures 4.8 – 4.12 for further discussion. The 5%-damped acceleration response spectra in these figures are compared against the design spectra defined in the current seismic code of Turkey (TBEC, 2019) for 475- and 2475-year return periods.

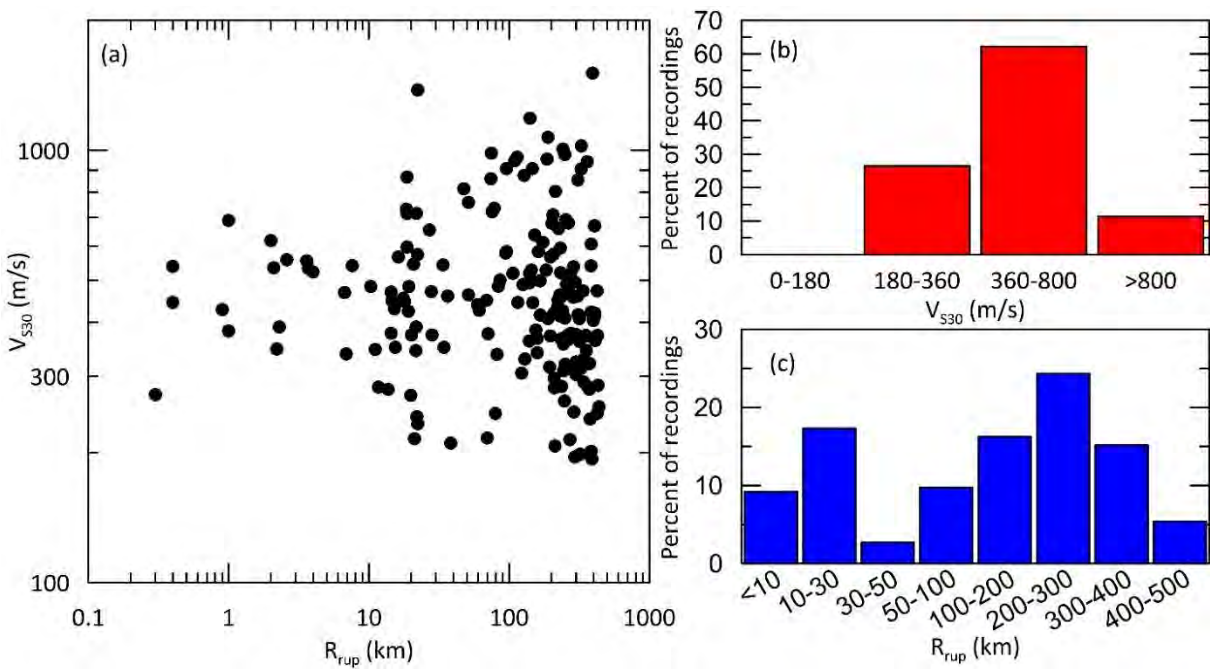

Figure 4.6. (a) R_{RUP} -V_{S30} distribution of the stations in the database, (b) percentage of recording stations in each site class defined in TBEC (2019), and (c) percentage of recording stations in each distance bin (Kahramanmaraş /Pazarcik earthquake with M_W=7.7).

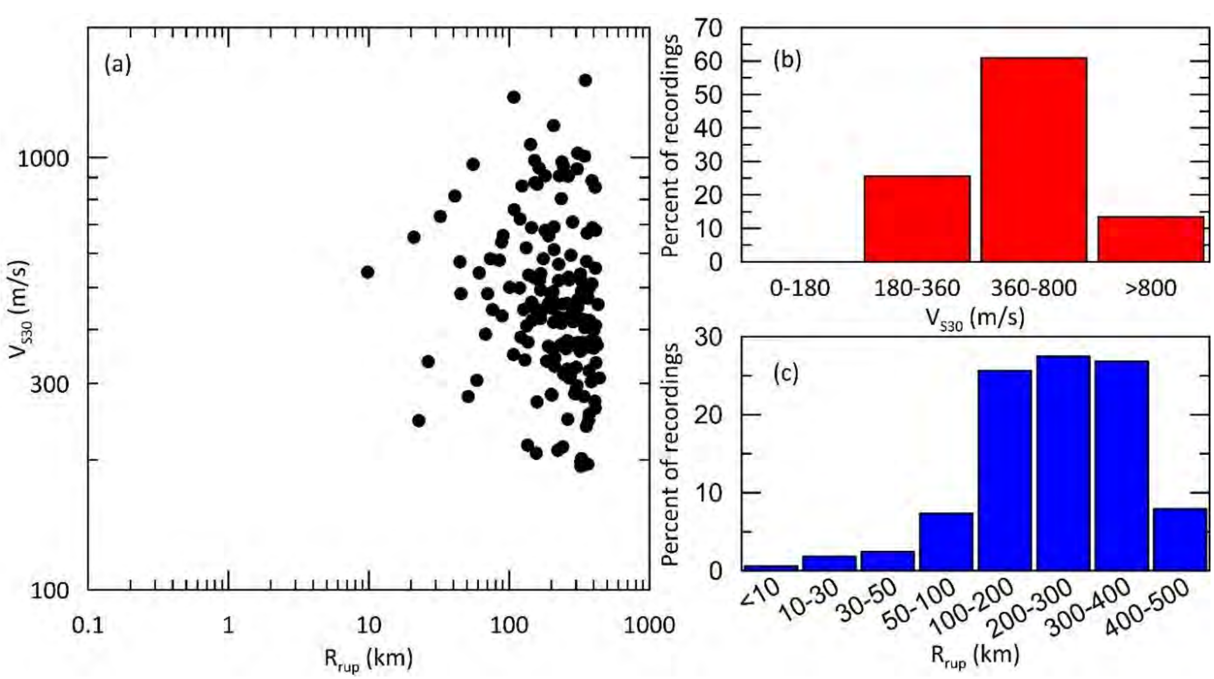

Figure 4.7. R_{RUP} -V_{S30} distribution of the stations in the database, (b) percentage of recording stations in each site class defined in TBEC (2019), and (c) percentage of recording stations in each distance bin (Elbistan earthquake with M_W=7.6).

Table 4.1 Information on Recorded Strong Ground Motions of Pazarcik earthquake for stations within 100 km rupture distance (unknown V_{S30}/Site Class values are shown with NA)

Station Code	City	District	Lat.	Long.	R_{rup}(km)	V_{S30} (m/s)	Site Class*	Comp.	PGA (cm/s^2)	PGV (cm/s)	Significant Duration (s)	Arias Intensity (cm/s)	Housner Intensity (cm)	Cumulative Absolute Velocity (cm/s)
119	Adana	Karataş	36.5680	35.3900	83.80	485	ZC	E-W	44.340	19.01	46.72	9.82	32.62	519.19
								N-S	42.835	8.48	58.2	6.51	20.73	442.90
								U-D	25.275	10.41	63.94	3.84	18.92	356.94
120	Adana	Yumurtalık	36.7701	35.7901	59.60	439	ZC	E-W	115.866	24.82	57.05	42.49	48.39	1034.78
								N-S	112.469	33.93	56.51	42.89	62.43	1051.25
								U-D	103.266	13.14	54.74	13.77	26.65	613.47
122	Adana	Kozan	37.4339	35.8202	86.10	501	ZC	E-W	52.378	8.32	52.43	15.09	20.16	666.06
								N-S	57.323	13.00	52.06	15.21	22.66	666.19
								U-D	33.184	8.94	51.44	4.73	17.19	368.11
125	Adana	Ceyhan	37.0152	35.7958	69.80	216	ZD	E-W	83.225	26.62	60.04	49.21	67.31	1216.86
								N-S	128.556	33.14	60.51	71.87	91.53	1377.95
								U-D	35.141	8.99	60.69	8.70	29.78	536.04
127	Adana	Feke	37.8162	35.9204	95.80	583	ZC	E-W	50.876	4.50	45.5	14.82	15.09	632.92
								N-S	55.088	8.21	41.62	12.79	18.90	550.08
								U-D	39.237	7.51	44.94	4.63	15.62	351.01
130	Adana	İmamoğlu	37.2519	35.6710	90.30	NA	NA	E-W	68.272	14.40	61.76	20.72	43.12	796.49
								N-S	81.197	17.33	55.05	25.44	53.69	856.36
								U-D	35.334	8.28	62.99	7.89	25.56	524.20
131	Adana	Saimbeyli	37.8566	36.1153	84.70	NA	NA	E-W	159.420	6.73	41.93	74.79	12.87	1360.83
								N-S	146.618	7.06	42.53	75.98	15.64	1383.10
								U-D	50.274	7.42	45.19	8.38	13.12	477.19
132	Adana	Saimbeyli	37.8559	36.1149	84.70	NA	NA	E-W	32.476	4.68	47.92	5.27	14.02	382.34
								N-S	37.774	6.05	46.47	6.90	15.19	433.59
								U-D	29.678	7.54	47.95	4.37	14.15	345.90
133	Adana	Feke	37.7455	35.8640	96.30	NA	NA	E-W	74.206	5.60	43.11	17.22	19.40	661.44
								N-S	77.882	6.88	44.02	10.91	21.21	517.13
								U-D	39.694	7.39	44.8	4.41	16.05	341.86
134	Adana	Feke	37.7443	35.8645	96.20	NA	NA	E-W	45.842	5.89	46.98	6.81	15.98	429.43
								N-S	68.712	7.32	42.35	12.43	21.72	555.86
								U-D	38.623	7.20	46	4.23	15.81	336.96

Station Code	City	District	Lat.	Long.	R_{rup}(km)	V_{S30} (m/s)	Site Class*	Comp.	PGA (cm/s^2)	PGV (cm/s)	Significant Duration (s)	Arias Intensity (cm/s)	Housner Intensity (cm)	Cumulative Absolute Velocity (cm/s)
2104	Diyarbakır	Ergani	38.2644	39.7590	99.70	NA	NA	E-W	88.006	13.13	46.3	17.75	66.55	694.58
								N-S	62.542	22.13	59.86	13.24	44.82	649.38
								U-D	42.838	8.70	72.97	6.72	28.38	500.67
2107	Diyarbakır	Çermik	38.1459	39.4838	74.70	NA	NA	E-W	112.283	16.51	43.8	28.72	66.62	858.16
								N-S	74.733	28.24	49.25	26.07	50.27	859.21
								U-D	44.231	7.88	56.72	8.13	32.05	489.21
2302	Elazığ	Maden	38.3923	39.6754	95.60	907	ZB	E-W	219.562	14.59	11.75	24.51	32.80	505.08
								N-S	197.116	14.05	13.23	20.65	24.32	491.13
								U-D	109.449	7.30	24.07	8.56	21.99	394.05
2308	Elazığ	Sivrice	38.4506	39.3102	68.90	450	ZC	E-W	163.792	29.35	37.31	35.35	98.63	808.03
								N-S	322.464	38.52	21.17	59.69	114.56	907.76
								U-D	400.053	11.53	10.14	39.50	32.90	600.52
2309	Elazığ	Keban	38.7991	38.7273	74.20	860	ZB	E-W	35.257	8.40	34.11	3.61	19.33	284.03
								N-S	36.858	6.67	40.39	4.19	14.58	326.56
								U-D	25.505	7.00	44.52	2.44	20.71	244.77
2310	Elazığ	Baskil	38.5727	38.8245	51.40	NA	NA	E-W	51.169	8.08	29.485	8.84	22.56	427.23
								N-S	60.480	14.85	22.055	10.56	33.19	443.03
								U-D	48.889	7.86	30.11	3.84	21.35	289.21
2703	Gaziantep	Şahinbey	37.0580	37.3500	51.40	758	ZC	E-W	160.131	16.67	53.08	120.01	49.54	1692.03
								N-S	150.388	13.32	52.5	114.58	43.44	1672.19
								U-D	80.294	8.02	52.08	31.18	29.32	882.75
2708	Gaziantep	İslahiye	37.0993	36.6484	4.00	523	ZC	E-W	1089.439	144.37	37.32	1154.32	488.24	3813.58
								N-S	812.734	126.86	39.91	963.64	361.96	3767.00
								U-D	977.012	55.92	20.57	439.64	149.64	2146.77
2711	Gaziantep	Yavuzeli	37.3174	37.5604	35.20	NA	NA	E-W	97.302	17.48	51.76	62.69	36.67	1251.38
								N-S	107.008	17.03	51.99	66.85	45.07	1270.04
								U-D	61.580	9.73	50.82	24.64	30.40	791.01
2712	Gaziantep	Nurdağı	37.1840	36.7328	1.00	NA	NA	E-W	602.742	110.46	33.96	744.30	332.38	3020.43
								N-S	555.436	83.02	36.7	628.04	197.28	2916.20
								U-D	343.814	26.90	38.09	237.04	97.04	1799.69

Station Code	City	District	Lat.	Long.	R_{rup}(km)	V_{S30} (m/s)	Site Class*	Comp.	PGA (cm/s^2)	PGV (cm/s)	Significant Duration (s)	Arias Intensity (cm/s)	Housner Intensity (cm)	Cumulative Absolute Velocity (cm/s)
2715	Gaziantep	İslahiye	36.8554	36.6856	9.80	NA	NA	E-W	340.021	55.52	46.99	132.07	82.08	1527.35
								N-S	457.193	36.99	45.29	110.24	66.06	1364.71
								U-D	76.072	13.61	49.12	14.02	44.61	533.71
2716	Gaziantep	İslahiye	36.8564	36.6883	10.00	NA	NA	E-W	228.890	55.57	48.72	232.49	147.00	2145.88
								N-S	255.463	60.13	49.91	266.12	142.58	2318.36
								U-D	164.684	17.00	50.73	100.29	54.05	1502.64
2717	Gaziantep	İslahiye	36.8555	36.6910	10.30	NA	NA	E-W	117.462	53.05	44.41	38.46	90.55	768.68
								N-S	138.367	32.96	49.92	29.18	58.59	703.65
								U-D	80.703	14.54	49.24	17.16	47.21	568.71
2718	Gaziantep	İslahiye	37.0078	36.6266	1.70	NA	NA	E-W	643.745	119.42	20.7	439.19	255.31	2229.45
								N-S	702.091	80.05	13.49	436.39	206.49	2125.73
								U-D	584.255	62.79	20.84	227.50	171.93	1564.41
3115	Hatay	Belen	36.5463	36.1646	19.10	424	ZC	E-W	211.134	50.82	37.52	172.62	153.67	1971.07
								N-S	274.824	42.12	29.65	321.62	166.45	2534.31
								U-D	214.353	20.58	30.79	114.75	78.51	1591.15
3116	Hatay	İskenderun	36.6162	36.2066	18.70	868	ZB	E-W	165.557	37.02	33.34	85.09	84.52	1216.03
								N-S	160.424	43.16	31.95	79.14	89.72	1227.89
								U-D	162.787	19.99	28.82	45.33	46.49	928.49
3123	Hatay	Antakya	36.2142	36.1597	14.40	470	ZC	E-W	594.043	101.98	17.68	754.41	401.08	3208.75
								N-S	655.302	188.44	13.58	935.11	579.51	3433.49
								U-D	868.061	52.67	14.09	487.14	215.76	2416.68
3124	Hatay	Antakya	36.2387	36.1722	11.70	283	ZD	E-W	637.793	101.28	18.86	776.20	391.19	3376.79
								N-S	572.431	113.10	21.39	622.95	444.00	3148.01
								U-D	577.756	42.70	17.08	317.40	144.70	1945.50
3125	Hatay	Antakya	36.2381	36.1326	14.60	448	ZC	E-W	1123.242	108.87	16.65	779.44	279.41	3057.58
								N-S	823.509	75.69	17.38	663.81	234.87	2956.75
								U-D	1136.121	65.49	9.74	823.35	144.35	2705.33
3126	Hatay	Antakya	36.2202	36.1375	15.40	350	ZD	E-W	1028.770	93.15	25.21	1134.59	274.03	4204.90
								N-S	1210.189	110.34	19.98	2096.96	380.30	5349.18
								U-D	1070.168	78.84	9.73	1288.69	207.89	3406.55

Station Code	City	District	Lat.	Long.	R_{rup}(km)	V_{S30} (m/s)	Site Class*	Comp.	PGA (cm/s^2)	PGV (cm/s)	Significant Duration (s)	Arias Intensity (cm/s)	Housner Intensity (cm)	Cumulative Absolute Velocity (cm/s)
3129	Hatay	Defne	36.1912	36.1343	17.90	447	ZC	E-W	1199.782	75.59	14.93	1829.59	286.96	4148.83
								N-S	1367.690	170.73	10.72	2501.64	545.19	4712.24
								U-D	826.167	43.85	10.22	705.19	165.12	2536.52
3131	Hatay	Antakya	36.1912	36.1633	16.20	567	ZC	E-W	339.689	44.24	8.98	164.62	222.30	1190.85
								N-S	349.297	51.49	9.06	127.52	168.36	974.83
								U-D	144.616	19.15	13.86	33.61	83.30	591.49
3132	Hatay	Antakya	36.2067	36.1716	14.40	377	ZC	E-W	514.114	53.85	17.58	439.50	221.47	2407.39
								N-S	515.074	67.69	13.52	372.47	294.44	2210.57
								U-D	353.840	34.28	13.64	193.77	154.21	1528.61
3133	Hatay	Reyhanlı	36.2432	36.5736	27.90	471	ZC	E-W	142.749	24.56	51.43	59.88	85.89	1215.67
								N-S	219.023	29.20	42.56	91.09	129.74	1387.28
								U-D	86.844	15.51	52.89	27.99	34.06	894.20
3134	Hatay	Dörtyol	36.8276	36.2049	28.20	374	ZC	E-W	203.742	41.95	45.6	127.59	108.57	1656.12
								N-S	245.988	40.58	45.58	143.25	136.27	1742.43
								U-D	140.627	19.87	43.68	57.74	46.07	1152.38
3135	Hatay	Arsuz	36.4089	35.8831	36.40	460	ZC	E-W	1367.456	66.09	22.78	688.44	232.35	2898.33
								N-S	741.091	51.94	23.33	558.60	183.14	2696.45
								U-D	589.311	37.45	25.25	244.53	95.77	1913.14
3136	Hatay	Altınözü	36.1159	36.2472	21.60	344	ZD	E-W	394.823	56.98	32.73	361.28	152.23	2619.67
								N-S	533.957	53.85	27.45	398.90	212.21	2604.43
								U-D	220.511	30.09	30.39	114.82	100.36	1469.17
3137	Hatay	Hassa	36.6929	36.4885	1.00	688	ZC	E-W	842.924	77.21	16.25	371.12	227.93	2183.54
								N-S	451.834	78.15	16.71	363.89	208.80	2239.28
								U-D	498.957	40.10	16.66	231.53	132.42	1760.51
3138	Hatay	Hassa	36.8026	36.5112	2.00	618	ZC	E-W	746.680	216.85	11.76	600.51	508.34	2281.25
								N-S	888.978	135.31	15.18	789.88	479.04	2596.21
								U-D	1068.095	83.22	4.99	325.55	331.92	1410.33
3139	Hatay	Kırıkhan	36.5838	36.4144	0.30	272	ZD	E-W	504.504	150.09	28.21	702.16	462.69	3216.46
								N-S	576.865	156.95	36.86	865.65	499.45	3675.59
								U-D	378.286	54.27	14.98	310.28	218.17	2078.78

Station Code	City	District	Lat.	Long.	R_{rup}(km)	V_{S30} (m/s)	Site Class*	Comp.	PGA (cm/s^2)	PGV (cm/s)	Significant Duration (s)	Arias Intensity (cm/s)	Housner Intensity (cm)	Cumulative Absolute Velocity (cm/s)
3140	Hatay	Samandağ	36.0816	35.9498	38.30	210	ZD	E-W	218.637	81.35	37.12	203.96	199.22	2117.51
								N-S	194.597	64.15	33.09	228.03	231.90	2174.74
								U-D	176.663	30.02	36.1	86.03	132.72	1381.62
3141	Hatay	Antakya	36.3726	36.2197	6.90	338	ZD	E-W	852.265	124.52	13.24	1535.79	409.43	4356.39
								N-S	944.346	83.15	16.02	1348.14	294.33	4356.39
								U-D	618.780	43.22	13.92	631.82	148.17	2808.10
3142	Hatay	Kırıkhan	36.4980	36.3661	0.40	539	ZC	E-W	746.416	76.48	12.01	606.18	208.40	2614.65
								N-S	647.205	87.84	11.65	568.60	214.84	2466.31
								U-D	503.662	30.59	12.97	224.09	74.89	1630.69
3143	Hatay	Hassa	36.8489	36.5571	0.40	445	ZC	E-W	351.295	106.44	26.4	252.12	253.16	1907.24
								N-S	381.318	129.53	23.32	273.54	272.79	1852.69
								U-D	411.649	28.96	18.2	171.59	107.58	1479.06
3144	Hatay	Hassa	36.7569	36.4857	2.10	535	ZC	E-W	763.724	138.98	39.83	386.29	250.32	2532.92
								N-S	611.555	138.07	31.9	356.72	271.92	2157.42
								U-D	452.311	80.17	15.92	138.31	235.81	1249.10
3145	Hatay	Kırıkhan	36.6454	36.4064	3.70	533	ZC	E-W	696.562	157.69	11.14	657.04	398.21	2350.18
								N-S	599.876	116.51	13.68	386.67	235.53	2053.54
								U-D	660.538	64.79	10.59	315.71	233.36	1713.35
3146	Hatay	Belen	36.4908	36.2270	11.50	NA	NA	E-W	346.000	54.23	17.68	330.91	117.21	1780.37
								N-S	481.686	39.20	15.83	494.37	124.40	2140.70
								U-D	340.118	19.07	18.91	205.62	73.36	1439.78
3147	Hatay	Yayladağı	35.9024	36.0644	48.80	NA	NA	E-W	47.500	27.15	34.59	8.28	42.59	439.66
								N-S	56.468	14.90	55.08	7.33	37.06	427.90
								U-D	29.130	8.12	43.22	4.15	28.59	324.59
4404	Malatya	Pütürge	38.1959	38.8739	22.30	1380	ZB	E-W	136.236	15.11	21.99	19.53	39.40	561.83
								N-S	135.323	21.21	21.29	20.68	42.58	580.56
								U-D	95.803	10.62	29.06	9.47	34.42	425.68
4405	Malatya	Hekimhan	38.8107	37.9396	94.50	579	ZC	E-W	126.383	15.88	21.91	19.27	26.12	537.06
								N-S	90.736	8.27	26.79	13.63	24.49	498.48
								U-D	77.207	7.55	26.47	9.81	26.90	424.74

Station Code	City	District	Lat.	Long.	Rrup(km)	Vs30 (m/s)	Site Class*	Comp.	PGA (cm/s^2)	PGV (cm/s)	Significant Duration (s)	Arias Intensity (cm/s)	Housner Intensity (cm)	Cumulative Absolute Velocity (cm/s)
4406	Malatya	Akçadağ	38.3439	37.9738	47.50	815	ZB	E-W	131.322	29.17	40.21	33.07	75.67	827.57
								N-S	108.849	14.16	46.01	24.16	36.53	757.00
								U-D	49.838	12.31	45.8	11.43	35.80	528.86
4407	Malatya	Arguvan	38.7807	38.2641	78.40	735	ZC	E-W	33.083	8.41	57.45	6.63	32.83	452.77
								N-S	43.351	13.41	52.11	8.31	34.17	494.37
								U-D	19.328	7.06	53.29	2.68	21.35	284.76
4408	Malatya	Doğanşehir	38.0962	37.8873	27.00	654	ZC	E-W	137.188	35.73	25.96	43.45	74.74	834.86
								N-S	100.331	24.95	28.43	23.98	46.41	665.23
								U-D	96.811	22.86	26.66	23.03	64.05	632.99
4409	Malatya	Darende	38.5606	37.4908	88.90	NA	NA	E-W	28.488	10.01	55.96	3.54	15.39	328.41
								N-S	38.057	7.34	51.24	4.71	19.69	365.29
								U-D	27.983	6.97	52.32	2.97	18.09	293.85
4412	Malatya	Yazıhan	38.5969	38.1839	63.50	NA	NA	E-W	68.867	48.20	50.09	45.56	71.11	1141.01
								N-S	63.657	27.18	45.2	31.35	68.41	970.82
								U-D	55.550	27.27	53.73	25.02	51.08	893.72
4611	Kahramanmaraş	Çağlayancerit	37.7472	37.2843	18.50	731	ZC	E-W	320.401	40.08	43.62	267.64	118.32	2349.00
								N-S	349.470	42.52	42.58	281.65	117.18	2371.06
								U-D	173.891	15.69	45.71	83.16	50.23	1331.88
4612	Kahramanmaraş	Göksun	38.0240	36.4819	79.70	246	ZD	E-W	122.210	14.90	55.12	127.63	65.19	1999.99
								N-S	140.979	20.54	56.74	102.01	59.11	1801.96
								U-D	54.192	5.24	57.98	20.14	18.80	808.91
4613	Kahramanmaraş	Andırın	37.5701	36.3574	48.80	NA	NA	E-W	153.576	10.87	40.18	63.02	28.89	1183.87
								N-S	146.858	15.80	41.11	50.95	27.48	1079.53
								U-D	75.032	14.33	42.27	21.59	17.23	710.82
4615	Kahramanmaraş	Pazarcık	37.3868	37.1380	10.30	484	ZC	E-W	581.134	131.96	47.1	605.26	314.76	3263.48
								N-S	583.931	152.43	46.65	584.93	247.03	3188.66
								U-D	664.518	77.88	35.66	305.41	159.44	2106.71
4616	Kahramanmaraş	Türkoğlu	37.3755	36.8384	2.30	390	ZC	E-W	505.824	87.46	41.03	387.30	202.84	2544.91
								N-S	615.281	97.90	41.8	658.17	224.19	3200.42
								U-D	398.751	25.86	39	226.83	72.11	1881.56

Station Code	City	District	Lat.	Long.	R_{rup}(km)	V_{S30} (m/s)	Site Class*	Comp.	PGA (cm/s^2)	PGV (cm/s)	Significant Duration (s)	Arias Intensity (cm/s)	Housner Intensity (cm)	Cumulative Absolute Velocity (cm/s)
4617	Kahramanmaraş	Onikişubat	37.5855	36.8303	22.20	574	ZC	E-W	114.831	28.24	44.49	57.19	72.96	1136.16
								N-S	145.430	29.44	44.33	74.46	83.33	1221.48
								U-D	110.736	20.70	45.61	47.88	48.26	1039.63
4620	Kahramanmaraş	Onikişubat	37.5857	36.8985	19.30	484	ZC	E-W	320.589	38.65	44.77	262.99	84.29	2259.75
								N-S	300.302	32.80	42.41	233.33	77.20	2070.83
								U-D	185.071	15.93	46.18	116.64	51.40	1552.32
4624	Kahramanmaraş	Onikişubat	37.5361	36.9177	13.70	280	ZD	E-W	319.801	62.40	45.84	437.35	201.39	2960.10
								N-S	357.389	60.48	45.96	389.34	199.05	2739.93
								U-D	161.694	35.76	43.39	112.44	82.91	1522.63
4625	Kahramanmaraş	Dulkadiroğlu	37.5387	36.9819	11.10	346	ZD	E-W	484.376	67.12	41.52	468.82	179.44	2815.40
								N-S	448.106	79.80	38.15	429.77	225.64	2702.33
								U-D	367.233	28.98	31.82	233.97	93.09	1989.10
4628	Kahramanmaraş	Afşin	38.2412	36.9228	81.90	337	ZD	E-W	82.565	11.91	58.19	56.67	28.65	1334.30
								N-S	91.116	9.74	55.09	44.83	22.60	1176.45
								U-D	55.744	4.10	57.43	10.22	11.99	548.17
6303	Şanlıurfa	Siverek	37.7524	39.3291	74.70	986	ZB	E-W	114.461	21.71	35.04	20.09	67.92	658.33
								N-S	117.418	17.11	40.51	17.22	56.21	610.16
								U-D	38.915	10.44	67.83	8.48	26.27	561.84
6304	Şanlıurfa	Bozova	37.3651	38.5132	70.70	376	ZC	E-W	237.995	16.55	46.29	181.45	54.76	2187.95
								N-S	210.759	21.30	44.07	152.30	63.06	1962.59
								U-D	89.436	11.23	53.65	34.88	23.26	1018.96
8002	Osmaniye	Bahçe	37.1916	36.5620	15.20	430	ZC	E-W	202.594	41.44	41.48	126.09	79.36	1558.71
								N-S	242.513	45.00	36.08	241.39	142.78	2089.51
								U-D	335.052	18.41	33.78	167.12	61.90	1669.63
8003	Osmaniye	Osmaniye Merkez	37.0842	36.2694	34.20	350	ZD	E-W	185.872	28.60	39.62	115.09	102.30	1587.76
								N-S	141.600	31.33	38.88	91.13	113.60	1363.10
								U-D	139.941	19.59	41.22	63.66	65.90	1159.75
8004	Osmaniye	Kadirli	37.3799	36.0976	61.20	426	ZC	E-W	178.978	22.00	44.16	96.90	70.54	1483.75
								N-S	168.388	19.05	41.88	80.42	58.55	1316.69
								U-D	71.815	12.04	51.62	18.86	36.19	718.60
NAR	Kahramanmaraş	Pazarcık	37.3919	37.1574	10.70	NA	NA	E-W	613.878	104.40	40.77	366.97	223.00	2494.04
								N-S	765.851	90.45	38.49	393.03	212.27	2484.29
								U-D	482.223	46.27	33.81	230.63	108.15	1868.44

*Site classes are given according to the site classification of the 2019 edition of earthquake code in Türkiye (TBEC, 2019).

Table 4.2 Information on Recorded Strong Ground Motions of Elbistan earthquake for stations within 100 km rupture distance (unknown V_{S30}/Site Class values are shown with NA)

Station Code	City	District	Lat.	Long.	R_{rup} (km)	V_{S30} (m/s)	Site Class*	Comp.	PGA (cm/s^2)	PGV (cm/s)	Significant Duration (s)	Arias Intensity (cm/s)	Housner Intensity (cm)	Cumulative Absolute Velocity (cm/s)
127	Adana	Feke	37.8162	35.9204	73.70	583	ZC	E-W	62.75	13.98	37.36	11.09	25.76	476.64
								N-S	56.07	16.16	39.62	8.04	21.29	406.54
								U-D	38.25	14.97	35.05	4.13	15.77	289.93
129	Adana	Tufanbeyli	38.2592	36.2109	55.40	965	ZB	E-W	172.34	15.85	23.97	33.59	24.02	700.45
								N-S	154.48	19.38	25.61	37.60	27.95	747.15
								U-D	85.49	14.49	28.42	13.35	22.38	455.09
131	Adana	Saimbeyli	37.8566	36.1153	56.00	NA	NA	E-W	331.27	27.35	16.16	91.60	26.80	1023.91
								N-S	397.23	27.44	14.21	120.83	31.20	1111.82
								U-D	83.37	18.65	23.30	11.38	26.20	415.91
132	Adana	Saimbeyli	37.8559	36.1149	56.10	NA	NA	E-W	59.45	14.02	31.21	5.12	17.08	305.73
								N-S	65.34	21.25	25.79	6.30	20.85	304.53
								U-D	53.67	17.42	26.92	6.45	26.08	318.86
133	Adana	Feke	37.7455	35.8640	80.80	NA	NA	E-W	80.24	18.23	33.42	13.07	23.24	491.70
								N-S	47.33	14.42	42.44	6.34	23.55	359.03
								U-D	36.93	13.14	42.31	3.77	16.75	282.31
134	Adana	Feke	37.7443	35.8645	80.80	NA	NA	E-W	46.53	18.86	38.42	6.13	22.36	343.00
								N-S	52.13	13.20	36.89	8.01	25.85	395.68
								U-D	35.49	13.83	41.51	3.49	17.00	271.08
138	Adana	Kozan	37.7049	35.7234	93.90	NA	NA	E-W	22.89	12.54	37.55	1.96	14.17	205.84
								N-S	25.02	12.56	40.50	1.61	13.98	185.09
								U-D	18.85	10.06	47.83	1.60	14.27	195.23
205	Adıyaman	Kahta	37.7918	38.6160	90.60	660	ZC	E-W	54.65	22.13	40.82	14.53	50.06	613.56
								N-S	44.88	16.00	47.30	12.16	48.73	579.42
								U-D	32.93	10.75	56.32	7.92	28.62	480.97
213	Adıyaman	Tut	37.7967	37.9296	39.90	NA	NA	E-W	126.66	24.00	29.76	79.91	102.01	1227.56
								N-S	121.24	26.68	30.35	73.64	83.89	1189.88
								U-D	71.36	9.93	31.81	18.33	30.87	594.91
3802	Kayseri	Sarız	38.4781	36.5036	59.00	305	ZD	E-W	220.92	27.65	47.84	111.97	138.82	1610.08
								N-S	196.54	25.73	44.60	122.52	113.17	1647.43
								U-D	121.64	12.59	57.00	44.66	63.26	1052.04

Station Code	City	District	Lat.	Long.	R_{rup} (km)	V_{S30} (m/s)	Site Class*	Comp.	PGA (cm/s^2)	PGV (cm/s)	Significant Duration (s)	Arias Intensity (cm/s)	Housner Intensity (cm)	Cumulative Absolute Velocity (cm/s)
3804	Kayseri	Pınarbaşı	38.7227	36.3779	88.30	637	ZC	E-W	37.97	6.62	34.96	3.52	19.88	252.56
								N-S	34.55	8.54	44.31	3.02	17.06	251.90
								U-D	27.89	4.81	45.80	2.13	13.48	220.64
4405	Malatya	Hekimhan	38.8107	37.9396	85.30	579	ZC	E-W	156.98	14.62	20.48	22.13	33.61	549.93
								N-S	152.09	7.96	20.30	22.85	34.37	571.37
								U-D	119.33	8.55	20.02	12.49	25.61	418.75
4406	Malatya	Akçadağ	38.3439	37.9738	41.00	815	ZB	E-W	410.95	36.95	17.42	287.52	97.76	1784.12
								N-S	472.03	22.36	18.37	326.12	94.34	1955.80
								U-D	315.16	19.11	16.98	144.70	62.52	1274.76
4409	Malatya	Darende	38.5606	37.4908	55.00	NA	NA	E-W	76.99	18.56	31.17	15.15	45.44	510.97
								N-S	72.04	9.19	27.40	15.17	33.30	511.09
								U-D	53.53	6.80	31.56	7.89	25.80	386.26
4410	Malatya	Kuluncak	38.8668	37.6790	87.70	NA	NA	E-W	127.27	17.64	25.61	25.78	48.18	659.64
								N-S	112.08	10.03	26.57	19.04	43.18	582.30
								U-D	54.04	5.36	31.38	7.03	24.49	382.82
4412	Malatya	Yazıhan	38.5969	38.1839	74.20	NA	NA	E-W	126.37	28.65	35.05	45.11	91.57	979.39
								N-S	158.97	39.50	35.32	50.21	101.56	1002.06
								U-D	79.91	29.18	52.34	37.08	63.22	1000.96
4611	Kahramanmaraş	Çağlayancerit	37.7472	37.2843	32.30	731	ZC	E-W	138.66	38.36	32.77	68.55	78.22	1080.46
								N-S	194.41	14.19	35.09	56.78	49.96	996.46
								U-D	69.66	11.35	35.43	14.90	30.36	532.72
4612	Kahramanmaraş	Göksun	38.0240	36.4819	22.70	246	ZD	E-W	523.19	75.57	25.33	317.38	314.81	1919.10
								N-S	635.48	174.05	20.01	417.35	410.67	2070.85
								U-D	367.81	55.89	9.99	89.83	129.34	875.16
4614	Kahramanmaraş	Pazarcık	37.4851	37.2978	61.30	541	ZC	E-W	203.92	34.77	33.63	51.91	33.49	952.45
								N-S	160.92	13.38	32.39	63.00	25.68	1081.29
								U-D	89.17	5.48	34.67	14.20	17.03	508.92
4615	Kahramanmaraş	Pazarcık	37.3868	37.1380	70.20	484	ZC	E-W	73.58	30.44	39.73	13.88	35.02	549.36
								N-S	44.44	10.99	39.04	8.73	20.99	426.76
								U-D	41.63	6.64	42.74	3.95	14.98	293.52

Station Code	City	District	Lat.	Long.	R_{rup} (km)	V_{S30} (m/s)	Site Class*	Comp.	PGA (cm/s^2)	PGV (cm/s)	Significant Duration (s)	Arias Intensity (cm/s)	Housner Intensity (cm)	Cumulative Absolute Velocity (cm/s)
4616	Kahramanmaraş	Türkoğlu	37.3755	36.8384	67.80	390	ZC	E-W	53.42	14.71	35.45	9.60	16.94	432.47
								N-S	57.55	10.69	37.61	11.35	16.67	479.10
								U-D	28.04	5.44	39.97	3.09	13.16	261.15
4617	Kahramanmaraş	Onikişubat	37.5855	36.8303	44.60	574	ZC	E-W	82.56	28.47	37.21	27.30	77.74	728.53
								N-S	55.90	23.46	39.76	19.15	60.60	642.67
								U-D	54.76	13.54	44.86	12.24	53.54	540.45
4620	Kahramanmaraş	Onikişubat	37.5857	36.8985	45.40	484	ZC	E-W	81.18	25.19	45.54	19.64	59.58	651.81
								N-S	66.83	21.99	37.52	15.83	50.54	583.58
								U-D	57.04	13.62	40.51	8.89	44.94	446.19
4624	Kahramanmaraş	Onikişubat	37.5361	36.9177	51.10	280	ZD	E-W	79.83	19.24	45.46	25.12	52.11	765.68
								N-S	65.03	18.78	42.96	26.06	65.10	770.11
								U-D	38.60	9.04	44.38	6.69	30.09	391.69
5807	Sivas	Gürün	38.7269	37.2475	76.10	445	ZC	E-W	71.85	17.86	33.78	17.60	47.48	571.91
								N-S	90.60	10.61	32.94	23.84	33.54	668.98
								U-D	41.84	7.43	39.05	9.11	29.98	444.45
8002	Osmaniye	Bahçe	37.1916	36.5620	89.00	430	ZC	E-W	45.52	18.16	36.32	6.51	23.88	387.75
								N-S	65.88	7.74	32.27	11.68	29.08	474.35
								U-D	28.81	6.81	47.19	4.02	16.28	317.22
NAR	Kahramanmaraş	Pazarcık	37.3919	37.1574	69.90	NA	NA	E-W	109.90	27.50	32.16	11.75	21.97	404.07
								N-S	126.47	8.65	28.54	9.79	17.30	362.86
								U-D	82.38	4.76	29.04	5.45	9.99	264.15

*Site classes are given according to the site classification of the 2019 edition of earthquake code in Türkiye (TBEC, 2019).

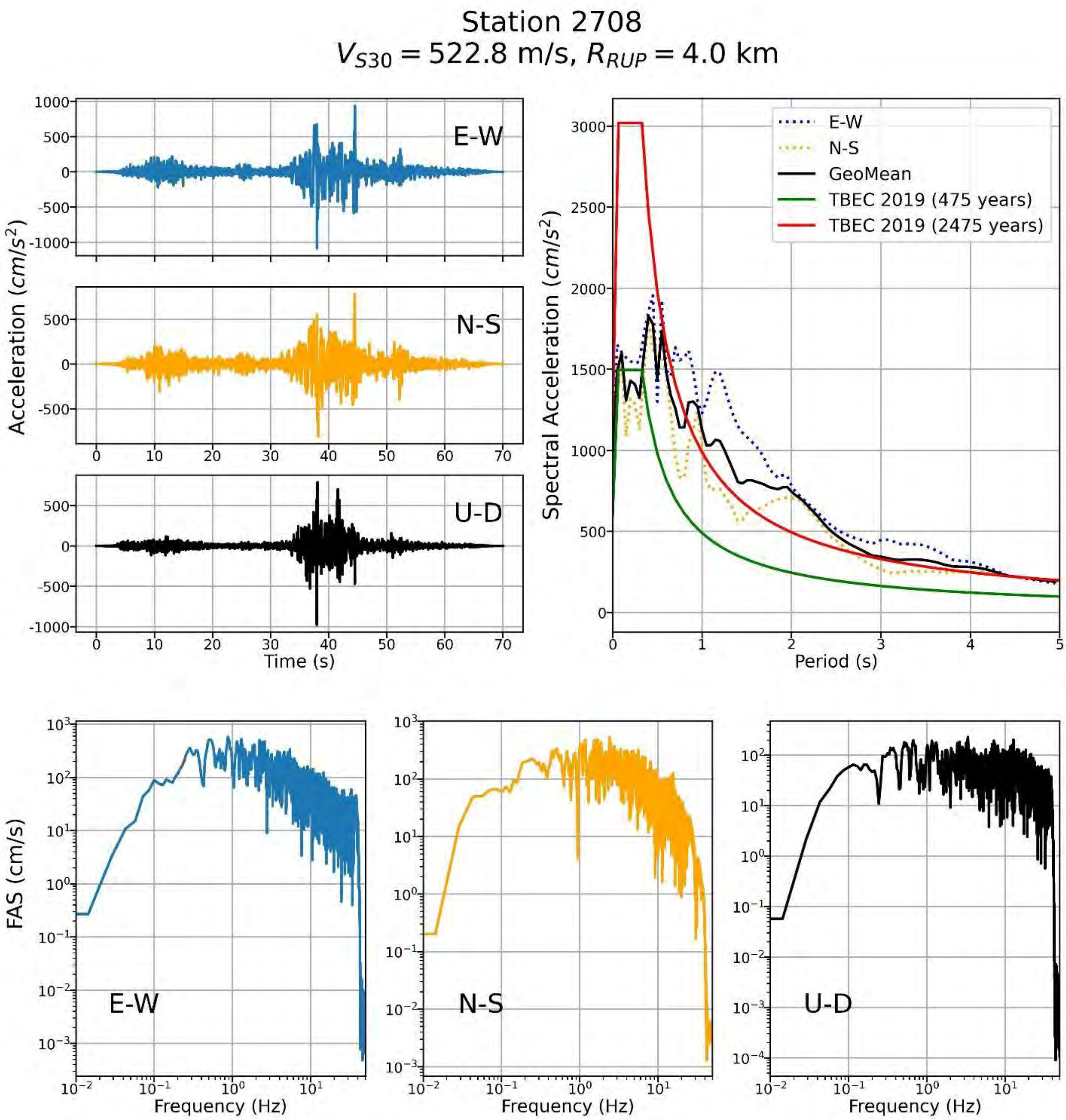

Figure 4.8. Recorded three-component ground accelerations, corresponding Fourier amplitude spectra (FAS) and response spectra (with 5% damping) in comparison with the most recent building code (TBEC, 2019) at selected station 2708 due to Pazarcik (Mw=7.7) event

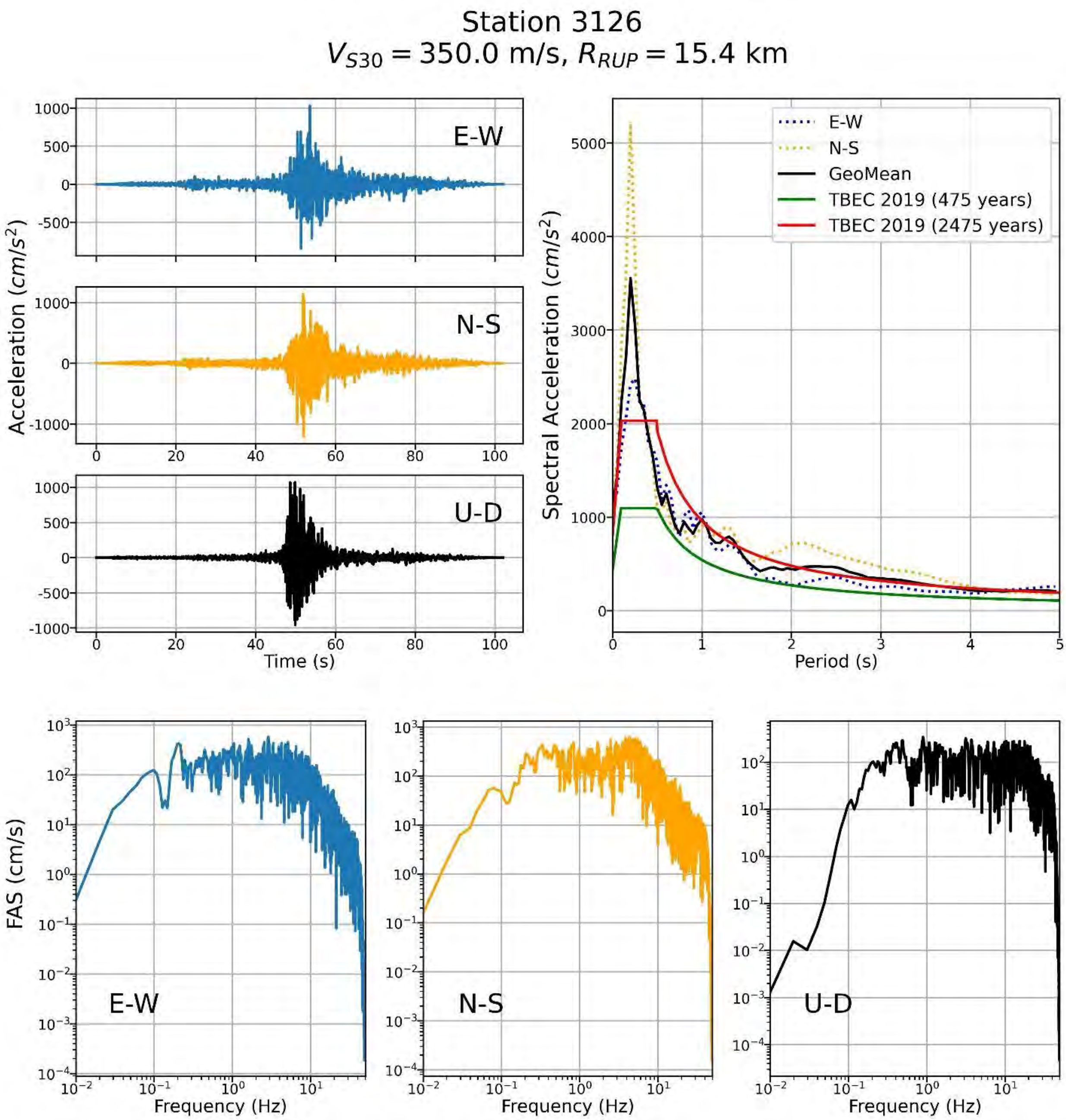

Figure 4.9. Recorded three-component ground accelerations, corresponding Fourier amplitude spectra (FAS) and response spectra (with 5% damping) in comparison with the most recent building code (TBEC, 2019) at selected station 3126 due to Pazarcik (Mw=7.7) event

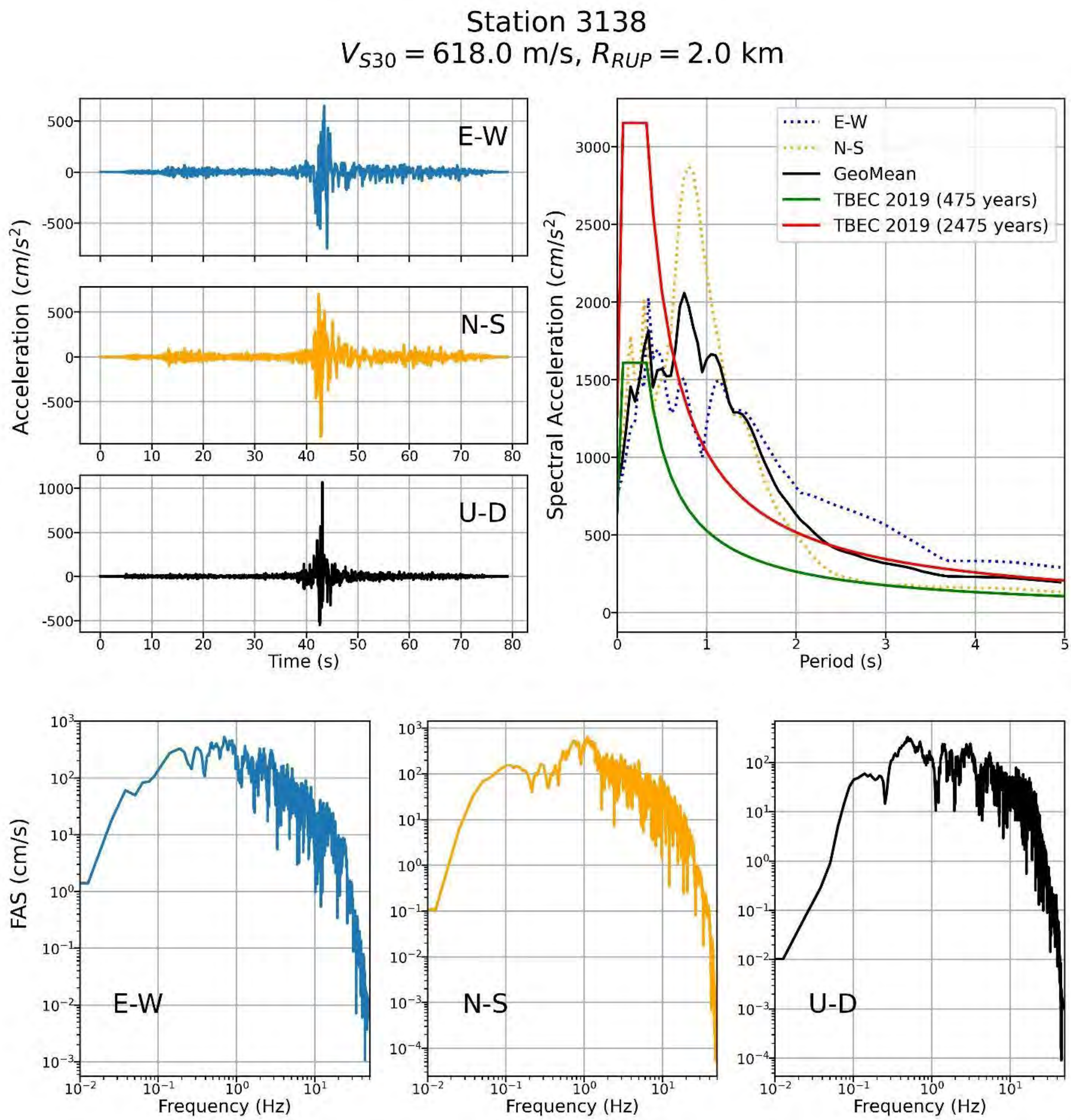

Figure 4.10. Recorded three-component ground accelerations, corresponding Fourier amplitude spectra (FAS) and response spectra (with 5% damping) in comparison with the most recent building code (TBEC, 2019) at selected station 3138 due to Pazarcik (Mw=7.7) event

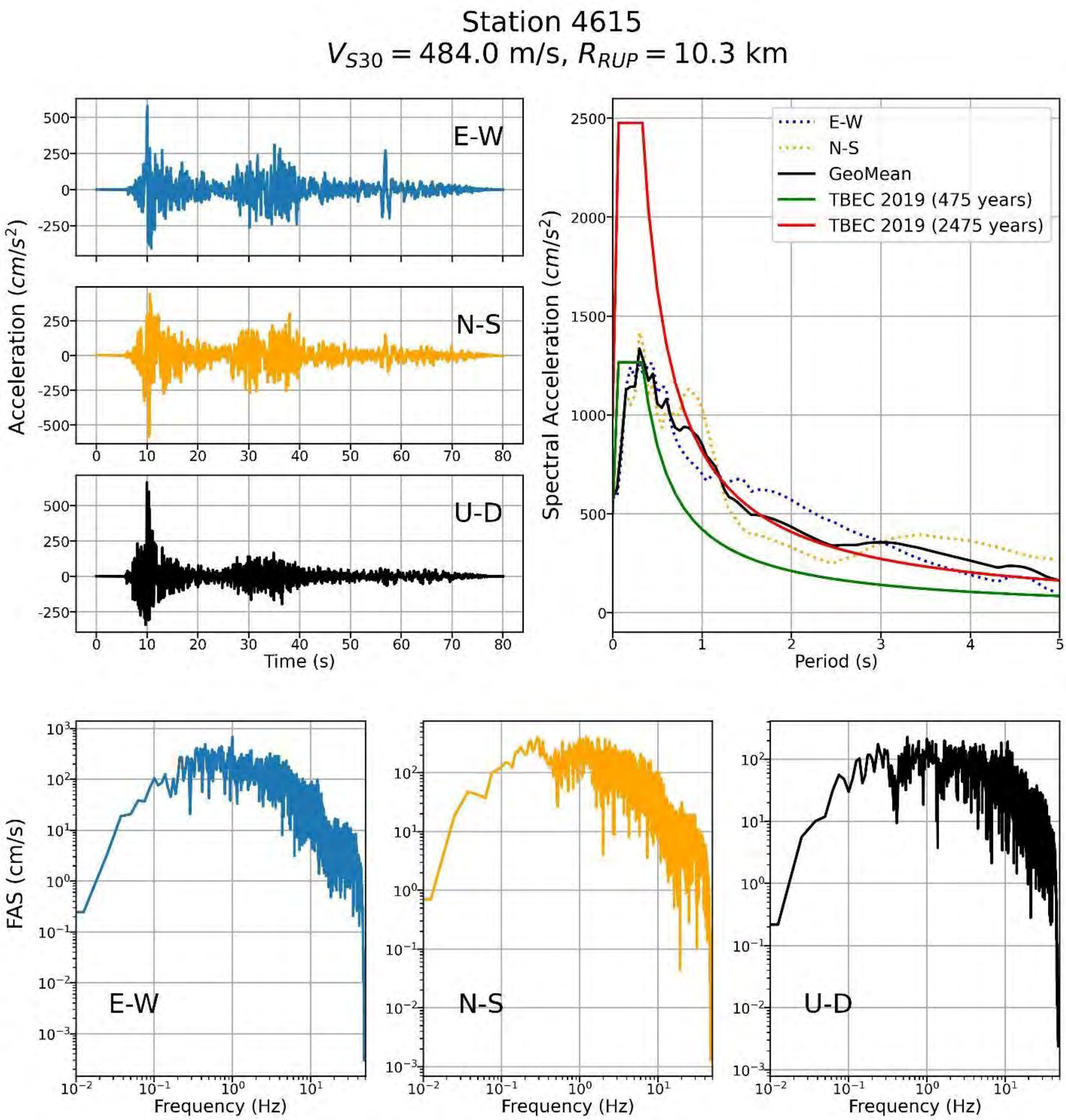

Figure 4.11. Recorded three-component ground accelerations, corresponding Fourier amplitude spectra (FAS) and response spectra (with 5% damping) in comparison with the most recent building code (TBEC, 2019) at selected station 4615 due to Pazarcik (Mw=7.7) event

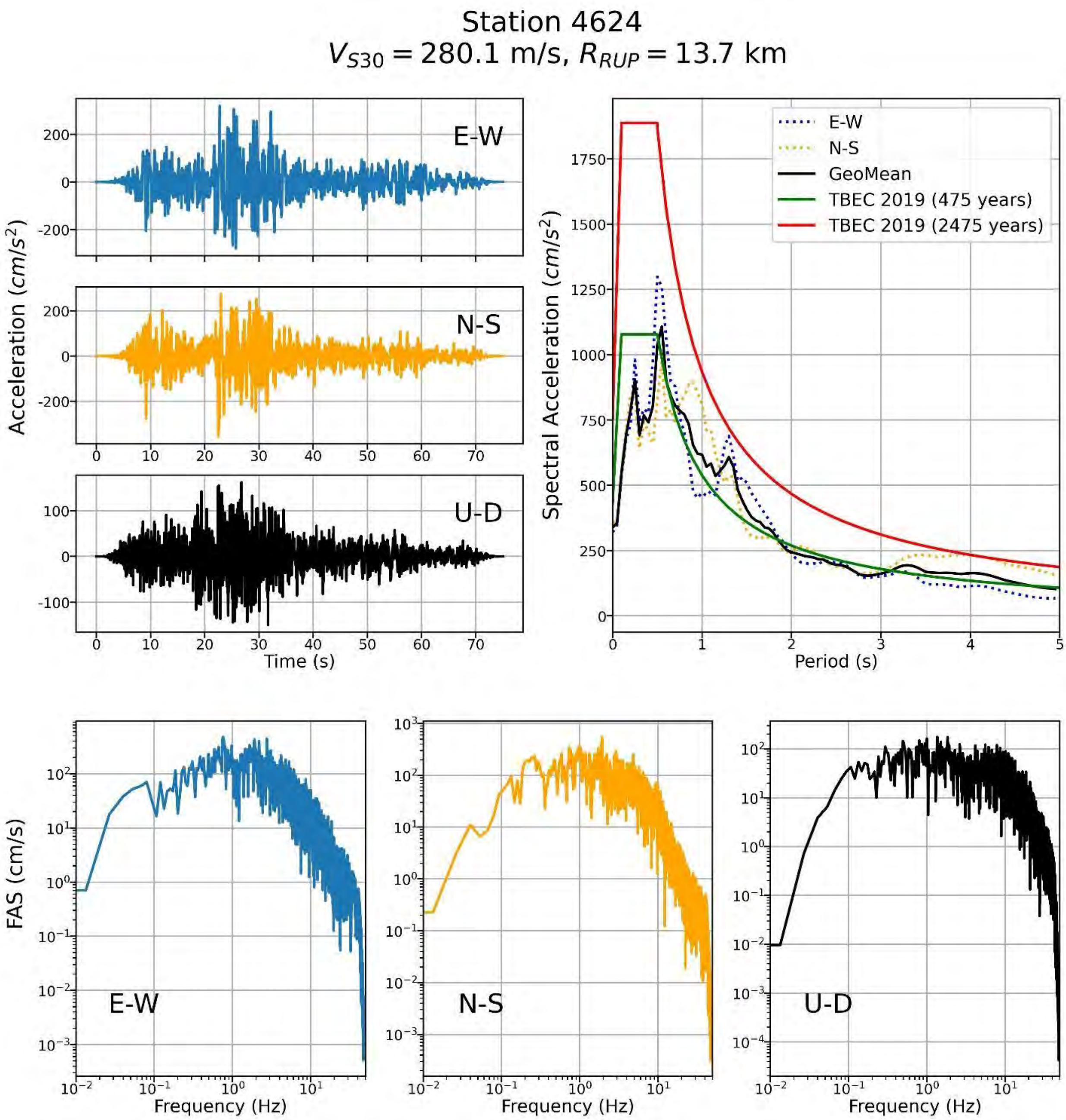

Figure 4.12. Recorded three-component ground accelerations, corresponding Fourier amplitude spectra (FAS) and response spectra (with 5% damping) in comparison with the most recent building code (TBEC, 2019) at selected station 4624 due to Pazarcik (Mw=7.7) event

Station 2708 is located in Islahiye, Gaziantep, on a site with NEHRP site class C (site class ZC of TBEC, 2019) and at a rupture distance of 4 km. We note that multiple wave packets were observed in the accelerogram. Both the FAS and response spectra were computed based on the entire time series, including all wave packets provided by AFAD. The maximum horizontal PGA is recorded in the EW direction as 1089 cm/s^2, while the vertical PGA value was recorded as 977 cm/s^2. The broadband nature of the response spectrum is attributed to the multiple wave packets observed in this large event. Response spectra from both horizontal components show peaks in the short period range. Despite being located on stiff soil conditions; the response spectra of the EW component show clear amplifications also in the longer periods with a particular peak around 1.2 seconds. The geometric mean of two horizontal response spectra exceeds the design spectrum corresponding to a return period of 475 years at almost all periods. The same geometric mean exceeds the design spectrum for a return period of 2475 years for periods longer than 0.7 seconds. We note that the most destruction was concentrated in this region based on the first observations in the field.

Station 3126 is located in Antakya, on a site with NEHRP site class D (site class ZD of TBEC, 2019) with a rupture distance of 15.4 km. The maximum horizontal PGA is recorded in the NS direction as 1210 cm/s^2. The vertical PGA value is 1070 cm/s^2. We observe that the acceleration recorded in the vertical direction are similar to those recorded in the horizontal direction in terms of frequency and amplitude content. The response spectra of both EW and NS components indicate amplifications around 0.3 seconds and both exceed the design spectrum for a return period of 475 years. The geometric mean is above the design spectrum for a return period of 2475 years for periods less than 0.4 seconds and below for longer periods.

Station 3138 is located in Hassa, Hatay on a site with NEHRP site class C (site class ZC of TBEC, 2019) with a rupture distance of 2 km. The acceleration records suggest potential directivity effects. When velocities are investigated, this record indicates forward directivity effects characterized by short-duration and high-amplitude, two-sided long-period velocity pulses. The geometric mean of horizontal response spectra indicates broadband period content and exceeds the design spectrum for a return period of 475 years for periods longer than 0.4 seconds.

Station 4615 is located in Pazarcik on a site with NEHRP site class C (site class ZC of TBEC, 2019) at a rupture distance of 10.3 km. This record also displays broadband response spectra, possibly due to the multiple wave packets. The maximum PGA value is recorded in the vertical component as 664 cm/s^2. The geometric mean spectrum is observed to exceed the 475-year design spectrum at periods larger than 0.5 s, and it is shown to be similar to the 2475-year design spectrum at periods larger than 1 s.

Station 4624, located in Onikisubat, Kahramanmaraş on a NEHRP site class D (site class ZD of TBEC, 2019) at a rupture distance of 13.7 km. The maximum horizontal PGA of 357 cm/s^2, which is relatively lower than the values at other stations. However, the geometric mean of the horizontal response spectra still exceeds the design spectrum for a return period of 475 years at periods longer than 0.7 seconds. The broadband content of the response spectra is consistent with the multiple wave packets observed in the accelerogram.

4. 3. MMI Distribution

Assessing seismic intensity measures after an earthquake is of great importance in identifying the effects of varying ground shaking over an area. One of the most common intensity measures for a rapid evaluation of seismic effects is macroseismic intensity distributions. Intensity levels can be assigned in the field, estimated via online surveys based on human responses, or can be computed via ground motion to intensity conversion equations (GMICEs). GMICEs mainly employ peak strong ground motion parameters such as PGA and PGV.

Within the scope of this report, Modified Mercalli Intensity (MMI) maps are used for the Pazarcik earthquake (7.7 M_w) and Elbistan earthquake (7.6 M_w) to identify the affected locations. Since the majority of the building stock in the mostly damaged regions is composed of rigid, low-to-mid-rise buildings, PGA could be a better identifier for macroseismic intensity distributions rather than PGV, which better correlates with the seismic behavior of ductile reinforced concrete structures (Erberik, 2008a; Erberik, 2008b). In this report, PGA-based ground motion to intensity conversion equations of Bilal and Askan (2014) and Albayrak et al. (2023) are employed. These GMICEs are both derived from local data compiled after past events in Türkiye. They both rely on geometric means of horizontal PGA values (in cm/s^2) from 244 strong ground motion stations for the defined earthquakes. The equations of Bilal and Askan (2014) and Albayrak et al. (2023) are as follows:

$$MMI = 0.132 + 3.884\, log\, log\, PGA \quad (4.1)$$

$$MMI = 1.290 + 3.766\, log\, log\, PGA \quad (4.2)$$

MMI levels can be related to anticipated damage levels. These damage levels are approximately moderate damage, moderate-to-severe damage and severe damage or total collapse as MMI levels of VI-VIII, VIII-X, and X-XII, respectively. Figure 4.13 shows the station-based MMI levels for Pazarcik Earthquake. Locations in the close vicinity of the epicenter exhibit MMI levels between X and XII. Figure 4.14 shows the station-based MMI levels for Elbistan earthquake. Locations in the close vicinity of the epicenter exhibit MMI levels between VIII and X.

It should be underlined that the Pazarcik earthquake had severe seismic effects not only around the epicenter but also along the surface rupture. In contrast, the MMI levels for Elbistan earthquake imply moderate-to-severe damage around the epicenter. It is important to note that MMI levels presented here express the effects of these two events independently. However, the occurrence of two large consecutive earthquakes in a relatively short time undoubtedly increased the damage levels in the structures located in the region. Finally, for regions with mid- and high-rise flexible reinforced concrete structures, PGV-based ground motion to intensity conversion equations should also be examined (Albayrak et al. 2023; Erberik, 2008a; Erberik, 2008b).

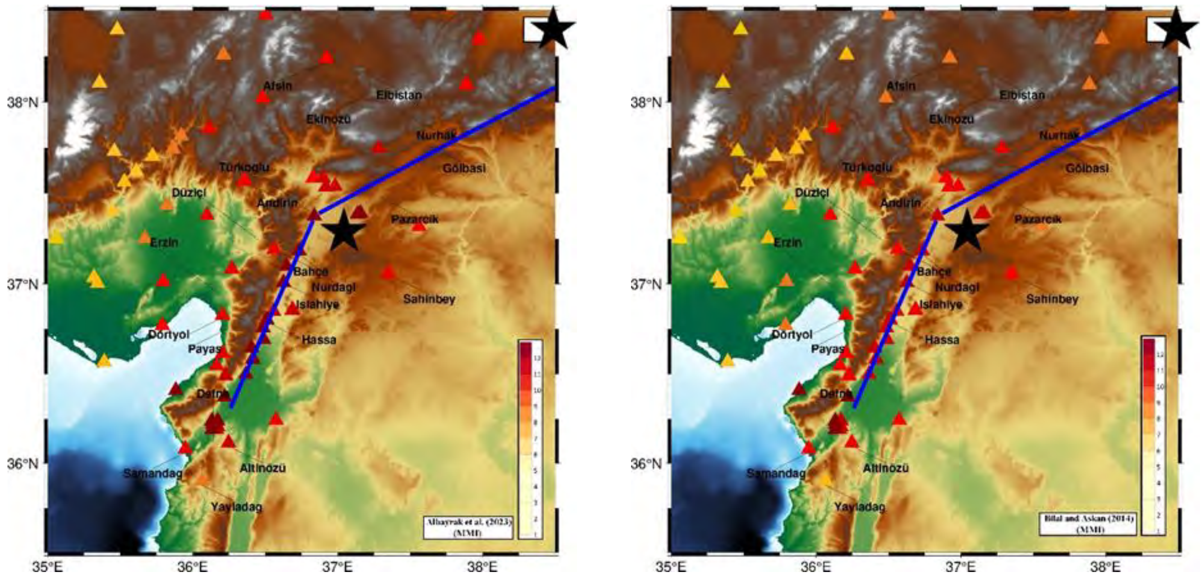

(a) (b)

Figure 4.13. Station based MMI levels for Pazarcik earthquake using recorded PGA values for (a) Equation 4.1 and (b) Equation 4.2.

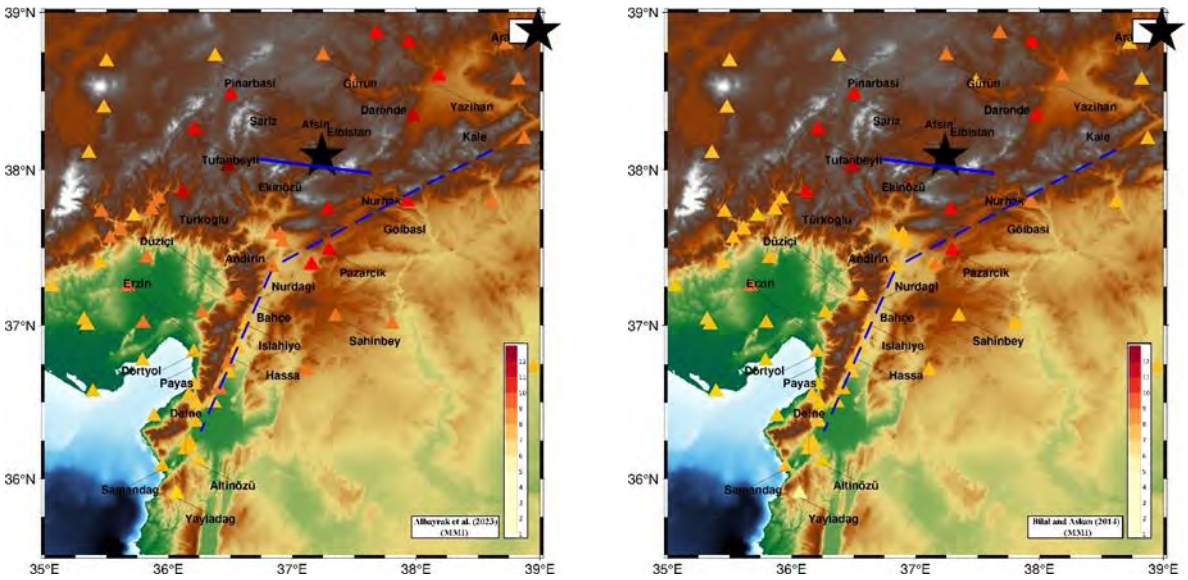

(a) (b)

Figure 4.14. Station based MMI levels for Elbistan earthquake using recorded PGA values for (a) Equation 4.1 and (b) Equation 4.2.

4. 4. Spatial Distribution of Peak and Spectral Accelerations

The spatial distribution of peak and spectral accelerations for the Pazarcik and Elbistan earthquakes is shown in Figures 4.15 and 4.16, respectively. Upon investigation of Figure 4.15, it becomes apparent that the highest PGA values are recorded in Antakya. In addition, very high PGA values between 500-1000 cm/s^2 are observed generally in the North-South direction, covering the provinces of Kahramanmaraş, Gaziantep, Osmaniye, Kilis and Hatay. The distribution of PGV and short-period spectral acceleration (at T=0.2 s) values are more homogeneous compared to the PGA, with very high intensities at all stations close to the rupture. Finally, the higher long-period spectral acceleration values (at T=1 s) observed in Antakya indicate potential forward directivity effects. As for the Elbistan earthquake (M_w=7.6), it is not as densely-recorded as the Pazarcik (M_w=7.7) event. As the rupture is located to the north of the first event (Figure 4.16), the effects of this event are felt more noticeably in the northern provinces, in addition to Kahramanmaraş, such as Adıyaman, Malatya and Kayseri. The highest ground motion intensities are generally observed in Kahramanmaraş.

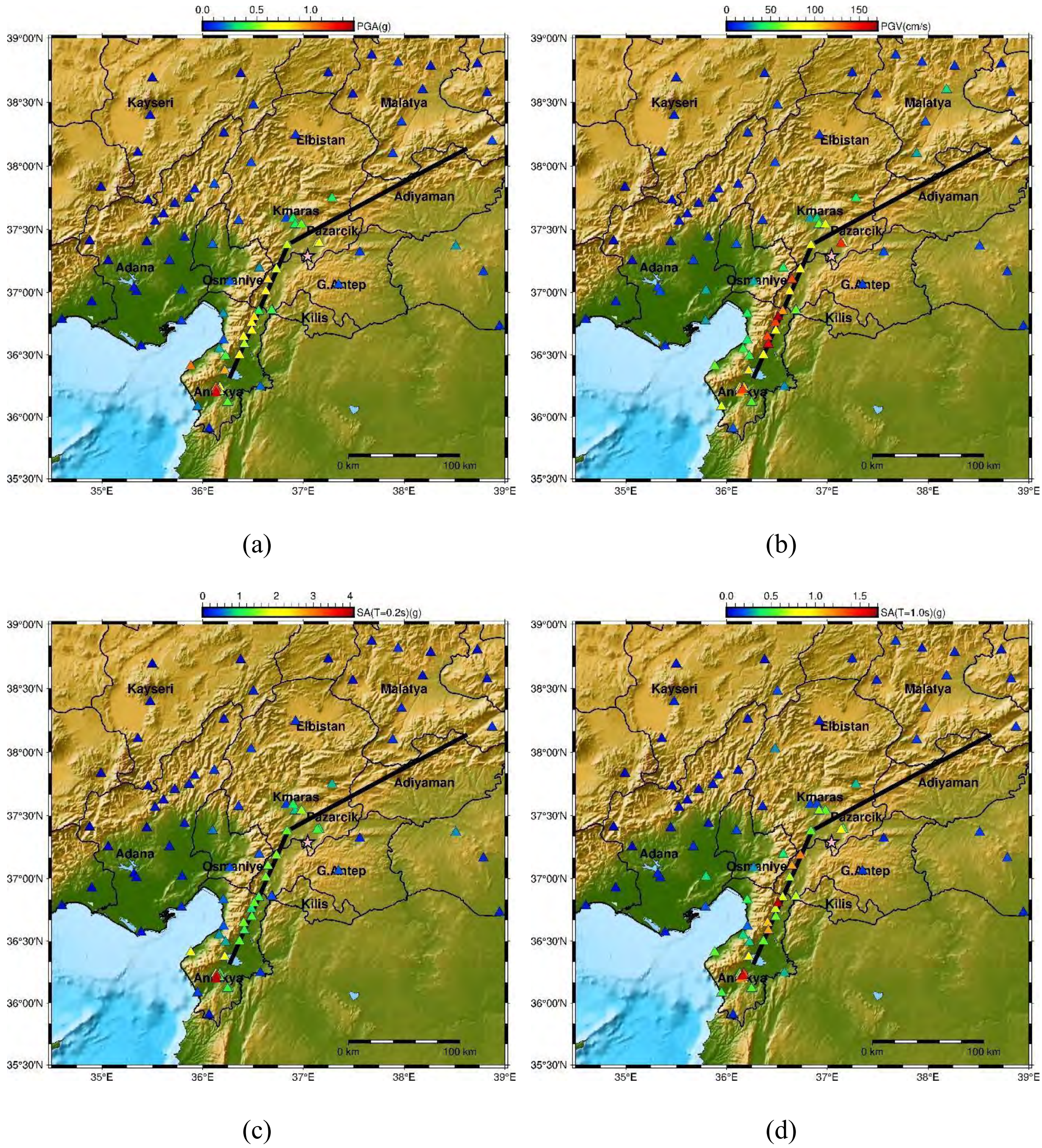

Figure 4.15. Spatial distribution of intensity measure of Pazarcik earthquake (a) PGA, (b) PGV, (c) T=0.2 s PSA and (d) T=1.0 s PSA

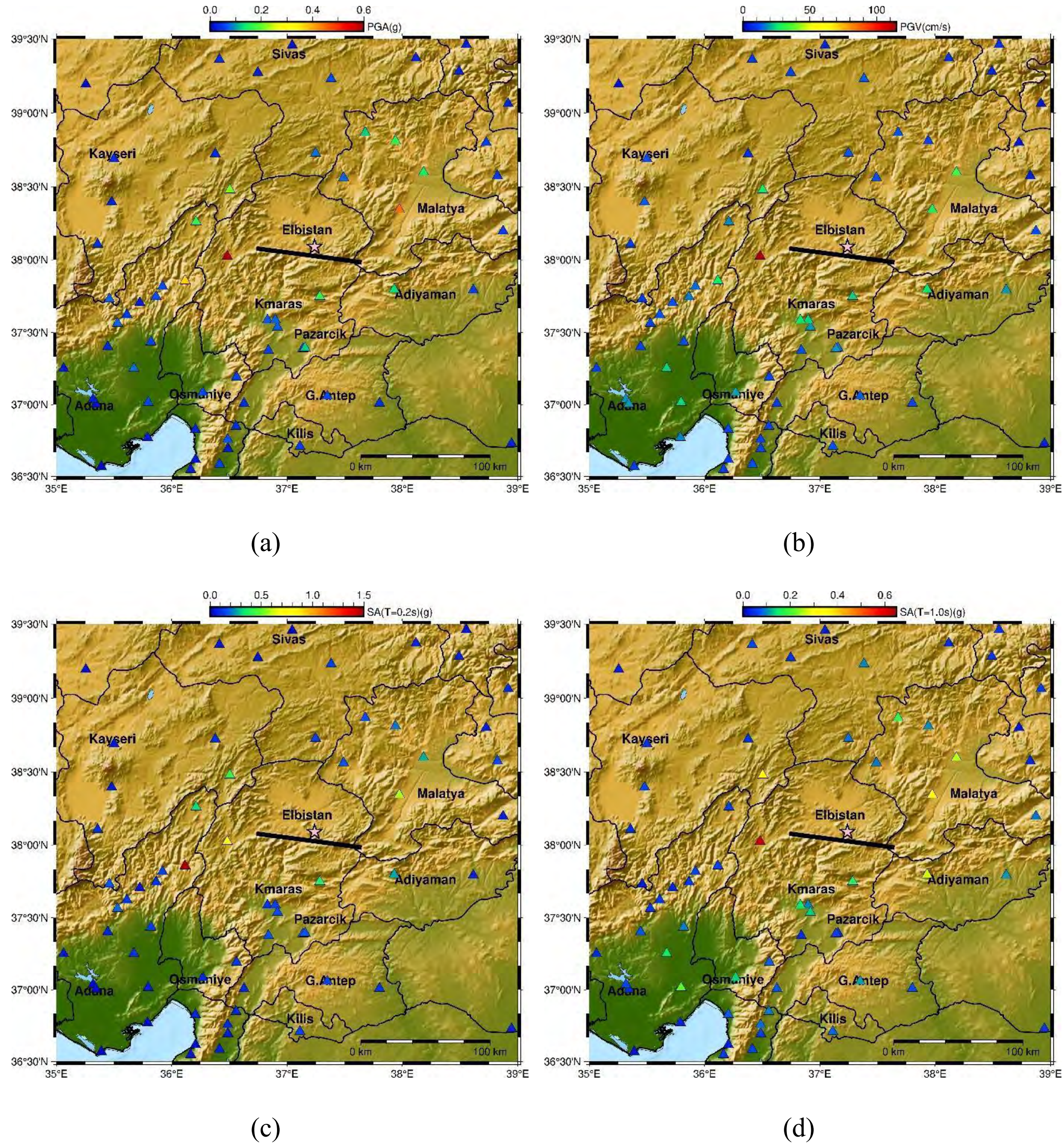

Figure 4.16. Spatial distribution of intensity measure of Elbistan earthquake (a) PGA, (b) PGV, (c) T=0.2 s PSA and (d) T=1.0 s PSA

4. 5. Performance of Current Ground Motion Models

Performance evaluation of ground motion models (GMMs) was conducted on a set of selected GMMs that represent the ground motion characteristics of the region. The best representative suit of GMMs for shallow active crustal tectonic regions was determined according to the proposals of Gülerce et al. (2016), Akkar et al. (2018), and Kale (2019), as well as the expert opinions. The final evaluation set includes the following GMMs:

- the local model of Kale et al. (2015) – KAAH15 developed by using the Turkish ground motion dataset,
- the Türkiye-adjusted version of the global NGA-W1 Chiou and Youngs (2008) model of Gülerce et al. (2016) - GCY16,
- the regional Pan-European models of Akkar et al. (2014) - ASB14 and Kotha et al. (2022) – KWBC22,
- the global Next Generation Attenuation (NGA) West 2 models of Boore et al. (2014) - BSSA14, and Chiou and Youngs (2014) - CY14.

The evaluations of the selected GMMs are based on the visual inspections between ground-motion model predictions and recorded ground-motion amplitudes. To this end, a subset of the ground motion dataset is compiled by selecting the strong motion stations with measured V_{S30} values, and R_{JB} and R_{RUP} < 300 km for each earthquake (Pazarcik and Elbistan). This distance limit falls within the model applicability ranges of GMMs, except for ASB14 and KAAH15, for which extrapolation of the models is considered. To obtain the model predictions, functional forms of the GMMs require a set of basic estimator parameters such as M_w, R_{JB}, R_{RUP}, V_{S30}, and style-of-faulting, whereas the global model of CY14 considers additional estimator parameters such as horizontal distance to the top edge of rupture measured perpendicular to the strike (R_X), depth-to-top of rupture (Z_{TOR}), dip angle, depth to the shear-wave velocity horizon of 1.0 km/s ($Z_{1.0}$), etc. Most of the parameters are computed by considering the ruptured fault plane, whereas the soil sediment parameter ($Z_{1.0}$) is estimated from the empirical relationship proposed by Chiou and Youngs (2014) as a function of V_{S30}.

To assess the distance attenuation of observed ground motions and compare them with the distance scaling of selected GMMs, we present the distribution of the geometric mean of the recordings at PGV, PGA, PSA at T=0.2 s, 1.0 s, and 3.0 s with R_{JB} for the Pazarcik and Elbistan Earthquakes separately. Although the figures show RJB as the distance metric to ensure consistency, the predictions of each GMM are calculated based on the original distance metric definition of the models. The median predictions of the BSSA14 model are calculated by considering the Turkiye-specific regional adjustment term (high-Q option) proposed by Boore et al. (2014). For the figures, recorded ground motions are converted to reference rock site conditions (V_{S30} = 760 m/s) using site amplification factors that are calculated for each recording and each GMM separately.

Figures 4.17 – 4.21 show the comparisons of the Pazarcik Earthquake:

- Recorded PGA values are generally higher than the median estimations of ASB14, KWBC22, and KAAH15 models for R_{RUP}<100km. In this distance range, the recorded motions are almost equally distributed around the median for GCY16, BSSA14, and CY14 models.
- The slope of the distance scaling in the recorded PGAs decays faster than the distance scaling implemented in almost all selected models for R_{RUP}>100km, except for KWBC22. This observation is consistent with the observations from recent large-magnitude events in Türkiye (e.g., Samos earthquake, Gülerce et al., 2021), underlining that the large distance scaling of the ground motions recorded in Türkiye calls for a critical and in-depth overview.
- Therefore, the event terms should definitely be estimated for an R_{RUP}<100km dataset in the early stages of regression for any future GMMs based on Turkish strong motion data.
- Median predictions of selected GMMs are quite different for PGV, hence the distribution of recorded PGVs with respect to median varies significantly. The median predictions of ASB14 and KAAH15 models are lower than the other models and eventually lower than the recorded motions, especially in the near field. Recorded motions are closer to the median plus one sigma range for the other models. At longer distances, median PGV predictions of all models are quite consistent with the recorded data.
- Predictive performance of all models is significantly good for PSA at T = 0.2 s for R_{RUP}<100km. Faster decay than the models' attenuation is also observed at large distances.
- Median to short distance predictive performance of selected GMMs for PSA at T = 1 s is similar to PGA. However, the distance scaling of GMMs and the distance scaling of 1-s spectral accelerations are very different for R_{RUP}>100km, except for KWBC22 and CY14 models. This observation underlines the need for evaluating the anelastic

attenuation terms in the GMMs developed (KAAH15) and calibrated for Türkiye (BSSA14 and GCY16).

- At T = 3 s, the predictive performance of BSSA14 and KWBC22 models are superior when compared to the other models. Recorded long-period ground motions are considerable, especially in the near-field region. This preliminary observation calls for a detailed analysis of the potential directivity effects, especially at or near the end of the rupture.

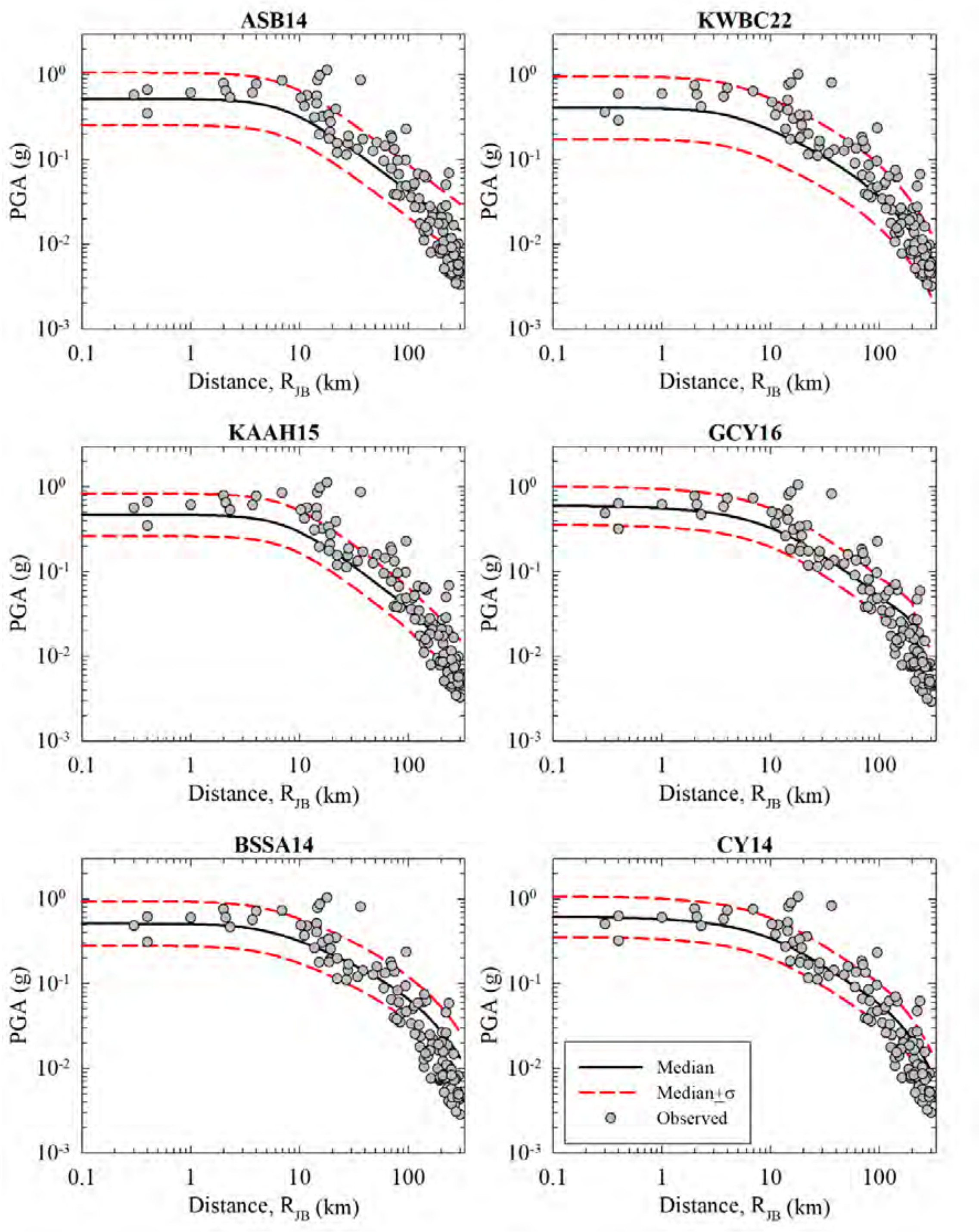

Figure 4.17. Comparison of the distance attenuation of ASB14, KWBC22, KAAH15, GCY16, BSSA14, and CY14 models with recorded strong motion data for PGA. Median and median ±1σ curves are given with black solid and red dashed lines, respectively. Gray points represent the V_{S30} normalized recorded strong motion data for Pazarcik Earthquake.

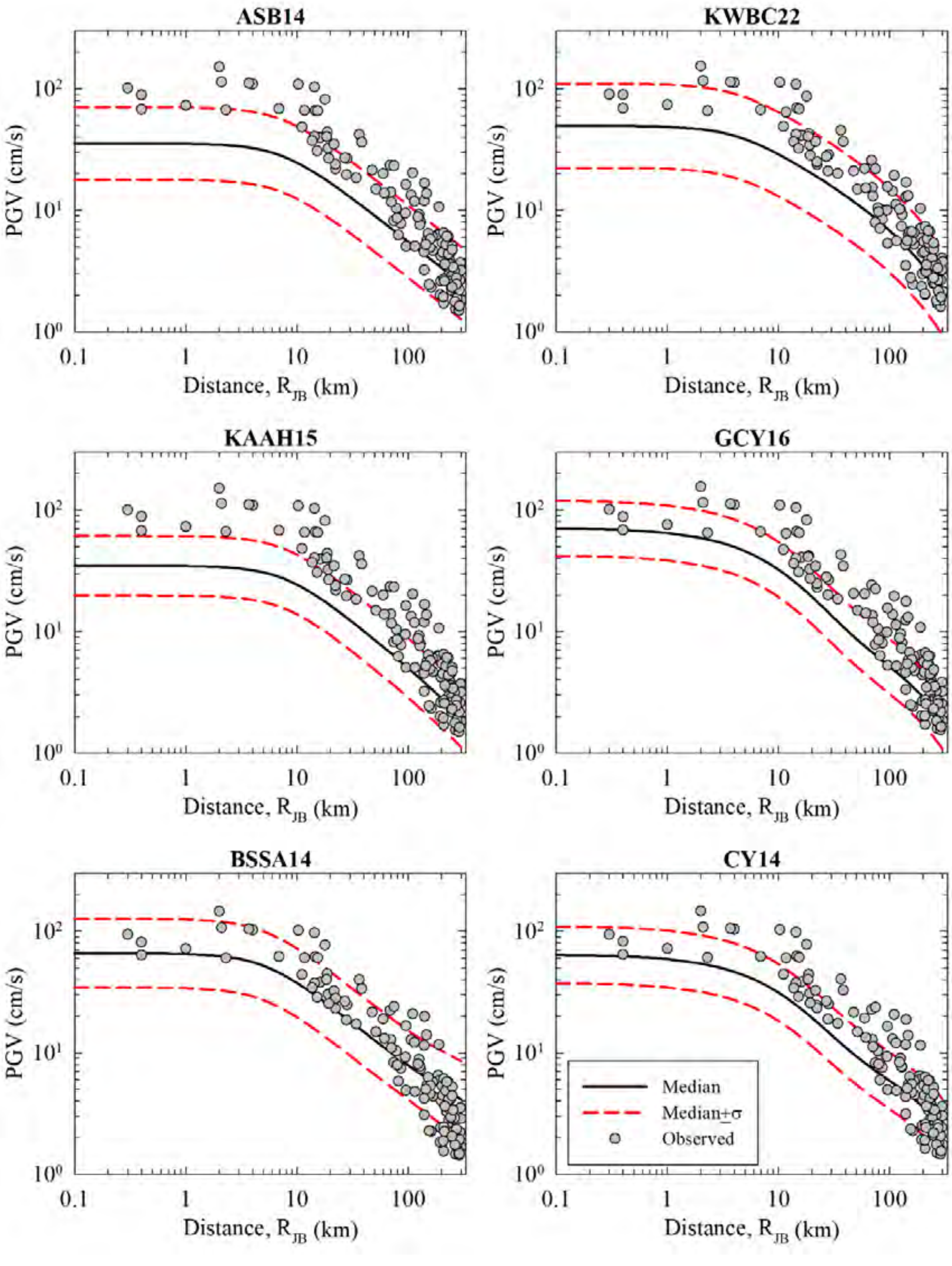

Figure 4.18. Comparison of the distance attenuation of ASB14, KWBC22, KAAH15, GCY16, BSSA14, and CY14 models with recorded strong motion data for PGV. Median and median ±1σ curves are given with black solid and red dashed lines, respectively. Gray points represent the V_{S30} normalized recorded strong motion data for Pazarcik Earthquake.

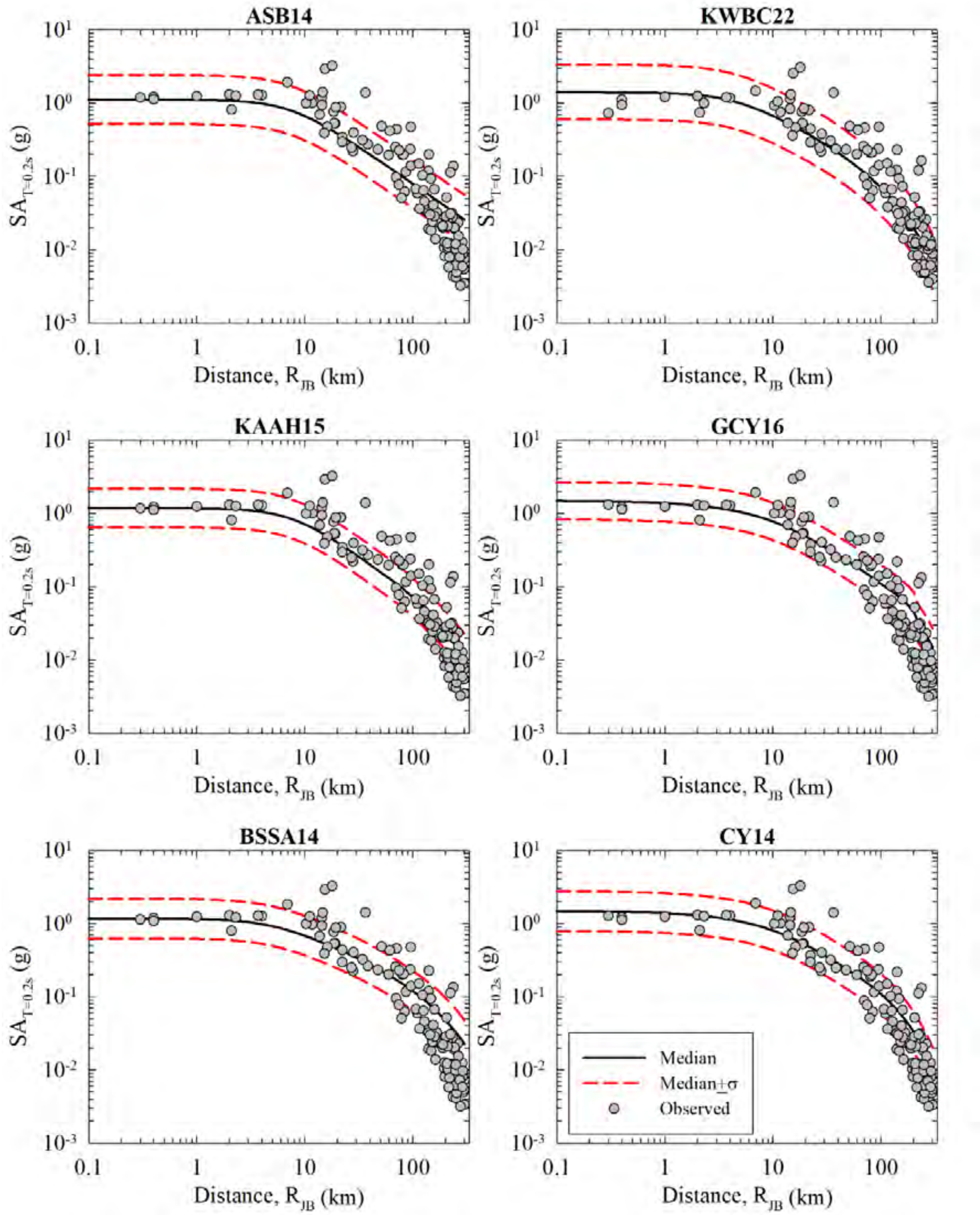

Figure 4.19. Comparison of the distance attenuation of ASB14, KWBC22, KAAH15, GCY16, BSSA14, and CY14 models with recorded strong motion data for T=0.2s PSA. Median and median ±1σ curves are given with black solid and red dashed lines, respectively. Gray points represent the V_{S30} normalized recorded strong motion data for Pazarcik Earthquake.

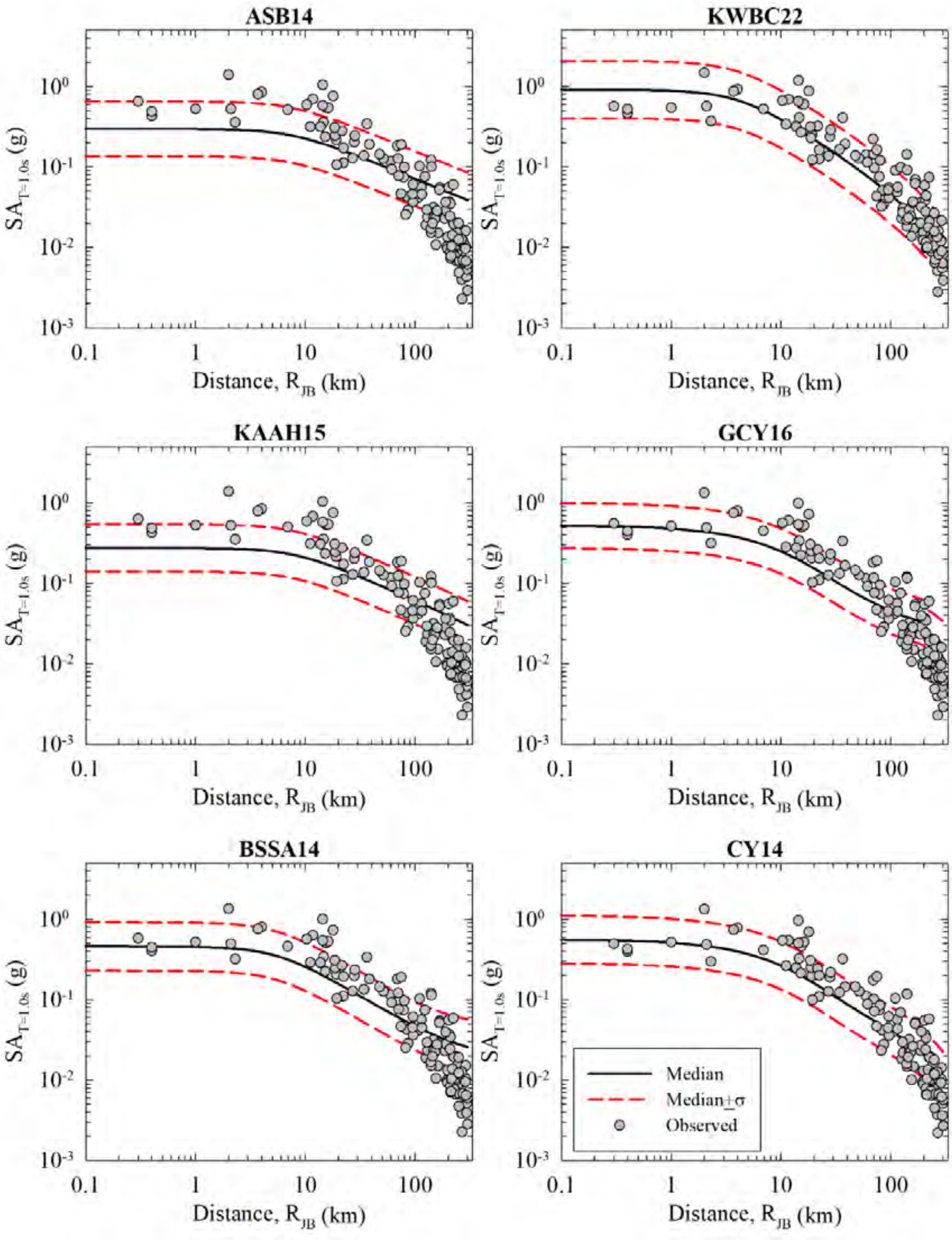

Figure 4.20. Comparison of the distance attenuation of ASB14, KWBC22, KAAH15, GCY16, BSSA14, and CY14 models with recorded strong motion data for T=1.0s PSA. Median and median ±1σ curves are given with black solid and red dashed lines, respectively. Gray points represent the V_{S30} normalized recorded strong motion data for Pazarcik Earthquake.

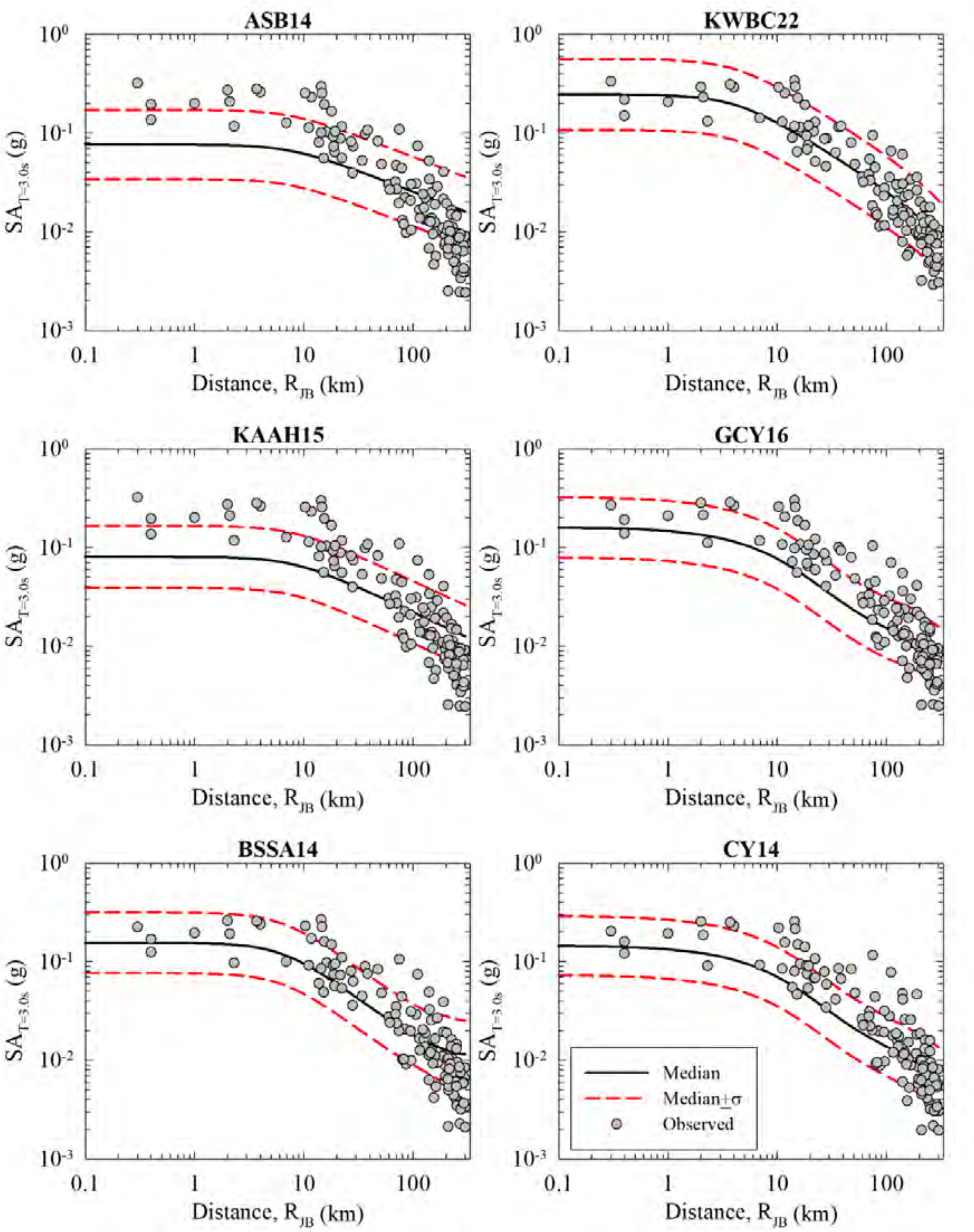

Figure 4.21. Comparison of the distance attenuation of ASB14, KWBC22, KAAH15, GCY16, BSSA14, and CY14 models with recorded strong motion data for T=3.0s PSA. Median and median ±1σ curves are given with black solid and red dashed lines, respectively. Gray points represent the V_{S30} normalized recorded strong motion data for Pazarcik Earthquake.

Figures 4.22 to 4.26 show the comparisons of the Elbistan Earthquake:

- The number of stations within the first 50 km of the rupture (that have passed the quality check) is very limited. Therefore, it is not meaningful to reach any conclusions on the geometrical spreading (short distance scaling) for this event.
- Except for a few outlying stations, the recordings at the R_{RUP}=50-100 km are generally in good agreement with the median predictions of the selected GMMs at all spectral periods, except for PGV.
- Interpretations for the first event, related to the large distance scaling, are also valid for this event. The large distance slope of the recordings is inconsistent with the large distance slope of almost all GMMs. The large distance predictive performance of CY14 and KWBC22 is superior to the other models at certain periods.
- Recorded PGV values are higher than the median predictions of all selected GMMs. The difference between the actual data and median estimations is most prominent for KAAH15 and GCY16 models, which were developed or calibrated by using Turkish strong motion recordings. This observation is striking and not easy to explain with the possible directivity effects.
- Recorded PGV values are larger than the median (or even larger than the median plus one sigma) but the long-period ground motions (PSA T = 1.0 s and PSA T = 3.0 s) are well distributed around the median for most models. This also supports the lack of long-period directivity pulse in the recorded motions.

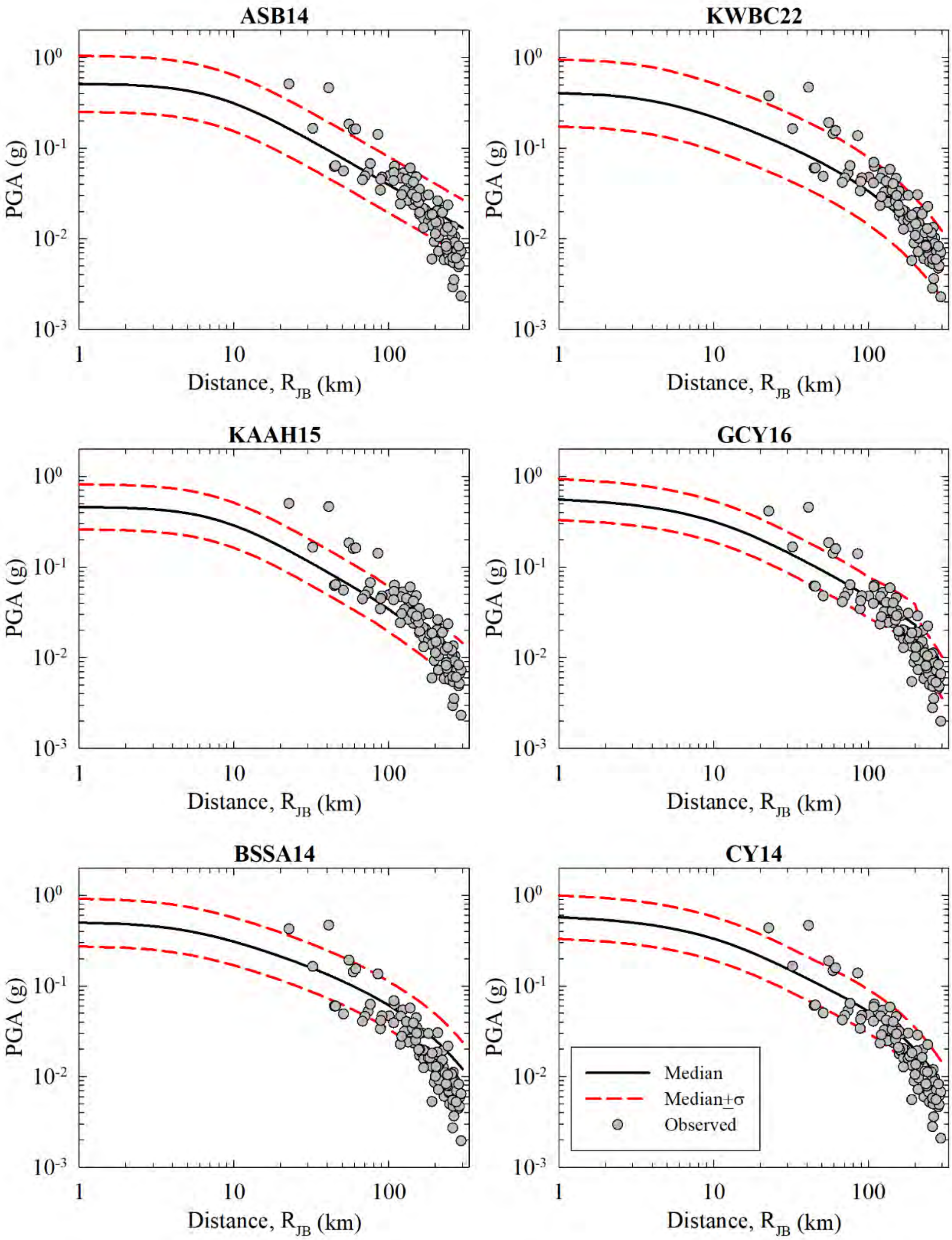

Figure 4.22. Comparison of the distance attenuation of ASB14, KWBC22, KAAH15, GCY16, BSSA14 and CY14 models with recorded strong motion data for PGA. Median and median ±1σ curves are given with black solid and red dashed lines, respectively. Gray points represent the V_{S30} normalized recorded strong motion data for Elbistan Earthquake.

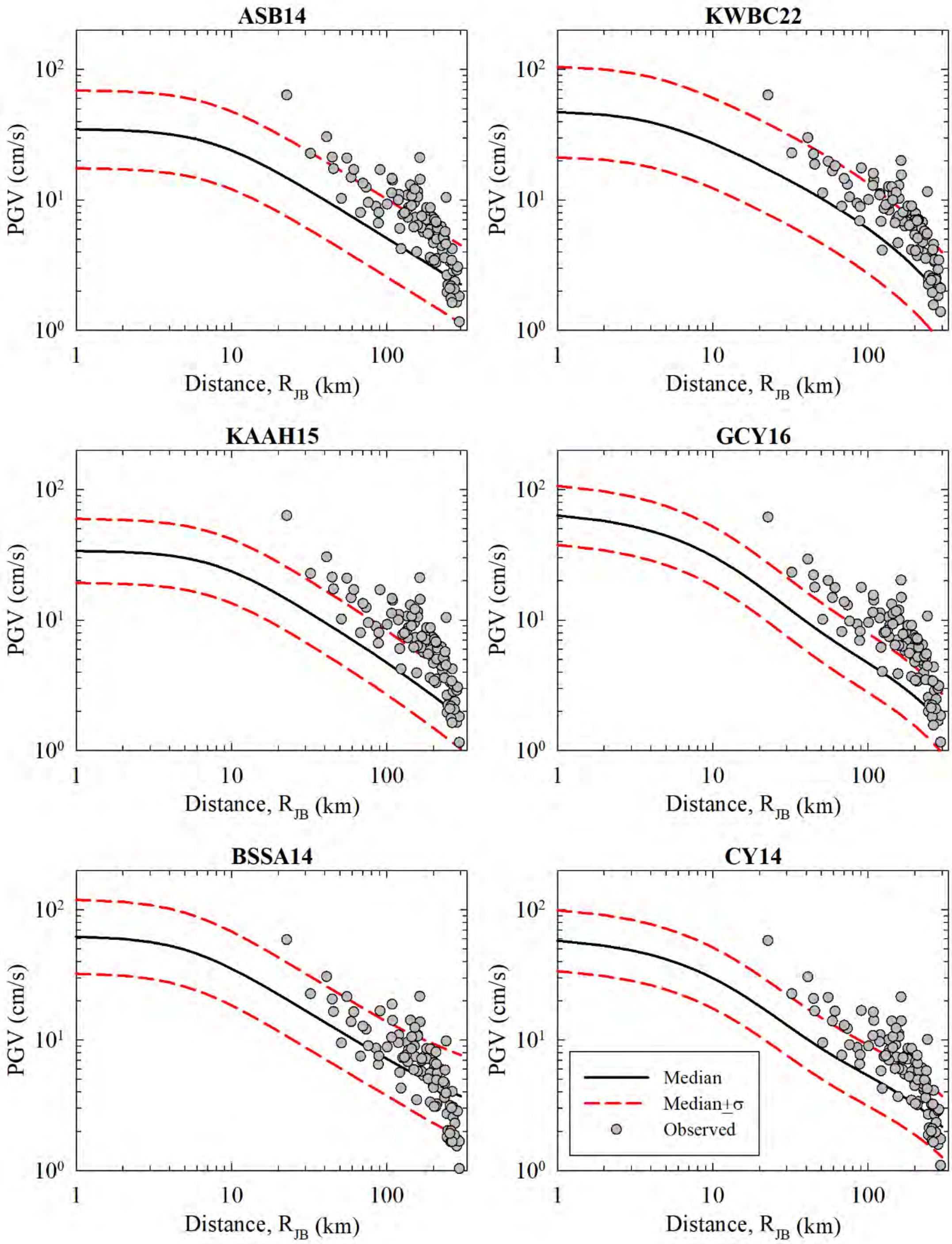

Figure 4.23. Comparison of the distance attenuation of ASB14, KWBC22, KAAH15, GCY16, BSSA14 and CY14 models with recorded strong motion data for PGV. Median and median ±1σ curves are given with black solid and red dashed lines, respectively. Gray points represent the V_{S30} normalized recorded strong motion data for Elbistan Earthquake.

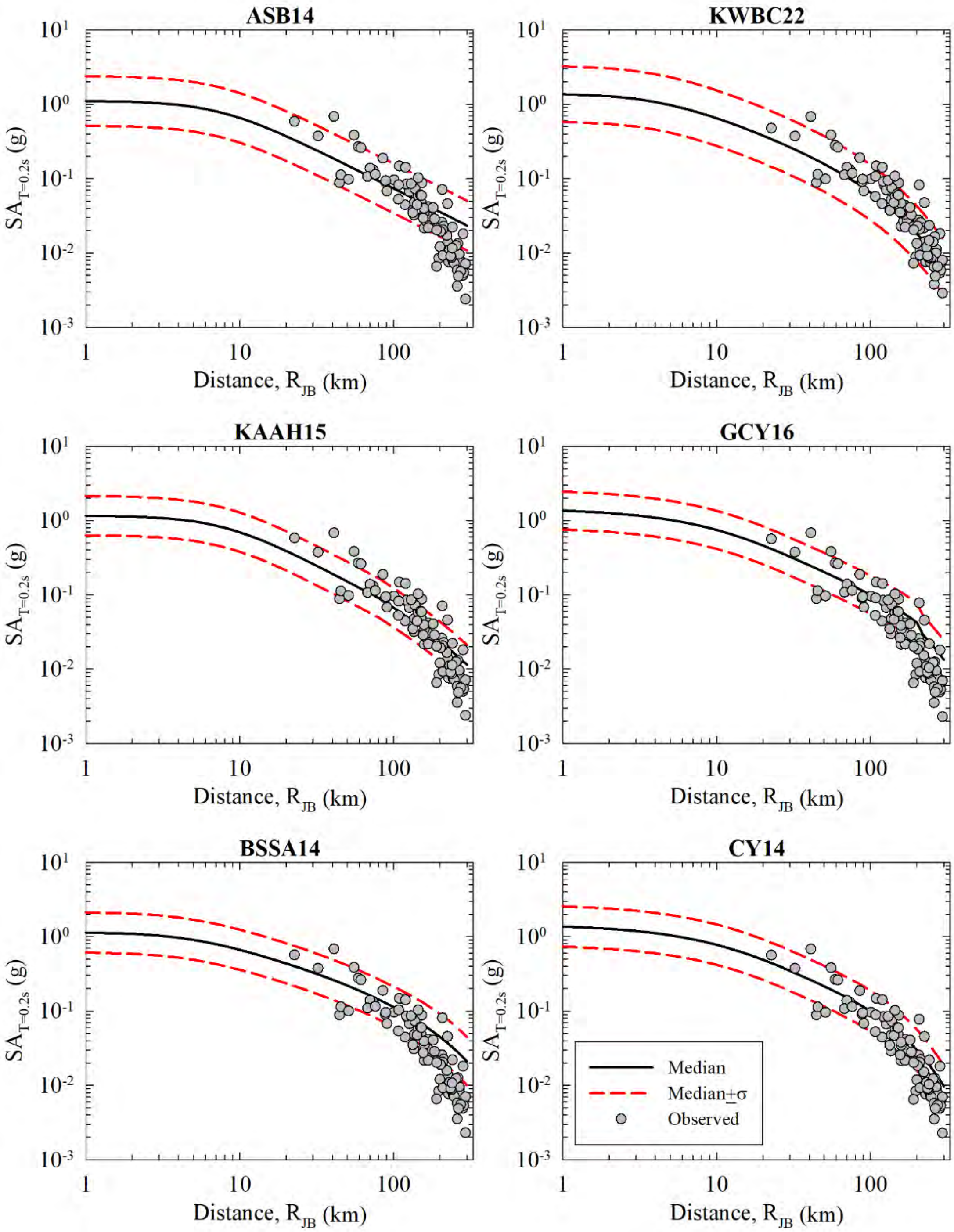

Figure 4.24. Comparison of the distance attenuation of ASB14, KWBC22, KAAH15, GCY16, BSSA14 and CY14 models with recorded strong motion data for T=0.2s PSA. Median and median ±1σ curves are given with black solid and red dashed lines, respectively. Gray points represent the V_{S30} normalized recorded strong motion data for Elbistan Earthquake.

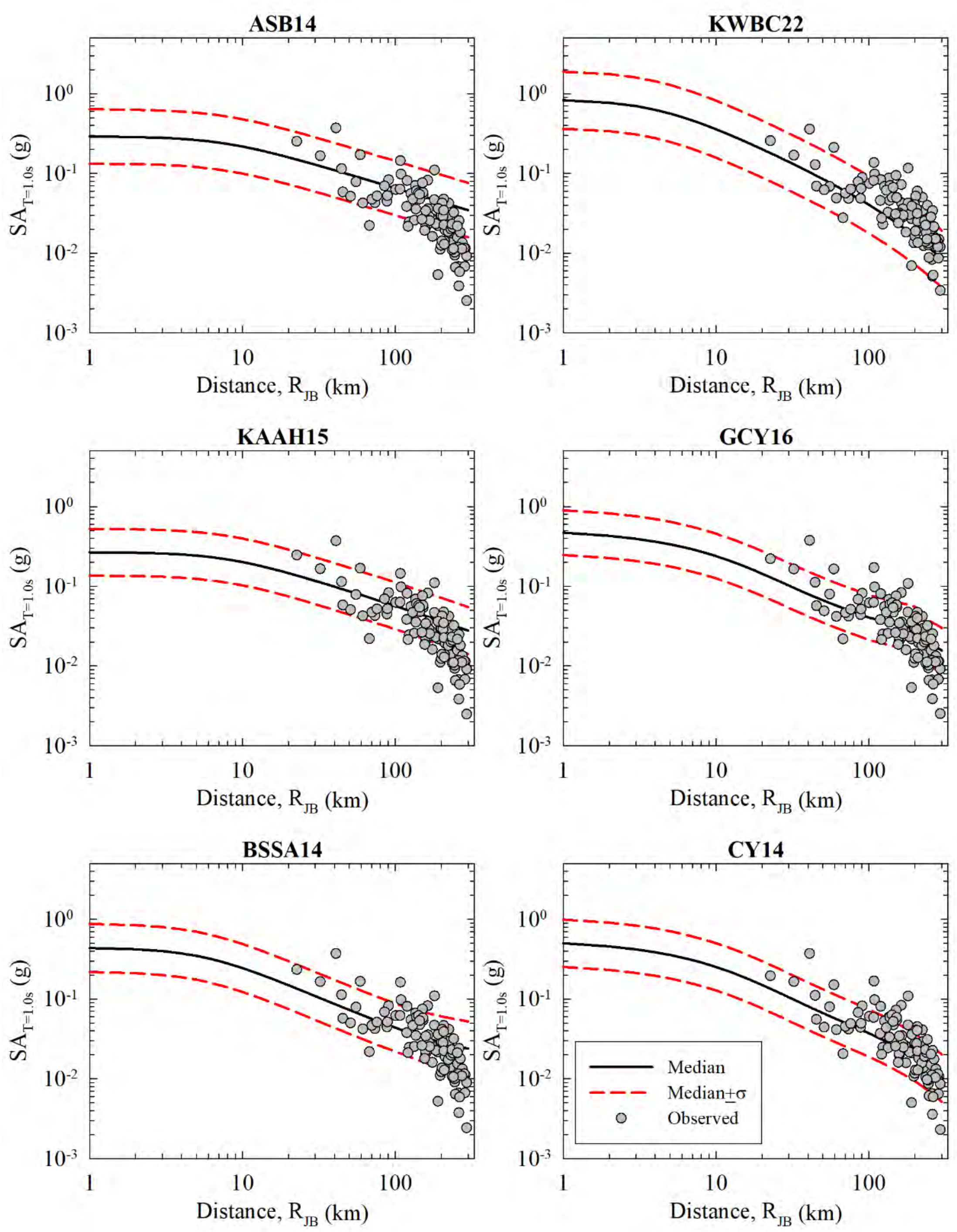

Figure 4.25. Comparison of the distance attenuation of ASB14, KWBC22, KAAH15, GCY16, BSSA14 and CY14 models with recorded strong motion data for T=1.0s PSA. Median and median ±1σ curves are given with black solid and red dashed lines, respectively. Gray points represent the V_{S30} normalized recorded strong motion data for Elbistan Earthquake.

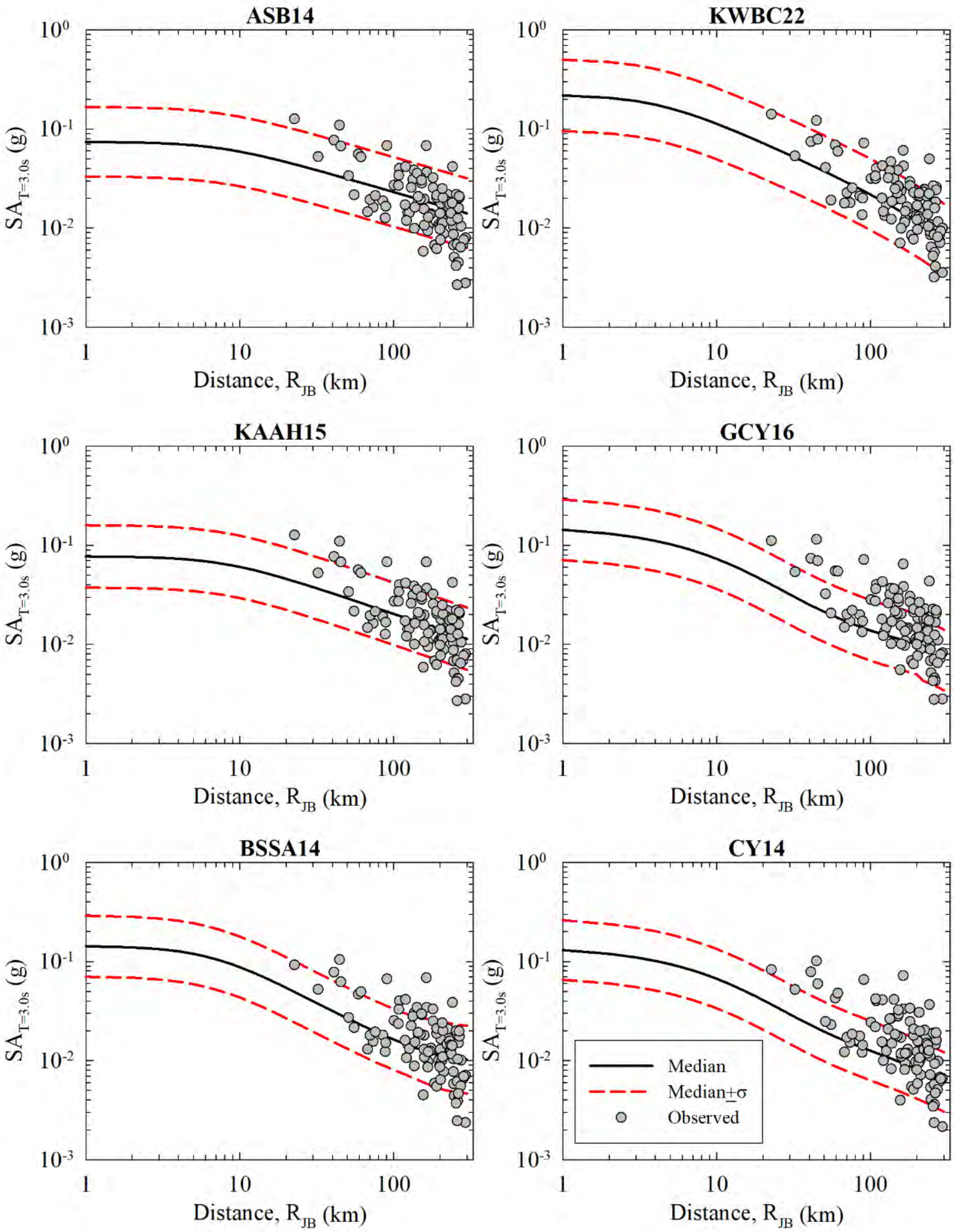

Figure 4.26. Comparison of the distance attenuation of ASB14, KWBC22, KAAH15, GCY16, BSSA14 and CY14 models with recorded strong motion data for T=3.0s PSA. Median and median ±1σ curves are given with black solid and red dashed lines, respectively. Gray points represent the V_{S30} normalized recorded strong motion data for Elbistan Earthquake.

4. 6. Spectral Amplifications and HVSR

Site amplification effects can significantly change the amplitude and frequency content of recorded ground motions. Various methods exist for calculating site amplifications and fundamental periods and frequency values of sites, which include both theoretical and empirical approaches. In this preliminary report, due to the limited availability of field investigation data (shear wave velocity measurement, soil profiles, etc.), the empirical HVSR method, also known as Nakamura's method, is used. This approach was developed by Nakamura (1989) following the original study of Nogoshi and Igarashi (1971). As part of this report, preliminary Horizontal-to-Vertical Spectral Ratio (HVSR) analyses are conducted using recorded strong motion data from selected stations located in Hatay, Gaziantep, and Kahramanmaraş after the M_w=7.7 Pazarcik earthquake on 6th February 2023.

HVSR method was originally developed for microtremor recordings, however, it can also be employed using single strong ground motion station measurements to estimate the natural resonant frequencies of near-surface layers. The fundamental assumption in this method is that the vertical motion remains constant during its propagation to the surface, while the horizontal component amplifies or de-amplifies due to site response. HVSR spectra are calculated by selecting the S-wave portion of the acceleration record, and FAS is computed for the two horizontal and vertical components at the surface. FAS for the S-wave portion is initially smoothed by Konno and Ohmachi (1998). Next, the geometric mean of the two smoothed horizontal component FAS is divided by the vertical component smoothed FAS to obtain HVSR. at the location. The resulting HVSR curve typically exhibits one or more peaks that correspond to the resonant frequencies of the subsurface layers.

HVSR curves are presented at five selected stations (Stations 2708, 3126, 3138, 4615, and 4624) located near the fault ruptures in Gaziantep, Kahramanmaraş, and Hatay. The selected stations are also shown in Figure 4.5a with a red rectangle.

HVSR values are calculated using Pizzaro (2017) HOVSR (Version 2.0) MATLAB code. Figure 4.27 – 4.31 present the acceleration time histories recorded at the stations and the corresponding HVSR curves, along with V_{s30} and rupture distances. It is observed that for the M_w=7.7 Pazarcik event, there are multiple wave packets. This is extensively discussed in Sections 4.2 and 4.3. This observation is also clearly recognized at stations 2708, 4615, and 4624, where the HVSR values from different S-wave packets are evaluated separately (named as 1st and 2nd packets on the corresponding HVSR curves).

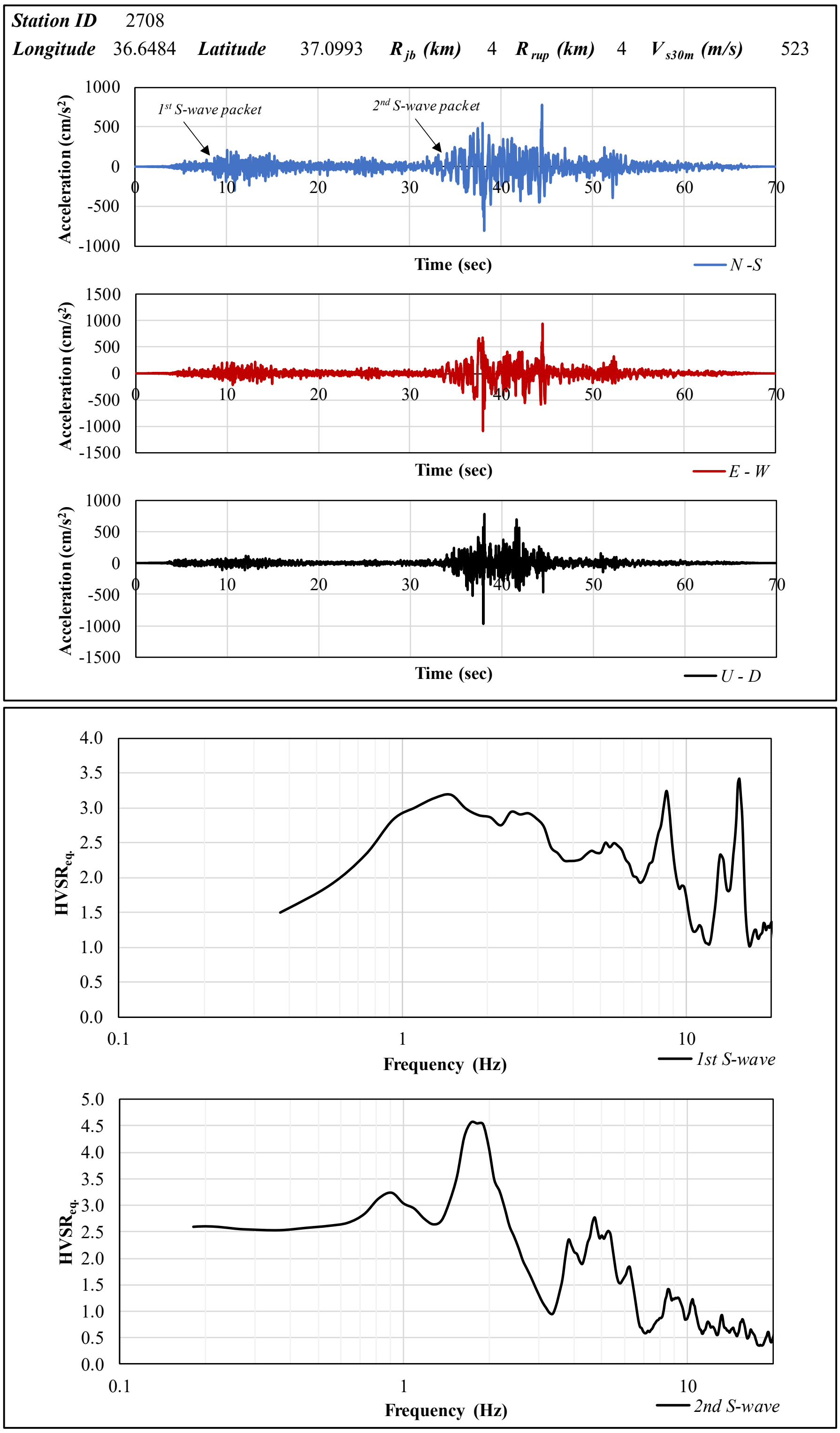

Figure 4.27. Resulting HVSR curve for station 2708

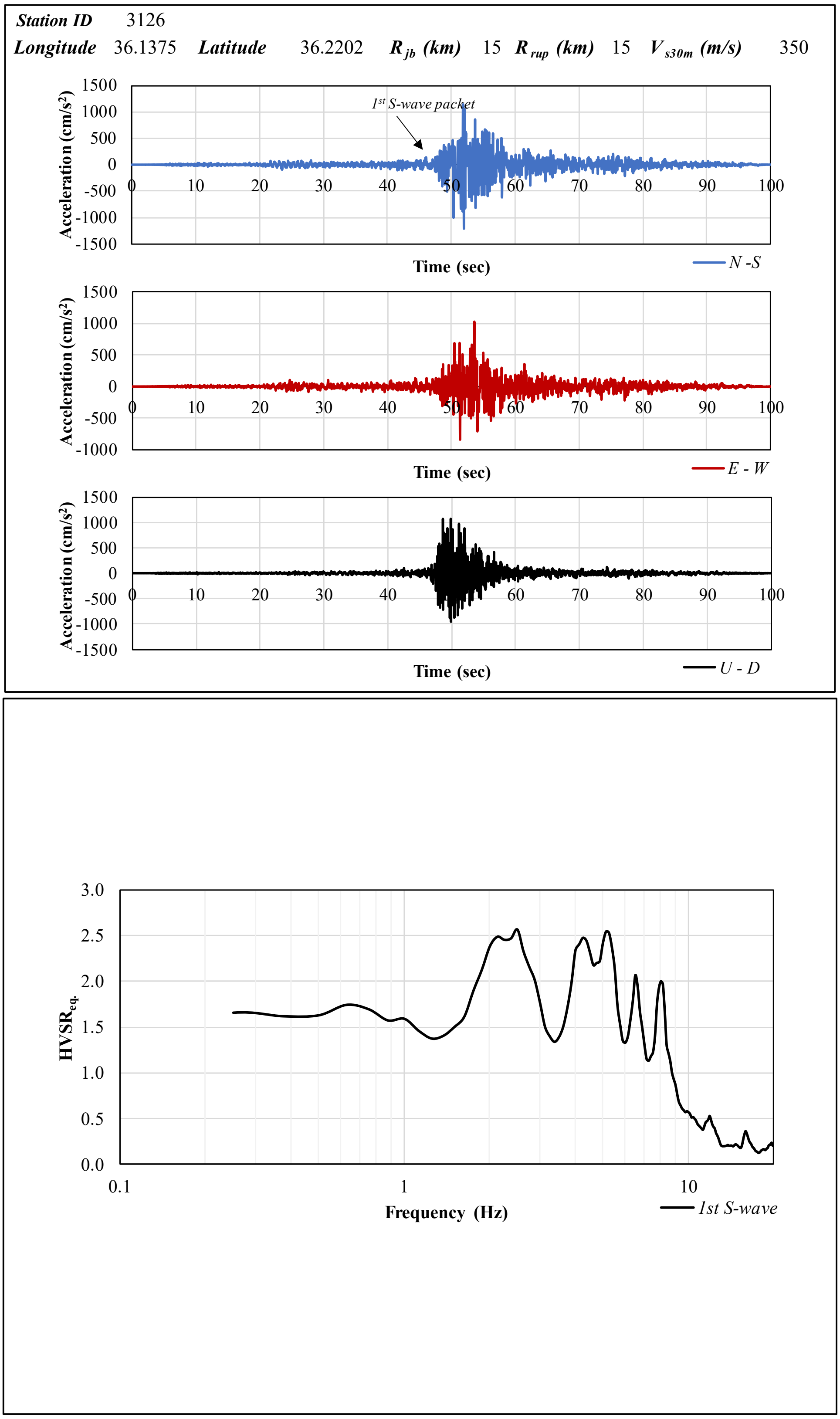

Figure 4.28. Resulting HVSR curve for station 3126

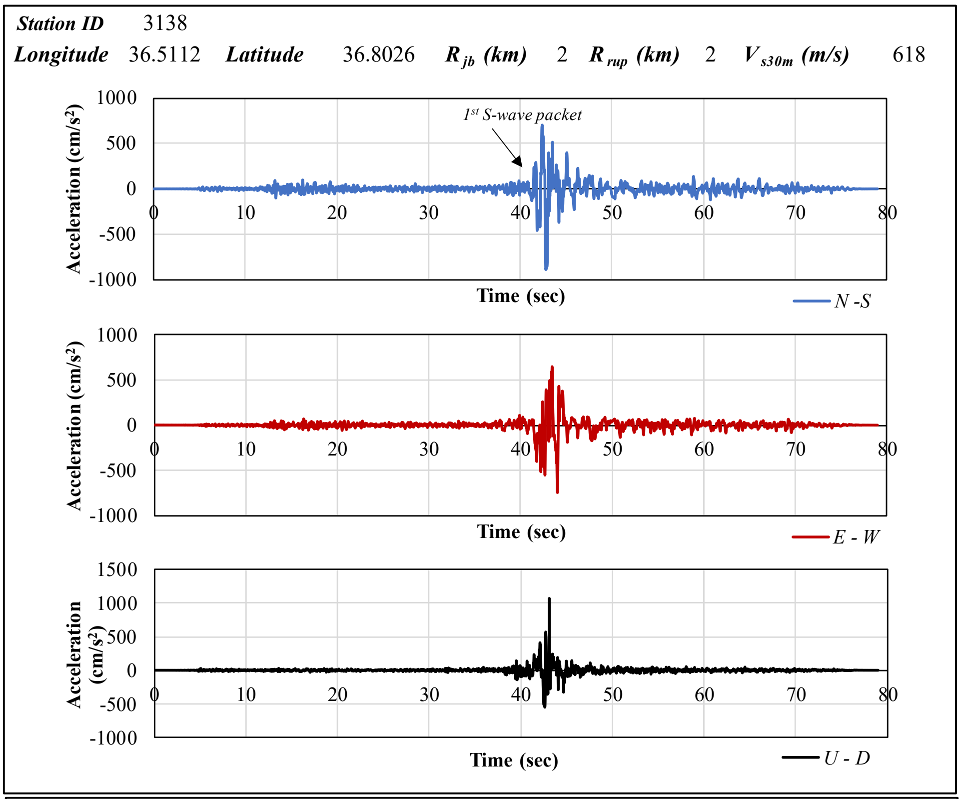

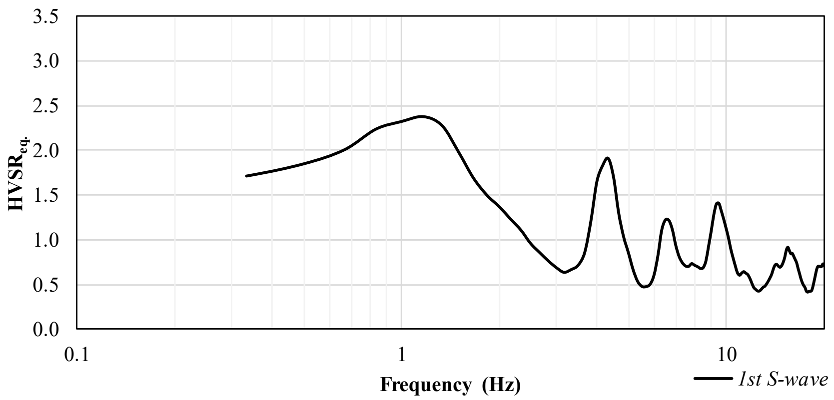

Figure 4.29. Resulting HVSR curve for station 3138

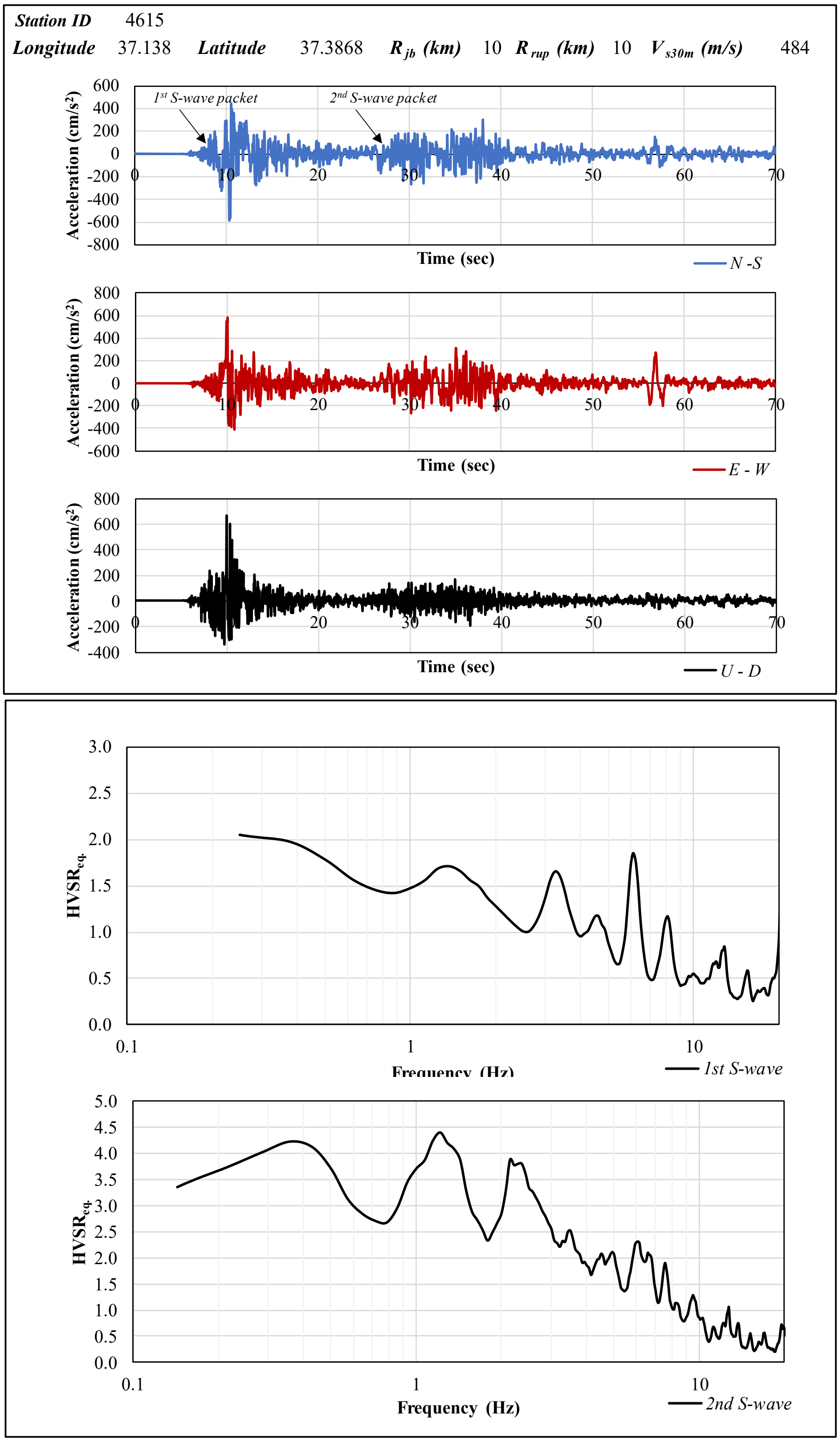

Figure 4.30. Resulting HVSR curve for station 4615

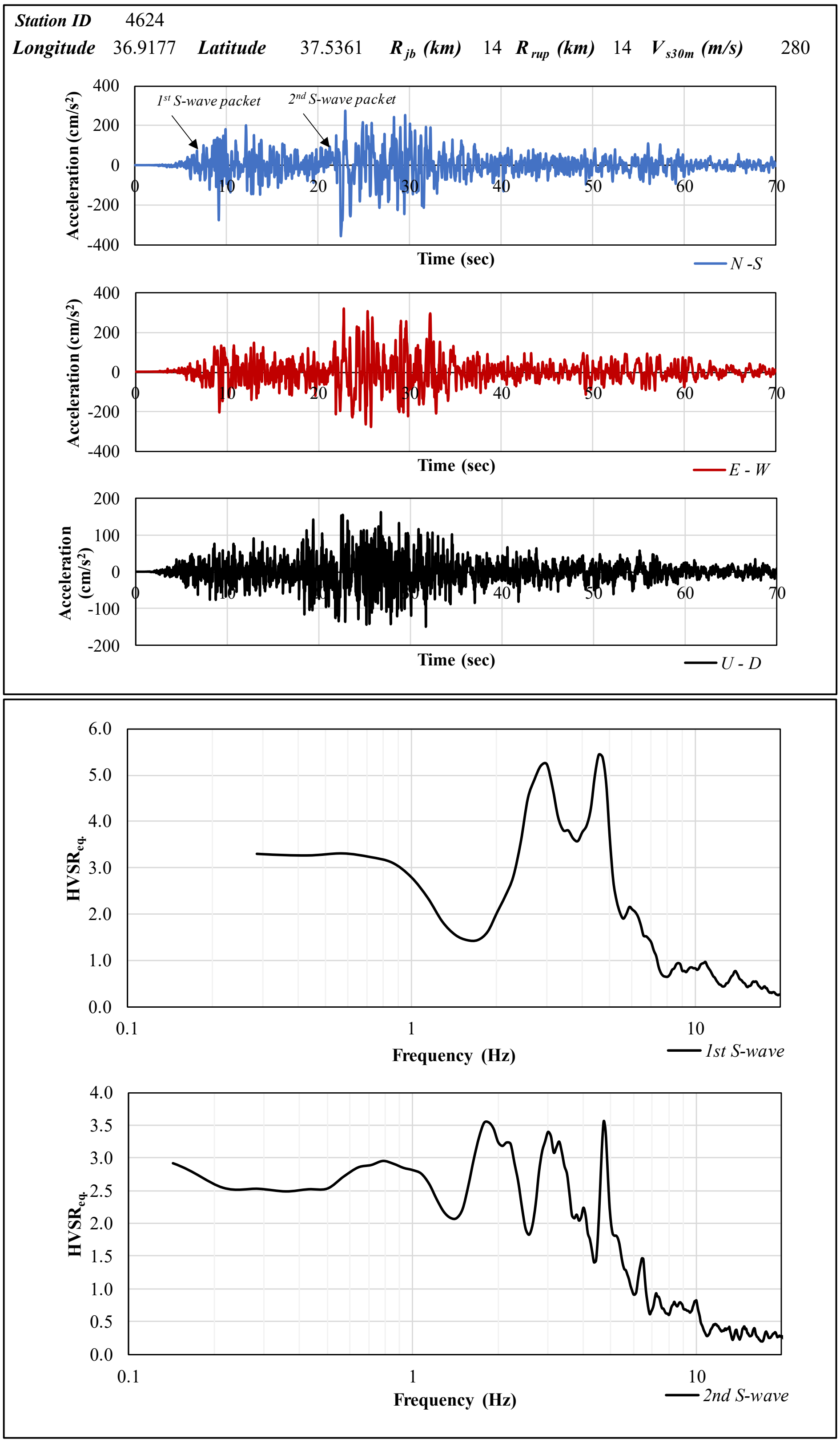

Figure 4.31. Resulting HVSR curve for station 4624

HVSR curves are commonly used to estimate the fundamental frequency values of sites, but their effectiveness in evaluating site amplifications is still being debated in the literature. To better assess site amplifications in future evaluations, amplification ratios using either the standard spectral ratio method (SSR), which normalizes outcrop soil response spectra to the nearest rock outcrop motion, or site-specific 1-D site response analyses at the selected stations. More specifically,

- Station 2708 (Figure 4.27) is located on either a very dense soil or a very soft rock site, where the $V_{s,30m}$ is 523 m/s and HVSR indicates peaks around 1.5 Hz (T=0.67 sec) and 7.5 Hz (T=0.13 sec) for the 1st S-wave portion and relatively low frequency 1.9 Hz (T=0.53 sec) and 5.0 Hz (T=0.2 sec) peak for the 2nd S-wave portion.
- Station 3126 (Figure 4.28) is located on a stiff soil site, where the $V_{s,30m}$ is 350 m/s and HVSR indicates peaks around 2.4 Hz (T=0.42 sec) and 5.3 Hz (T=0.19 sec).
- Station 3138 (Figure 4.29) is located on either a very dense soil or a very soft rock site, where the $V_{s,30m}$ is 618 m/s and HVSR indicates peaks around 1.2 Hz (T=0.83 sec) and 4.3 Hz (T=0.23 sec).
- Station 4615 (Figure 4.30) is located on either a very dense soil or a very soft rock site, where the $V_{s,30m}$ is 484 m/s and HVSR indicates peaks around 1.5 Hz (T=0.67 sec) and 2.5 (T=0.4 sec) Hz for the 1st S-wave portion and relatively low frequency 0.4 Hz (T=2.5 sec) and 1.2 Hz (T=0.83 sec) peak for the 2nd S-wave portion.
- Station 4624 (Figure 4.31) is located on a stiff soil site, classified as a NERHP Site Class D ($V_{s,30m}$ = 280 m/s) and HVSR indicates peaks around 3 Hz (T=0.33 sec) and 5 Hz (T=0.2 sec) for the 1st S-wave packet and relatively low frequency 0.8 Hz (T=1.25 sec) and 2 Hz (T=0.5 sec) peak for the 2nd S-wave packet.

To summarize, when the HVSR is assessed from the first and second wave packets, different fundamental frequencies are estimated. This suggests a shift in site periods, which could be attributed to strain-dependent softening of individual soil layers, as well as the softening of the overall site. These factors, along with others are to be studied as part of more in-depth site response assessments. The use of the entire time series in the development of HVSR curves may have produce a wider range of amplified frequencies, which also requires further evaluations.

References

Akkar, S., Sandıkkaya, M.A., Şenyurt, M., Azari Sisi, A., Ay, B.Ö., Treversa, P., Douglas, J., Cotton, F., Luzi, L., Hernandez, B., Godey, S. 2014. "Reference Database for Seismic Ground Motion in Europe (RESORCE)". Bulletin of Earthquake Engineering, 12:311–339. https://doi.org/10.1007/s10518-013-9506-8

Akkar, S., Sandikkaya, M. A., Bommer, J. J. 2014c. "Empirical ground-motion models for point- and extended-source crustal earthquake scenarios in Europe and the Middle East". Bulletin of Earthquake Engineering, 12: 359–387. https://doi.org/10.1007/s10518-013-9461-4

Akkar, S., Kale, Ö., Yakut, A., Çeken, U. 2018. "Ground-motion characterization for the probabilistic seismic hazard assessment in Turkey", Bulletin of Earthquake Engineering, 16: 3439–3463. https://doi.org/10.1007/s10518-017-0101-2

Albayrak, K., Askan, A., Yerlikaya, F. 2023. "Ground Motion to Intensity Conversion Equations (GMICEs) for Turkey: Evaluation of Regional Differences with Parametric and Non-Parametric Regression Methods", [Working paper].

ASCE 7-16 (2017). "Minimum Design Loads and Associated Criteria for Buildings and Other Structures in Seismic Design Requirements for Building Structures: Structural Engineering Institute" (pp. 89-121). https://doi.org/10.1061/9780784414248

Atkinson, G., Silva, W., 2000. "Stochastic Modeling of California Ground Motions". Bulletin of the Seismological Society of America, 90(2), pp.255-274. https://doi.org/10.1785/0119990064

Bilal, M., Askan, A. 2014. "Relationships between felt intensity and recorded ground-motion parameters for Turkey". Bulletin of the Seismological Society of America, 104:1. https://doi.org/10.1785/0120130093

Boore, D. M., Bommer, J. J., 2005. "Processing of strong-motion accelerograms: needs, options and consequences". Soil Dynamics and Earthquake Engineering, 25 93-115. https://doi.org/10.1016/j.soildyn.2004.10.007

Boore, D. M., Sisi, A. A., Akkar, S. 2012. "Using pad-stripped acausally filtered strong-motion data". Bulletin of the Seismological Society of America, 102751-760. https://doi.org/10.1785/0120110222

Boore, D. M., Stewart, J. P., Seyhan, E., Atkinson, G. M. 2014. “NGA-West 2 equations for predicting PGA, PGV, and 5%-damped PSA for shallow crustal earthquakes”. Earthquake Spectra, 30: 1057–1085. https://doi.org/10.1193/070113EQS184M

Building Seismic Safety Council (BSSC) 2020. " NEHRP Recommended Seismic Provisions for New Buildings and Other Structures 2020 Edition". FEMA P-2082, Washington, D.C.

Chiou, B. S.-J., Youngs, R. R. 2008. “An NGA Model for the Average Horizontal Component of Peak Ground Motion and Response Spectra”, Earthquake Spectra; 24: 1: 173–215. https://doi.org/10.1193/1.2894832

Chiou, B. S.-J., Youngs, R. R. 2014. “Update of the Chiou and Youngs NGA model for the average horizontal component of peak ground motion and response spectra”. Earthquake Spectra, 30: 1117–1153. https://doi.org/10.1193/072813EQS219M

Douglas, J. 2003. “What is a poor quality strong-motion record?”. Bulletin of Earthquake Engineering, 1: 141-56. https://doi.org/10.1023/A:1024861528201

Douglas, J, Boore, D.M. 2011. “High-frequency filtering of strong-motion records”. Bulletin of Earthquake Engineering, 9: 395-409. https://doi.org/10.1007/s10518-010-9208-4

Erberik, M. A. 2008a. “Generation of fragility curves for Turkish masonry buildings considering in-plane failure modes”, Earthquake Engineering and Structural Dynamics, 37: 387–405. https://doi.org/10.1002/eqe.760

Erberik, M. A. 2008b. “Fragility-based assessment of typical mid-rise and low-rise RC buildings in Turkey”, Engineering Structures, 30: 1360–1374. https://doi.org/10.1016/j.engstruct.2007.07.016

Gülerce, Z., Kargıoglu, B., Abrahamson, N. A. 2016. “Turkey-adjusted NGA-W1 horizontal ground motion prediction models”. Earthquake Spectra, 32: 75–100. https://doi.org/10.1193/022714EQS034M

i4Works 2023. “SiteEye: Cloud-based Photogrammetry and Project Management”, [Computer Software]. Available from: https://siteeye.co [Last accessed on February 13, 2023]

Kale, Ö., Akkar, S., Ansari, A., Hamzehloo, H. 2015. “A ground-motion predictive model for Iran and Turkey for horizontal PGA, PGV and 5%-damped response spectrum: Investigation of possible regional effects”. Bulletin of the Seismological Society of America, 103: 963–980. https://doi.org/10.1785/0120140134

Kale Ö. 2019. "Some discussions on data-driven testing of Ground-Motion Prediction Equations under the Turkish ground-motion database. Journal of Earthquake Engineering, 23: 160–81. https://doi.org/10.1080/13632469.2017.1323047

Konno, K., Ohmachi, T. 1998. "Ground-motion characteristics estimated from spectral ratio between horizontal and vertical components of microtremor". Bulletin of the Seismological Society of America, 88: 1: 228–241. https://doi.org/10.1785/BSSA0880010228

Kotha, S.R., Weatherill, G., Bindi, D., Cotton, F. 2022. "Near-source magnitude scaling of spectral accelerations: analysis and update of Kotha et al. (2020) model", Bulletin of Earthquake Engineering, 20: 1343–1370. https://doi.org/10.1007/s10518-021-01308-5

Nakamura, Y. 1989. "A method for dynamic characteristics estimation of subsurface using microtremor on the ground surface". QR of Railway Technical Research Institute, 30: 25-33.

Nogoshi, M., Igarashi, T. 1971. "On the amplitude characteristics of microtremors". Journal of the seismological society of Japan, 24: 24-40 (in Japanese with English abstract).

Pizzaro 2017. "HOVSR (Version 2.0)". https://github.com/ppizarror/HOVSR [Downloaded on February 02, 2023]

Turkish Accelerometric Database and Analysis System (AFAD TADAS). Disaster and Emergency Management Presidency, Department of Earthquake, Ankara, Türkiye. https://tadas.afad.gov.tr/map [Last accessed on February 19, 2023].

Turkish Building Earthquake Code (TBEC) 2019. Ministry of Interior, Disaster and Emergency Management Presidency (AFAD), Ankara, Turkey.

Chapter 5. Geotechnical Findings and the Performance of Geo-Structures

Chapter Coordinators: Kemal Önder Çetin and Makbule Ilgaç

Main Contributors in alphabetical order:

- Abd Alhamed Arif, Civil Engineer Aleppo, Syria
- Alaa Elsaid, Middle East Technical University, Department of Civil Engineering, Ankara, Türkiye
- Ali Fırat Çabalar, Gaziantep University, Department of Civil Engineering, Gaziantep, Türkiye
- Alper Özmen, İnönü Univertsity Departmant of Civil Engineering, Malatya, Türkiye
- Alper Sezer, Ege University, Department of Civil Engineering, İzmir, Türkiye
- Arda Burak Ekmen, Harran University, Department of Civil Engineering, Şanlıurfa, Türkiye
- Arda Şahin, Middle East Technical University, Department of Civil Engineering, Ankara, Türkiye
- Aşkın Özocak, Sakarya University, Department of Civil Engineering, Sakarya, Türkiye
- Ayhan Gürbüz, Gazi University, Department of Civil Engineering, Ankara, Türkiye
- Berkan Söylemez, Middle East Technical University, Department of Civil Engineering, Ankara, Türkiye
- Berna Unutmaz, Hacettepe University, Department of Civil Engineering, Ankara, Türkiye
- Bilal Umut Ayhan, İstanbul Bilgi University, Department of Civil Engineering, İstanbul, Türkiye
- Çağlar Tuna, Yaşar University, Department of Civil Engineering, İzmir, Türkiye
- Candan Gökçeoğlu, Hacettepe University, Department of Geology Engineering, Ankara, Türkiye
- Cem Demir, Hacettepe University, Department of Civil Engineering, Ankara, Türkiye
- Cem Kıncal, Dokuz Eylül University, Department of Geological Engineering, & Geographical Information Systemsö İzmir, Türkiye
- Duygu Köksal, Department of Geographical Information Systemsö İzmir, Türkiye
- E. Ece Eseller Bayat, İstanbul Technical University, Department of Civil Engineering, İstanbul, Türkiye
- Elife Çakır, Middle East Technical University, Department of Civil Engineering, Ankara, Türkiye
- Erkut Sayın, Fırat University, Department of Civil Engineering, Elazığ, Türkiye
- Ertan Bol, Sakarya University, Department of Civil Engineering, Sakarya, Türkiye
- Eylem Arslan, Sakarya University, Department of Civil Engineering, Sakarya, Türkiye
- Eyyüb Karakan, Kilis 7 Aralık University, Department of Civil Engineering, Kilis, Türkiye
- Faik Cüceoğlu, The General Directorate of State Hydraulic Works Ankara, Türkiye
- Gizem Can, Royal Haskoning DHV Resilience& Maritime-BL Maritime & Water, Netherlands

- Gökhan Şahin, Hacettepe University, Department of Civil Engineering, Ankara, Türkiye
- Halil Murat Alğın, Harran University, Department of Civil Engineering, Şanlıurfa, Türkiye
- Hayri Güzel, Middle East Technical University, Department of Civil Engineering, Ankara, Türkiye
- Hilal Uğurlu, Ankara Yıldırım Beyazıt University, Department of Civil Engineering, Ankara, Türkiye
- Hüseyin Akkuş, Gazi University, Technology Faculty Department of Civil Engineering, Ankara, Türkiye
- İsmail Dinçer, Nevşehir Hacı Bektaş Veli University, Faculty of Engineering, and Architecture Department of Geology Engineering, Cappadocia Geological Heritage and Rock-Hewn Structures Application and Research Center
- Kemal Önder Çetin, Middle East Technical University, Department of Civil Engineering, Ankara, Türkiye
- Kübra Sertkaya, Fırat University, Department of Civil Engineering, Elazığ, Türkiye
- M. Murat Monkul, Yeditepe University, Department of Civil Engineering, İstanbul, Türkiye
- Makbule Ilgaç, University, of California, Civil and Environmental Engineering, Berkeley, USA
- Mehmet Göncü, Civil Engineer, Türkiye
- Mehmet Salih Keskin, Dicle University, Department of Civil Engineering, Diyarbakır, Türkiye
- Mehmet Türkezer, Middle East Technical University, Department of Civil Engineering, Ankara, Türkiye
- Mesut Gör, Fırat University, Department of Civil Engineering, Elazığ, Türkiye
- Metehan Başer, Abdullah Gül University, Department of Civil Engineering, Kayseri, Türkiye
- Moutasem Zarzour, Middle East Technical University, Department of Civil Engineering, Ankara, Türkiye
- Müge Akın, Abdullah Gül University, Department of Civil Engineering, Kayseri, Türkiye
- Muhammet Çınar, Kahramanmaraş Sütçü İmam University, Department of Civil Engineering, Kahramanmaraş, Türkiye
- Mustafa Kerem Kockar, Hacettepe University, Department of Civil Engineering, Ankara, Türkiye
- Mustafa Tolga Yılmaz, Middle East Technical University, Department of Engineering, Sciences Ankara, Türkiye
- Mutluhan Akın, Nevşehir Hacı Bektaş Veli University, Faculty of Engineering, and Architecture Department of Geology Engineering, Cappadocia Geological Heritage and Rock-Hewn Structures Application and Research Center
- Nihat Sinan Işık, Gazi University, Technology Faculty Department of Civil Engineering, Ankara, Türkiye
- Ogün Ozan Varol, Van Yüzüncü Yıl University, Department of Mining Engineering, Van, Türkiye
- Ömer Faruk Taş, Fırat University, Department of Civil Engineering, Elazığ, Türkiye
- Özgün Numanoğlu, Consultant Schnabel Engineering, Seattle WA, USA
- Özgür Yıldız, Malatya Turgut Özal University, Civil Engineering, Department Malatya, Türkiye

- Pelin Tohumcu Özener, Yıldız Technical University, Department of Civil Engineering, İstanbul, Türkiye
- Sallama Alosman, Gaziantep University, Department of Civil Engineering, Gaziantep, Türkiye
- Sedat Sert, Sakarya University, Department of Civil Engineering, Sakarya, Türkiye
- Selim Altun, Ege University, Department of Civil Engineering, İzmir, Türkiye
- Senem Tekin, Adıyaman University, Adıyaman, Türkiye
- Serhat Erinmez, i4 Construction Software Energy Education Consultancy Research and Development Ankara, Türkiye
- Seyhan Fırat, Gazi University, Technology Faculty Department of Civil Engineering, Ankara, Türkiye
- Soner Ocak, Tunge Proje, Ankara, Türkiye
- Sultan Kocaman Gökçeoğlu, Hacettepe University, Department of Geomatics Engineering, Ankara, Türkiye
- Taha Taşkıran, Ankara Yıldırım Beyazıt University, Department of Civil Engineering, Ankara, Türkiye
- Tolga Çan, Çukurova University, Department of Geological Engineering, Adana, Türkiye
- Tuğçe Başer, University, of Illinois Urbana-Champaign Department of Civil Engineering, Urbana IL, USA
- Volkan Kalpakcı, Hasan Kalyoncu Univesity Gaziantep, Türkiye
- Yaren Birşen, İstanbul Technical University, Disaster Management Institute İstanbul, Türkiye

5. 1. Geotechnical Observations

This chapter presents the preliminary findings of ongoing geotechnical reconnaissance studies after the earthquakes. Several geotechnical reconnaissance teams were mobilized to the field to collect and document perishable data. More specifically, these discussions will focus on the documentation and preliminary assessments of geotechnical aspects observed at 12 cities in the region, namely Kahramanmaraş, Gaziantep, Diyarbakır, Malatya, Elazig, Adıyaman, Hatay, Mersin, Sanliurfa, Kilis, Osmaniye, and Kayseri, along with findings from Republic of Syria. Discussion topics include: i) seismic soil liquefaction, ii) rockfalls, iii) landslides, iv) retaining structures, v) deep excavations, vi) foundations, and the seismic performance of vii) earth dams, viii) harbors, ix) airports, and x) tunnels. Also, as part of discussions, the use of photogrammetry and remote sensing techniques in reconnaissance assessments are also presented.

5. 1. 1. Kahramanmaraş

Kahramanmaraş, at 37.75° N 36.95° E and 67-meter elevation, is a city with more than a million population in the southern-central Türkiye and lies in one of the most seismically active regions in the country (GDDA 2019). It is within the zone of influence of the Bitlis Thrust Zone, East Anatolian Fault Zone (EAFZ), and the Dead Sea Fault Zone (DSFZ) in southern-central Türkiye, located at the junction of African, Anatolian, and Arabian plates in southern-central Türkiye. The city and its vicinity are located in an area, where the potential of destructive earthquakes is high due to the influence of the EAFZ and the DSFZ (Biricik and Korkmaz 2001). The city has an area of 25.622 hectars, and the urban settlement is located within the Kahramanmaraş thrust system (Akil and Ecemis 2011).

The collision along Arabian and Anatolian Plates formed the Kahramanmaraş territory. The basin was filled out by heavy alluvial sediments and dense turbiditic flysch sequences (Sengor and Yilmaz, 1981; Karig and Kozlu, 1990). The area is surrounded by active faults of the EAFZ (i.e., Surgu Segment, Savrun Segment, Cardak Segment, Toprakkale Segment, Cokak Segment, Amanos Segment, and Golbasi Segment), Kahramanmaraş Fault Zone, Engizek Fault Zone, and Narli segment of the Dead Sea Fault Zone (DSFZ) (Palutoglu and Sasmaz, 2017).

Kahramanmaraş is a tectonic-based alluvium plain, whose boundaries are under the control of fault lines. The length of Kahramanmaraş plain lying between Cimen and Ahir Mountains is 40 km, and the width from north to south is nearly 20 km. Gul et al. (2005) suggest that limestone and claystone deposits can be found in the basin, on top of which lies shallow marine deposits.

Regarding the fault rupture in Kahramanmaraş, it was observed that, the Amanos segment located in the south of the Pazarcık segment was ruptured. This is confirmed with field observations. The damage levels in Nurdağı, Islahiye, Hassa, and Kırıkhan located on the Pazarcık and Amanos segments are attributed to fault displacements along with many other factors.

As part of the Türkoğlu-Narlı State Road Survey and Project (13), geological units were identified and listed starting from the oldest to the youngest as; Late Oligocene aged Ophiolithic rocks (Ktohd) consisting of Peridotite, Harzburjit, Dünit, Serpentine interleaved Basalt-Basalt Lava, Middle Miocene aged Yavuzeli Bazaltı (Tmy) formed by Agglomerates, Clayey, gravel, silty SAND/ silt, sandy, blocky pebbles, sandy, silty clay /clayey silt feature Quaternary aged Alluviums (Qa). The dominant unit in the region is Alluvium.

The project route is quite often interrupted by streams. The most important surface waters that cut the route along the project route are the irrigation/drying channel at Km: 1+650, the DSI irrigation channel at Km: 3+730, the irrigation channels at Km: 16+612 and Km: 16+720, the Aksu stream at Km: 18+210 and Km: 18+265, and apart from these waters, there are also many irrigation/drying channels that cut the route or continue parallel to the route.

Kahramanmaraş is located at the western end of the orogenic belt, known as the Bitlis-Zagros dock belt in the south-southeast of Türkiye in a highly complex system where oceanic crust and continental crust are intertwined with tectonics. The area in which the study area is located is divided into four zones (Righi and Cortesini, 1964). These belts are the Orogenic Belt, the Edge Bends Belt, the Fold Belt, and the Front Country from north to south. The study area is located on the Orogenic belt and the Edge folds belt.

5. 1. 1. 1. City Center of Kahramanmaraş

In Kahramanmaraş city center, no significant geotechnical-related damage was reported. The totally collapsed buildings were concentrated in the southern parts of the city. Many deep cracks were observed in the road route along the villages of Kocalar, Öksüzlü, Tevekkeli and Kapıçam (Fig. 5.1). Many buildings in the villages were either damaged with manifestations of severe cracking or collapsed. Electric poles on the same road routes were folded (Fig. 5.2).

Rock falls were also observed on the same road (Fig. 5.3). Some pictures from geotechnical and road structure damages are given in Fig. 5.4-5.8.

Figure 5.1. Cracks on the roads along Tevekkeli village photo by Dr. Eyyüb Karakan

Figure 5.2. Electric poles on the roads folded by Tevekkeli village photo by Dr. Eyyüb Karakan

Figure 5.3. Rockfalls observed in Tevekkeli village photo by Dr. Eyyüb Karakan

Figure 5.4. Translational slides observed on northern highway in Kahramanmaraş city center photo by Dr. Muhammet Çınar

Figure 5.5. Liquefaction-induced slope instability of a retaining wall by State Hydraulic Works Canal in Kahramanmaraş city center photo by Dr. Volkan Kalpakçı

Figure 5.6. Fault offset on Kahramanmaraş – Gaziantep Road photo by Dr. Volkan Kalpakçı

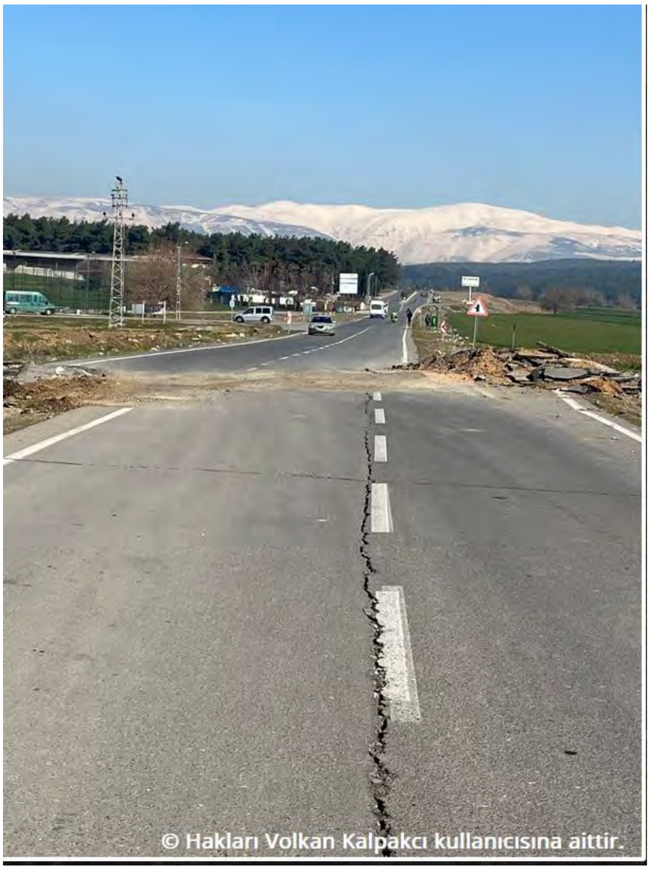

Figure 5.7. Fault offset on Kahramanmaraş – Gaziantep Road photo by Dr. Volkan Kalpakçı

Figure 5.8. Fault offset on Kahramanmaraş – Gaziantep Road photo by Prof. Dr. Selim Altun

5. 1. 1. 2. Afşin

No major geotechnical-induced damage features were observed in the Afşin city center. The damage was mainly due to poor construction quality and lack/inadequacy of structural element lateral capacity. Some examples of partially collapsed buildings are shown in Figures 5.9 and 5.11 in Afşin city center.

Figure 5.9. Heavily damaged buildings – Afşin city center

Figure 5.10. Shear cracks on partition walls– Afşin city center

Figure 5.11. Heavily damaged buildings – Afşin city center

5. 1. 1. 3. Elbistan

The district of Elbistan, which is approximately 140 kilometers away from the city center of Kahramanmaraş, is surrounded by Darende, Malatya in the north, Ekinözü in the south, Afşin in the west and Akbayır districts in the east.

No geotechnical damage was observed in and around Elbistan. This is mostly due to the snow covering the area. The surface manifestations of lateral spread and/or liquefaction were covered by snow. The damage was mainly due to poor construction quality and lack/inadequacy of structural elements, some examples are presented in Figures 5.12-5.15.

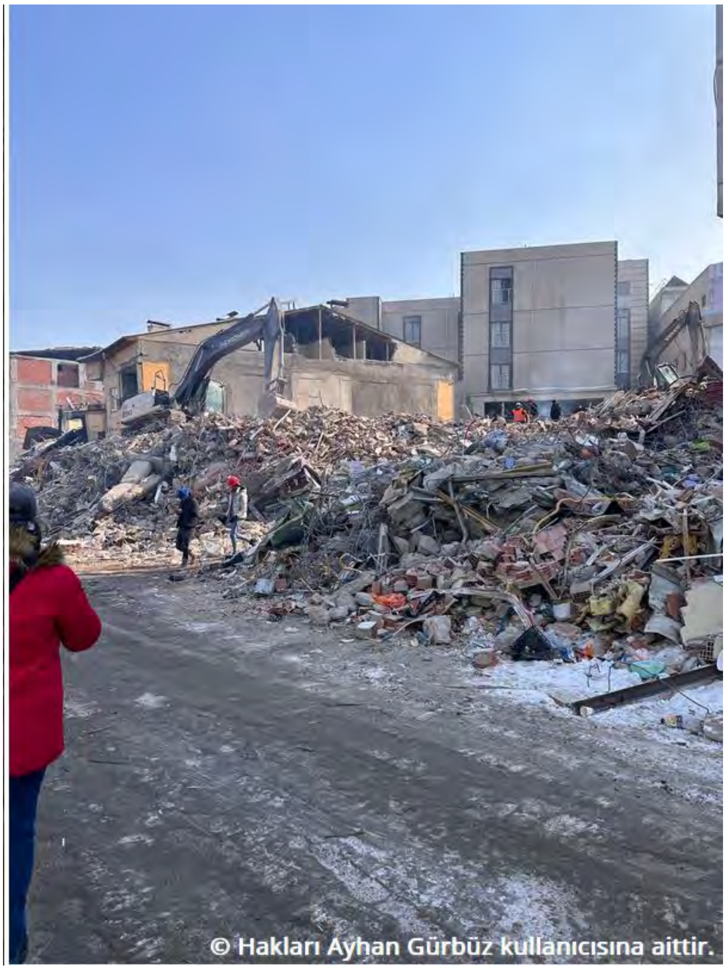

Figure 5.12. Collapsed buildings – Elbistan city center.

Figure 5.13. Collapsed building – Elbistan city center.

Figure 5.14. Heavily damaged residential building – Elbistan city center

Figure 5.15. Pancaked ground floor – Elbistan city center.

On the road from Elbistan to Malatya, there were no significant manifestation of geotechnical-induced failures or features. No ground cracks, no slope failures, etc. were observed along the road. The retaining walls by the benches of (about 5 m high), and the slopes behind the walls were not damaged as can be seen in Figure 5.16.

Figure 5.16. Stable retaining wall – Elbistan-Malatya Road

5. 1. 1. 4. Pazarcık

The district of Pazarcık, which is approximately 47 kilometers from the city center of Kahramanmaraş, is surrounded by Çağlayancerit in the north, Gaziantep Yavuzeli, Şehitkamil and Nurdağı in the south, Türkoğlu in the west and Adıyaman, Gölbaşı, Besni and Araban districts in the east.

In the Pazarcık district, which is very close to the epicenter of 6 February 2023 M_w:7.8 earthquake, rock units from the Upper Eocene to the Maestrichtian crop out on the site (Sümegen, 2014). Some part of the district is also located on the Quaternary alluvial deposits. Surface faulting is clearly visible on the rock units. Structural damages due to surface faulting were observed in the district center and villages. Quaternary-aged alluvial deposits contributed to elevated structural damage.

Lateral spreading is observed on alluvial soils along the stream bed in Çöçelli district, Adana-Şanlıurfa highway Narlı entrance location (Fig. 5.17). In addition, ground deformations were apparent along the access road pavements on alluvial sediments (Fig. 5.18). The bridge crossing was affected due to large lateral spreading (Fig. 5.19).

Rock mass failures due to rockfall were observed on the slopes along the road crossings in the Çöçelli neighborhood, which is close to the epicenter of the February 6, 2023 (M_w:7.7) earthquake (Fig. 5.20).

In the city center, the damage was mainly due to poor construction quality and lack/inadequacy of structural elements. Some examples of partially collapsed buildings are shown in Figure 5.21 in the Pazarcık city center. Some geotechnical structures protected its stability during earthquakes (Figure 5.22).

Figure 5.17. Lateral spreading observed in Pazarcık

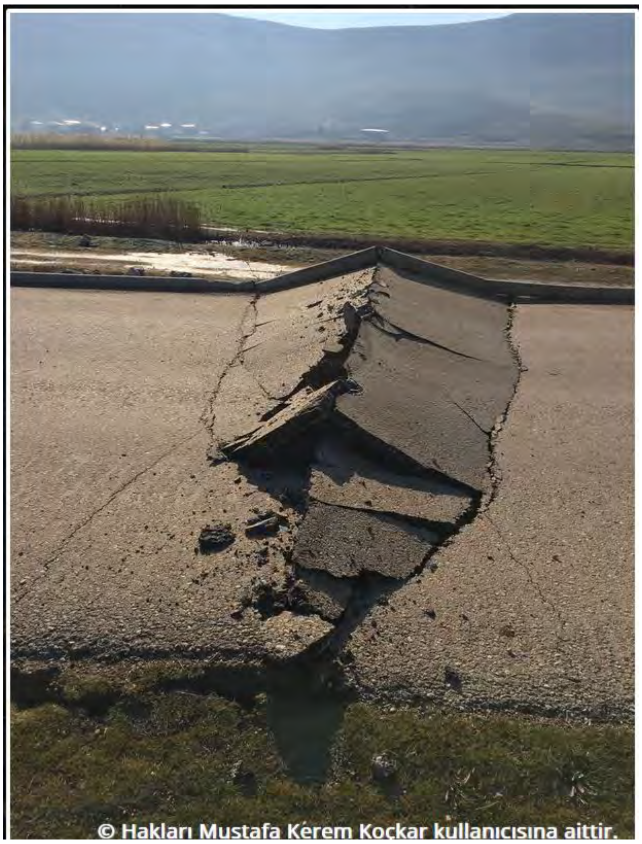

Figure 5.18. Compression cracks observed in Pazarcık

Figure 5.19. Lateral spreading along the road in Pazarcık

Figure 5.20. Rock falls observed in Pazarcık

Figure 5.21. A partially collapsed building in Pazarcık

Figure 5.22. Safe retaining wall in Pazarcık Photo by Prof. Dr. Selim Altun

5. 1. 1. 5. Türkoğlu

Türkoğlu district, which is located 22 km south of Kahramanmaraş province, is adjacent to Kahramanmaraş city center in the north, Nurdağı of Gaziantep province in the south, and Pazarcık districts of Kahramanmaraş province in the east.

In the west of the district, a Paleozoic basement and overlying Mesozoic deep marine sediments and carbonate rock series with a predominance of ophiolitic rocks were outcropped. In the district center and east of the district, Quaternary aged alluvial deposits were deposited in an approximately NE-SW trending plain (Gül, 2000).

Traces of surface faulting formed along the EAFZ as a result of February 6, 2023, Kahramanmaraş earthquakes are clearly observed in the NE_SW trending in the Quaternary aged alluvial units along the Türkoğlu -Nurdağ (D825) main highway route from the east of the district center. Since a significant part of the district is located on alluvial deposits, structural damage was documented in the city center and the industrial area in the south and north.

Lateral spreading (Fig. 5.23) and liquefaction manifestations (Fig. 5.24) were observed at the irrigation dam road crossing located on the Aksu Stream in the northeast of the district, respectively. Lateral spreading was also encountered at the railway crossing on the east side of the river (Fig. 5.25). Damages also occurred in the retaining structure of the water channel passing through the district (Fig. 5.26).

Along the road crossing connecting the Yeşilyurt neighborhood of the Türkoğlu district to the Şekeroba neighborhood, rockfalls on the side slopes and structural damage along the highway were observed (Fig. 5.27).

Figure 5.23. Liquefaction in free field

Figure 5.24. Lateral spreading

Figure 5.25. Lateral spreading

Figure 5.26. Lateral spreading

Figure 5.27. Landslide

5. 1. 2. Gaziantep

Gaziantep Basin is located at 37.08 N 37.36 E and 855 m elevation. It has a population of about 2,5 million, situated in southern Türkiye, to the south of the suture zone formed due to the collision of the Arabian and Anatolian plates in late Cretaceous (Maastrichtian) and Miocene times (Coskun and Coskun, 2000). From the studies Rigo de Righi and Cortesini (1964), Terlemez et al. (1992), and Robertson (2000), it can be concluded that the region entails autochthonous units and allochthonous units. Basic seismicity: Following the analysis of historical earthquakes through northern part of the Dead Sea Fault (DSFZ) and the East Anatolian Fault (EAF), the most probable locations of disastrous earthquakes in these zones were predicted for the 21st century (Balakani and Moskvina, 2004). Furthermore, the study of Westaway (2003) on the Kinematics of the Middle East and Eastern Mediterranean noted that the seismicity on the region, which behaves as a 'geometrical lock', appears to provide a possible basis for an advance warning system of future destructive earthquakes on the North Anatolian Fault (NAF).

The region entails autochthonous units as well as allochthonous units. Allochthonous units that outcrop in Gaziantep are the Karadut Complex, the Koçali Complex, and the Hatay Ophiolite Nappe that tectonically overlies the Karadut and Koçali Complexes. The Maastrihtiyen-Lower Miocene autochthonous units are represented by an 1800 m thick sequence. The autochthonous units are the Besni formation, German formation, Gercis¸ formation, Ardıçlı Tepe formation, Hoya formation and Upper Eocene-Oligocene aged Gaziantep formation. The Oligocene-Lower Miocene aged Fırat formation, which is composed of reef limestones, unconformably overlies these units. The Middle-Upper Miocene Şelmo formation, Upper Miocene Yavuzeli Basalt, and Pliocene aged Harabe formation are emplaced over the older units with an unconformity (Terlemez et al., 1992). The general distribution or deposition of lithology within the boring logs appeared to be relatively variable due to the presence of different units ranging from recent alluvial sedimentary units to competent rock in the central districts of Gaziantep. It should be noted that the thickness of alluvium varies between 5 and 15 m from the surface.

The lithologies were spatially differentiated based on geotechnical and seismic data obtained from the compiled boreholes (i.e., standard penetration test results, SPT-N) and seismic measurements (i.e., shear wave velocity). For the site characterization study, the data from 1450 borings along with the standard penetration test results were classified as soil and rock information as a function of depth based on the characteristics of the depositional setting.

Similarly, the near-surface seismic measurements of the shear wave velocities were compiled with existing data from 262 locations that were obtained from previous studies in Quaternary alluvial to Upper Miocene sediments. Then, the V_{S30} results have been directly determined from these seismic field survey measurements. The estimated V_{S30} values have been calculated based on the empirical correlations from reliable index measurements according to the SPT-N. The calculated V_{S30} values were verified with the V_{S30} results compiled from the seismic measurements in the field. In summary, the estimated V_{S30} values compiled from the direct field measurement locations in the project area have been determined considering the near-surface geologic units in the region. As a result, the mean V_{S30} value for the Quaternary Alluvium deposits is 493 m/s (range varies between 420-550). The mean values for the rock units are 670 (Sandstone-conglomerate-limestone; range: 600-750) and, 810 (Limestone; range: 760-850) and 905 m/s (Basalt; range: 760-1050), respectively from younger to older rock units (Kelam et al., 2022).

Field visit covering Gaziantep was carried within the first week after the two consecutive earthquakes and site observations were made by researchers. The first findings regarding these observations are presented in this report. Within the scope of the field study, important engineering structures in the region, soil behavior such as landslide, slope failure, liquefaction, lateral spreading and surface fracture, and damage to buildings were observed.

As a result of the geological studies carried out within the scope of Gaziantep-Nizip-Birecik State Road, Yavuz Sultan Selim Overpass Bridge Project (7), the units surface along the project area and its immediate surroundings are Alluvial (Qa), Colluvium (Qc) and Gaziantep Formation (Tmga). In the project area, only Gaziantep Formation (TMGA) is being surfaced.

Within the scope of the project, two 30 meters long boreholes were drilled. In SK – 1 drilling; between depths of 0 – 0,80m; vegetative soil; between depths of 0,80 – 15,00m; light coffee-beige colored, low-medium hard, medium-medium weak strength, low-moderately decomposed. Thin-medium layered, clay-limestone units are cut. No groundwater was observed in this drilling. In SK – 2 drilling; between depths of 0 – 2,10m; amixture of vegetable soil and high plasticity, coffee-coloured very solid clay and at depths of more than 2,10m; beige- off-white colored, friable - medium hard, medium - very decomposed, clay - limestone units are cut. No groundwater was observed in this drilling. As a result of the studies carried out, it was evaluated that the ideal ground profile of the foundation ground where the bridge legs will sit consists of small – medium decomposed and medium – weak strength clay limestone units.

The evaluations observed in the field as a result of the geotechnical and mass movements on the sediments in Nurdağı and İslahiye-Fevzipaşa districts in Gaziantep are presented below.

5. 1. 2. 1. City Center of Gaziantep

Local authorities have recently stated that at least 25 multi-story buildings collapsed in the city center due to the consecutive earthquakes (Fig. 5.28). A few collapsed one-story buildings in the villages close to the city center were observed (Fig. 5.29). Slope failures caused by the earthquakes were observed both in the city center (Fig. 5.30) and its vicinity area (Fig. 5.31). Liquefaction was not observed in the areas, where liquefaction was likely expected due to the presence of high groundwater level and silt/sand/gravel with low density (Fig. 5.32). Walls of the Gaziantep Castle, whose history dates back to the Hittite Empire, was severely damaged by the two consecutive earthquakes. However, no serious damage was observed on the slopes (greater than about 45°) carrying the castle walls. This gave the impression that the geogrid application made a few years ago on the slopes was found to be quite successful (Fig. 5.33).

Figure 5.28. An 8-storey building collapsed in the city (Coordinates; 37.0824, 37.3269). Photo by Prof. Dr. Ali Fırat Çabalar

Figure 5.29. A 1-storey building collapsed in the village Akpinar (Coordinates; 37.0370, 37.1767). Photo by Prof. Dr. Ali Fırat Çabalar

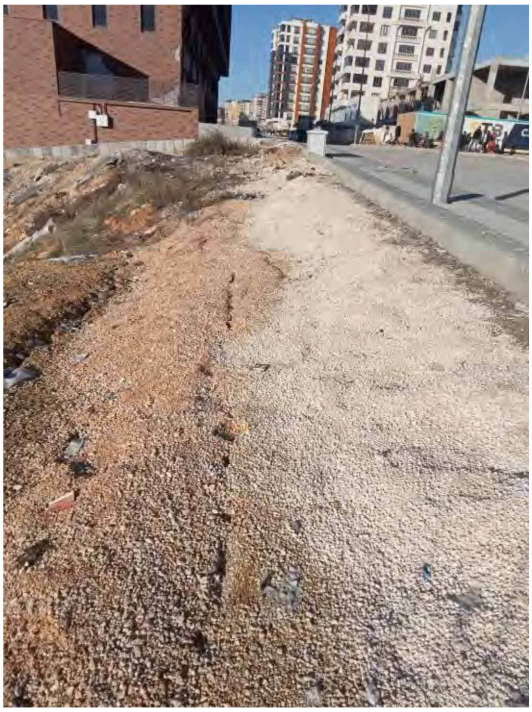

Figure 5.30. A slope failure in the city center (Coordinates; 37.0793, 37.3237). Photo by Prof. Dr. Ali Fırat Çabalar

Figure 5.31. A slope failure in the vicinity area (Coordinates; 37.0209, 37.1509). Photo by Prof. Dr. Ali Fırat Çabalar

Figure 5.32. Non-liquefied area (Coordinates; 37.0628, 37.3363). Photo by Prof. Dr. Ali Fırat Çabalar

Figure 5.33. Gaziantep castle (Coordinates; 37.0665, 37.3832). Photo by Prof. Dr. Ali Fırat Çabalar

In Gaziantep, one of the cities most affected by the 7.7 and 7.6 magnitude earthquakes that occurred in Kahramanmaraş and affected 11 provinces, a giant sinkhole was formed in Aydın Baba Park, located in Şenyurt suburb, Derinçukur street in Şahinbey district. As the park collapsed with the force of the earthquake, the surrounding houses were also damaged. The sinkhole in the park is approximately 30 meters long, 8 meters wide and 10 meters deep (Fig. 5.34).

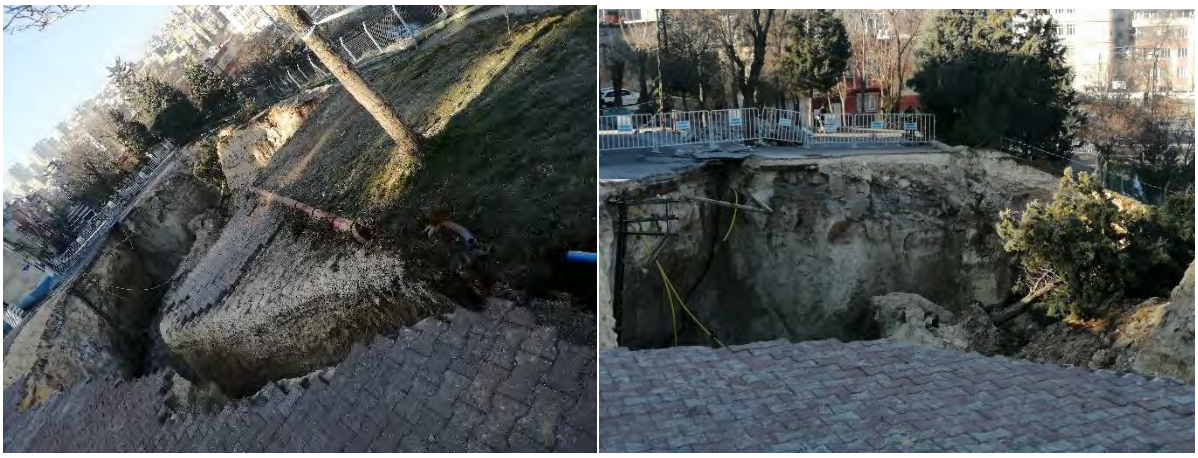

Figure 5.34. Sinkhole in Aydınbaba park, Derinçukur Street, Şahinbey district in Gaziantep Photo by Assist. Prof. Dr. Eyyüb Karakan

5. 1. 2. 2. Nurdağı

The district of Nurdağı, which is approximately 68 kilometers from the city center of Gaziantep, is surrounded by Turkoğlu, Kahramanmaraş in the north, Islahiye in the south, Osmaniye district in the west and Gaziantep districts in the east.

The damage was mainly due to poor construction quality and lack/inadequacy of structural elements in City center of Nurdağı. Some geotechnical damage was observed surrounding the city center. An example of partially collapsed buildings are shown in Figures 5.35 in the Nurdağı city center.

The Nurdağı region and its surroundings vary in terms of geological features. Paleozoic, Mesozoic, Tertiary, and Quaternary aged rock and soil units are encountered in the region. Surface faulting, which is the primary effect of the earthquake, is visible on the rock units. Structural damages due to surface faulting have been effective in the district center and villages. The Quaternary-aged alluvial deposits were also effective in increasing structural damage due to their loose soil characteristics.

Large deformations and settlements occurred in the access road pavements on the rock units due to surface rupturing in the Nurdağı district (Figure 5.36).

Large mass failures due to landslides and rockfalls were encountered at the Kahramanmaraş-Gaziantep (D825) main road crossing and on the slopes of the village roads in the Belpınar neighborhood of Nurdağı district of Gaziantep (Figure 5.37).

Rock mass failures due to rockfalls were observed along the slopes on the Gaziantep Osmaniye Road (D400) to the east of Nurdağı (Figure 5.38).

Figure 5.35. Heavily damaged building

Figure 5.36. Surface rupture in Nurdağı

Figure 5.37. Rock debris flows in Nurdağı

Figure 5.38. Rockfalls in the Nurdağı

Figure 5.39. Bridge failure on the highway between Nurdağı and Turkoğlu

,

Figure 5.40. Retaining structure failure

Observations at Bahçe Railway Underpass: The construction of the underpass that will connect the Osmaniye Bahçe district to the Osmaniye - Gaziantep Road continues. Although the construction works are not completed yet, no damage was observed in the piled excavation support system. A jet grout base curtain was designed and under construction during earthquakes. No significant deformations or failures was observed in the reinforced earth wall and panels, built for the main road embankments (Figs. 5.41& 5.42).

Figure 5.41. Bahçe Railway Underpassage Photo by Prof. Dr. Kemal Önder Çetin and Prof. Dr. Candan Gökçeoğlu

Figure 5.42. The reinforced earth wall. Photo by Prof. Dr. Kemal Önder Çetin and Prof. Dr. Candan Gökçeoğlu

Bahçe-Nurdağı Railway Tunnels Bahçe Portal:

The longest railway tunnels in Türkiye, with a length of approximately 10 km, are between Bahçe and Nurdağı. T2 tunnel has been completed and excavations of T1 tunnel are about to be completed with TBM. TBM will exit from the Bahçe Portal. Starting from Bahçe Portal, an approximately 1200 m long cut-and-cover tunnel passage located under the Adana - Gaziantep State Highway was designed. Cut-and-cover tunnels were completed, and some sections of the TBM is supported by struts and kept waiting for the extraction. However, the Bahçe exit portal is in a paleo landslide. Conventional railway passage approximately 15 m above the portal, is located at just north of the cut-cover tunnel and Adana-Gaziantep State Highway to the south. As a result, investigations were made in the portal area, where many buildings are present in a narrow area along the route.

As can be seen from the Figure 5.43, no damage was observed at cut-and-cover tunnel exit section and the reinforced concrete support walls.

Figure 5.43. Cut-and-cover tunnel Photo by Prof. Dr. Kemal Önder Çetin and Prof. Dr. Candan Gökçeoğlu

The photo in Figure 5.44, is taken from an angle extending from west to east, showing the TBM exit portal, the conventional railway line is running just above it. An L-shaped retaining wall was constructed between the top of the portal and the conventional railway. A small landslide occurred, but the retaining wall prevented the landslide from continuing, preventing damage to both the portal and the conventional railway (Fig. 5.44).

Figure 5.44. A small landslide occurred. Photo by Prof. Dr. Kemal Önder Çetin and Prof. Dr. Candan Gökçeoğlu

Struts (steel pipes) were designed to support pile elements in Bahçe. A certain section of the cut-and-cover tunnel built right in front of the garden portal is temporarily supported by struts and kept open for the removal of the TBM, which is currently being excavated in the tunnel. As can be seen from the photos below, all struts performed well as designed and no damage was occurred (Figs. 5.45 & 5.46).

Figure 5.45. A certain section of the cut-and-cover tunnel Photo by Prof. Dr. Kemal Önder Çetin and Prof. Dr. Candan Gökçeoğlu

Figure 5.46. Cut-and-cover tunnel supported by struts. Photo by Prof. Dr. Candan Gökçeoğlu and Prof. Dr. Kemal Önder Çetin

Various rockfalls and failures caused by local discontinuity were observed in the metamorphic blocky rock masses on the slopes of the State Highway between Bahçe and Nurdağı. In the photo below, the block falls observed on the northern slope of Bahçe-Nurdağı Highway can be observed (Fig. 5.47).

Figure 5.47. Rockfall at Bahçe-Nurdağı Highway. Photo by Prof. Dr. Candan Gökçeoğlu and Prof. Dr. Kemal Önder Çetin

Failures were observed in the road embankment and the stone wall supporting the embankment between Bahçe and Nurdağı. These changes can be seen in the photos below (Figs. 5.48-5.49).

Figure 5.48. Failures in the road embankment and the stone wall supporting the embankment between Bahçe and Nurdağı. Photo by Prof. Dr. Kemal Önder Çetin and Prof. Dr. Candan Gökçeoğlu

Figure 5.49. Failures in the road embankment and the stone wall supporting the embankment between Bahçe and Nurdağı. Prof. Dr. Candan Gökçeoğlu and Prof. Dr. Kemal Önder Çetin

Figure 5.50. Failures in the road embankment and the stone wall supporting the embankment between Bahçe and Nurdağı. Photo by Prof. Dr. Kemal Önder Çetin and Prof. Dr. Candan Gökçeoğlu

Surface ruptures and landslides triggered by many landslides were observed around Gökçedere village of Nurdağı district (Figs. 5.51-5.54).

Figure 5.51. Surface ruptures and landslides around Gökçedere. Prof. Dr. Candan Gökçeoğlu and Prof. Dr. Kemal Önder Çetin

Figure 5.52. Minor surface ruptures around Gökçedere. Prof. Dr. Candan Gökçeoğlu and Prof. Dr. Kemal Önder Çetin

Figure 5.53. Fault ofsett across a village graveyard. Photo by Prof. Dr. Kemal Önder Çetin and Prof. Dr. Candan Gökçeoğlu

Figure 5.54. Minor surface ruptures around Gökçedere. Photo by Prof. Dr. Candan Gökçeoğlu and Prof. Dr. Kemal Önder Çetin

No damage was observed at the portal of the Bahçe-Nurdağı tunnels. However, some rockfalls are observed. However, the surface fracture passes approximately 50 m in front of the portal (Fig. 5.55).

Figure 5.55. The portal of the Bahçe-Nurdağı tunnels. Photo by Prof. Dr. Candan Gökçeoğlu and Prof. Dr. Kemal Önder Çetin

5. 1. 2. 3. Islahiye

The district of Islahiye, which is approximately 91 kilometers from the city center of Gaziantep, is surrounded by Nurdağı in the north, Hassa, Hatay in the south, Osmaniye district in the west and Gaziantep and Kilis districts in the east.

The damage was mainly due to poor construction practices and inadequacy of lateral structural element capacity in city center of Islahiye. Some geotechnical damage was observed surrounding the city center. Some examples of partially collapsed buildings are shown in Figures 5.56 and 5.57 in the Islahiye city center.

Islahiye State Hospital did not suffer from damage during earthquake despite it is proximity to the fault rupture (Fig. 5.58-5.59)

Figure 5.56. Partially collapsed building in Islahiye

Figure 5.57. Settled building in Islahiye

Figure 5.58. Deformed surface concrete panels in front of Islahiye State Hospital

Figure 5.59. No structural damage in Islahiye State Hospital. Minor cracks at infill walls

Approximately north-south trending surface ruptures are commonly observed in Islahiye district. The rupture passing in front of the Islahiye State Hospital cuts the railway to the south. In addition, flowering was observed on the natural ground. Left lateral displacement was clearly observed in the surface fractures (Figs. 5.60-5.63).

Figure 5.60. Surface rupture Photo by Prof. Dr. Candan Gökçeoğlu and Prof. Dr. Kemal Önder Çetin

Figure 5.61. Fault rupture. Photo by Prof. Dr. Candan Gökçeoğlu and Prof. Dr. Kemal Önder Çetin

Figure 5.62. Fault rupture and flowering surface manifestations. Photo by Prof. Dr. Kemal Önder Çetin and Prof. Dr. Candan Gökçeoğlu

Figure 5.63. Fault offset. Photo by Prof. Dr. Candan Gökçeoğlu and Prof. Dr. Kemal Önder Çetin

Mass failures due to rockfall were observed on the slopes parallel to the railway in the Fevzipaşa neighborhood of the Islahiye district (Fig. 5.64). In addition, along the water channel on the same route, the retaining structure collapsed towards the channel for approximately 150 m due to lateral spreading (Fig. 5.65).

Large deformations occurred on the railway in the Fevzipaşa region due to surface rupturing. Large tension cracks at the crown of the landslide were encountered along the cut slope to the east of the station (Fig. 5.66). In a certain section, the retaining structure along this landslide was also destroyed and tilted due to the sliding movement.

Figure 5.64. Rockfalls in Islahiye

Figure 5.65. Lateral spreading in Islahiye

Figure 5.66. Slope slides in Islahiye

5. 1. 3. Diyarbakır

The city area is composed of 5 geological formations. They are divided into two groups as soil and rock. The soil sites are composed of Yeniköy Formation, which is clay and silt layers, Gölpınar Formation which is sandstone, and quaternary aged old and new alluviums. The rock sites are described by some basalt units of Karacadağ Volcanism. In the field studies carried out in Diyarbakır, surface manifestations of geotechnical problems (liquefaction, settlement, etc.) were observed. The geological profile in the city is generally composed of rock. The collapses were mostly attributed to structural design and material defects. No damage was observed in the retaining structures in the city center. Also, slope stability and liquefaction were not observed.

In and around Diyarbakır, the Miocene-Pliocene aged Shelmo Formation and the Quaternary aged Karacadağ volcanites are available. Karacadağ volcanites are incompatible on the Upper Miocene-Pliocene aged Shelmo Formation, which consists of pebbles, sandstones, and mudstones.

As a result of the geological studies carried out within the scope of the State Road Junction Underpass Bridge (11) Project, it was seen that the idealized ground profile included fills extending to a depth of approximately 1.5m from the surface, high-strength basalt up to a depth of 11.3m and then low-strength consolidated - claystone units.

When the results obtained in the drilling carried out within the scope of the Air Regiment Interchange Bridge (12) project were examined, it was seen that the idealized ground profile is composed of fills extending to a depth of approximately 1.5m from the surface, silty hard clay up to a depth of 10.8m, altered basalt with gravel block size between 10.8m and 13.7m and then low-strength concubine - claystone units.

5. 1. 4. Malatya

The Malatya region is composed of geologically metamorphic rocks. Paleozoic, Mesozoic, and Tertiary age Arabic platform autochthonous sediments are represented by the best studied and defined platform type sediments in Türkiye paleontologically and lithologic ally, and which have not undergone metamorphism. The allochthonous units that settled on the metamorphics of the Arabian Platform and Pütürge were later settled in the form of gravitational shifts with the rise of this massif. Allocton units include ophiolite-type oceanic mantle and shell material and their pelagic deep-sea sediments, as well as continental slope sediments of the "Pacific Arabian Platform".

In the drilling carried out within the scope of the Malatya Northern State Road Project (14), it was observed that the terrestrial sediments surface in the examination area belong to the completely separated siltstone-sandstone-pebbles-conglomerate units within the Beylerderesi formation and that these units are mostly rocks. The dissociated units are mostly ground and have been observed to consist of large pebbles of irregular size in places. The unit that has a weak binding feature among the pebbles is the clay units. Since the clay units have weak binding properties, it causes the pebbles in the pebble-conglomerate units to disperse and not to have the nature of rock. Pebbles are usually semi-round and half-cornered, usually limestone, dolomite origin. It was determined that the claystone-siltstone and sandstone units were again weak bindings and surfaced as decomposed-residual grounds. In the study area, it was also seen that in the Km: 20 + 288.300 section, which was determined as weak zone, the alluvial units including pebble, sand, silt, and clay size units were surfaced at the upper levels. Groundwater levels of varying levels (1-17m) have been determined in the boreholes.

For the structure projected in the Hekimhan West State Road region within the scope of the Hekimhan Bridge Project (16), first of all, the type of structure and foundation was decided. In the research studies, it was observed that the idealized ground profile was slope rubble up to a depth of 10 m from the surface for SK-1, 0.45 m from the surface for SK-2 and 5.2 m from the surface for SK-3. After the aforementioned depths, limestone was seen in all boreholes.

There was no damage to the retaining structures located on the Elazığ and Malatya highway as seen in Figure 5.67. Also, insignificant slope stability was seen (Figure 5.68). Large cracks were not observed on the Elazığ-Malatya highway and in the Malatya city center. Only small cracks were observed in the roads of Malatya, as seen in Figure 5.69. It can be said that geotechnical problems such as submersion, swelling, liquefaction etc., were not observed in the Malatya city center. Due to the old building stocks, structural design and material defects, some residential structures were heavily damaged or collapsed.

Figure 5.67. Elazığ-Malatya highway (Kömürhan Bridge-Photo by Erkut Sayın)

Figure 5.68. Elazığ-Malatya highway (Photo by Mesut Gör)

Figure 5.69. Road conditions in Malatya city center (Photo by Mesut Gör)

5. 1. 5. Elazığ

In Elazığ city center and its surrounding districts, liquefaction or slope stability were not seen. Only one old building was collapsed after the earthquakes. In Elazığ city center, liquefaction, and settlement, etc., were not observed. Also, no damage was reported in the retaining structures. This is due to following reasons:

1. Clay soil profiles with high plasticity are typically found in the southern portions of the city (Sürsürü District, Ataşehir District, etc.), where groundwater is found at more than 15-20 m depths. Plasticity Index of fine-grained soils is greater than 12%.

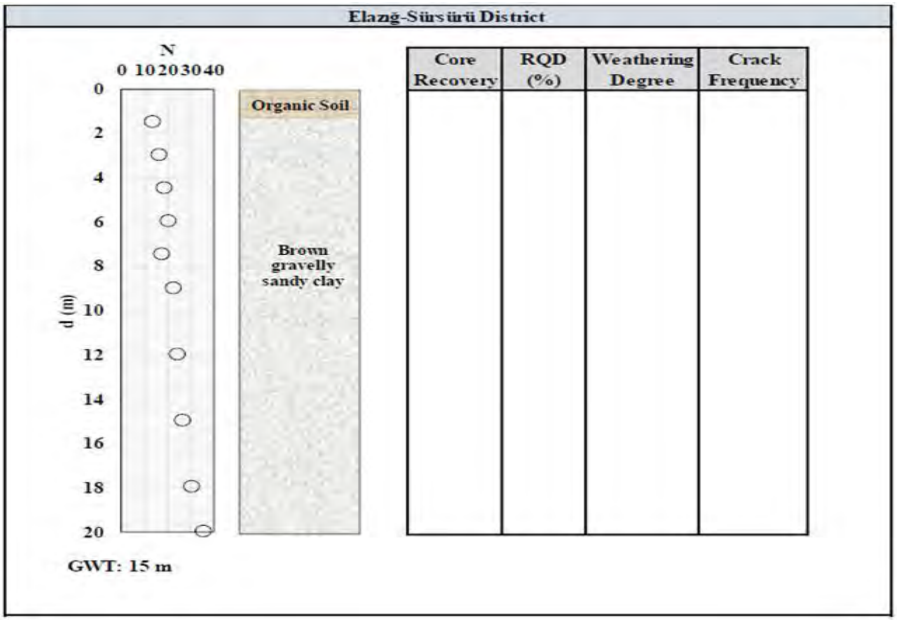

Idealized soil profile (Sürsürü District)-1

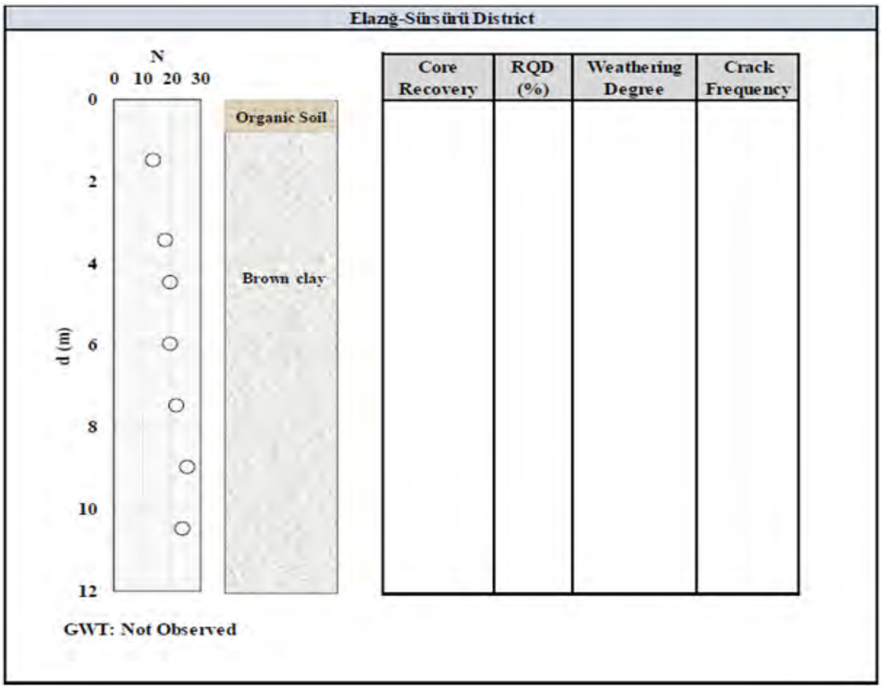

Idealized soil profile (Sürsürü District)-2

2. Coarse pebbly, sandy, and silty units are found in the eastern portion of the city (Zafran Mah., Mustafapaşa Mah., Hüseynik Mah., etc.), and groundwater is typically not encountered within 20 m depths. In addition, the soil profile is quite stiff and the corrected SPT data is generally >30.

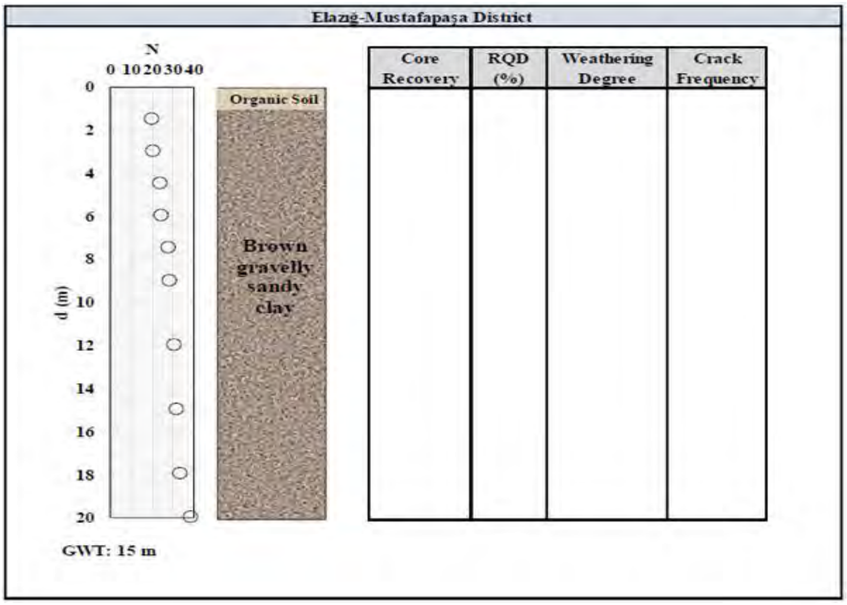

Idealized soil profile (Mustafapaşa District.)

3. There is no ground water found in the northern areas of the city (Cumhuriyet Mah., Şahinkaya Mah., etc.), which are typically made up of rock soil profiles (sandstone, claystone, and basalt alternations).

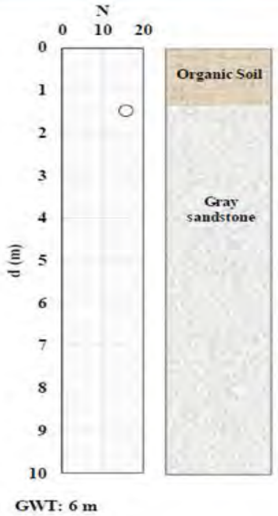

Core Recovery	RQD (%)	Weathering Degree	Crack Frequency
23	0	W5	>50
66	0	W5-W4	10--50
46	28	W3	3--10
66	28	W3	3--10
80	56	W3	3--10
90	14	W3	3--10

Idealized soil profile (Şahinkaya District.)-1

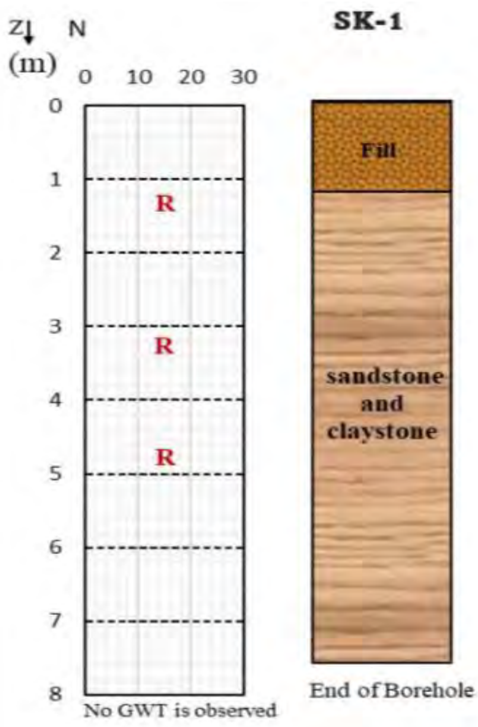

Weathering degree	RQD
	0
W1	5
W1	5
W1	10
W1	10

Idealized soil profile (Şahinkaya District.)-2

4. The groundwater level is deeper than 15 m or not found at most locations, and the soil profiles in the western portions of the city (Abdullahpaşa Mah. Bızmişen Mah., etc.) are composed of pebbly, coarse gravel, sandy clayey soil profiles, pebbly sandy soils, and rock soil profiles.

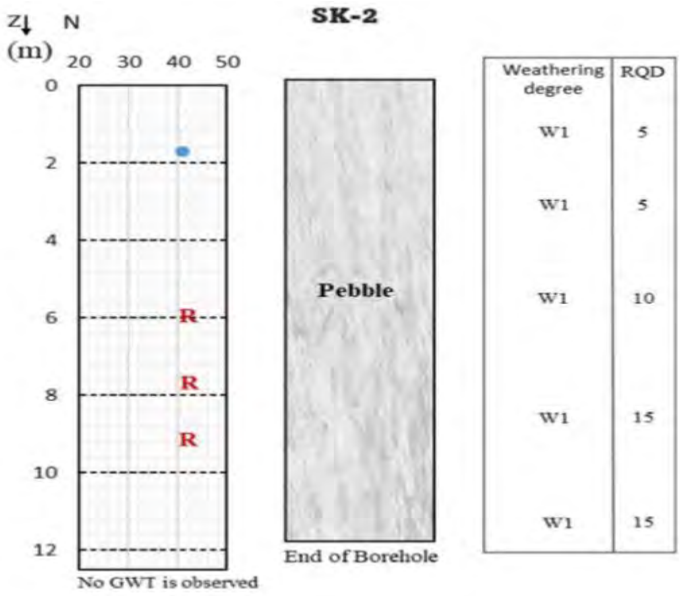

Idealized soil profile (Abdullahpaşa District.)

5. 1. 6. Adıyaman

The Adıyaman central district and its vicinity is composed of Neogene aged weakly cemented sedimentary rocks and Quaternary alluviums. Neogene aged sedimentary rocks are composed of conglomerates, sandstones, siltstones, and mudstones. The topography of Adıyaman central district is gentle, having slopes less than 10 %. There are two strong ground motion stations in the central district, one of them has MASW measurements. According to measurements shear wave velocity increases with depth and average shear wave velocity is 391 m/sec.

Approximately 45 % of the buildings in the central district collapsed during the first earthquake (M_w=7.7) and 15 % collapsed during the second earthquake (M_w=7.6). The majority of the remaining structures were heavily damaged (Figure 5.70, 71, 72, 73). Most of the buildings constructed after 2016 are inhabitable, their elevator reinforced concrete walls are damaged. Liquefaction phenomenon was not observed in the Adıyaman central district. The number of totally collapsed buildings in the Pazarcık and Gölbaşı districts are less compared to the central district. Ground deformations in the form of collapses and cracks are observed in the highway around the Pazarcık and Gölbaşı districts.

Figure 5.70. Photograph taken in the Adıyaman central district showing earthquake damage (https://www.gazeteduvar.com.tr/depremden-etkilenen-Adıyamandaki-hasar-havadan-goruntulendi-galeri-16020839.

Figure 5.71. Collapsed building in the Adıyaman central district (photo taken by Dr. Senem Tekin).

Figure 5.72. Partially collapsed building in the Adıyaman central district (photo taken by Dr. Senem Tekin).

Figure 5.73. Heavily damaged buildings in the Adıyaman central district (photo taken by Dr. Seyhan Fırat).

The Gölbaşı basin is a depression formed by pull-apart mechanism. Main geological unit observed in the district is Quaternary gravelly sandy soils with clay – silt intercalations (Akıl et. al., 2008). Observations made in the Gölbaşı district, revealed very intense structural damage and ground deformations, such as total and differential settlements due to liquefaction (Figures 5.74 and 5.75). In addition to settlement, lateral spreading was also observed in some areas (Figure 5.78).

Some of the building tilted and overturned due to bearing capacity losses after seismic soil liquefaction. Widespread sand boils with water outlets were observed in some places (Figure 5.79). In addition, rockfalls involving large blocks were also encountered around the Karamağara locality (Figure 5.80). No loss of life due to the rockfall was reported, but the road was closed, and transportation was disrupted.

Figure 5.74. Settlement due to liquefaction in the Adıyaman Gölbaşı district (photo taken by Dr. Müge Akın).

Figure 5.75. Overturned building without structural damage in the Adıyaman Gölbaşı district (photo taken by Dr. Müge Akın).

Figure 5.76. Sand boils observed in the Adıyaman Gölbaşı district (photo taken by Dr. Müge Akın).

Figure 5.77. Large rockfall observed in the Adıyaman Gölbaşı district, Karamağara locality (photo taken by Dr. Müge Akın).

5. 1. 7. Hatay

5. 1. 7. 1. Antakya

Antakya is tectonically in the center of Dead Sea (DSFZ) and East Anatolian faults (EAFZ) and the Cyprus arc. There had been major and devastating earthquakes in the historical period. And there are several attempts to perform seismic hazard analyses for this region (Kurnaz and Ince, 2020). The seismicity and filling of the quaternary age in Antakya and its surrounding area have been controlled by these active major faults and geological map including city center is given Figure 5.78

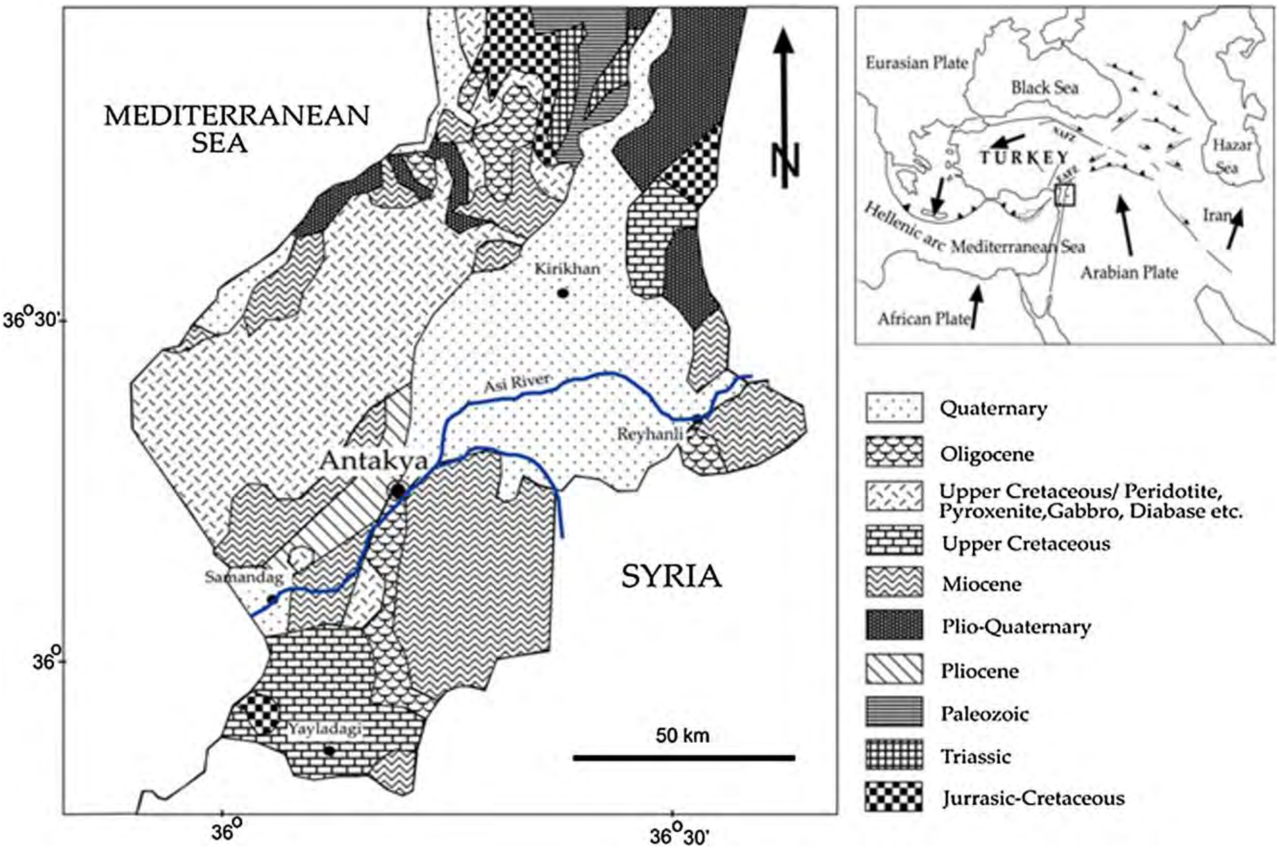

Figure 5.78. Geological map of Antakya and surroundings (Over et al. 2011).

The sediments are primarily composed of Quaternary alluvial fill that consist of clayey, sandy, silty, and gravelly material. The soil layers were classified for the region including V_{s30} values. The related soil classification is given in Figure 5.79.

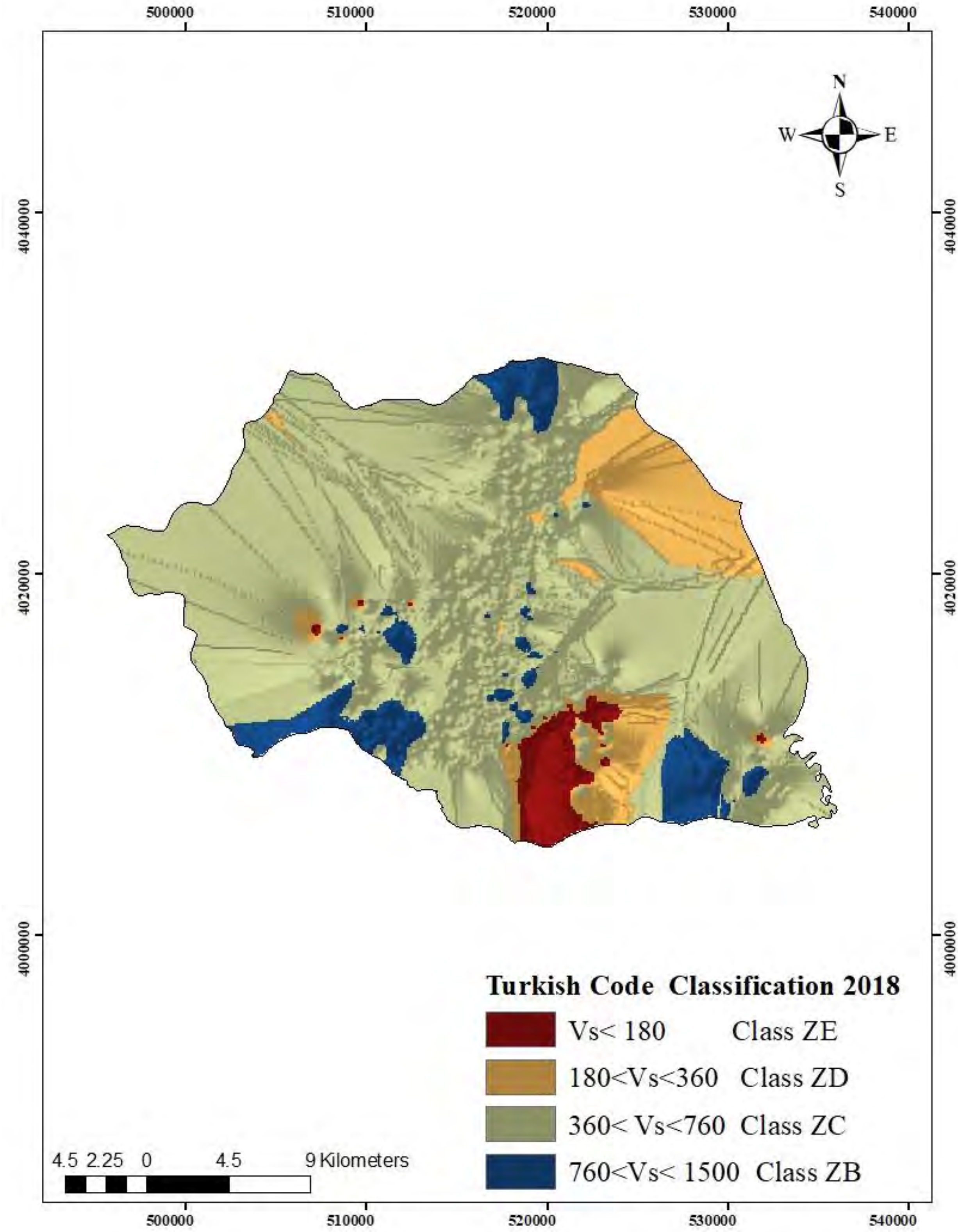

Figure 5.79. Site classification based on Vs30 values (Prepared by Sallama Alosman, 2023).

Data on the near-surface geological conditions were examined and two deep borehole logs (Figure 5.80) provide a vertical profile of the surface deposits up to 60 m (W1) and 100 m (W2), respectively in the previous studies (Table 5.1) (Buyuksarac et al., 2014).

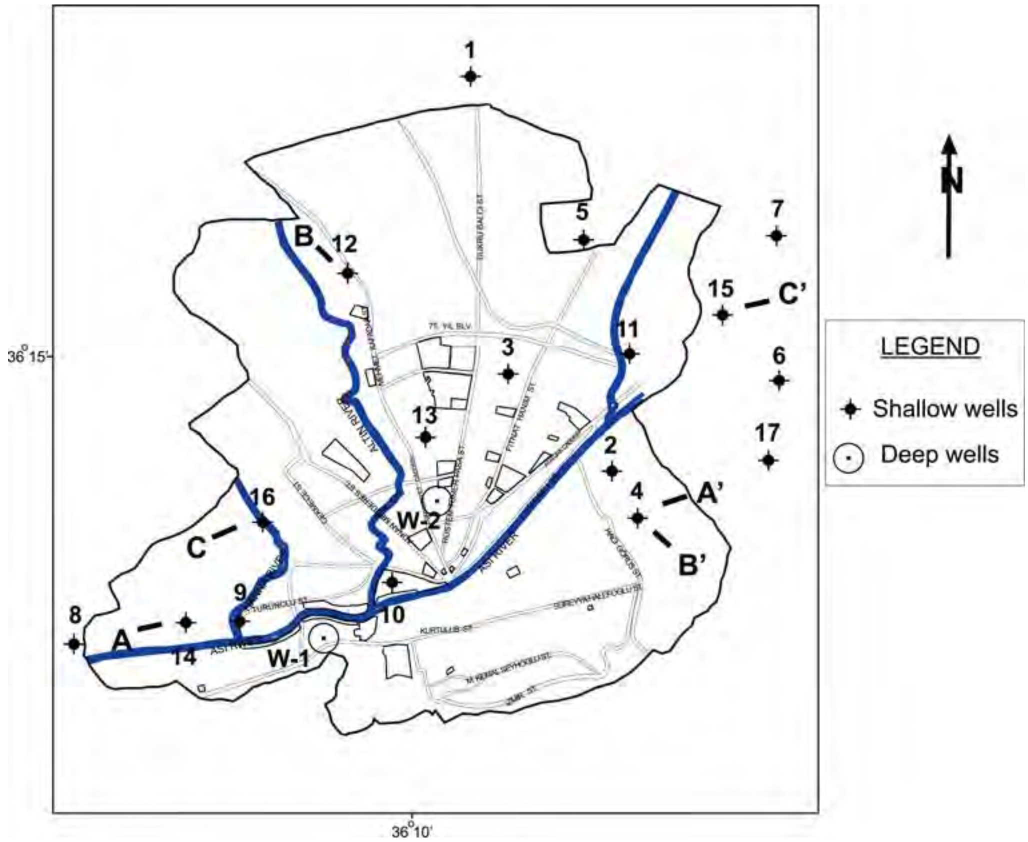

Figure 5.80. Location of deep wells (Taken from Buyuksarac et al., 2014)

Table 5.1 Deep boreholes in the study area (W1=60 m and W2=100 m) (Over et al., 2008)

W1	
Depth (m)	**Formation**
0 - 1	Agricultural Soil table
1 - 7	Gravel
7 - 11	Clay stone
11 - 18	Clay Stone with Gravel
18 - 22	Gravel
22 - 26	Conglomerate
26 - 29	Conglomerate with Clay
29 - 33	Conglomerate
33 - 53	Conglomerate with Clay
53 - 60	Clay Stone

W2	
Depth (m)	**Formation**
0 - 7	Gravel with clay
7 - 26	Clay
26 - 36	Gravel
36 - 76	Clay
76 – 80	Gravel
80 - 90	Clay
90 - 100	Gravel with clay

The soil description in the borehole logs show that the surface soil consists of quaternary materials composed of clay, gravel detritic formations of conglomerates and alluvial sands. The average ground water level in the area is 3 m according to the deep boreholes.

Antakya is in the seismically dangerous region and the largest city of a former civilization. It had been demolished many times by earthquakes in its history and the historical earthquakes are compiled from ancient time to recording times (Table 5.2). A view from the great destruction in Antakya centered in Pazarcık and Elbistan on February 6, 2023, is shown in Figure 5.81.

Table 5.2 Historical earthquakes (modified from Bikce et al., 2009)

Date	Coordinates	Earthquake Intensity	Location	Magnitude
69 BC	36.25 N–36.10 E	IX	Antakya, Syria	
245	36.25 N–36.10 E	X	Antakya	
334	36.25 N–36.10 E	IX	Antakya, Beirut, Cyprus	
14.09.458	36.25 N–36.10 E	IX	Antakya and North of Syria	
10.09.506	36.25 N–36.10 E	IX	Antakya, Samandag	
29.05.526	36.25 N–36.10 E	IX	Antakya, Samandag	
29.11.529	36.25 N–36.10 E	IX	Antakya	
561	37.20 N–35.90 E	VIII?	Anazarba, Ceyhan-Adana, Antakya	
30.09.587	36.25 N–36.10 E	IX	Antakya (60,000 dead)	
08.04.859	36.25 N–36.10 E	IX	Antakya, Lazkiye	
867	36.25 N–36.10 E	IX	Antakya	
10.08.1114	36.25 N–36.10 E	IX	Ceyhan, Antakya, K.Maras (Tsunami)	
13.08.1822	37.35 N–35.80 E	X	Antakya, Iskenderun (20,000 dead)	
02.04.1872	36.40 N–36.20 E	IX	Antakya, Samandag (1,800 dead)	
14.06.1936	36.5 - 36.0		Iskenderun bay	5.5
08.04.1951	36.6 - 36.1		Iskenderun	5.7
22.10.1952	36.5 35.3		Ceyhan	5.0
24.03.1953	37.0 37.0		Gaziantep	5.1
07.04.1967	37.4 36.1		Yumurtalik-Ceyhan	5.0
15.07.1976	37.5 35.9		Yumurtalik-Ceyhan	5.0
29.06.1971	37.1 36.8		Aslantas-Berke	5.0
11.07.1971	37.2 36.8		Aslantas-Berke	5.0
24.06.1989	36.2 36.1		Antakya	5.1
10.04.1991	37.5 35.7		Yumurtalik-Ceyhan	5.4
03.01.1994	36.9 35.8		Yumurtalik - Ceyhan	5.3
22.01.1997	36.1 36.1		Antakya	5.5
22.01.1997	36.2 36.0		Samandag	5.2
27.06.1998	36.8 35.5		Ceyhan	6.3
04.07.1998	36.8 35.4		Ceyhan	5.4
25.06.2001	37.2 36.1		Osmaniye	5.4

Figure 5.81. A view from the great destruction in Antakya after the great earthquakes in Pazarcık and Elbistan on February 6, 2023, https://www.sozcu.com.tr.

Among these provinces, one of the most affected cities was Hatay. In Hatay, where 1200 buildings were destroyed, 872 of our citizens lost their lives, while 2766 of our citizens were injured.

Data from satellites (Figure 5.82 and 5.83) show that after the quakes, much of the region lost electric power. The following maps show the amount of light emitted by Antakya's city center and surrounding communities before and after the earthquake taken from Nasa webpage.

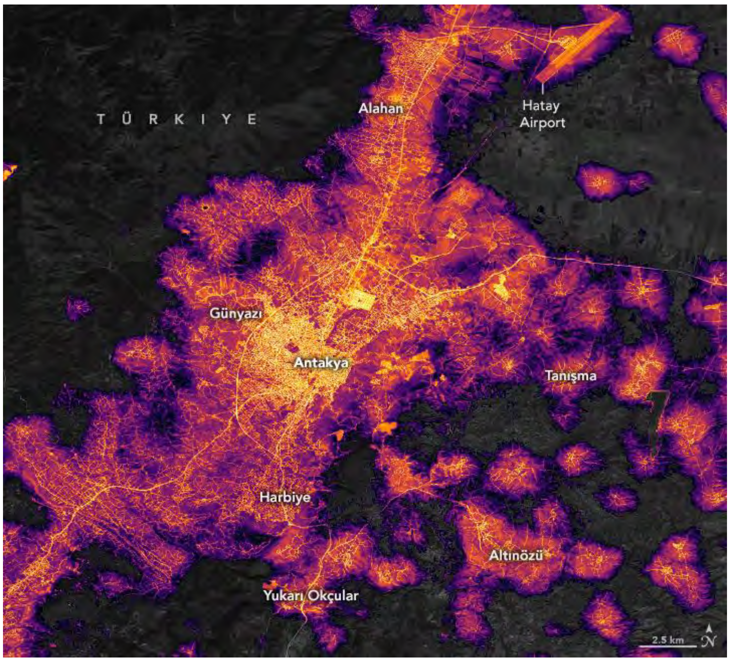

Figure 5.82. Satellite images on February 4, 2023, showing the region lost electric power (resource https://earthobservatory.nasa.gov/images/151029/dark-nights-in-antakya)

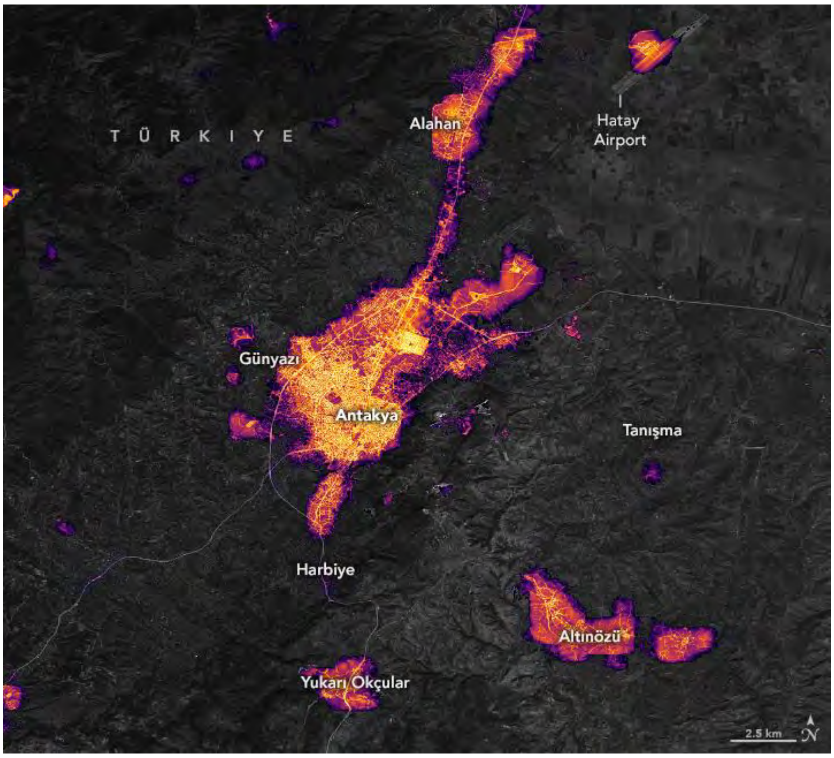

Figure 5.83. Satellite images on February 8th, 2023 showing the region lost electric power February 8, 2023 (resource https://earthobservatory.nasa.gov/images/151029/dark-nights-in-antakya)

Figure 5. 84-87 presents examples of structurally stable and damaged to collapsed building in Hatay.

Figure 5.84. Museum Hotel in Antakya (photo by Müge Akın)

Figure 5.85. Hospital building in Hatay (photo by Müge Akın)

Figure 5.86. Collapsed building in Hatay (photo by Müge Akın)

Figure 5.87. Damaged building in Hatay (photo by Müge Akın)

5. 1. 7. 2. İskenderun

February 6, 2023, Kahramanmaraş-Pazarcık (Mw=7.7) and Elbistan (Mw=7.6) Earthquakes heavily affected the city of İskenderun. There were many totally collapsed and heavily damaged 2-6 stories residential buildings in the province of Hatay-Iskenderun center as shown in Figure 5.88. Some of the damaged buildings were tilted or settled probably due to a foundation bearing capacity failure. Some of them had structural damage from the first or second story. The number of buildings collapsed at the city center is reported to be approximately 300. Main roads and street along Atatürk Boulevard The major findings of the reconnaissance studies performed immediately after the earthquake by Turkish teams are discussed in the below sections under the titles of performance of building foundations, seismic soil liquefaction and performance of retaining structures.

The generalized stratigraphy of Iskenderun and its bottom units are Paleozoic aged, quartzite, partially phyllite and schist and occasionally dolomite. Triassic, Jurassic and Cretaceous ged limestone, dolomite phyllite, and shale come discordantly on top of bottom units. In general, quaternary-aged alluvium and debris cover the surface. The general stratigraphy of Iskenderun is shown in Figure 5.89.

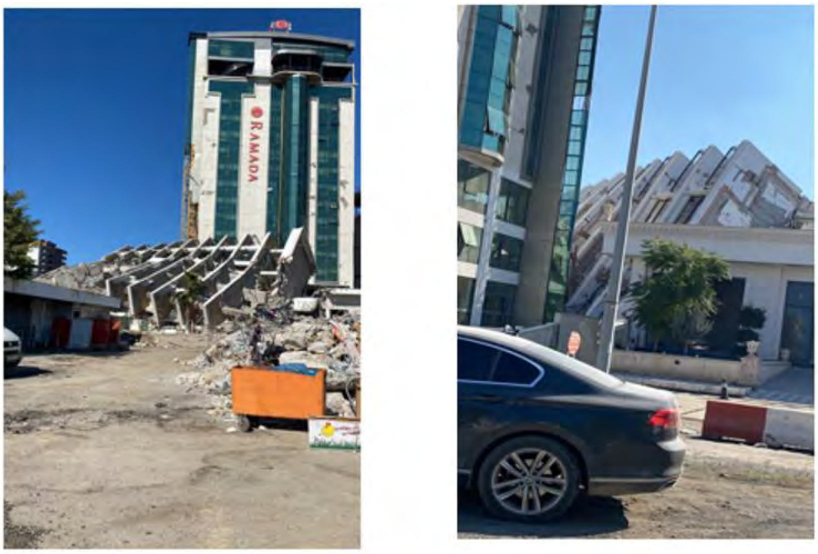

Figure 5.88. Collapsed and overturned buildings in İskenderun/Hatay (36°35'22.0 "N/ 36° 10'37.5"E, Photo by: Ece Eseller Bayat, Yaren Birşen)

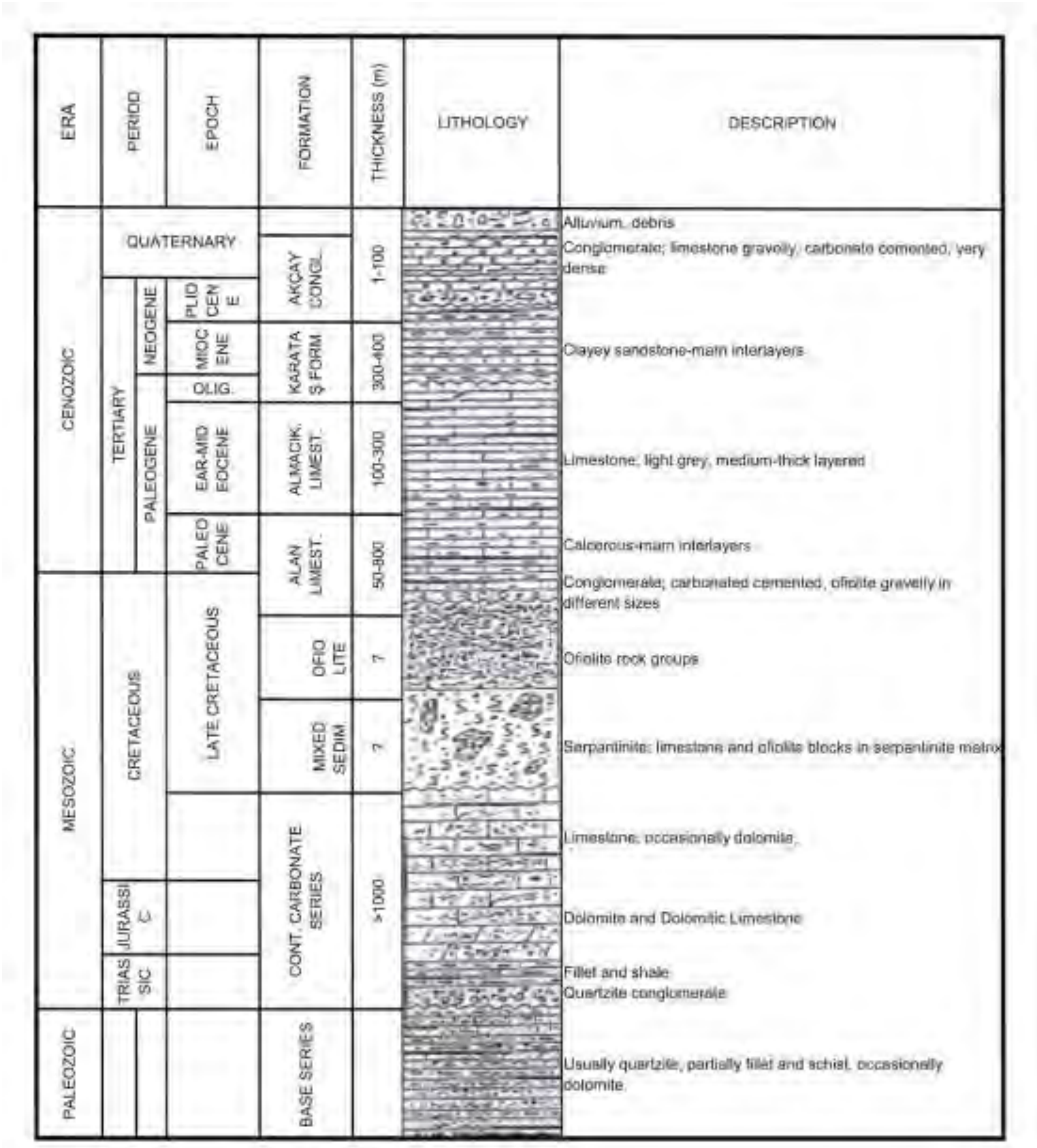

Figure 5.89. General stratigraphy of Iskenderun and its vicinity

5. 1. 7. 2. 1. Seismic Soil Liquefaction Manifestations

Consistent with the subsoil conditions and geology of the region, surface manifestations of seismic soil liquefaction including lateral spreading, sand boils, soil ejecta, and subsidence were observed in İskenderun region as shown in Figure 5.90 through Figure 5.92.


Yellow arrows indicate the length or diameter of observed sand boils.

(a)

(b)

(c)

(d)

(e) (f) (g)

Figure 5.90. Seismic soil liquefaction-induced surface manifestation: sand boils in free field conditions: a) Ataturk Boulevard/İskenderun/Hatay (36°35'26.86"N/ 36° 10'40.39"E, Photo by: Tugce Baser, Ozgun Numanoglu, Serhat Erinmez) b) Tennis Courts on Ataturk Boulevard İskenderun/Hatay (36°35'26.95"N/ 36° 10'28.39, Photo by: Tugce Baser, Ozgun Numanoglu, Serhat Erinmez) c) Çay District / İskenderun /Hatay (36.591334°N, 36.178781°E, Photo by: Ertan Bol, Aşkın Özocak, Sedat Sert, Eylem Arslan) d) Çay District / İskenderun /Hatay (36.591326°N 36.178147°E, Photo by: Ertan Bol, Aşkın Özocak, Sedat Sert, Eylem Arslan) e) İskenderun Port / İskenderun /Hatay (36.73221°N 36.19618°E, Photo by: Pelin Özener, M. Murat Monkul) f) Çay District / İskenderun / Hatay (36.59133°N, 36.17888°E, Photo by: Kemal Önder Çetin, Elife Çakır) g) Ataturk Boulevard/İskenderun/Hatay (36°35'29.50"N, 36° 10'20.23"E, Photo by: Tugce Baser, Ozgun Numanoglu, Serhat Erinmez)

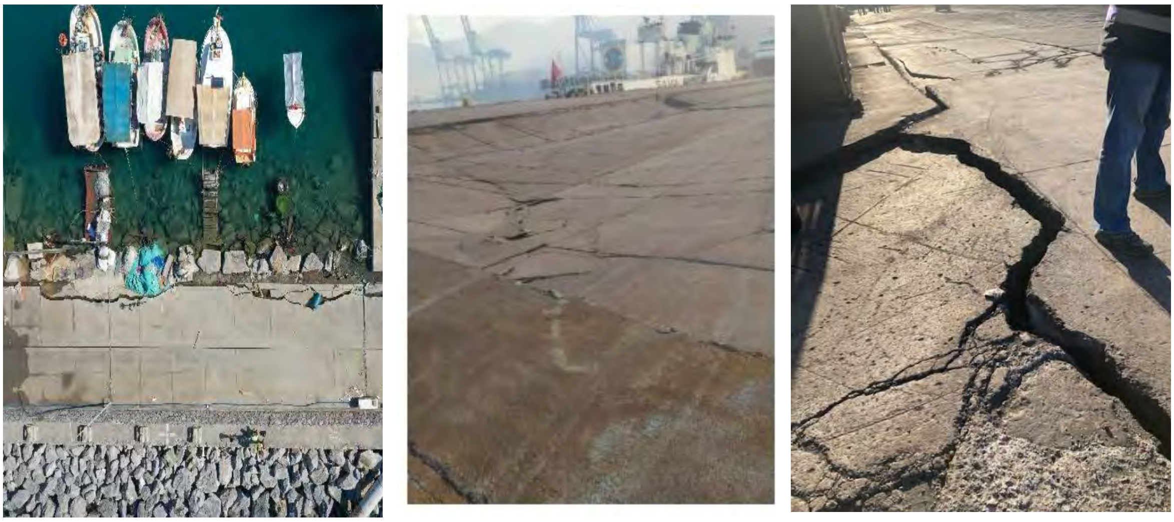

(a) (b) c)

Figure 5.91. Seismic soil liquefaction induced lateral spreadings **a)** Iskenderun Dock/İskenderun/ Hatay (36°35'40.67"N/, 36° 10'38.69"E, Photo by: Tugce Başer, Özgun Numanoglu, Serhat Erinmez) b) İskenderun Port Area /İskenderun/ Hatay *(*36.59991°N, 36.19274°E , Photo by: Kemal Önder Çetin*)* c) İskenderun Port Area/İskenderun/Hatay (36.73011°N, 36.19681°E, Photo by: Pelin Özener, M. Murat Monkul)

(a) **(b)** **(c)**

Figure 5.92. Seismic soil liquefaction induced bearing capacity and settlement problems in **a)** Çay District / İskenderun.

5. 1. 7. 2. 2. Performance of Foundation Systems

Many foundations of residential buildings in İskenderun region were subjected liquefaction induced settlements and bearing capacity failures The foundation settlements are observed to vary within 3 cm to 15 cm in İskenderun city Center and reach approximately 30-35 cm in Karaağaç – Cumhuriyet Districts. Additionally, differential settlements that reach 30 cm were observed that caused the tilting of buildings as shown in Figure 5.93. On the other hand, no settlements were observed for high buildings that have pile foundation system, but damages attributed to inadequate structural design was observed in those buildings.

Figure 5.93. Tilted Buildings due to seismic soil liquefaction (36°35'11.4 N/, 36° 10' 27.5, Photo by: Ece Eseller Bayat, Yaren Birşen)

Moreover, performance of improved sites was observed to perform well during earthquake with no severe damage although the neighboring buildings collapsed. Çivisöken building shown in Figure 5.94 is surrounded by diaphragm wall penetrating to 12m depth from the ground surface and improved with jet grout columns of 3m in length and 60cm in diameter.

Figure 5.94. Performance of Çivisöken building with no damage resting on improved soil conditions in Çay District / İskenderun /Hatay (36.590761°N, 36.175848°E, Photo by: Ertan Bol, Aşkın Özocak, Sedat Sert, Eylem Arslan)

5. 1. 7. 2. 3. Performance of Viaducts and Overpass Bridges

Performance of viaducts at Çankaya-Belen and Payas-İskenderun intersections were inspected. Seismic shear keys were mainly observed to be damaged as shown in Figure 5.95. But in general, elastomeric bearings were observed to perform well up to a certain acceleration level and the displacement bridge deck was observed to be restrained by shear keys and parapet walls of abutment (Figure 5.96). These damages mainly indicate that shear keys functioned well and prevent the excess displacement and fall of bridge deck.

Figure 5.95. Damaged seismic shear keys beneath the viaduct deck at Çankaya-Belen intresection (36.54796°N, 36.15087°E, Photo by: Pelin Özener)

Figure 5.96. Bridge deck restrained by the performance of shear keys and paraphet at İskenderun-Payas Intersection (36.740734°N, 36.224845°E, Photo by: Pelin Özener)

5. 1. 7. 2. 4. Performance of İskenderun Airport

Deformation cracks and signs of vertical settlement were observed at the entrance of domestic arrivals lounge as shown in Figure 5.97. The vertical settlement was observed to be in the order of 35-40 cm, but no severe structural damage was observed in Airport building.

Figure 5.97. Settlements observed at the entrance of domestic arrivals lounge (Hatay Airport, 36.366025˚N, 36.272742˚E, Photo by M. Murat Monkul and Pelin Özener)

5. 1. 7. 2. 5. Performance of Port and Harbors

İskenderun fishery port and an industrial port located in Payas were observed to be severely damaged during the earthquake. Ground Settlements and Lateral displacements were also observed at Iskenderun Fishery Port indicating liquefaction induced type of deformations (Figure 5.98).

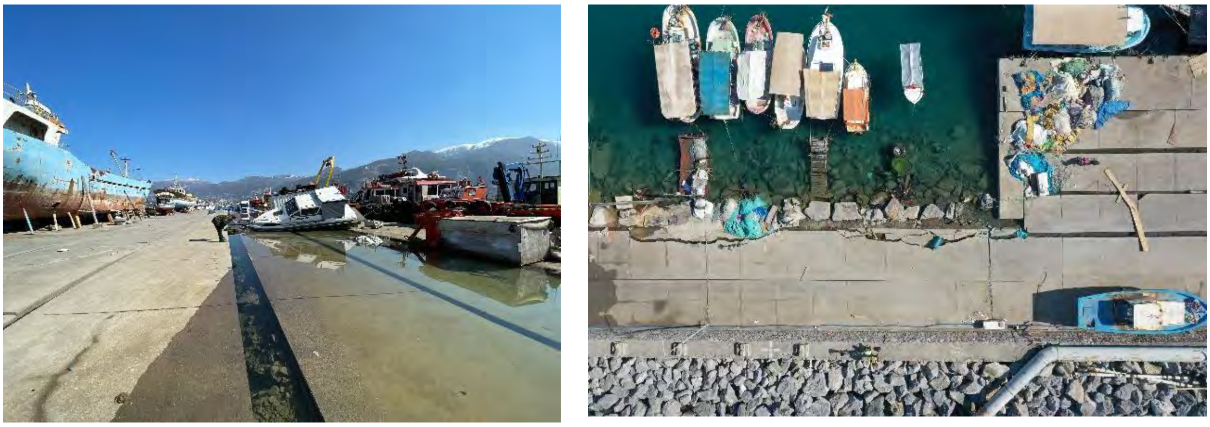

(a) (b)

Figure 5.98. Ground Settlements and Lateral Displacements at Iskenderun Fishery Port (36°35'40.67"N/ 36° 10'38.69"E, Photo by: Tugce Baser, Ozgun Numanoglu, Serhat Erinmez)

The port located in Payas was mainly constructed as block type gravity quay wall and in 2006 after a modernization study, a new port was constructed which is founded on driven steel piles. Deformation cracks were observed in block type gravity quay wall part during the February 6, 2023, Earthquake as shown in Figure 5.99. Due to the damages occurred at the port, cranes and weighbridges were reported to be tilted (Figure 5.99).

Figure 5.99. Deformation cracks in block type gravity quay wall and tilted cranes (36.73011°N, 36.19681°E, Photo by: Pelin Özener, M. Murat Monkul)

Vertical and lateral displacements were also observed and documented in the vicinity of sand ejecta most probably due to lateral spreading of the quay wall. The vertical and lateral displacements were observed to be in the order of 85 cm and 57 cm, respectively (Figure 5.100). The port way over No.2 and No.3 ports collapsed as shown in Figure 5.101 most probably due to lateral spreading that took place during earthquake and this part of the port is not in service now.

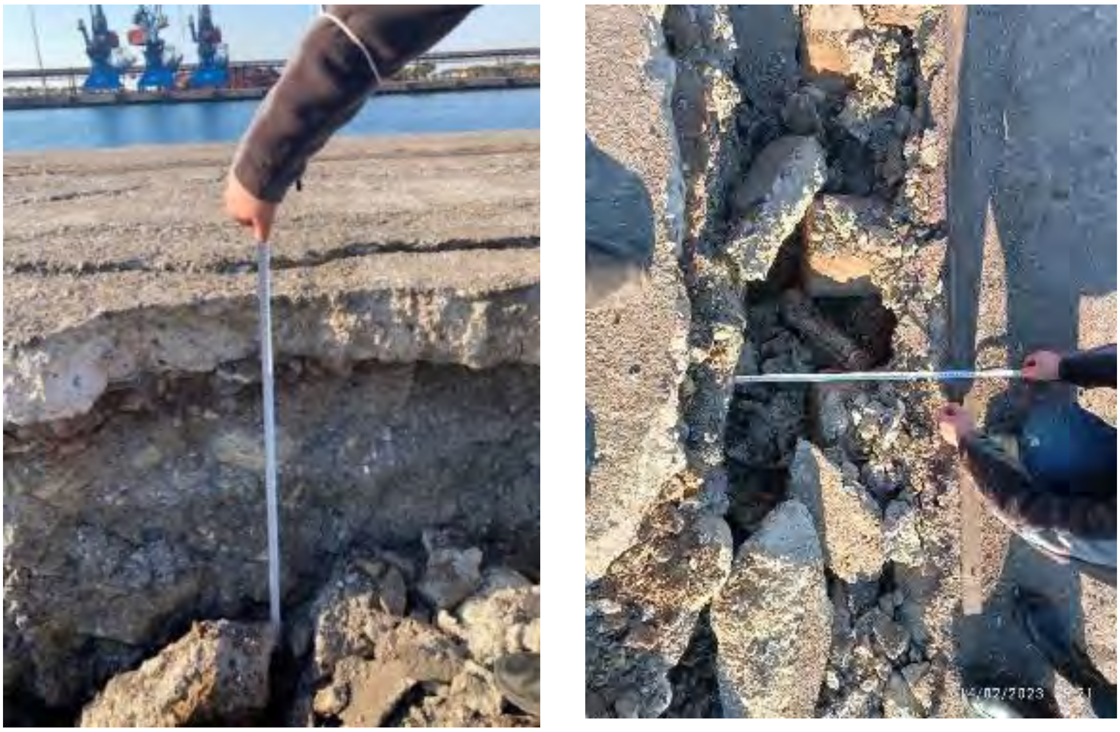

Figure 5.100. Vertical and Lateral displacements occurred in block type gravity quay wall (36.73011°N, 36.19681°E, Photo by: Pelin Özener, M. Murat Monkul)

Figure 5.101. The collapse of Port way over No.2 and No.3 ports due to liquefaction induced lateral spreading (36.73208°N, 36.19735°E, Photo by: Pelin Özener, M. Murat Monkul)

On the other hand, no damage was observed in the new port founding on driven steel piles as shown in Figure 5.102.

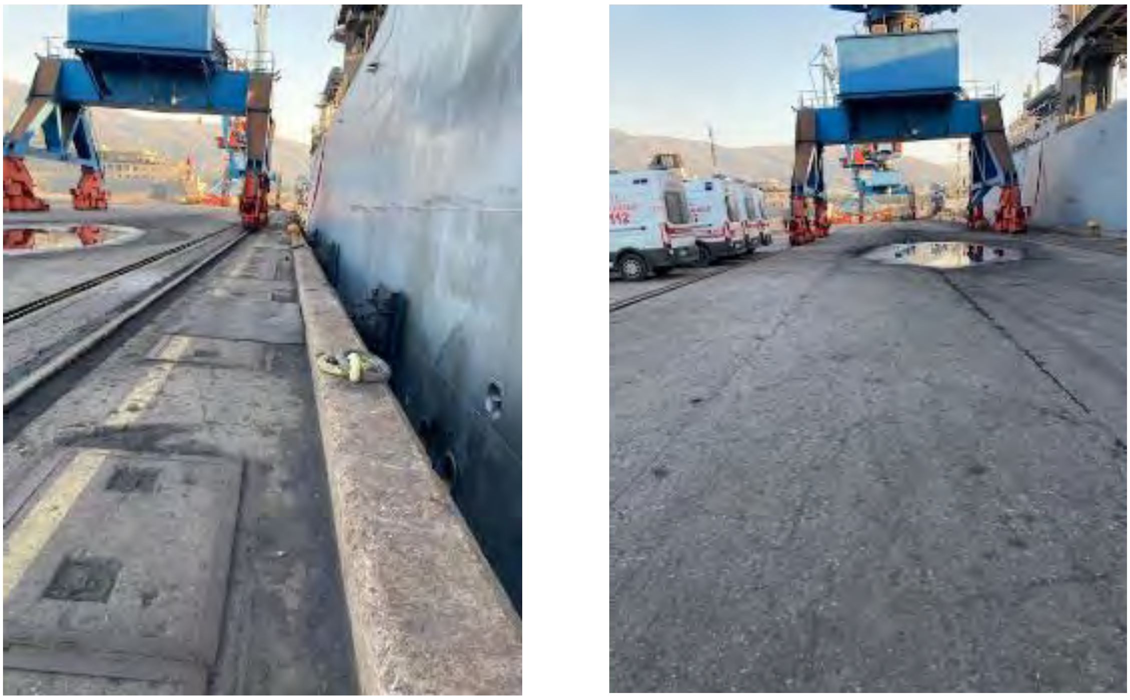

Figure 5.102. No damage was observed in the new port founding on driven steel piles.

5. 1. 7. 2. 6. Performance of Retaining Structures

Mechanically Stabilized Earth Wall (MSEW) and gravity type retaining walls were observed along the transportation network. General performance of the retaining walls was observed to be good and no visible damages were observed for the investigated walls due to seismic shaking as shown in Figure 5.103.


Figure 5.103. No damage on retaining walls due to seismic shaking.

5. 1. 8. Mersin/Tarsus

Mersin and its district of Tarsus are one of those places experienced the negative impacts of the Kahramanmaraş earthquakes followed by the Hatay earthquake occurred on February 13, 2023. These impacts include a tilting of a multistory building in the Mezitli district of Mersin, and five of school building damages in the district of Tarsus. Most of the damages are structural and are relatively slight compared to the damages in the cities near the epicenter of the earthquake; however, they have caused disruptions in the educational operations both in Tarsus and Mersin. All the buildings impacted in the region was built in years between 1987 and 1995, therefore they do not comply with the building codes implemented after the ’98 Ceyhan and ’99 Kocaeli earthquakes.

There are three buildings in the Baykent complex, which was built in 1995, and only one of them was damaged. The locals reported that there were several structural problems with the building even before the earthquake. The subsurface profile in the coastal strip of Mersin mainly consists of loose alluvial deposits. Considering that the majority of the urban development (multistory buildings) is in the coastal strip of Mersin, this area deserves a further attention.

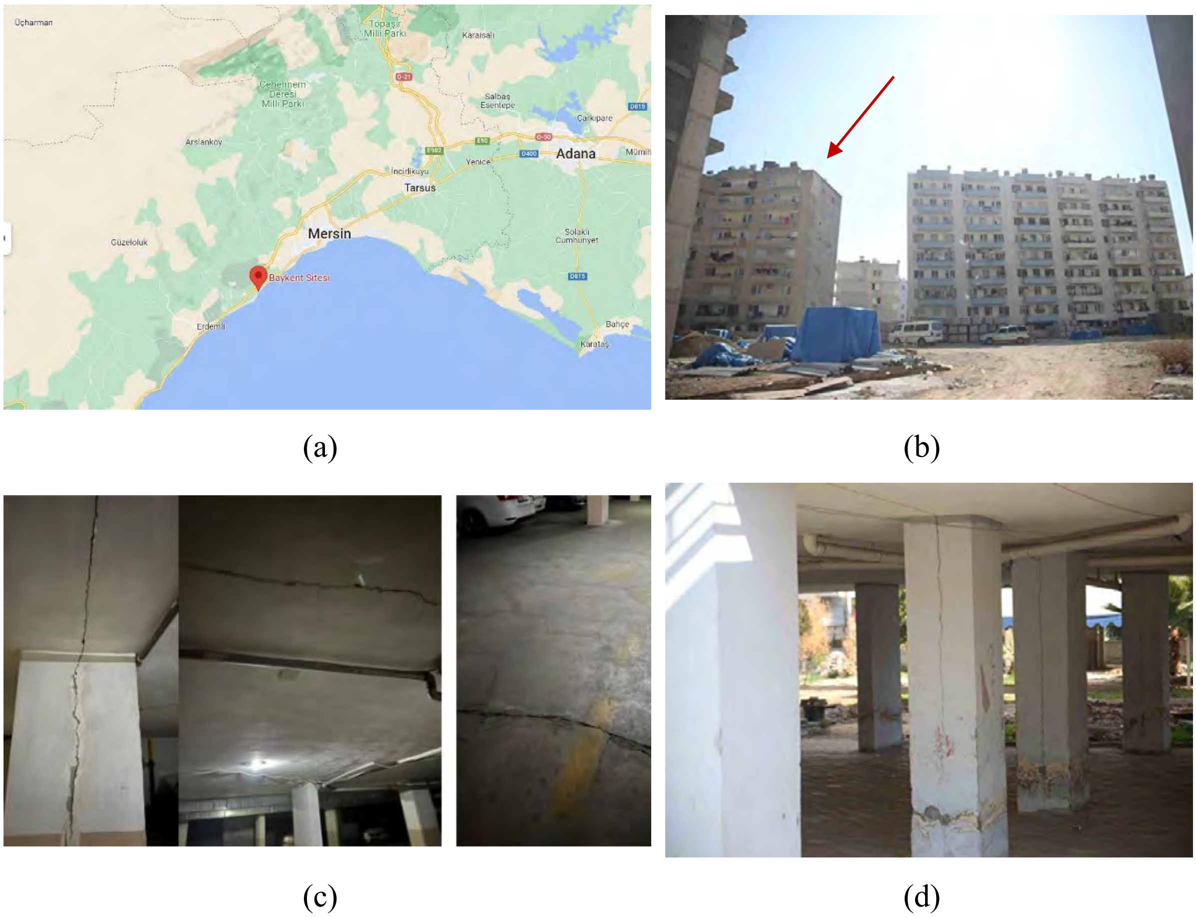

Figure 5.104. Tilted building (Baykent complex) in Mezitli, Mersin (36.68888N, 34.44277E): (a) Location; (b) Overview; (c) Cracks in the concrete panels in the parking lot; (d) column cracks Photo by (Ozgun Numanoglu, Tugce Baser, Serhat Erinmez)

Five of school buildings in Tarsus are evacuated the right after the Kahramanmaraş earthquakes mainly because of the cracks in the load carrying columns and beams in addition to the walls. Our conversations with locals and authorities revealed that the evacuations are prevention at this stage. The map overview of the impacted buildings is given in Figure 5.105.

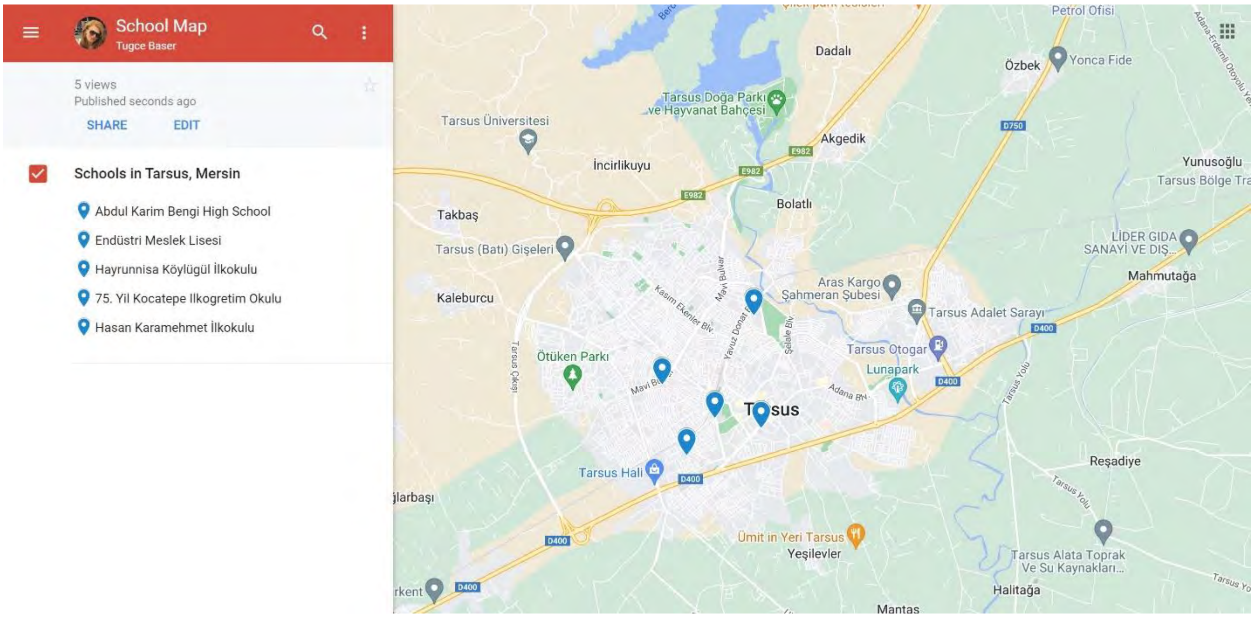

Figure 5.105. Locations of the damaged and evacuated school buildings

(a) (b) (c)

Figure 5.106. Damages in several school buildings in Tarsus: (a) Interior cracks in Hayrunnisa Koylugil (36.90946, 34.87914); (b) Column cracks in AKBAL (36.92016, 34.87463); (c) Sidewalk and wall damages in AKBAL Photo by (Ozgun Numanoglu, Tugce Baser, Serhat Erinmez)

5. 1. 9. Sanliurfa

5. 1. 9. 1. General Information about the Damage

February 6, 2023, Kahramanmaraş-Pazarcık (M_w=7.7) and Elbistan (M_w=7.6) Earthquakes also affected the city of Şanlıurfa. Accordingly, the number of buildings that collapsed in the city center is 19. Some buildings collapsed progressively or tilted during the earthquake indicating geotechnical problems. A photo indicating the damage at the city center is given in Figure 5.107 According to the municipality, 4727 buildings were reported to be damaged (personal communication). The damage assessment studies have been carried out in 124,569 independent units in a total of 18333 buildings in Şanlıurfa. It was determined that 1,481 independent units in 263 buildings were heavily damaged and collapsed, requiring urgent demolition. Additionally, 2,431 independent units in 291 buildings were moderately damaged, 59,362 independent units in 5,959 buildings were slightly damaged, and 46,274 independent units in 8,875 buildings were reported as undamaged.

Figure 5.107. Collapsed building at Bahçelievler (top left), damaged minaret of the Balıklıgöl Mosque (top right), Fountain of Harran University Mosque (bottom)

5. 1. 9. 2. Situation and Ground/Soil Profile at the City Center

Şanlıurfa province shows the character of the polyocene age. It was formed together with a part of the old world. The northeastern region of Şanlıurfa, especially Siverek, Hilvan and Viranşehir, is composed of basalts gushing from Karacadağ. A part of the province is covered with limestone formation. The province exhibits a very complex structure in terms of geology.

There are many local districts in the city center of Şanlıurfa. The most affected districts are Yenişehir, Bahçelievler, İpekyol, Yeşildirek, Paşabağı, Sırrın, and Bamyasuyu. In the Yenişehir district, most buildings are mid-aged or old (between. 10 and 30 years). The ground profile typically comprises weak, weathered rock formations (with RQD 0.4-0.45 indicating poor rock quality). The groundwater table (GWT) varies excessively from 15 to 30 meters. This district has some damaged and collapsed buildings. Some of the collapsed buildings are shown in Figure 5.108.

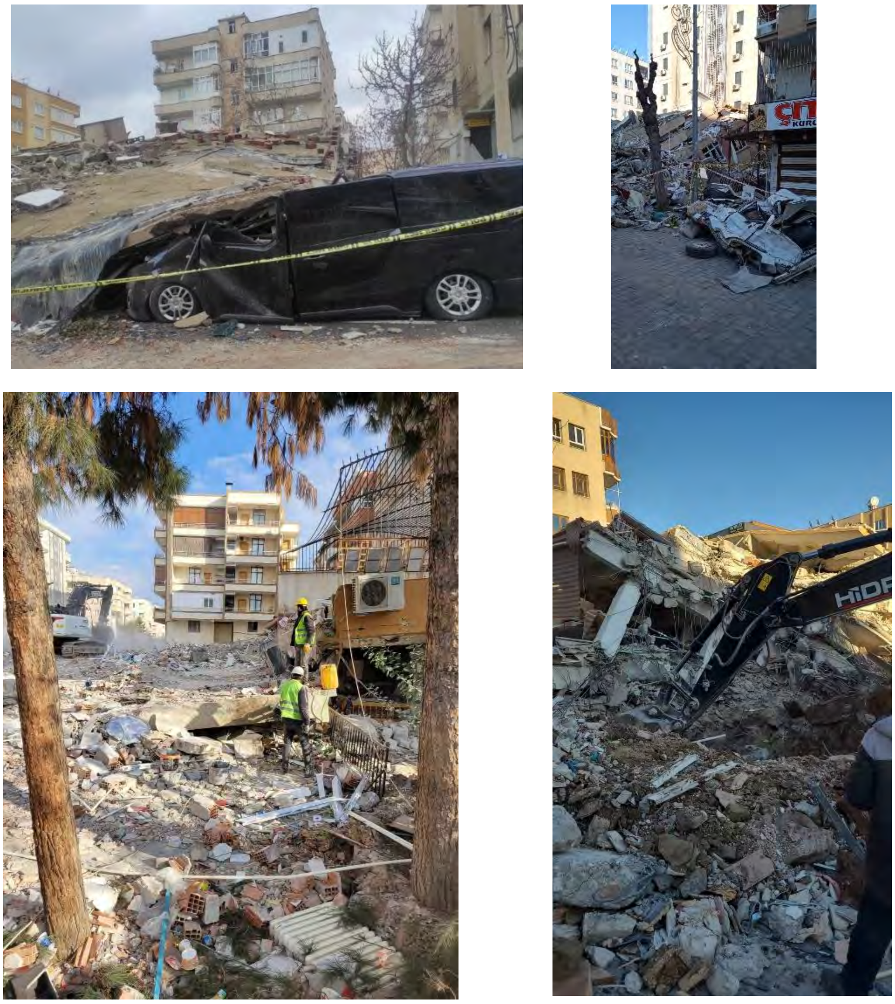

Figure 5.108. Some of the collapsed buildings

In the Bahçelievler district, the general reinforced concrete building profile is quite old, typically 40-50 years of age. The ground profile generally has low-quality (RQD 0.25-0.30) and slightly weathered rock formations. The groundwater table (gwt) varies excessively from 4 to 30 meters. This district has several collapsed buildings, but the number of damaged buildings is greater than the Yenişehir district. The structural damage at the newly constructed Abide Junction bridge is shown in Figure 5.109. Bahçelievler/ İpekyol districts are the most critical and severely damaged locations of the Şanlıurfa city center. There are many old structures in this district, and they are relatively more affected in terms of damage and collapse. Some of the collapsed buildings in this district are shown in Figure 5.110. Also, some tilted buildings were observed.

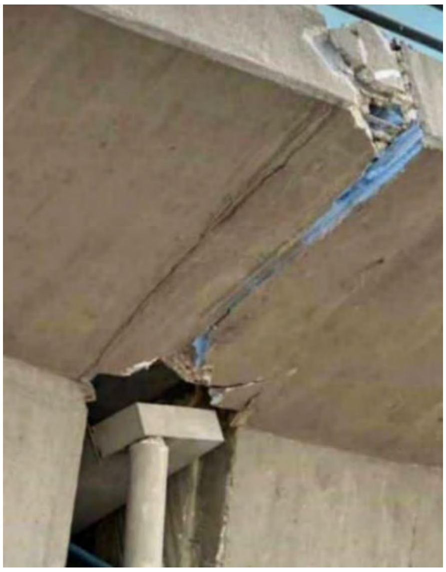

Figure 5.109. Damage at the newly constructed bridge on Abide Junction located between the İpekyol and Bahçelievler districts.

Paşabağı district typically has new buildings whose foundations primarily rest on Holocene alluvial deposits. The primary soil type in this district is composed of a significant amount of silt/clay soils, indicating the fine-grained nature of the typical soil profile at the top 7m. Some progressively collapsed and damaged buildings were observed at the buildings in this district.

In the Sırrın District, about 2 out of 3 multi-story buildings are old age. This district is close to the Paşabağı district and predominantly has fine-grained soil of high plasticity clay. The gwt depth is shallower than most of the other districts at the city center (i.e., about 4-20 m deep from the surface). Interestingly, the structural damage is relatively low compared to the Bahçelievler and Yenişehir districts, despite the highly plastic soil profile and shallower gwt.

This observation is probably due to the fewer stories of reinforced concrete buildings and their interaction with the local soil profile.

Figure 5.110. Collapsed buildings at Bahçelievler

5. 1. 9. 3. The situation in Suburbans

There are also two crucial municipal regions near the city: Karaköprü and Eyyübiye districts. Typically, new, and relatively high-rise (5 to 15 stories) reinforced concrete buildings exist in the Karaköprü district. Some severely damaged structures (e.g.: mosque shown in Figure 5.111) are located in the region.

Figure 5.111. Damage at Eyüp el Ensari Mosque in Karaköprü district

Eyyübiye district is famous for its touristic attractions, with the most well-known Balıklıgöl and the nearby Dergah Mosque. Structural damage and collapse are observed in both the tourist attractions (Figure 5.112), mosques (Figure 5.113), and buildings (Figure 5.114).

Figure 5.112. Damage to Urfa House at Eyyübiye (left) and brownish-colored water in the pool of Balıklıgöl with the fractured minaret of Dergah Mosque (right)

Figure 5.113. Damage at Ulu Mosque in Eyyübiye

Figure 5.114. A collapsed building in Eyyübiye district

In addition, a retaining wall in the organized industrial zone of Eyyübiye was damaged due to the earthquake as shown in Figure 5.115.

Figure 5.115. A collapsed retaining wall in organized industrial zone of Eyyübiye

5. 1. 9. 4. The situation of Transportation Network and Airport

The initial observations on the transportation network and highways indicated no severe damage. Fortunately, GAP Airport, located northeast of the city, is in service with its runways functioning.

5. 1. 9. 5. Observations on Liquefaction Hazard

Due to the nature of the city's soil/ground profile, no soil liquefaction was observed at the city center.

5. 1. 9. 6. Conditions Regarding Search, Rescue, and Residents

As of February 9, 2023, AFAD announced that the search and rescue teams located at Şanlıurfa are started to be transferred to other cities where there is an urgent need for such teams. As of

February 10, 2023, a great migration from the city center was observed; many local inhabitants have left and migrated to villages or other cities.

5. 1. 10. Kilis

Surrounded by three major cities, Gaziantep, Antakya, and Aleppo, Kilis lay at the crossroads of Anatolia and Syria. Due to its proximity to the Mediterranean Sea, it is located in a region where the climate changes from a Mediterranean to a continental character. It is also on the Fertile Crescent, which has been home to settlements since the dawn of history. The Syrian border crossing Öncüpınar is 5 km to the south and the major city of Gaziantep is 60 km to the north. In fact, Kilis was a district of Gaziantep Province until 1996, made a province by Tansu Çiller after an open vote gain in the 1995 general election. The Syrian border crossing Öncüpınar is 5 km to the south and the major city of Gaziantep is 60 km to the north. In fact, Kilis was a district of Gaziantep Province until 1996, made a province by Tansu Çiller after an open vote gain in the 1995 general election.

If the general geology of Kilis Province is examined from top to bottom; Alluvium is at the top and Yavuzeli Basalt is at the bottom. Beneath the basalt layer is the Şelmo Formation with alternations of conglomerate, sandstone, shale, tuffite and marl. Below the Şelmo Formation is the Euphrates Formation, which consists of cream colored massive and very densely bedded reef limestones. Below the Euphrates Formation is the Gaziantep Formation with alternating clayey limestone and calcareous limestone interspersed with limestone surfaces and very small chert nodules. Beneath this formation is the Ardıçlı Tepe Formation and an alternation of clastic limestone and Cretaceous limestone is observed at ground level. Below the Ardıçlı Tepe formation is the Aslan Su formation. In this formation, alternating marl at the bottom and clayey chert limestone at the top are observed.

The Cengin Formation, composed of agglomerate and tuff and containing a limestone lens, is present over the Aslan-Su Formation. Below the Cengin Formation is the Germav Formation, which consists of marl and clayey limestone at the bottom and marl at the top. Underneath the Germav Formation is the Koali Complex, which contains ultrabasic rocks, serpentinite, radiolarite, Cherty limestone and blocks of limestone of various ages. The Karadut Complex lies beneath the Koali Complex and contains silicified limestone, radiolarite, chert, cherty limestone and argillaceous limestone beds. Below the Black Mulberry Complex is the Bozova Formation, composed of clayey limestone.

These ground motions caused the collapse of many buildings while resulting in considerable damage to many structures, particularly in Hatay, Kahramanmaraş, Gaziantep, Malatya, Osmaniye, Kilis, Adıyaman, Diyarbakır, Şanlıurfa provinces. Field observations in Kilis revealed that, despite the devastating effect of the earthquake which took 10 provinces under its influence, the damage observed was lower in Kilis in comparison with above-mentioned cities. Between 8.02.2023 and 11.02.2023, field surveys were carried out in Kilis city center, Polateli, Elbeyli and Musabeyli districts. In our investigations, it was observed that weak columns/strong beam problems in buildings caused collapse or heavy damage in buildings. It has been determined that the Karakadı (1611) (Figure 5.116) and Şıh Hıdır (1569) (Figure 5.117), mosques from the 16-17th century in the city center of Kilis were heavily damaged and the minarets were destroyed, although restoration works were carried out. It was also observed that there are limited cleavages and the stone falls in the vicinity of transportation structures between Kilis city center and Musabeyli town (Figure 5.118), where ground motions had the most impact and loss of lifes in the province were more concentrated. In addition, it has been determined that the retaining walls made of briquettes have partially collapsed in the city center and also in the organized industrial zone of Kilis (Figure 5.119). No liquefaction or sand boiling was observed in the vicinity of Kilis city center and surrounding districts, which was attributed to the relatively deep groundwater table level. In the field observations, no road pavement damage, electricity pole damage, drinking and wastewater pipe damage and natural gas pipe damage were detected in Kilis city center.

Figure 5.116. Karakadı Mosque (heavily damaged) Photo by Assist. Prof. Dr. Eyyüb Karakan and Prof. Dr. Alper SEZER


KİLİS MÜFTÜLÜĞÜ
ŞIH HIDIR CAMİİ
ŞEYH HIDIR CAMİİ

Figure 5.117. Şıh Hıdır Mosque (heavily damaged) Photo by Assist. Prof. Dr. Eyyüb Karakan and Prof. Dr. Alper SEZER

Figure 5.118. Limited cleavages and the stone fall in the vicinity of transportation structures between Kilis city center and Musabeyli town. Photo by Assist. Prof. Dr. Eyyüb Karakan and Prof. Dr. Alper SEZER

Figure 5.119. Briquettes have partially collapsed in the city center and also in the organized industrial zone of Kilis. Photo by Assist. Prof. Dr. Eyyüb Karakan and Prof. Dr. Alper SEZER

5. 1. 11. Osmaniye

The documentation of performance of Ariklikas dam is presented in Figure 5.120. Figure 5.120b shows that the approximately 8-meter-wide crest has continuous cracks through the longitudinal direction which intensifies towards the center of the dam more than 4 meters wide openings. Similarly, towards the center of the dam, upstream slope is observed to have settled significantly near the crest. In parallel to these settlements, toe of the upstream slope was observed to bulge significantly which indicates potentiall slope instability. Furthermore, D400 highway connecting Osmaniye to Nurdagi experienced several earthquake-induced rockfall hazards as shown in Figure 5.121. Moreover, several partial or complete collapse of the buildings at the city center of Osmaniye is documented in Figure 5.122.

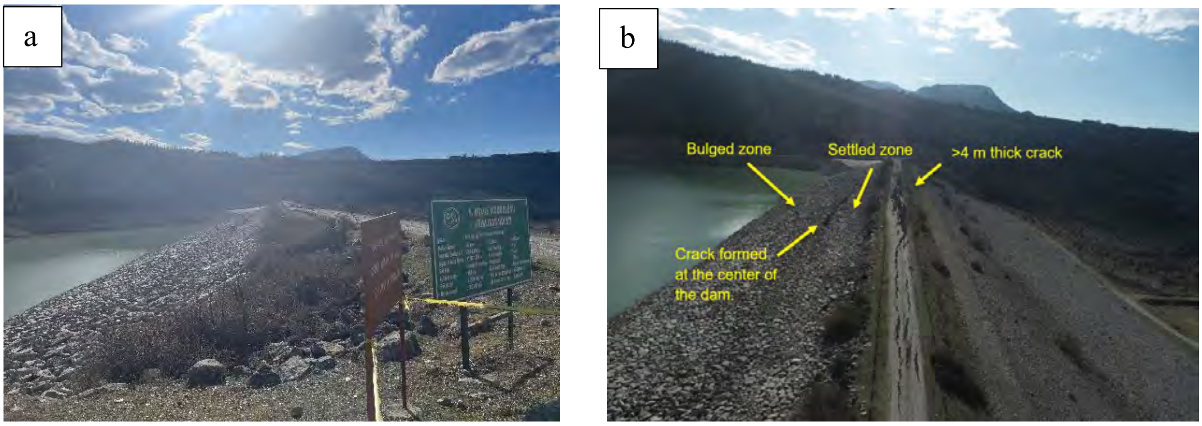

Figure 5.120. a) Ariklikas Dam (side view); b) Ariklikas dam (bird's-eye view) (~37°09'25.70"N/ 36°30'55.96"E). (Photo by Ozgun Numanoglu, Tugce Baser, Serhat Erinmez)

Figure 5.121. Earthquake-induced rockfall hazard at D400 connecting Osmaniye to Nurdagi(~37°10'48.17"N/ 36°42'45.62"E). (Photo by Ozgun Numanoglu, Tugce Baser, Serhat Erinmez)

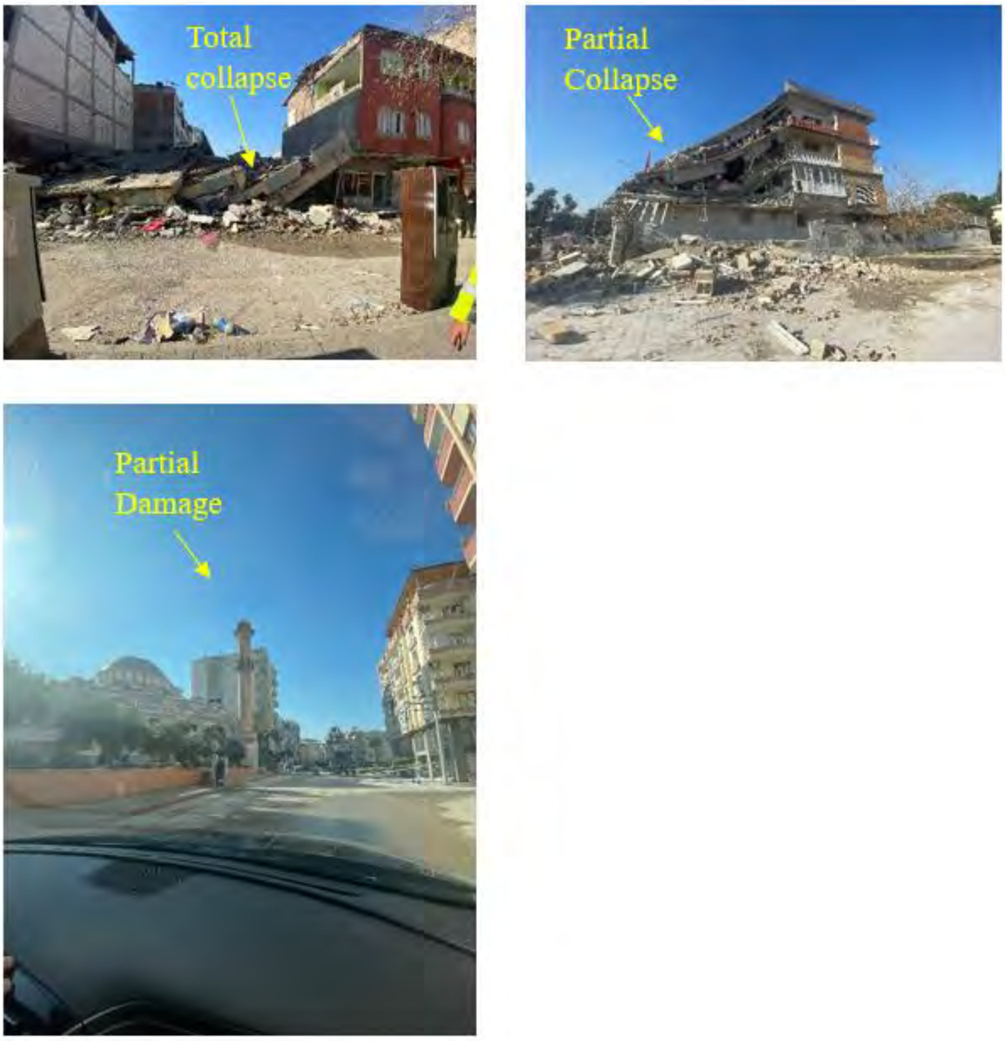

Figure 5.122. Total or partial collapse / damage documented fort the buildings in Osmaniye City Center: a) Total collapse case (~37°04'28.75"N/ 36°14'55.78"E); b) partial collapse case (~37°04'30.97"N/ 36°14'50.00"E); c) partial damage case (~37°04'15.08"N/ 36°14'46.00"E) (Photo by Ozgun Numanoglu, Tugce Baser, Serhat Erinmez)

5. 1. 12. Kayseri

Kayseri and its vicinity in the Central Anatolia Region are under the effect of some important fault zones. One of the most important fault zones is the NE-SW trending Central Anatolian Fault Zone with a left lateral strike slip within the continent that controls Kayseri and its vicinity and the eastern part of Central Anatolia (CAFZ) (Koçyiğit and Beyhan, 1998), as shown in Figure 5.123.

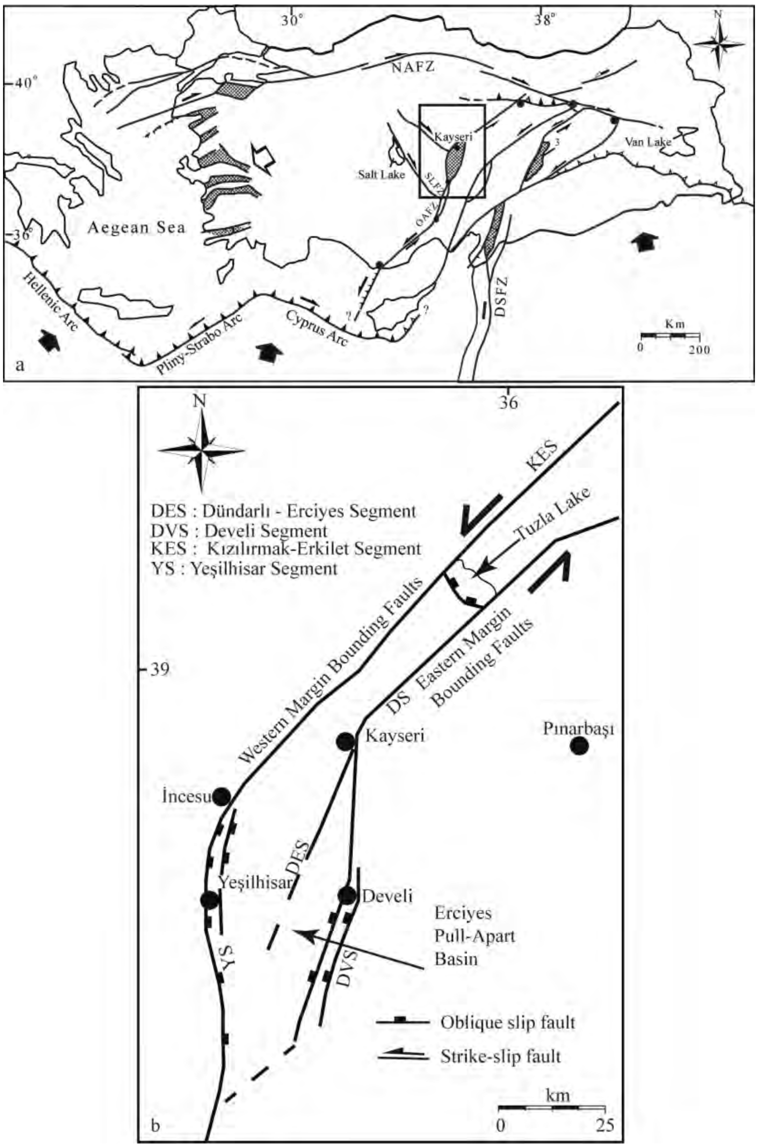

Figure 5.123. Simplified neotectonics map of Türkiye and the environment (DSFZ: Dead Sea Fault Zone, SLFZ: Salt Lake Fault Zone, NAFZ: North Anatolian Fault Zone (modified from Koçyiğit and Beyhan, 1998; taken from Cilsaar and Temiz, 2020), b) Neotectonic map of the Erciyes pull-apart basin included in the Central Anatolian Fault Zone modified from (Koçyiğit and Erol, 2001; taken from Cilsaar and Temiz, 2020).

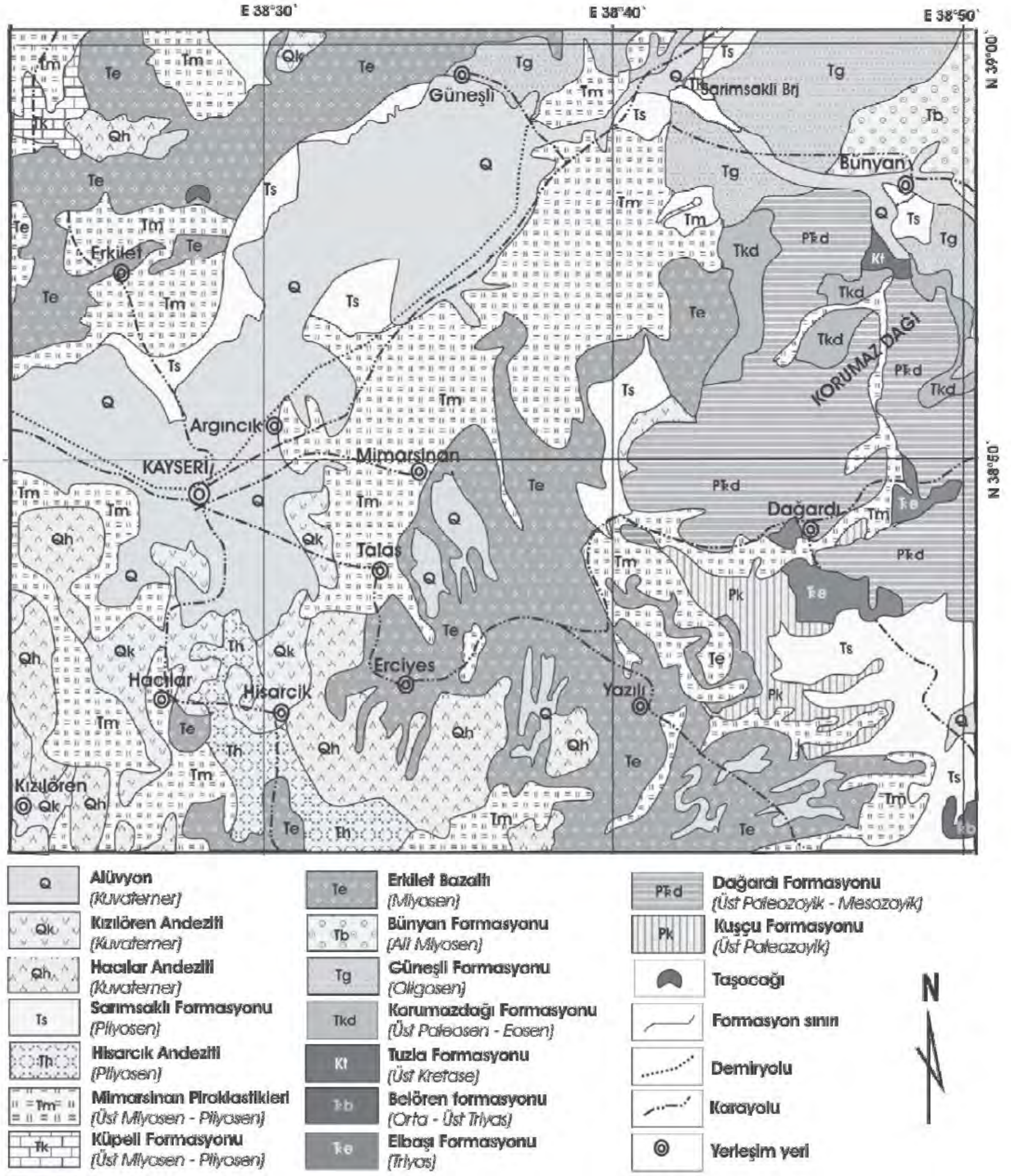

Figure 5.124. Geological map of the study area (modified from 1/500000 scaled geological map edited by MTA, 2002)

NE trending fault, which is approximately 730 km long and 2 to 80 km wide, consists of 24 segments while covering the Anatolian plate (Koçyiğit and Erol, 2001). This fault zone is bending in the region of Kayseri and forms Erciyes pull-apart basin and Erciyes volcanic complex. The current deformation of Central Anatolia lasts on several second-order faults like the CAFZ, which extends about 730 km from Erzincan in the northeast Türkiye to the Eastern

Mediterranean Sea in the south (Koçyiğit and Beyhan, 1998). It is considered as a large shear zone, formed by the reactivation and propagation of a paleotectonic structure (Şengör and Yılmaz, 1981). Although, it is seismically less active than other fault zones in Türkiye, it is considered that it will form the eastern boundary of the Anatolian plate in the future, instead of the Eastern Anatolian Fault Zone (Koçyiğit and Beyhan, 1998). CAFZ shows many geomorphic features characterized by strike-slip faulting, comprising volcanic emplacements in a double-bended left lateral pull-apart basin (Erciyes–Sultansazlığı pull-apart basin). The fault zone comprises several segments, including the Ecemiş Fault (Sarıkaya et al., 2015).

An earthquake catalogue is organized including events between 1900 and 2018, and magnitude of these earthquakes are higher than 4 (AFAD, 2019).

Table 5.3 Historical earthquakes in Central Anatolia between the years 240-2023 (modified after Cilsar and Temiz, 2020).

Date (year/month/day)	Coordinates	Location	Intensity	Magnitude
240	-	Kayseri-Sivas	IX	
1104	-	Niğde	IX	
1205	38.70-35.50	Kayseri	VIII	
1695.01.01	-	Sivas	-	
1704.06.09	-	Kayseri	-	
1714	-	Kayseri	VII	
1717.05.09	38.70-35.50	Kayseri	VIII	
1754.09.16	39.75-37.00	Kangal (Sivas)	VII	
1779.03.14	-	Divriği (Sivas)	-	
1835.08.23	38.30-35.50	Develi (Kayseri)	VIII	
21.02.1940	38.70-35.30	Erciyes		5.3
21.02.1940	38.40-35.30	Yeşilhisar		5.2
31.08.1960	39.09-35.98	Sarıoğlan		4.7
18.09.1989	38.97-35.54	Felahiye		4.3
10.10.1989	39.01-35.40	Felahiye		4.2
14.12.1998	39.06-35.84	Sarıoğlan		4.5
14.12.1998	39.04-35.84	Sarıoğlan		4.7
15.12.1998	39.04-35.88	Sarıoğlan		4.3
12.11.2008	38.83-35.56	Çavuşağa-Kocasinan		4.8
04.08.2021	38.92-35.66	Sayacık-Kocasinan		4.1

After the 7.7 Pazarcık (K.Maraş) and 7.5 Elbistan (K.Maraş) earthquakes, which were intensely felt in the center of Kayseri, people experienced panic, especially on 6 February and 7 February, and they could not enter their homes and spent their nights in cars, school gyms, large sports halls, and university buildings. Accordingly, a detailed examination was carried out for the damaged building, especially in the city center, and its details are given below. In the observations made, it was determined that the damages were of structural origin.

Although there was no totally collapsed building in the city center, it was decided to demolish 4 multi-storey buildings that were heavily damaged, and more than 5 thousand homeowners requested damage assessment due to the concern of cracks and plaster spillage. After the examinations, it was announced that 73 buildings were heavily damaged. The minarets of all four mosques built recently were destroyed and the mosque was damaged to a large extent Besides general structural failures are depend on the quality of the structures (https://www.canligaste.com/son-dakika-depremin-ardindan-kayseri-de-yikilacak-bina-sayisi-belli-oldu/307798/).

Since it is close to the earthquake zone, it is seen that the damage is high in Sarız district. During our work there, 48 houses, 11 barns and 1 small school were severely damaged. Beyond that, 2,432 damage assessment studies were carried out throughout the province. Of these, 73 were severely damaged. We also have minarets inside these buildings. An emergency demolition decision was made for 3 residences in the city center. According to the earthquake analysis report Kayseri authorities have made, there are 9 schools in total. 3 schools are evacuated because they were in danger of collapsing. The authorities mentioned that the process continues for the remaining 6 schools.

Kayseri city center is located on generally alluvial material. Kayseri city center is one of the provinces where active faults pass under the buildings in the city center. For this reason, it is expected that Kayseri will be damaged in a possible earthquake greater than 6.5 due to both the severe shaking caused by the earthquake and the danger of surface faulting.

Kayseri was one of the provinces affected by the 7.7 magnitude earthquake that occurred on 06.02.2023 at around 04:17, the epicenter of which was Kahramanmaraş. After the first earthquake, around 13:15, the epicenter was again in Kahramanmaraş and after the second earthquake with a magnitude of 7.6, some structures were damaged in the center and districts of Kayseri. One of the most damaged buildings in the center of Kayseri is the building (Gevher Nesibe Neighborhood Street, located at 38.7265, 35.5047 Figure 5.123).

Figure 5.125. Map view of damaged building

Considering the examinations performed after the earthquake, visible damage was found in some columns of the building (Figures 5.126 and 127). When the damage in the columns was examined closely, it was noticed that the reinforcement used was non-ribbed bar. In addition, when the facade of the building is examined, cracking in the plaster can be seen easily. In addition, cracks are evident on the walls of the business center and shop on the first four floors (Figures 5.128 and 129). In addition, diagonal breaks on the facade are also clearly visible. According to the evaluations of municipal officials, civil engineers it was concluded that the building was heavily damaged (Figures 5.130 and 131).

Figure 5.126. Column damage, plastic hinging

Figure 5.127. Damaged building, plastic hinging

Figure 5.128. Partition wall damage

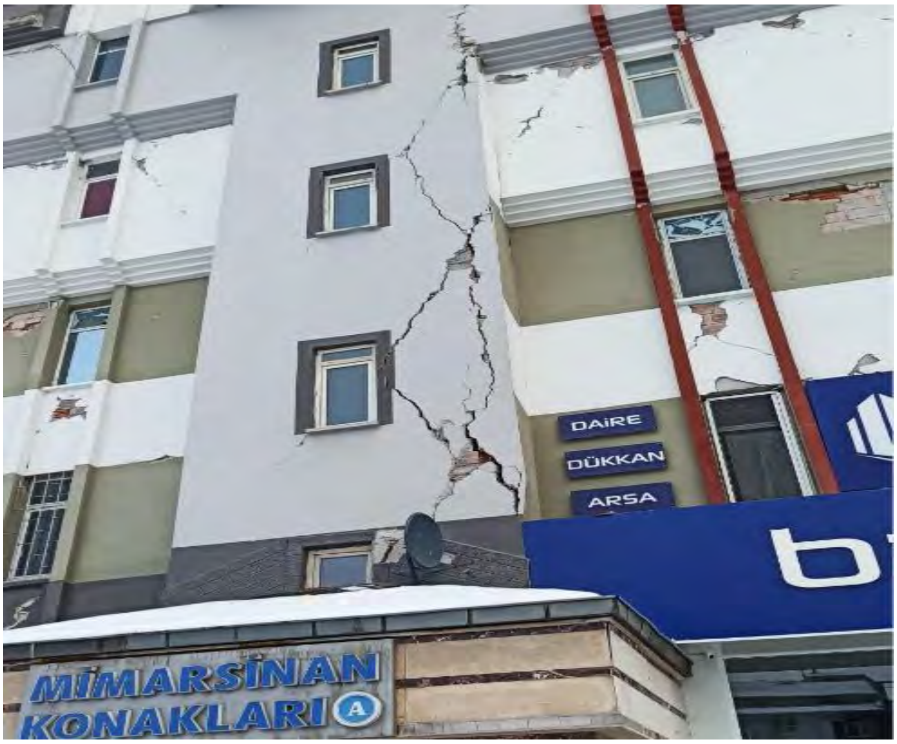

Figure 5.129. Shear cracking

Figure 5.130. Facade damages

Figure 5.131. Front view of a damaged building complex

5. 1. 13. Damage in Republic of Syria

Syria is located to the southeast of Türkiye on the north of the Arabian plate and bordered by the Dead Sea fault to the west, the East Anatolian fault to the north, and the Eurasian plate to the northeast and east, Figure 5.132.

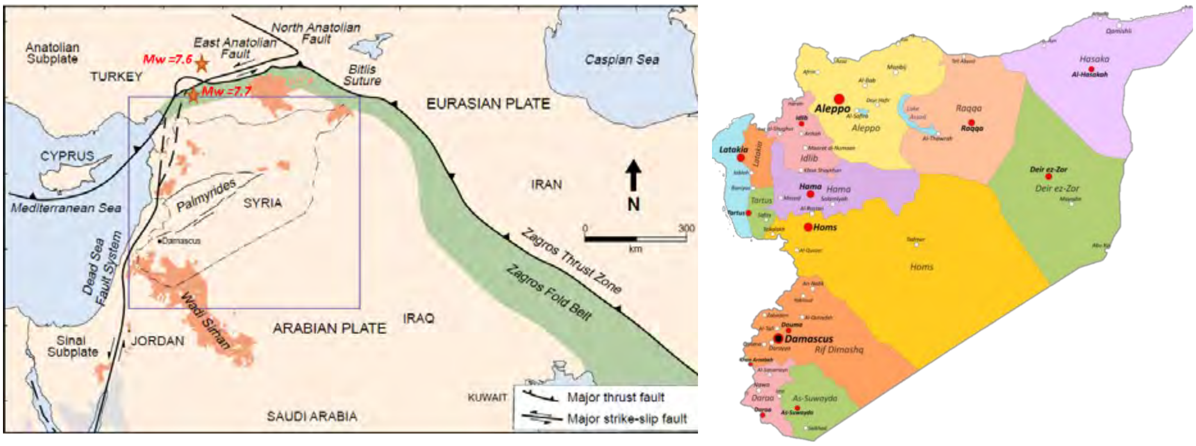

Figure 5.132. Syria and its location in correspondence to tectonic plates, showing the epicenters of the earthquake events, (After Brew et al., 2001, ontheworldmap.com).

Syria was greatly affected by the earthquake events that occurred in Türkiye, especially, in the northwestern region of the country resulting in to the date of writing this report, more than 8.8 million people affected, 6000 deaths, and 12000 injuries. Regarding structures, more than 1700 were destroyed and 5700 were partially damaged buildings according to United Nation Humanitarians Affairs.

The affected cities in Syria are Aleppo, Idlib, Latakia, and Hama, respectively, along with relatively less damage in the other cities of the country. The severity of the damage was gradually decreasing with increased distance to Türkiye's border and in turn the earthquake's epicenter proximity.

The greatest damage was in the city of Aleppo and its northwestern suburbs (Mostly in Jindires, Afrin, A'zaz, and Sawran). Figure 5.133 shows an example of the destruction in Jindires, where most of the buildings have been totally collapsed or damaged severely.

Figure 5.133. Destruction in Jindires – Afrin, Aleppo, approximate location (36°23'46.76"N, 36°41'14.26"E)

Nevertheless, in Idlib North suburban (Mostly in Harem, Sarmada, Aldana, Salqin, and Armanaz). Figure 5.134 shows the destruction in Harem due to the earthquake.

Figure 5.134. Destruction in Harem, Idlib, approximate location (36°12'45.01"N, 36°31'13.72"E)

Regarding affected service structures, it was spoken of 17th April or Medanki dam in Afrin as being damaged due to the earthquake. But, as per reported by a committee of civil engineers who inspected the dam, there is no visible damage in the body of the dam and there is no water leakage observed. The seen cracks at the top road constructed over it are just in the asphalt layer of the road with a 4cm width and 40cm depth, Figure 5.135.

It is an earth-fill dam with 980 x 10 / 325 x 75 m and has a capacity of 190 million m3.

Figure 5.135. Medanki dam showing the cracks in the road at the crest, (36°37'18.56"N, 36°52'17.19"E), (syria.tv).

In the Tloul village in the subdistrict Salqin, Idlib, a flood occurred due to an increase in the AlAsi river water level due to the winter season and damage to the constructed mud shoulders on the sides of the river in the mentioned village and its neighborhood resulting in approximately 1000 home affected and evacuation of 7000 people, Figure 5.136.

Figure 5.136. Flooded village of Tloul in Salqin, Idlib, (36°12'42.82"N, 36°23'40.89"E), (nasnews.com).

In the subdistrict of Afrin, collapsed electricity supply tower as a result of a stability problem in the foundation soil, Figure 5.137.

Figure 5.137. Slope failure in the proximity of the Afrin subdistrict.

Also, due to the earthquake historical buildings sustained limited damage. In the case of Aleppo castle, some parts of the ottoman mill, and the northeastern defensive walls. Also, historical buildings in Hama and Banias have sustained similar light to moderate damage, (Directorate General of Monuments and Museums, Syria).

As a reminder, the damage due to the earthquake is not limited to the above-mentioned, many other areas were stroked by the earthquake and sustained different levels of damage in a country worn out by 12 years of civil war. Even before the earthquake events, the living conditions were harsh and now many families are still under the rubble due to the earthquake, waiting for help and the local capabilities are lacking to machinery tools to be able to rescue these people, especially in the north and northwestern parts of the country.

5. 1. 14. Landslides

In the observations made, it was seen that many landslides occurred due to the earthquake effect in the studied locations. Landslides are categorically classified as:

- Landslides in road cuts
- Landslides in road embankments
- Landslides in mixed section

Since the acceleration and duration of the earthquake were high, it was noted that the permanent displacement levels after the earthquake were relatively high, and the tension crack widths were similarly high. On the other hand, it is thought that road ruptures caused by elastic earthquake waves or fault lines on the road/ the side of the road and vertical displacements (subsidence or uprise) encountered can be confused with landslides from time to time and it is an important detail that they should be carefully distinguished. These images were also taken within the scope of the study, but they are not included here.

Figure 5.138. Planar sliding mass on the roadside (hekimhan-sivas Road)

Figure 5.139. Planar sliding mass on the roadside (hekimhan-sivas Road)

Figure 5.140. Failure of reinforced concrete elements at the landslide heel (hekimhan-sivas Road)

Figure 5.141. Shallow planar slips (hekimhan-sivas Road)

Figure 5.142. Partial landslide development due to earthquake at the roadside (bingol-elazig road junction)

Figure 5.143. Earthquake-induced tension cracks in the road fill zone (bingol-elazig road junction)

Figure 5.144. Landslide tension cracks on the roadside (bingol-elazig road junction)

Figure 5.145. Development of tension cracks in the landslide crown zone, possibly on the mixed ground, on the roadside (bingöl-elazig road junction)

Figure 5.146. Landslide occured due to earthquake (Bingöl-Elazig road junction)

Figure 5.147. Landslide induced by earthquake (Bingöl-Karlıova road)

Due to the hihg level of accelaration it is observed that the displacement amount of slope become high

Figure 5.148. Landslide induced by earthquake (Bingöl-Karlıova road)

Figure 5.149. Earthquake induced Landslide occured at Sancak road

Figure 5.150. Earthquake induced Landslide occured at Sancak road

Figure 5.151. Earthquake induced Landslide occured at Sancak road

Figure 5.152. Flow and mass slides in the talus on the bedrock (Sancak road)

5. 1. 15. **Rockfalls**

(ENG) As a result of Kahramanmaraş-centered earthquakes (M_w 7.7 and 7.6) February 6, 2023, 11 provinces were destroyed and many of our citizens lost their lives. In addition to the destruction caused by the earthquake, it triggered the rockfalls and as a result of that transportation routes and some settlements were affected and caused disruption of transportation. On the other hand, the rock blocks that fell during the earthquake in Gaziantep province Islahiye district, Fevzipaşa neighborhood caused the death of two people. In general, rockfalls are locally observed mass movements. Because of the Kahramanmaraş earthquakes, intense rockfalls were encountered in many areas where earthquakes were effective. Especially on the slopes of highways, many blocks in the source zones broke off from the slopes and reached the transportation routes. In the site observations made after the earthquake, rockfalls were detected in many areas. Rockfalls were encountered in Hatay-Belen, Gaziantep-Islahiye Fevzipaşa, Gaziantep Nurdağ-Sakçagözü, Malatya-Erkenek regions. Although the dimensions of the falling blocks are variable, rockfalls with dimensions exceeding 3 m have been detected in these investigations (Figure 5.153 through 5.156). This study was also supported by TUBITAK with 1002 – C Natural Disaster Focused Field Study Emergency Support Program

Figure 5.153. Hatay-Belen rockfall (Photo by Müge Akın)

Figure 5.154. Gaziantep-Islahiye Fevzipaşa rockfall (Photo by Ogün Ozan Varol)

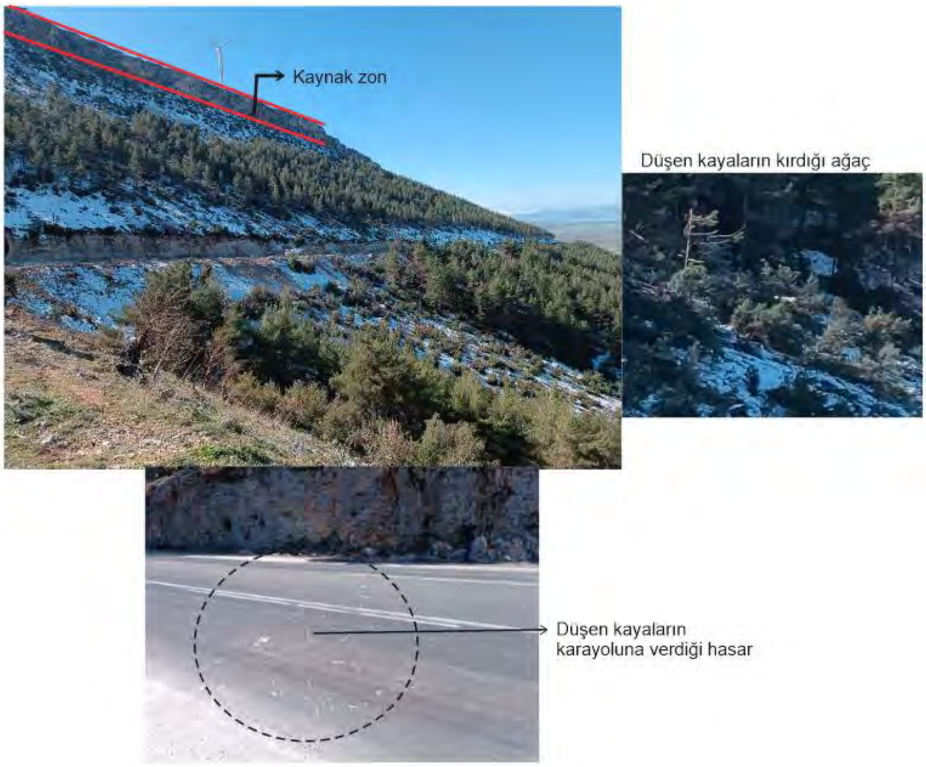

Figure 5.155. Gaziantep Nurdağ-Sakçagözü rockfall (Photo by Ogün Ozan Varol)

Figure 5.156. Malatya-Erkenek rockfall (Photo by Metehan Başer)

Figure 5.157. Adıyaman, Gölbaşı district Karamağara rockfall (Photo by Ayhan Gürbüz)

Figure 5.158. Another view of Adıyaman, Gölbaşı district Karamağara rockfall (Photo by Seyhan Fırat)

Figure 5.159. Rock falls along Altınözü road (Photo by Eylem Arslan)

Figure 5.160. Rock falls and rockslides along Hatay Büyük Karaçay Dam Skirts, Power Plant transportation road (Photo by Faik Cüceoğlu)

Figure 5.161. Rock falls and rockslides along Hatay Büyük Karaçay Dam Skirts, Power Plant transportation road (Photo by Faik Cüceoğlu)

Figure 5.162. Rock falls along Osmaniye Kalecik Dam bottom sluice transportation road (taken by Faik Cüceoğlu)

5. 1. 16. Airports and Harbors

This section summarizes the preliminary findings of ongoing geotechnical reconnaissance studies after the earthquakes focusing on the performance of airports and harbors. Several geotechnical reconnaissance teams were mobilized to the earthquake area to investigate the performance of critical infrastructure. The discussion here will focus on harbors, and airports.

5. 1. 16. 1. Airports

There exist 11 airports located 250 km away from the epicenter of the M_w 7.7. Kahramanmaraş -Pazarcik Earthquake as shown in Figure 5.163.

Figure 5.163. Location of the airports in the earthquake-affected area

Kahramanmaraş, Gaziantep, Hatay airports were closed after the earthquakes due to damages or inspection of the state of the airports (https://www.afad.gov.tr/kahramanmaras-pazarcikta-meydana-gelen-deprem-hk-basin-bulteni6) as announced by AFAD on 06.02.2023 at 03:35pm. At the airports in Elazig and Diyarbakır, no damage was reported by the field reconnaissance teams, and the required services were available. Malatya Airport, on the other hand, is reportedly partially structurally damaged and closed for commercial flights, but open for relief and rescue supplies. Şanlıurfa GAP Airport, located northeast of the Urfa city center, is in service with its runway functioning. No structural or geotechnical damage occurred during the earthquakes as reported by the teams in the field. Gaziantep and Şanlıurfa airports were announced to be open only to aid flights while Malatya, Adana, Diyarbakır, Adıyaman airports were open to service (https://www.afad.gov.tr/Kahramanmaraş -pazarcikta-meydana-gelen-deprem-hk-basin-bulteni10) as stated by AFAD on 07.02.2023 at 12:15 pm. On 12.02.2023 at 04:14 am, Ministry of Transport and Infrastructure, Republic of Türkiye announced that Hatay airport was open to service from the official Twitter account.

Reconnaissance studies are performed in Hatay Airport on 09.02.2023. A full mapping of the earthquake-induced damage in Hatay Airport was reported by the researchers. Figure 5.164 shows the observation of the fault rupture and fault displacement, liquefaction in the form of lateral spreading, soil ejecta, and excessive settlement at the airport. Another reconnaissance team visited the Hatay Airport (HTY), on 14.02.2023 (8 days after the first main shock). The airport was in service with its runway functioning during the investigations. No visible damage was observed in the Domestic Terminal Building. Vertical deformations, accompanying, cracks, and signs of liquefaction were observed through the soil between the apron and Domestic Terminal Building Section L. Significant vertical settlements were observed at the free field between the Domestic Terminal Building and the apron, where a recently constructed ramp for passengers can also be seen. Preliminary measurements indicate that the apron side settled about 40 cm relative to the terminal building side.

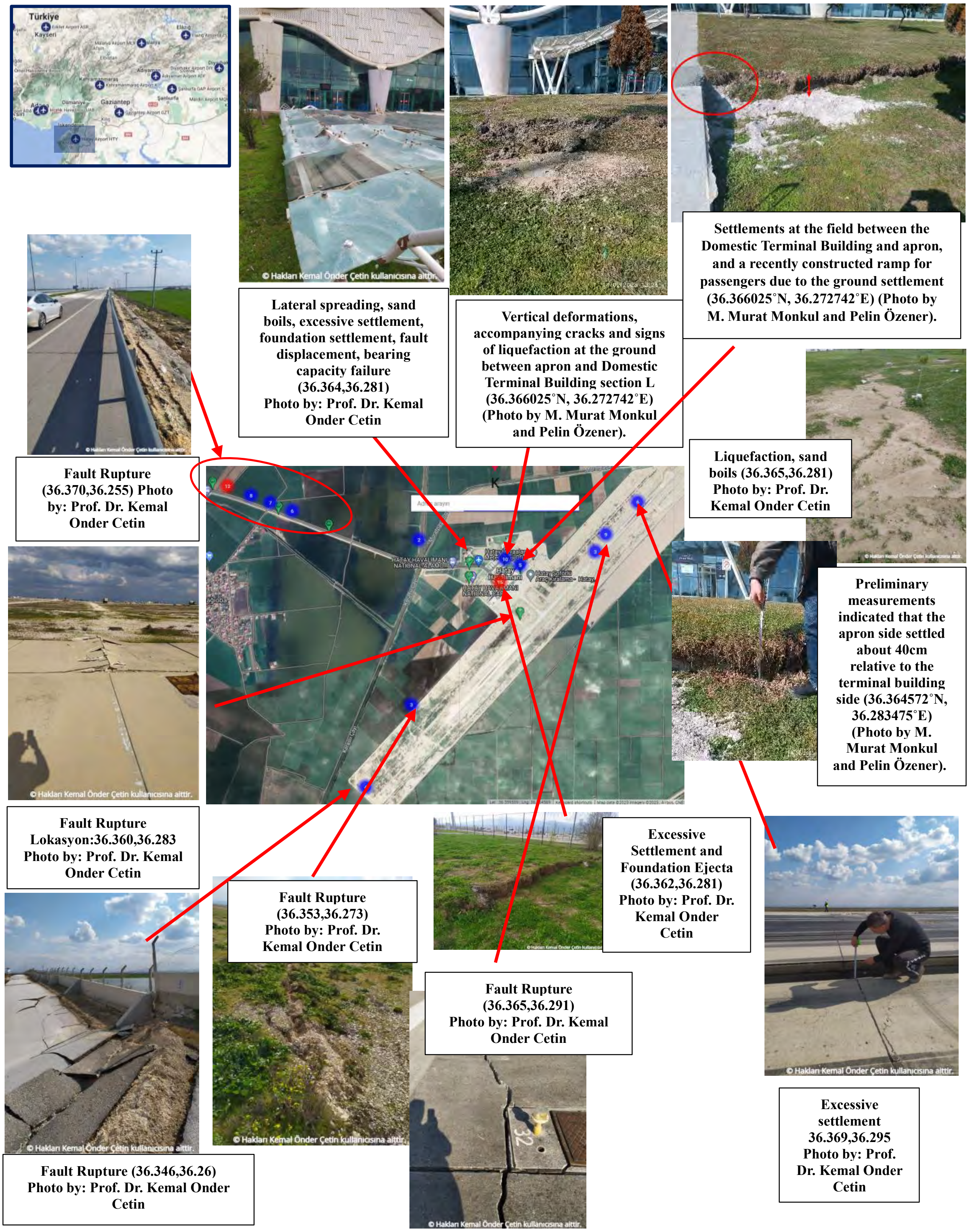

Figure 5.164. Hatay Airport ground deformation and liquefaction features

5. 1. 16. 2. Harbors

Along the route, several ground deformations due to seismic soil liquefaction were mapped by reconnaissance teams. The liquefaction phenomena were widely observed at the Dörtyol municipality public beach and shoreline, in several ports of Iskenderun Bay area and in Iskenderun Customs and Fishery port regions.

5. 1. 16. 2. 1. Dörtyol Municipality Public Beach

Seismic soil liquefaction-induced surface manifestations in the form of ejecta, lateral spreading, subsidence, and structural damage were accompanied to liquefaction triggering at these sites as displayed in Figure 5.165 to 168. Some of these manifestations were observed at free field sites. In addition to free field sites, liquefaction surface manifestations were also observed in the vicinity of building foundations.

(a)

(b)

Figure 5.165. Seismic soil liquefaction induced ground deformations in Dörtyol / Hatay a) 36.82043,36.17322 b) 36.82071, 36.17359 (photo taken by Dr. Robb Moss).

(a) (b)

Figure 5.166. Seismic soil liquefaction induced lateral spreading in Dörtyol / Hatay a) 36.82067,36.17367, b) 36.82072,36.17372 (photo taken by Dr. Kemal Onder Cetin).

(a) (b)

Figure 5.167. Seismic soil liquefaction induced settlements in Dörtyol / Hatay a) 36.82085,36.17402, b) 36.82117,36.17458 (photo taken by Dr. Kemal Onder Cetin).

(a) (b)

Figure 5.168. Seismic soil liquefaction induced surface manifestation in the form of soil ejecta in Dörtyol / Hatay a) 36.82108,36.17467, b) 36.82109,36.17468 (photo taken by Dr. Kemal Onder Cetin).

5. 1. 16. 2. 2. Dörtyol Shoreline

The second stop on the reconnaissance route was the coast of Dörtyol district. Like the municipality beach, several surface manifestations due to seismic soil liquefaction were observed in the form of ejecta, lateral spreading at the sites as displayed in Figure 5.169 and 170. Here the majority of the manifestations were observed at free field sites.

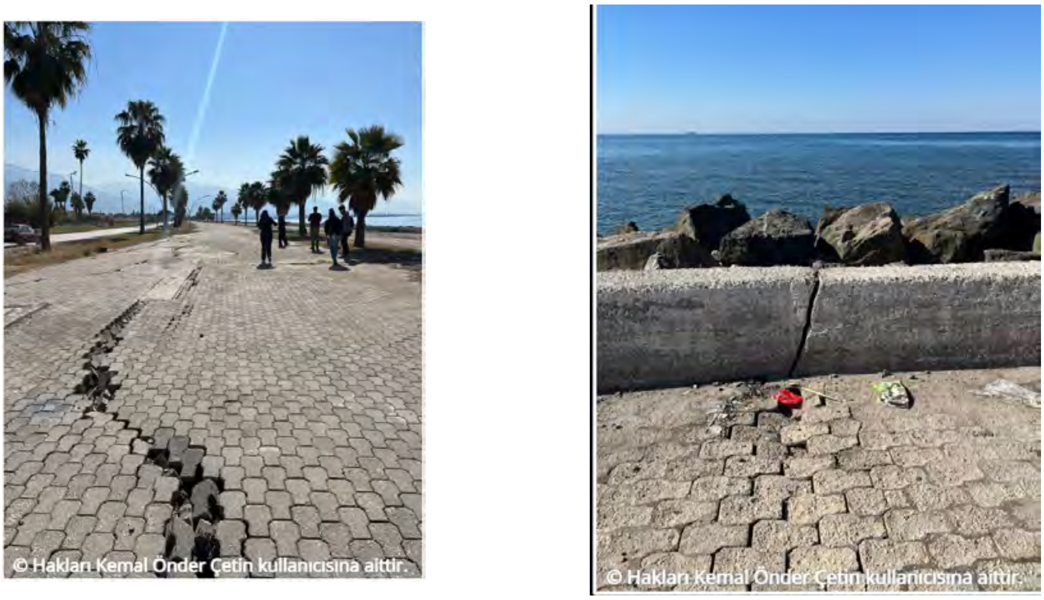

(a) (b)

Figure 5.169. Seismic soil liquefaction induced surface manifestation in the form of soil ejecta in Dörtyol / Hatay a) 36.81295,36.18141, b) 36.81269,36.18138 (photo taken by Dr. Kemal Onder Cetin).

(a) (b)

Figure 5.170. Seismic soil liquefaction induced surface manifestation in the form of soil ejecta in Dörtyol / Hatay a) 36.81274, 36.18147, b) 36.81283, 36.18182 (photo taken by Dr. Kemal Onder Cetin).

5. 1. 16. 2. 3. Port and Industrial Facilities in İskenderun Bay

Seismic soil liquefaction-induced surface manifestations in the form of ejecta, lateral spreading, subsidence, and structural damage were accompanied to liquefaction triggering at these sites as displayed in Figure 5.171 to 175. Some of these manifestations were observed at free field sites. In addition to free field sites, liquefaction surface manifestations were also observed in the vicinity of building foundations.

(a) (b)

Figure 5.171. Seismic soil liquefaction induced ground deformations in Iskenderun Bay a) 36.78337,36.20344 b) 36.77877,36.20430 (photo taken by Dr. Robb Moss).

(a)

(b)

Figure 5.172. Seismic soil liquefaction induced lateral spreading in Iskenderun Bay a) 36.78331,36.20211, b) 36.78343,36.20270 (photo taken by Dr. Kemal Onder Cetin).

(a)

(b)

Figure 5.173. Seismic soil liquefaction induced settlements in Iskenderun Bay a) 36.78331,36.20379, b) 36.78189,36.20447 (photo taken by Dr. Kemal Onder Cetin).

(a)

(b)

Figure 5.174. Seismic soil liquefaction induced surface manifestation in the form of soil ejecta in Iskenderun Bay a) 36.78236,36.20439, b) 36.78209,36.20302 (photo taken by Dr. Kemal Onder Cetin).

(a)

(b)

Figure 5.175. Seismic soil liquefaction induced structural damage in Iskenderun Bay a) 36.78212,36.20376, b) 36.78328,36.20373 (photo taken by Dr. Kemal Onder Cetin).

At the İskenderun district, another major port typically handling raw and manufactured industrial products was also visited. The investigated section of the port was mainly constructed in 1974 as a block type gravity quay wall, where significant cracks, vertical and horizontal deformations were observed in concrete blocks. The approximate values for the vertical and lateral deformations are measured as 90 cm and 60 cm respectively as shown in Figure 5.176.

Figure 5.176. Vertical and horizontal deformation measurements in a port section (Photo by M. Murat Monkul and Pelin Özener).

Seismic soil liquefaction-induced surface manifestations in the form of ejecta, lateral spreading, subsidence was accompanied to liquefaction triggering at the site as displayed in Figure 5.177.

Figure 5.177. Seismic soil liquefaction induced settlements in Iskenderun Bay 36.72949,36.19893 (photo taken by Dr. Pelin Ozener and Dr. Murat Monkul).

At various locations of the port, sand ejecta was observed on the surface indicating liquefaction of the underlying soils, which could also be considered among the main reasons for the large lateral deformations of the quay walls. A sand ejecta was observed on the surface of the port deck as shown in Figure 5.178.

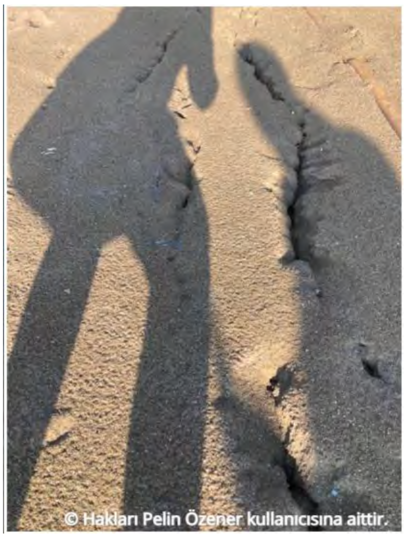

(a) (b)

Figure 5.178. Seismic soil liquefaction induced surface manifestation in Iskenderun Bay a) 36.72998,36.19625, b) 36.72996,36.19689 (photo taken by Dr. Pelin Ozener and Dr. Murat Monkul).

Some sections of the port way, being used by the loading trucks, were collapsed into the sea during the earthquake as shown in Figure 5.179 below. Deformations effecting the quay walls also caused damages in the rails and tilted some of the cranes at the port as shown in Figure 5.180.

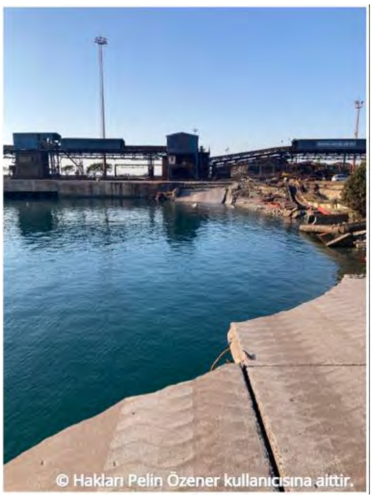

(a) (b)

Figure 5.179. a) Collapsed port way during the earthquake, where tire tracks of the loading trucks are 36.73208,36.19735, b) Significant deformations tilted crane 36.72059,36.20166 (photo taken by photo taken by Dr. Pelin Ozener and Dr. Murat Monkul)

In 2006, a modernization study was conducted, and some sections of the port was extended on steel pipe piles. It was observed that the extended port section supported by piles performed quite well during the earthquakes. As shown in Figure 5.180 no damage was observed on the extended section of the port.

Figure 5.180. Extended section of the port on steel pipe piles performed well during the earthquake (Photo by M. Murat Monkul and Pelin Özener).

5. 1. 16. 2. 4. The Zones of Ports-Iskenderun

Seismic soil liquefaction-induced surface manifestations in the form of ejecta, lateral spreading, subsidence was accompanied to liquefaction triggering at these sites as displayed in Figure 5.181 and 182. Some of these manifestations were observed at free field sites. In addition to free field sites, liquefaction surface manifestations were also observed by structural foundations.

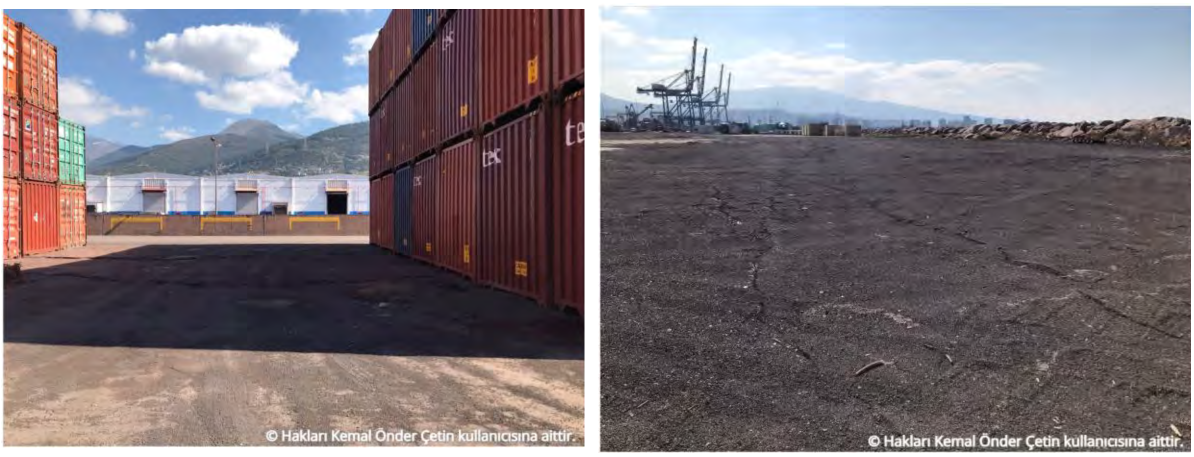

Figure 5.181. Seismic soil liquefaction induced lateral spreading in Iskenderun Zones of Ports / Hatay a) 36.60558,36.19426, b) 36.60356,36.19233 (photo taken by Dr. Kemal Onder Cetin).

(a) (b)

Figure 5.182. Seismic soil liquefaction induced surface manifestation in the form of soil ejecta in Iskenderun Zones of Ports / Hatay a) 36.60429,36.19297, b)36.60346,36.19299 (photo taken by Dr. Kemal Onder Cetin).

5. 1. 16. 2. 5. Iskenderun Customs Region

Seismic soil liquefaction-induced surface manifestations in the form of ejecta, lateral spreading, subsidence, and structural damage were accompanied to liquefaction triggering at these sites as displayed in Figure 5.183 to 185. Some of these manifestations were observed at free field sites. In addition to free field sites, liquefaction surface manifestations were also observed in the vicinity of building foundations.

Figure 5.183. Seismic soil liquefaction induced lateral spreading in Iskenderun Customs / Hatay a) 36.59361,36.18735, b) 36.59389,36.18539 (photo taken by Dr. Kemal Onder Cetin).

Figure 5.184. Settlement due to seismic soil liquefaction in Iskenderun Customs / Hatay 36.59284,36.18582 (photo taken by Dr. Kemal Onder Cetin).

Figure 5.185. Seismic soil liquefaction induced surface manifestation in the form of soil in Iskenderun Customs Region / Hatay a) 36.59198,36.18390, b) 36.59313,36.18532 (photo taken by Dr. Kemal Onder Cetin).

5. 1. 16. 2. 6. Iskenderun Fishery Port

Seismic soil liquefaction-induced surface manifestations in the form of ejecta, lateral spreading, subsidence, and structural damage were accompanied to liquefaction triggering at these sites as displayed in Figure 5.186 through 188. Some of these manifestations were observed at free field sites. In addition to free field sites, liquefaction surface manifestations were also observed in the vicinity of building foundations.

(a) (b)

Figure 5.186. Seismic soil liquefaction induced lateral spreading in Iskenderun Fishery Port / Hatay a) 36.59218,36.17319, b) 36.59159,36.17426(photo taken by Dr. Kemal Onder Cetin).

Figure 5.187. Settlement due to Seismic soil liquefaction in Iskenderun Fishery Port / Hatay a) 36.59274,36.17267, b) 36.5927,36.17263 (photo taken by Dr. Kemal Onder Cetin).

Figure 5.188. Seismic soil liquefaction induced surface manifestation in the form of soil ejecta in Dörtyol / Hatay a) 36.5914,36.175675, b) 36.59134,36.17894 (photo taken by Dr. Kemal Onder Cetin).

5. 1. 17. Seismic Soil Liquefaction Manifestations

In this section seismic soil liquefaction manifestations will be presented.

Hatay-Iskenderun Coast Line

Along the Iskenderun coastal line, sand ejects were encountered on the edges of many buildings and free field. Figure 5.189 shows sand ejecta locations and their spread areas in Iskenderun, Hatay. Figure 5.190 shows the points where pictures were captured, and green arrows indicate their directions in the field. Building settlements were recorded approximately 35-50 cm on the coastline of Piri Reis, Savaş, Süleymaniye and Çay districts. Swelling has occurred in the parcels between two high-rise buildings and single-storey light structures. After the earthquake on the Iskenderun coast, especially in the Çay District, it has been understood that the water spreading in the 200-300 m wide area from the coastline inwards was due to the liquefaction of the uniform silty sands and their coming to the surface together with the water. A part of Atatürk Boulevard on the beach was filled with sand and water. After the recession of the waters, the remaining sand was removed from the roads by the authorities and the coastal road was opened for use. Some points where sand outflows are observed, it has been observed that ejected sands spread up to 700 m2 has occurred. It is noteworthy that almost all of the settlements in the coastal area were uniform. It is understood that the foundation settlements of the structures in this part of the Iskenderun coast are the result of widespread liquefaction in this area. The manhole covers on the Atatürk Boulevard Road have risen a little above the road level or the whole area has settled as a result of liquefaction. It is thought that the entire coastal part was completely settled due to the liquefaction, as a result, the manhole covers appeared to have risen. Figures 5.191 and 192 show structural deformations because of soil liquefaction on the Bahçeli Sahil Evler Street, here it can be seen that these buildings have sand ejecta points in their foundation borders.

Figure 5.189. Hatay, Iskenderun, Sand Ejecta Locations (Çay District, East Coast of Atatürk Boulevard)

Figure 5.190. Hatay, Iskenderun, location and numbers of the pictures (East Part of Atatürk Boulevard)

Figure 5.191. Structural deformations because of soil liquefaction (captioned by Ertan Bol, 1: Ersöz Apt.: B+6S, Lat: 36.590118 - Long: 36.177205; 2: Yenerer Apt.: B+5S, Lat: 36.59011 - Long: 36.17739; 3: Uğur Apt.: B+5S, Lat: 36.590119 - Long: 36.177459; 4: East neighbour building of Ugur Apt. B+5S, Lat: 36.590137 - Long: 36.177771)

Figure 5.192. Sand boils on Bahçeli Sahil Evler Street (captioned by Ertan Bol, 5: Lat: 36.589992 - Long: 36.177186; 6a and b: Lat: 36.590044 - Long: 36.177747)

Structural deformations because of soil liquefaction were observed in the structures on Bahçeli Sahil Evler Street (Figure 5.193). As can be seen in Pic. 7, there has no bending in the building, the settlement of the building is equivalent in every border and the amount of settlement is about 25-30 cm. No sand outflow was observed at the building boundaries. It was observed that the single story building swelled (about 20-25 cm) due to the settlement of the surrounding buildings due to liquefaction (Pic 8). There are no structural defects in the 7-storey building (Çivisöken Apartment) located just to the west of these buildings (Pic. 9a and b). Behind this structure, two buildings collapsed during the earthquake. There are vertical deformations in the existing structures, roads and pavements around the Çivisöken Apartment due to settlements caused by liquefaction. In the interviews with the authorized persons of the Çivisöken Apartment, it was stated that there is a diaphragm wall up to 12 meters deep around the building, and that there are jet grout columns with a diameter of 60 cm and a length of 3 meters under the building foundation, spaced two meters apart. It has been declared that the foundation of the building with two basements is formed as a raft 6 meters below the surface. It seems that even if the soils show liquefaction, no damage occurs in the structures where adequate geotechnical investigation has been made and precautions have been taken against liquefaction. In the water storage plant located right across this building, it was observed that a swelling occurred due to liquefaction (Pic. 10).

Figure 5.193. Structural deformations because of soil liquefaction on Bahçeli Sahil Evler Street (captioned by Ertan Bol, 7: 36.590859 - 36.178742; 8: 36.590709 - 36.177793; 9a and b: 36.590761 - 36.175848)

In Figure 5.194, the sand ejecta points of the liquefied soils in the coastal park area are shown. Widely liquefied sands in this park cover almost the entire area in the areas whose distribution is shown in Figure 5.189. In Figure 5.194, there is an image of the liquefied sands accumulated on the road. Along this street, there were sands to completely cover the asphalt, but the sands were stripped and removed in order to open the road to traffic.

Figure 5.194. Sand ejecta points of the liquefied area in the coastal park on Bahçeli Sahil Evler Street (captioned by Ertan Bol, 11: 36.591343 - 36.179531; 12: 36.591416 - 36.179457; 13: 36.591636 - 36.179500; 14: 36.591423 - 36.179390; 15: 36.591334 - 36.178781; 16: 36.591130 - 36. 178106; 17: 36.591326 - 36.178147; 18: 36.590959 - 36.178157; 19a: 36.591289 - 36.178264; 19b: 36.591386- 36.178672; 20: 36.591386 - 36.177916)

Figure 5.195 shows the satellite photo and the locations of the field studies carried out in the Nihal Atakaş Mosque. Pic. 21 shows the settlement of the ground around the mosque seen in the garden and the exit points of the liquefied sands. This site was determined by the research group as the westernmost point on the Iskenderun coast where liquefaction was observed in the field.

Figure 5.195. Iskenderun Beach, Pirireis District, Ataturk Boulevard, Nihal Akkaş Mosque (captioned by Ertan Bol, 21: 36.593336 - 36.157473)

In Figure 5.196, the eastern border of the Nihal Atakaş Mosque, that is, the coastline covering the west of the research area and the photo directions are shown. In this region, signs of widespread liquefaction were observed both at the surroundings of the buildings and in the free field. (Fugure 5.197)

Figure 5.196. Hatay, Iskenderun, location, and numbers of the pictures (West Part of Atatürk Boulevard)

Figure 5.197. Sand ejecta points of the liquefied area in the coastal park on west part of the Atatürk Boulevard, Iskenderun, Hatay (captioned by Ertan Bol, 22: 36.593954 - 35.161100; 23: 36.59445 - 36.164121; 24: 36.595002 - 36.162275; 25: 36.59445 - 36.164121; 26: 36.593447- 36.166074; 27: 36.593007 - 36.166749; 28: 36.592703 - 36.167629; 29: 36.593031 - 36.166686; 30: 36.592281- 36.169286)

In Figure 5.198, video images of the liquefaction event that occurred 27 minutes after the earthquake at the coordinates 36.593954 - 36.161100 are shown. As can be seen from the figure, a swelling has occurred on the surface where liquefaction will occur first (Figure 1b). Then, the water outlet point appeared and after about 5 second (Figure c), the sand-water outlet reached its maximum level with approximately 2.50 m (Figure d), and the outlet continued for a certain period of time (Figure e).

Figure 5.198. Sand ejecta video pictures of the liquefied area in the Atatürk Boulevard, Iskenderun, Hatay (The region in Figure 5.197, Pic. 22: 36.593954 - 36.161100)

Figure 5.199 shows the middle sections of Atatürk Boulevard. Traces of liquefaction are also widely observed in this section (Figure 5.200). The liquefied sands found the opportunity to exit from the electrical connection points where the concrete was drilled in the ornamental channel and filled a certain part of the channel (Pic. 31). It was observed that the Ziraat Bank in the same region did not show any ground and pavement damage (Pic. 33). This building is thought to have basement floors or deep foundation. Residues of sand fill the street as a result of liquefaction are still observed.

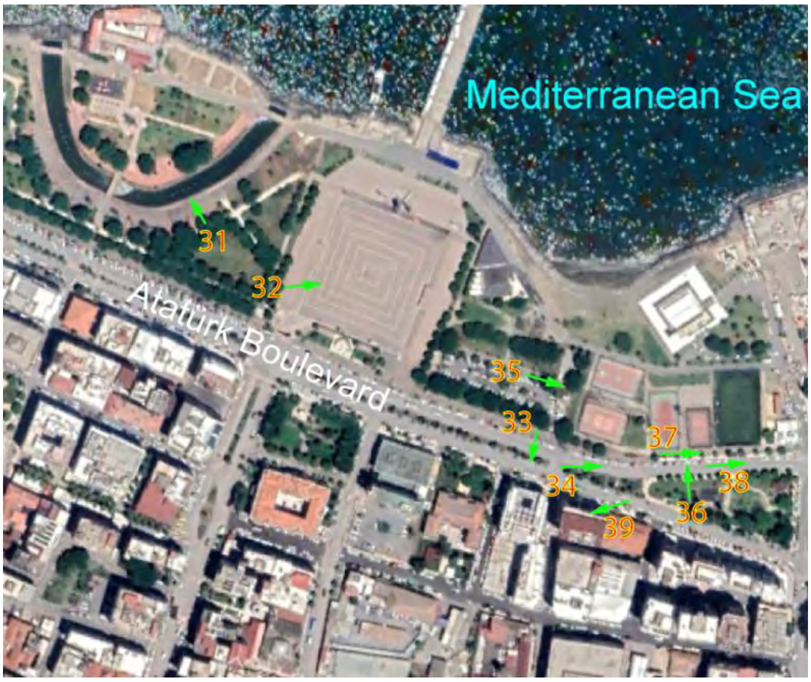

Figure 5.199. Hatay, Iskenderun, location, and numbers of the pictures (Middle Part of Atatürk Boulevard)

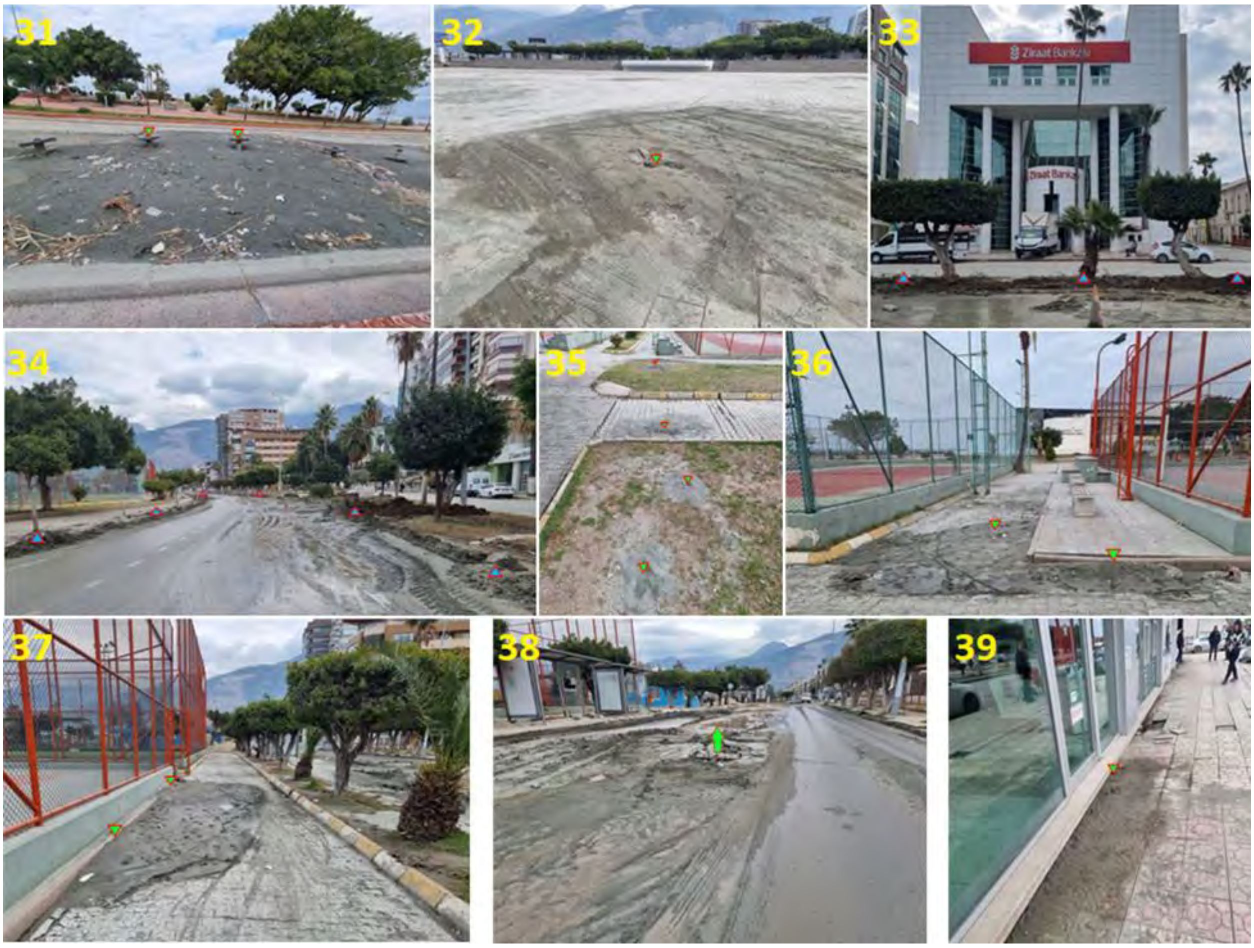

Figure 5.200. Sand ejecta points of the liquefied areas in the coastal park on west part of the Atatürk Boulevard, Iskenderun, Hatay (captioned by Ertan Bol, 31: 36.592195 - 36.170998; 32: 36.591758 - 36.172110; 33: 36.590815 - 36.173540; 34: 36.590613 - 36.173995; 35: 36.591123 - 36.173782; 36: 36.590755 - 36.174565; 37: 36.590755 - 36.174565; 38: 36.590692 - 36.175006; 39: 36.590492 - 36.173901)

Figure 5.201 shows the determined liquefaction areas in Arsuz district, just south of Iskenderun. In this section, Defne Blocks, Elif Site and Güney Deniz Site were investigated in detail (Figure 5.202). In these blocks, which are adjacent to each other, the sand deposits coming out of the water well in the Güney Deniz Site are shown in the Figure 5.203-Pic. 40. While there was no damage in the Güney Deniz Site blocks, the settlements in some buildings in the Elif Site reached 40 cm (Figure 5.203, Pic. 40 and 41). These settlements were generally uniform. In the same region, settlement or any soil problem were not observed in even higher buildings (Defne Blocks) where pile foundation system was applied, but heavy damage was observed in the structural elements of these structures. It should be emphasized that soil engineering was good, but superstructure engineering was found to be weak in the Defne Blocks (Figure 5.203, Pic. 42). Additionally, excessive sand outflows were also observed in front of the Iskenderun Technical University Library building and in the south-west corner in same region (Figure 5.203, Pic. 43, 44 and 45).

Figure 5.201. Hatay Provience, Arsuz Municipal Liquefaction Areas

Figure 5.202. Hatay Provience, Arsuz Municipal Liquefaction Sites

Figure 5.203. Sand ejecta points of the liquefied area in Arsuz, Hatay (captioned by Ertan Bol, 40: 36.577111 - 36.142776; 41: 36.577082 - 36.142006; 42: 36.577424 - 36.142169; 43: 36.577082 - 36.151119; 44: 36.577453 - 36.151857; 45: 36.577758 - 36.152203)

Demirköprü Village, Antakya- Hatay

Demirköprü village is located on the Amik basin and near the Asi River (Figure 5.204). Both lateral and vertical deformations of up to 2 m were observed as a result of collapse in the road embankments (Figure 5.205, Pic. 46 and 47). In this region lateral spreading up to 7-8 meters towards the Asi River has been observed (Figure 5.205, Pic. 48-54). The shifted structures were submerged obliquely towards the soil. Village residents declared that during the earthquake, water erupted several meters high.

Figure 5.204. Lateral Spreading sites Demirköprü Village, Antakya, Hatay

Figure 5.205. Lateral spreading sites of Demirköprü Village, Antakya, Hatay (captioned by Ertan Bol, 46: 36.245483 - 36.362605; 47: 36.245843 - 36.362492; 48: 36.248304 - 36.354500; 49: 36.249344 - 36.353289; 50: 36.249726 - 36.353004; 51: 36.249892 - 36.352822; 52: 36.250295 - 36.352775; 53: 36.250735 - 36.352309; 54: 36.251264 - 36.351299)

Dörtyol- Hatay

A linear deformation was detected in Dörtyol, 300 meters from the beach and 900 meters in length parallel to the seacoast. As a result of lateral spreading, this part has moved slightly towards the sea. Figure 5.206 shows the northern end of the lineament. In the Hatay Dörtyol region, horizontal and vertical deformations up to 80 cm occurred as a result of liquefaction and lateral spreading. Sand boils and surface fractures were observed even in the field, and excessive deformations were observed in the structures on the linearity (Figure 5.207, Pic. 55-60).

Figure 5.206. Lateral Spreading sites Dörtyol, Hatay (North Part)

Figure 5.207. Lateral spreading sites of Dörtyol, Hatay (North Part) (captioned by Ertan Bol, 55: 36.821664 - 36.178360; 56: 36.821689 - 36.178636; 57: 36.821738 - 36.178602; 58: 36.821353 - 36.178545; 59: 36.821392 - 36.178267; 60: 36.821153 - 36.178988)

Figure 5.208 shows the south end section of linearity observed in the field. In this region, there are again both sand ejecta and a clear fracture line in the field (Figure 5.209, Pic. 61-64).

Figure 5.208. Lateral spreading sites Dörtyol, Hatay (South Part)

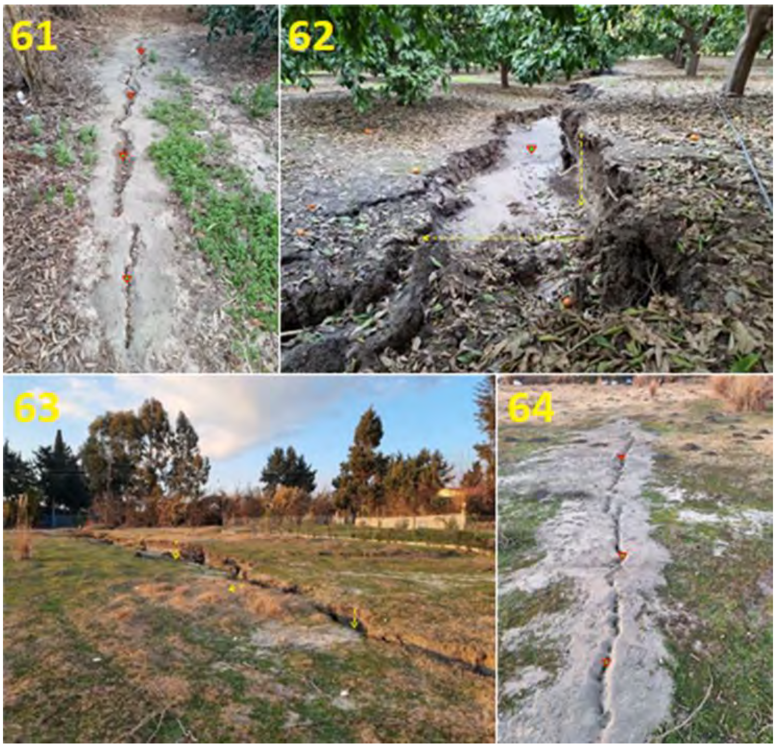

Figure 5.209. Lateral spreading sites of Dörtyol, Hatay (South Part) (captioned by Ertan Bol, 61: 36.817179 - 36.182109; 62: 36.817450 - 36.182037; 63: 36.816813 - 36.182482; 64: 36.816198 - 36.182913)

Hatay Airport

In the Hatay Airport region (Figure 5.210), horizontal and vertical deformations have occurred on the airport connection road and the retaining wall. It has been determined that the road has become undulated due to the earthquakes. The vertical deformations occurred in the southern extension of the fracture line that locates in the southern part of the terminal entrance of the airport have reached approximately 70 cm. It is thought that this phenomenon is lateral spreading because of sand boilings were detected on the airport connection road (Figure 5.211, Pic. 65-70 and Figure 5.212).

Figure 5.210. Satellite photo and locations of field studies in the Hatay Airport (Antakya)

Figure 5.211. Lateral spreading sites of Dörtyol, Hatay (South Part) (captioned by Ertan Bol, 65: 36.367796 - 36.261389; 66: 36.367698 - 36.261591; 67: 36.363901 - 36.277886; 68: 36.363901 - 36.277886; 69: 36.363037 - 36.277857; 70: 36.362907 - 36.277540)

Figure 5.212. Hatay Airport and sand ejecta (captioned by Kemal Önder Çetin 1: 36.3646˚N, 36.281492˚E; 2: 36.362518˚N, 36.280952972˚E; 3: 36.364491972˚N, 36.281483˚E; 4: 36.362479˚N, 36.281070972˚E)

Dörtyol-Payas-Hatay Coastal Line

Along Dörtyol-Payas coastal line a number of liquefaction manifestations were reported as shown in Figure 5.213 and 214.

Figure 5.213. Liquefaction induced sand ejecta in Payas, near Hatay-Dörtyol district (captioned by Kemal Önder Çetin 1: 36.7819583˚N, 36.20253˚E; 2: 36.782358˚N, 36.204391972˚E; 3: 36.78184167˚N, 36.20233056˚E; 4: 36.782199˚N, 36.20472˚E)

Figure 5.214. Sand ejecta and cracks near Hatay Dörtyol beach (captioned by Kemal Önder Çetin 1: 36.81589167˚N, 36.1845972˚E; 2: 36.81283056˚N ,36.1818194˚E; 3: 36.812789˚N, 36.1814583˚E; 4: 36.8183278˚N, 36.177867˚E; 5: 36.82108056˚N, 36.17467˚E)

Hatay-Kırıkhan Route

Along Hatay-Kırıkhan route, a number of liquefaction manifestations were reported as shown in Figure 5.215.

Figure 5.215. Sand ejecta fields and sand cones near Hatay Kırıkhan road (captioned by Kemal Önder Çetin 1: 36.356901972˚N, 36.393472˚E; 2: 36.350989˚N, 36.379424˚E; 3: 36.351291˚N, 36.380054972˚E; 4: 36.3512089722˚N, 36.379545972˚E)

Iskenderun Portal Region

Liquefaction phenomenon was widely observed in Iskenderun. Surface manifestation of liquefaction includes lateral spreading, sand boils, soil ejecta, and settlements. Several of these indicators were observed during the reconnaissance. Figure 5.216 documents the observations regarding liquefaction, liquefaction induced lateral spreading and ground deformations, and seismic deformations.

Figure 5.216. Areas with liquefaction induced sand ejecta in İskenderun Port Region (captioned by 1: SahaGözü Team, 36.60231389˚N, 36.1928˚E; 2: SahaGözü Team, 36.604289˚N, 36.192972˚E; 3: Kemal Önder Çetin, 36.6033278˚N, 36.194472˚E; 4: Kemal Önder Çetin, 36.60402˚N, 36.1921083˚E

Iskenderun-Nihal Atakas Mosque

Liquefaction manifestations were documented in Iskenderun Nihal Atakas Mosque facility. Surface manifestation of liquefaction includes lateral spreading, sand boils, soil ejecta, and settlements. Several of these indicators were observed during the reconnaissance. Figure 5.216

documents the observations regarding liquefaction, liquefaction induced lateral spreading and ground deformations, and seismic deformations.

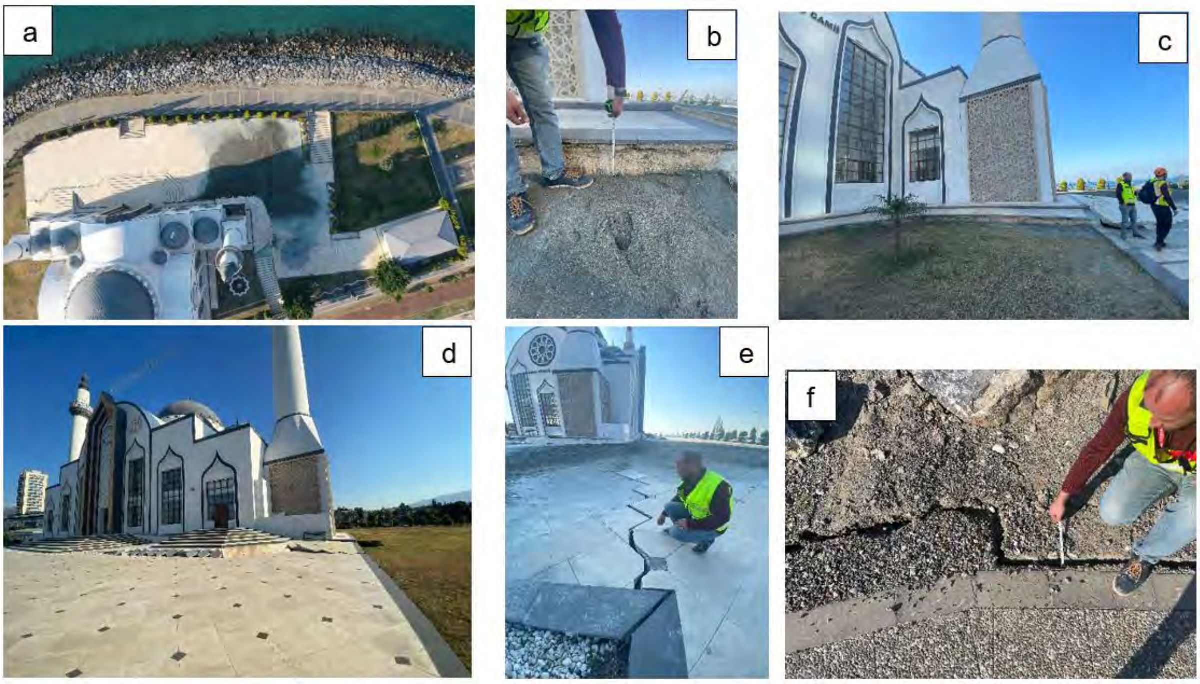

Figure 5.217. Liquefaction manifestations in Nihal Atakas Mosque (~ 36°35'35.27"N/ 36° 9'26.74"E): a) Bird's-eye view of the sand ejecta at the corner; b) settlements of the sand near the mosque; c) front view outlining the settlements; d) severe deformations observed on the marble ground due to liquefaction induced settlements; e) lateral spreading in front of the mosque; f) lateral spreading near the mosque towards the sea. Photo by Ozgun Numanoglu, Tugce Baser, and Serhat Erinmez

Iskenderun-Çay District Atatürk Boluvard

Liquefaction manifestations were documented in Iskenderun Cay District along Ataturk Boulevard Surface manifestation of liquefaction includes lateral spreading, sand boils, soil ejecta, and settlements. Several of these indicators were observed during the reconnaissance. Figure 5.218 through 5.222 document the observations regarding liquefaction, liquefaction induced lateral spreading and ground deformations, and seismic deformations.

Figure 5.218. Liquefaction manifestations on Ataturk Boulevard near Forbes Shopping Center (~ 36°35'36.52"N/ 36° 9'34.67"E): a) sand boils on Ataturk Boulevard; b) cracks formed due to lateral deformation; c) cracks formed due to lateral deformation; d) liquefaction induced settlements; e) cracks formed due to lateral deformation. Photo by Ozgun Numanoglu, Tugce Baser, *and* Serhat Erinmez

Figure 5.219. Liquefaction manifestations (sand boils) on Ataturk Boulevard near Ataturk (~ 36°35'29.50"N/ 36° 10'20.23"E) Photo by Ozgun Numanoglu, Tugce Baser, and Serhat Erinmez

Figure 5.220. Liquefaction manifestations (sand boils) on Ataturk Boulevard (~ 36°35'26.86"N/ 36° 10'40.39"E) *Photo by* Ozgun Numanoglu, Tugce Baser, *and* Serhat Erinmez

Figure 5.221. Liquefaction manifestations on Ataturk Boulevard near Tennis Courts (~ 36°35'26.95"N/ 36° 10'28.39"E): a) water accumulation and sand boils; b) sand boils; c) ground settlement. *Photo by* Ozgun Numanoglu, Tugce Baser, *and* Serhat Erinmez

Figure 5.222. Liquefaction manifestation): a) Odeo Bank corner: sand ejecta and liquefaction induced settlements (~ 36°35'25.92"N/ 36° 10'25.46"E); b) Civilim building corner: sand ejecta (~ 36°35'23.48"N/ 36° 10'23.89"E). Photo by Ozgun Numanoglu, Tugce Baser, and Serhat Erinmez

Iskenderun-Dock

Liquefaction manifestations were documented in Iskenderun Dock which include lateral spreading, and settlements, which are shown in Figure 5.223.

Figure 5.223. Ground Settlements and Lateral Deformations on Iskenderun Dock (~ 36°35'40.67"N/ 36° 10'38.69"E): a) Ground subsidence at the pier and the lighthouse; b) Ground subsidence at the dock; c) Ground subsidence and lateral deformations of the concrete panels; d) lateral deformations and cracks on the concrete panel Photo by Ozgun Numanoglu, Tugce Baser, and Serhat Erinmez

Adıyaman-Gölbaşı

The seismic soil liquefaction phenomena, show a great effect in Adıyaman Gölbaşı as well. The liquefaction-induced sand ejecta, lateral spreading and excessive settlements were observed in Gölbaşı both in the free field and in the vicinity of buildings. Similar surface manifestions were also documented by Gölbaşı Lake. These are shown in Figures 5.224 through 5.224 through 228.

Figure 5.224. Liquefaction induced sand ejecta in Adıyaman Gölbaşı region (captioned by 1: Kemal Önder Çetin 37.7840417°N, 37.63517°E; 2: Kemal Önder Çetin 37.7865194°N, 37.630925°E; 3: Ayhan Gürbüz 37.7862917°N, 37.631728°E; 4: Kemal Önder Çetin 37.7877694°N, 37.642589°E; 5: Kemal Önder Çetin 37.78166°N, 37.62913056°E)

Figure 5.225. Cracks and fractures caused by liquefaction in the Gölbaşı district of Adıyaman (captioned by 1: Mustafa Kerem Koçkar 37.78880278°N, 37.64811389°E; 2: Ayhan Gürbüz 37.7827083°N, 37.62888056°E; 3: Kemal Önder Çetin 37.786661972°N, 37.632413972°E; 4: Kemal Önder Çetin 37.7863083°N, 37.63233056°E)

Figure 5.226. Uniform building settlements caused by liquefaction in Gölbaşı district of Adıyaman (captioned by 1: Ayhan Gürbüz 37.7873167°N, 37.6430083°E; 2: Berna Unutmaz 37.7875861°N,37.642125°E; 3: Kemal Önder Çetin 37.7827194°N, 37.6362°E; 4: Kemal Önder Çetin 37.7839694°N, 37.63324°E; 5: Kemal Önder Çetin 37.7866972°N, 37.631078°E)

Figure 5.227. Liquefaction induced deformations in Gölbaşı district of Adıyaman (captioned by 1 and 2: Müge Akın 37.794105,37.648625)

Figure 5.228. Sand ejecta in Gölbaşı, Adıyaman (captioned by Sedat Sert, 37.781342 37.635246)

Kahramanmaraş-Türkoğlu

The seismic soil liquefaction manifestations were also observed in Turkoglu. The liquefaction-induced sand ejecta observed near Kuyumcular Village is illustrated in Figure 5.229.

Figure 5.229. Sand ejecta near the fault rupture in Kuyumcular Village, Türkoğlu, Kahramanmaraş (captioned by Sedat Sert, 37.412425, 36.910369)

Malatya-Kahramanmaraş Road

The seismic soil liquefaction manifestations were also observed along the route from Malatya to Kahramanmaraş. The liquefaction-induced sand ejecta along with lateral spreading were documented as illustrated in Figure 5.230 and 5.231.

Figure 5.230. Sand ejecta and lateral spreading observed on Malatya-Kahramanmaraş Road (captioned by 1: Kemal Önder Çetin 37.86305278°N, 37.7677083°E; 2: Kemal Önder Çetin 37.86312°N, 37.76752°E; 3: Berna Unutmaz 37.865°N, 37.77116°E; 4: Berna Unutmaz 37.865367°N, 37.771156°E; 5: Ayhan Gürbüz 37.86551389°N, 37.771183°E)

Osmaniye-Adıyaman Road

The seismic soil liquefaction manifestations were also observed along the route from Osmaniye to Adıyaman. The liquefaction-induced sand ejecta was documented as illustrated in Figure 5.231.

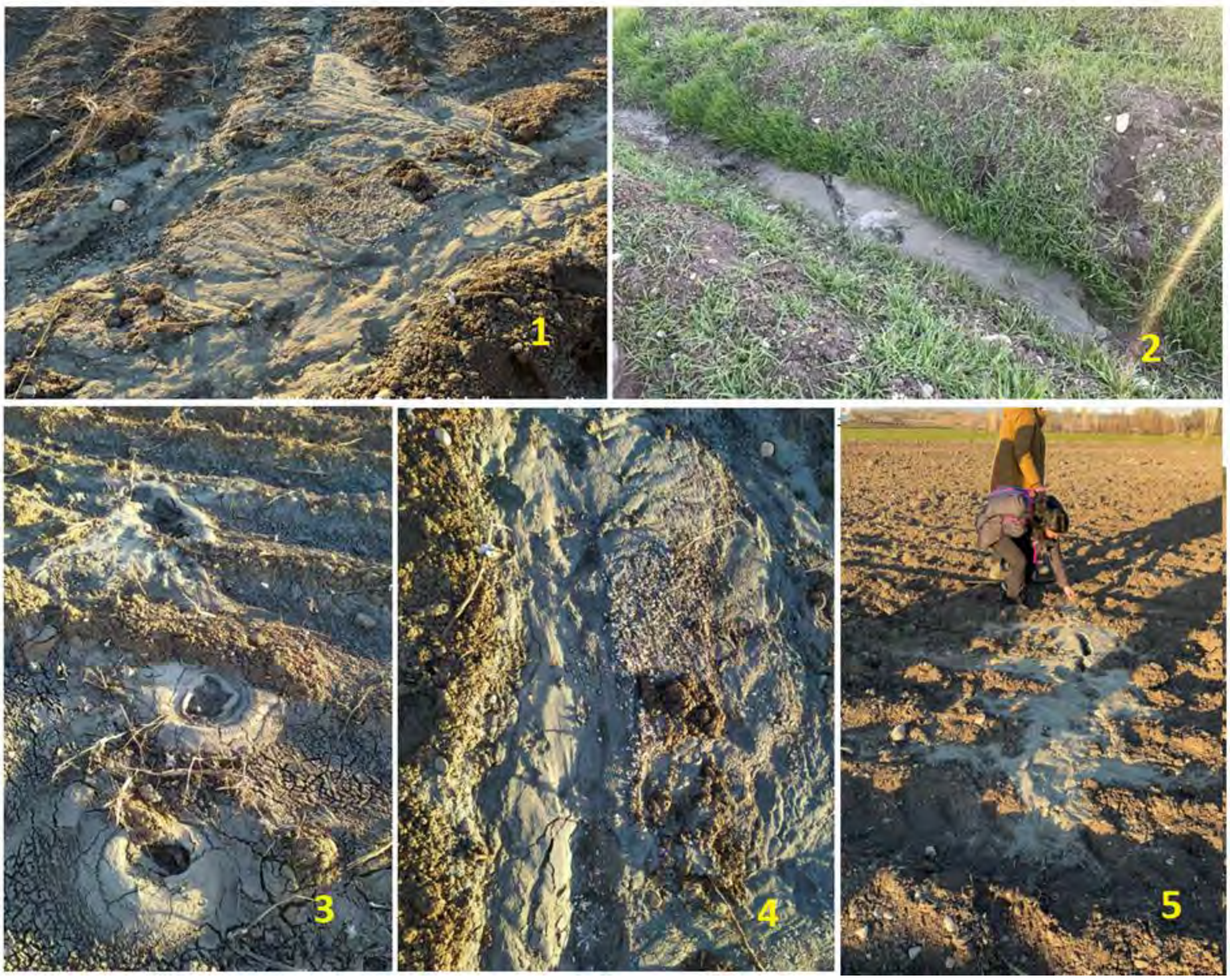

Figure 5.231. Liquefied areas on Osmaniye - Adıyaman road (captioned by Kemal Önder Çetin 1: 37.33691°N, 37.04542°E; 2: 37.3372°N, 37.0454056°E; 3: 37.336745°N, 37.0452559°E; 4: 37.336956972°N, 37.045499972°E; 5: 37.337375°N, 37.0455083°E)

5. 1. 18. Retaining Structures, Deep Excavations, Foundation Performance/Tunnel:

The failures on the retaining structures, deep excavations, foundations, and tunnels among all the earthquake area will be presented within this section. This section is organized according to the structure types and the damage patterns.

5. 1. 18. 1. Stone Walls:

Along the road from Elbistan to Malatya, there was no signs of geotechnical-related problems were observed on the retaining walls of about 5m high (Figure 5.232) and the slopes behind the walls were not damaged. It should be noted that, no cracks, no slope failures, etc. were observed along the road.

Figure 5.232. Stable retaining wall – Elbistan-Malatya Road

Along the road from Malatya to Gölbaşı, on Km: 74+600-75+800, near the entrance of Erkenek Tunnel, the retaining walls performed well with light damage.

Figure 5.233. Stone retaining wall performed relatively well in the entrance of Erkenek tunnel.

Figure 5.234. Stone retaining wall lightly damaged in the entrance of the tunnel.

However, on Malatya-Gölbaşı Road, approximately around the coordinates 37.86345N, 37.76782E, near Göksu Çayı, probably because of the liquefied soil and slope, some cracks were observed at the stone retaining walls.

Figure 5.235. Location of cracked stone walls (marked as 4 in the figure)

Figure 5.236. Collapsed/cracked stone walls, Location: around37.86345N, 37.76782E

At the similar location very close to the green mark in Figure 5.235, a small, reinforced concrete retaining wall was observed to fail due to slope failure as can be seen in Figure 5.237.

Figure 5.237. Reinforced concrete retaining wall failed due to slope failure, location: 37.863208,37.767095

Similarly, at the location of the mark 7 in Figure 5.235, a total view of the wall can be seen and the cracked part is observed as can be seen in Figure 5.238.

Figure 5.238. Collapsed/cracked stone walls.

On the steep highway slopes between Iskenderun and Hatay, rock overturns and falls can be widely observed on steep slopes possibly composed of clayey limestone. However, the failure of the stone retaining wall and fill constructed on the same road was observed. Stone walls often perform poorly.

Figure 5.239. Stone walls, performed poorly on Iskenderun-Hatay Road, Photo by Prof. Dr. Kemal Önder Çetin and Prof. Dr. Candan Gökçeoğlu

Figure 5.240. Stone walls, performed poorly on Iskenderun-Hatay Road, Photo by Prof. Dr. Kemal Önder Çetin and Prof. Dr. Candan Gökçeoğlu

Figure 5.241. Photo by Prof. Dr. Kemal Önder Çetin and Prof. Dr. Candan Gökçeoğlu, Location: 36.483029,36.27101797

Figure 5.242. Photo by Prof. Dr. Kemal Önder Çetin ve Prof. Dr. Candan Gökçeoğlu

Figure 5.243. Photo by Prof. Dr. Kemal Önder Çetin ve Prof. Dr. Candan Gökçeoğlu

Near Pazarcık/Kahramanmaraş, a composite wall observed no damage as can be seen in Figure 5.244.

Figure 5.244. No damage stone (composite) wall, Location: 37.50768,37.33958

On Yeşilyurt – Gündüzbey yolu, although some cracks were observed along the road, no damage has been seen in the adjacent retaining wall (Figure 5.245).

Figure 5.245. No damage on stone wall, Location: 38.30536289,38.23547732

5. 1. 18. 2. Anchored Walls/Reinforced Earth Walls/Piled Walls/Stabilized Wall:

Although the construction works are not completed yet, no damage was observed in the piled excavations system in Osmaniye Bahçe.

Figure 5.246. Photo by Prof. Dr. Kemal Önder Çetin and Prof. Dr. Candan Gökçeoğlu

Figure 5.247. Photo by Prof. Dr. Kemal Önder Çetin and Prof. Dr. Candan Gökçeoğlu

As can be seen from the Figure 5.248, no damage was observed at the cut-and-cover of T2 tunnel exit on Bahçe and Nurdağı railway and the reinforced concrete support walls following it.

Figure 5.248. Photo by Prof. Dr. Kemal Önder Çetin ve Prof. Dr. Candan Gökçeoğlu

The photo in Figure 5.249 is a view from west to east, showing the TBM exit portal, the conventional railway running just above it. An L-shaped retaining wall was constructed between the top of the portal and the conventional railway. A small landslide occurred, but the retaining wall separated it from portal structure, prevented further progress of the slide and damage to both the portal and the conventional railway.

Figure 5.249. Photo by Prof. Dr. Kemal Önder Çetin and Prof. Dr. Candan Gökçeoğlu

The anchored retaining walls along the road from Malatya to Gölbaşı and Hatay Ceyhan to İskenderun performed well as can be seen from the figures below:

Figure 5.250. Anchored wall, Malatya to Gölbaşı road, location 37.90435,37.81127

Figure 5.251. Anchored wall, Hatay Ceyhan-İskenderun road, Location 36.684127199,36.217725899

A piled and buttressed retaining wall at Hatay-İskenderun is reported to have no damage:

Figure 5.252. Buttressed wall, Hatay-İskenderun, Location 36.5431584,36.1459744

Mechanically Stabilized Earth Wall (MSEW) and gravity type retaining walls were observed along the transportation network. General performance of the retaining walls was observed to be good, and no visible damages were observed for the investigated walls due to seismic shaking as shown in Figure 5.253.

Figure 5.253. No damage on retaining walls due to seismic shaking.

Some damage has been reported along the retaining walls adjacent to hydraulic structures and rivers. For example, as can be seen in Figure 5.254 below, near Asi River in Hatay, the retaining wall has collapsed. Similarly, near this crack, the retaining wall under the bridge abutments (Figure 5.255) has failed.

Figure 5.254. Cracked reinforced concrete retaining wall, location 36.21571742,36.16185614

Figure 5.255. Failed retaining structure, location 36.21548476,36.16233899

At a different location still along Asi River, a failure of the retaining wall is presented in Figure 5.256.

Figure 5.256. Failed retaining structure, Location 36.221139,36.1641857

A similar failure (Figure 5.257) of the has been reported along the water channels in Kahramanmaraş. This failure is going along with a slope failure (Figure 5.258)

Figure 5.257. Failed retaining structure, Location 37.56588,36.872208

Figure 5.258. Slope failure behind a retaining wall, Location 37.56598,36.871731

5. 1. 18. 3. Deep Excavations:

The longest railway tunnels in Türkiye, with a length of approximately 10 km, are between Bahçe and Nurdağı. T2 tunnel has been completed and excavations of T1 tunnel are about to be completed with TBM. TBM will exit from the Bahçe Portal. Starting from Bahçe Portal, an approximately 1200 m long cut-and-cover tunnel passage located under the Adana - Gaziantep State Highway was designed. Cut-and-cover tunnels were completed, and some sections of the TBM is supported by struts and kept waiting for the extraction. However, the Bahçe exit portal is in a paleo landslide. Conventional railway passage approximately 15 m above the portal, is located at just north of the cut-cover tunnel and Adana-Gaziantep State Highway to the south. As a result, investigations were made in the portal area, where many buildings are present in a narrow area along the route.

The photo in Figure 5.259, is taken from an angle extending from west to east, showing the TBM exit portal, the conventional railway line is running just above it. An L-shaped retaining wall was constructed between the top of the portal and the conventional railway (Figure 5.260) A small landslide occurred, but the retaining wall prevented the landslide from continuing, preventing damage to both the portal and the conventional railway (Fig. 5.259).

Struts (steel pipes) were designed to support pile elements in Bahçe. A certain section of the cut-and-cover tunnel built right in front of the garden portal is temporarily supported by struts and kept open for the removal of the TBM, which is currently being excavated in the tunnel. As can be seen in Figures 5.259 and 5.260, all struts performed well as designed and no damage was occurred.

Figure 5.259. General overview of temporary struts over the cut section, Photo by Prof. Dr. Kemal Önder Çetin and Prof. Dr. Candan Gökçeoğlu

Figure 5.260. Temporary struts over the cut section, Photo by Prof. Dr. Kemal Önder Çetin and Prof. Dr. Candan Gökçeoğlu

5. 1. 18. 4. Tunnels:

No damage was observed at the portal of the Bahçe-Nurdağı tunnels. However, some rockfalls are observed. However, the surface fracture passes approximately 50 m in front of the portal.

Figure 5.261. Photo by Prof. Dr. Kemal Önder Çetin and Prof. Dr. Candan Gökçeoğlu, Location: 37.16989197,36.708058

The traffic along the Erkenek tunnel was flowing in only one of the tunnels, the one in the direction of Malatya to Gölbaşı. However, some spalling and rock pieces were observed along the tunnel.

Figure 5.262. Panels and rock failures along Erkenek tunnel (in the direction from Malatya to Gölbaşı)

5. 1. 19. Preliminary findings with Photogrammetry and Remote Sensing Techniques

Photogrammetry and remote sensing data of the earthquake region have been collected from various platforms (Unmanned Aerial Vehicle, airplane, Earth Observation satellites), sensors (optical and radar) and with diverse resolutions (20 cm to 1 km). A significant part of the public and private sector-sourced data has been made open and freely available. The datasets have various characteristics, advantages and disadvantages depending on the platform, sensor and resolution, surface cover (e.g., snow), analysis scale (e.g. local, district, regional), weather conditions (cloud), determination of surface changes (compatibility), level of detail and temporal characteristics (pre- and post-earthquake).

Optical and radar weather and satellite data taken at different resolutions and at different dates before the earthquake exist in the archives. Although optical data could be partially utilized soon after the earthquake due to adverse weather conditions (rain, snow, wind), images from Maxar, Planet Skysat and the Pleiades satellites were quickly provided free of charge. However, due to their very high resolution (50 cm and better) and smaller swath width, these datasets cover only a part of the region.

ESA Sentinel-2 optical satellites, taken on February 9, 2023, with 10 m resolution, provided an important opportunity for regional analysis with low cloud coverage. Sentinel-2 products also have high geometric and radiometric quality and provide bottom-of-atmosphere (BOA) reflectances. At the same time, synthetic aperture radar (SAR) data from JAXA ALOS-2/PALSAR-2 (February 8) and ESA Sentinel-1 (February 9) satellites were provided free of charge for the regional deformation analysis and the analysis results were published by different organizations. Some of the results are presented by NASA[1].

On the other hand, post-disaster damage mapping studies have been carried out by public institutions, the EU Copernicus Programme[2] and volunteers.

2 days after the earthquake, the General Directorate of Mapping (HGM), Türkiye initiated aerial photogrammetric flight missions and provided aerial orthophotos with 20 cm resolution free of charge on the 4th day via the HGM Küre application and the Atlas web service[3]. In the HGM Küre application, pre-earthquake orthoimages are also presented simultaneously. However, the acquisition date of the pre-event orthoimages are unknown. They have been possibly taken during regular aerial photogrammetric mapping missions carried out in summer months of previous years. In addition, the images after the earthquake do not cover the whole area due to data volume (very high-resolution imagery) and dense cloud cover.

The surface deformation map obtained from ALOS-2 data analysis and provided by JAXA and GSI is given in Figure 5.263. The line of sight (LOS) displacements with respect to the satellite orbit indicate a south-north movement (up to 2 m) in the south of Pazarcik fault lines and again up to -2 m displacement in the north of the Pazarcik.

---

[1] https://maps.disasters.nasa.gov/arcgis/apps/MinimalGallery/index.html?appid=cb116456d682456abc38b90d96a72713

[2] https://activations.emergency.copernicus.eu/#EMSR648

[3] https://atlas.harita.gov.tr/mobile/#7.69/36.991/35.726

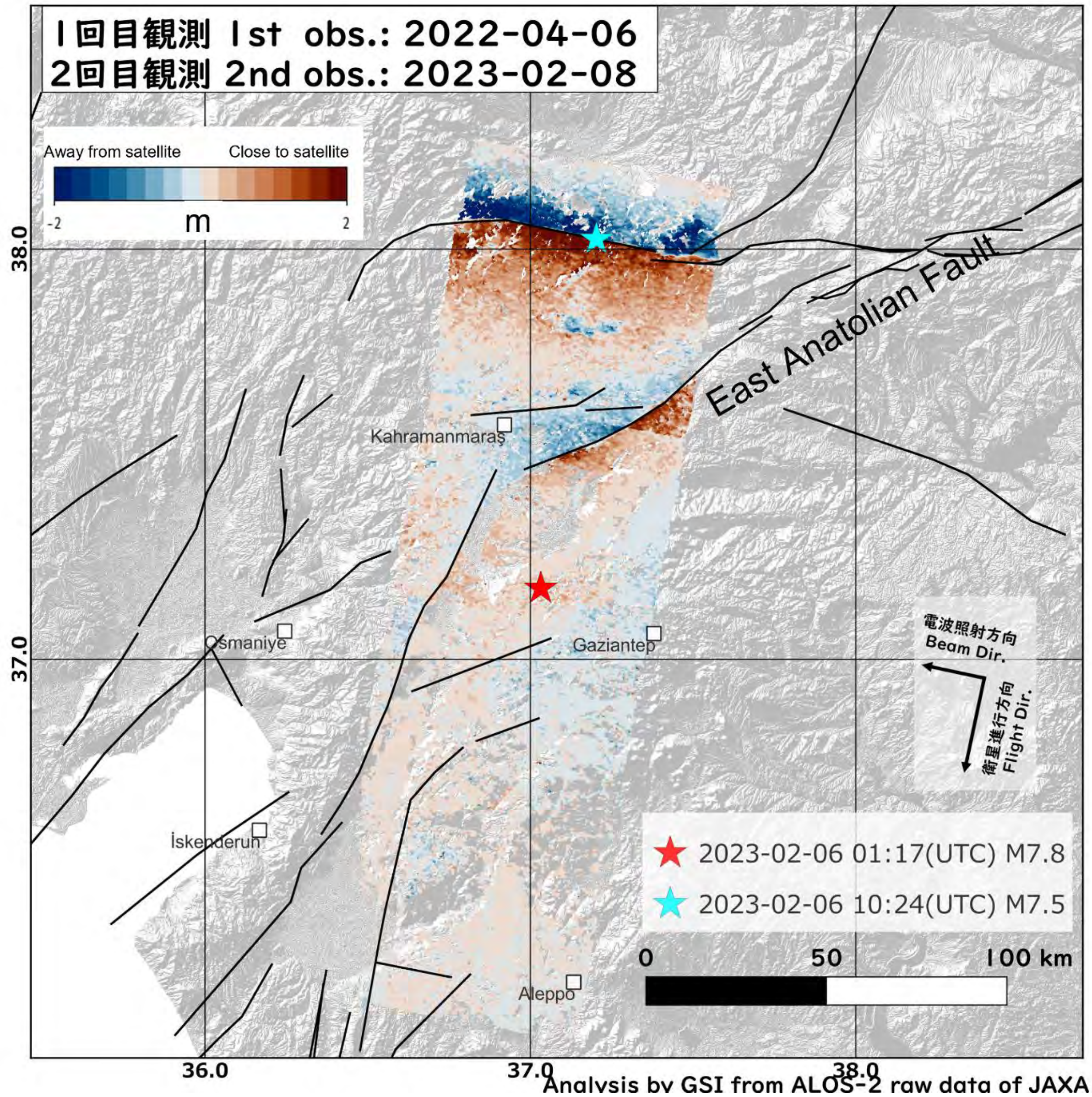

Figure 5.263. Regional deformations (movements relative to satellite orbit) obtained by GSI Japan from JAXA's ALOS-2/PALSAR-2 sensor. Source: https://www.gsi.go.jp/cais/topic20230206-e_Turkey.html

Sentinel-2 deformation analyses by Comet (Figure 5.264) indicate larger movements in the North-South direction (± 5 m) than East-West direction (± 3 m).

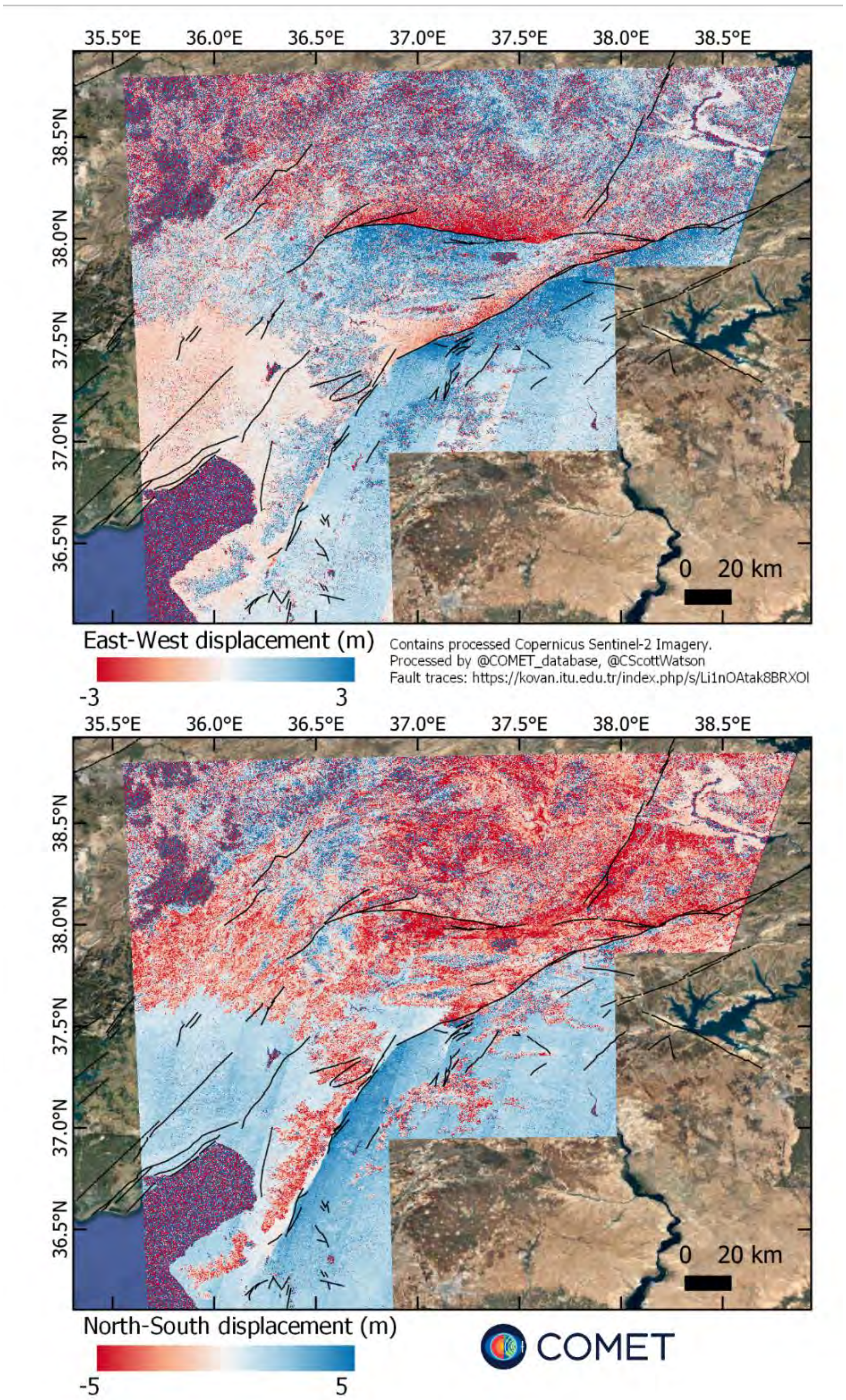

Figure 5.264. Sentinel-2 deformation analyses provided by COMET [4]

---

[4] https://drive.google.com/drive/folders/1z0CEHySRjDc0S71Vq2Bq7ux9Sj8PiXSE

Images published on HGM Küre with 20 cm resolution illustrate the fault lines, surface changes and damages, although there are cloud and data availability (coverage) restrictions (Figures 5.265-270).).

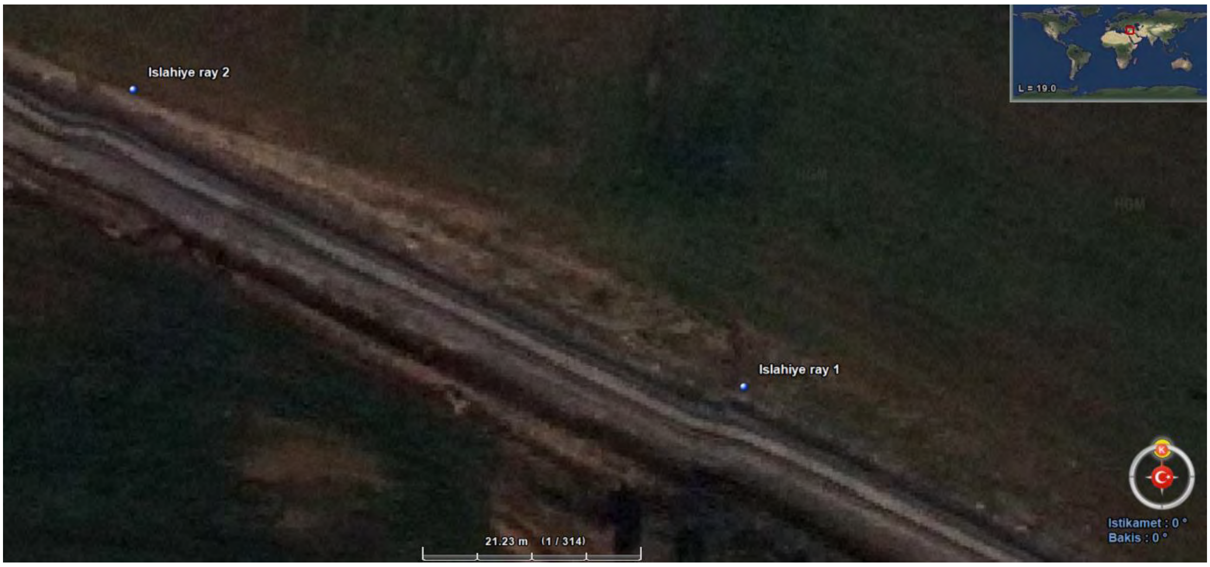

Figure 5.265. İslahiye railway deformations. Source: HGM küre

Figure 5.266. İslahiye surface rupture. Source: HGM küre

Figure 5.267. Hatay-Hassa fault line displacement. Source: HGM küre

Figure 5.268. Hatay-Hassa fault line displacement. Source: HGM küre

Figure 5.269. Hatay-Hassa fault line displacement. Source: HGM küre

Figure 5.270. Hassa Hacılar district, surface rupture. Source: HGM küre

Local deformations were obtained by mapping Sentinel-2 optical images taken on 25 January 2023 and 9 February 2023. Since motion vectors were determined with respect to the reference Sentinel-2 image dated January 25, 2023, the vectors are relative and need to be converted to absolute values. Examples to the displacement vectors are shown in Figures 5.271-276.

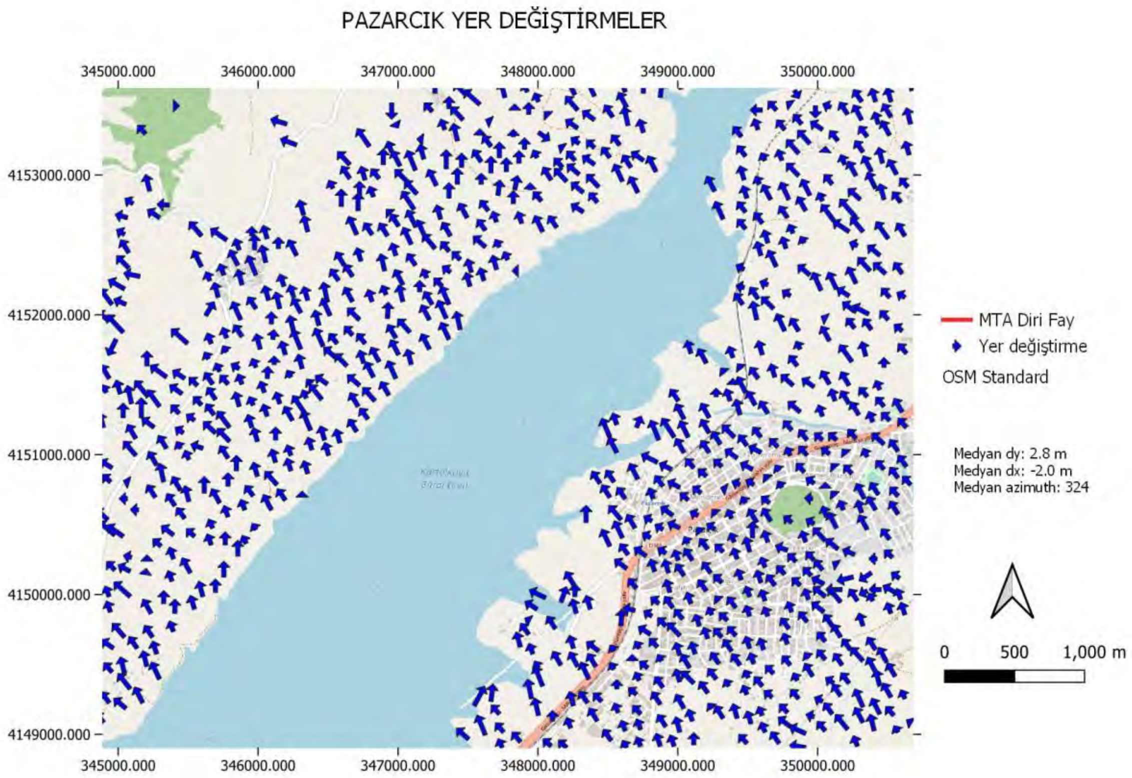

Figure 5.271. Local surface changes obtained from Sentinel-2 images: Pazarcık, Kahramanmaraş (median values were obtained from all points in the image)

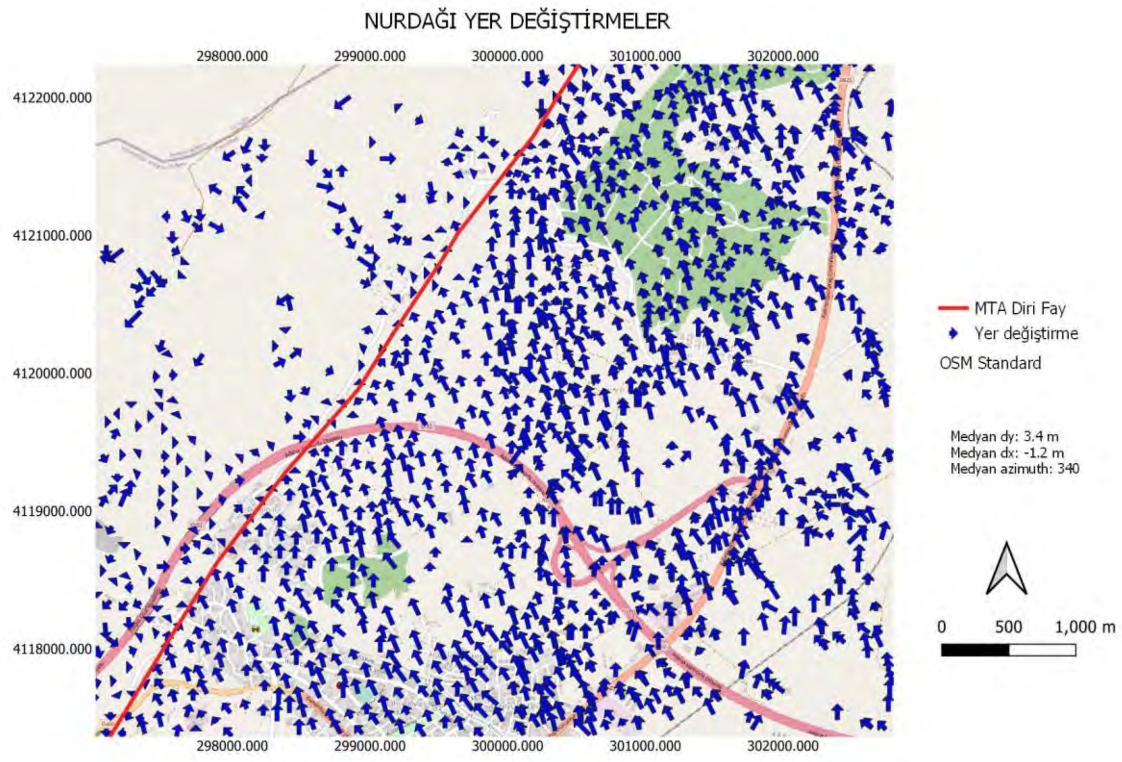

Figure 5.272. Local surface changes obtained from Sentinel-2 images: Nurdağı, Gaziantep (median values were obtained from the points located in the east of the fault line in the image)

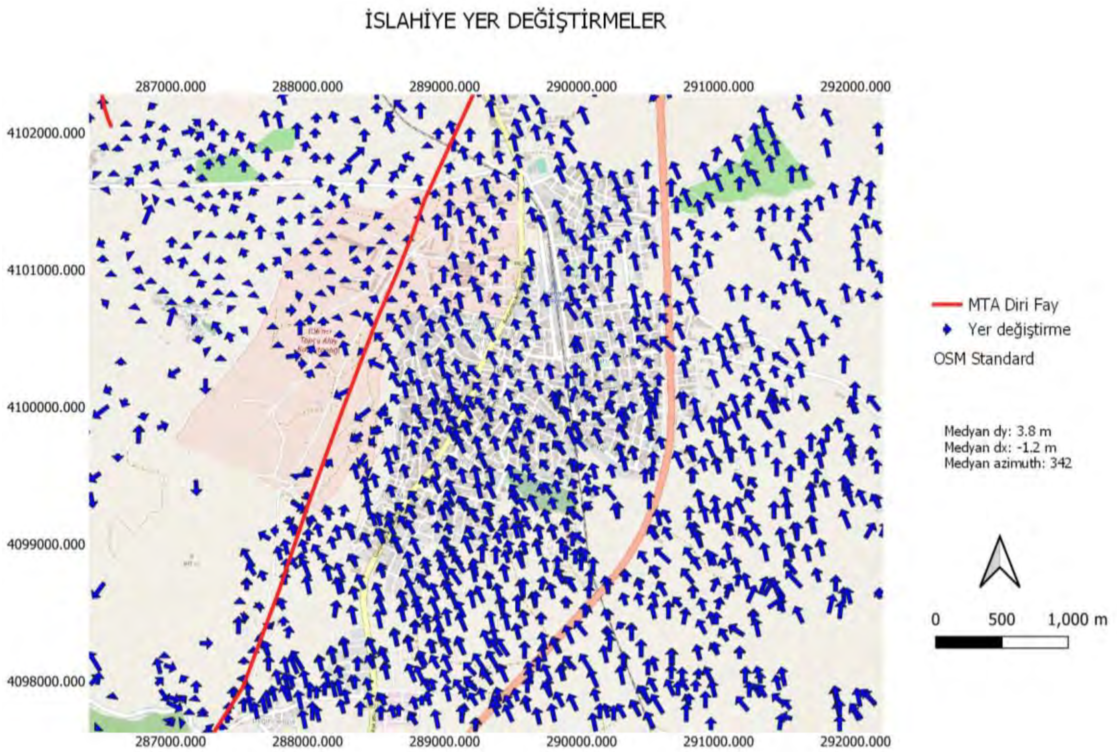

Figure 5.273. Local surface changes obtained from Sentinel-2 images: İslahiye, Gaziantep (median values were obtained from the points located in the east of the fault line in the image)

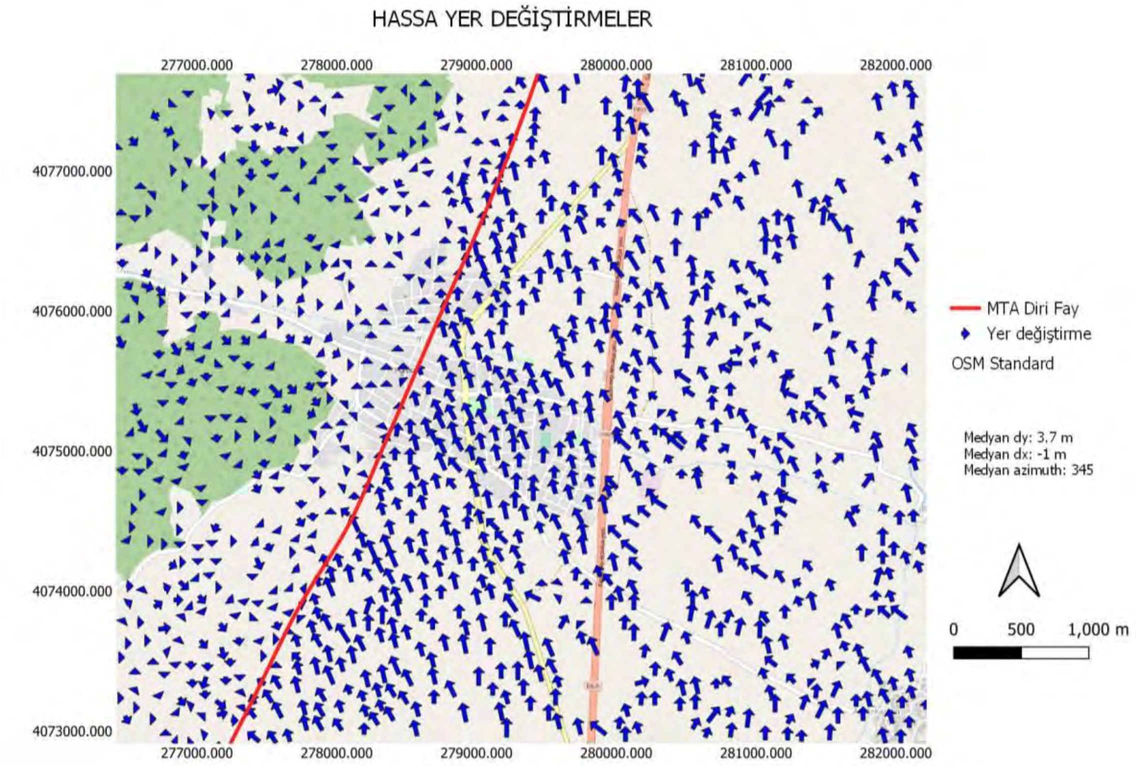

Figure 5.274. Local surface changes obtained from Sentinel-2 images: Hassa, Hatay (median values were obtained from the points located in the east of the fault line in the image)

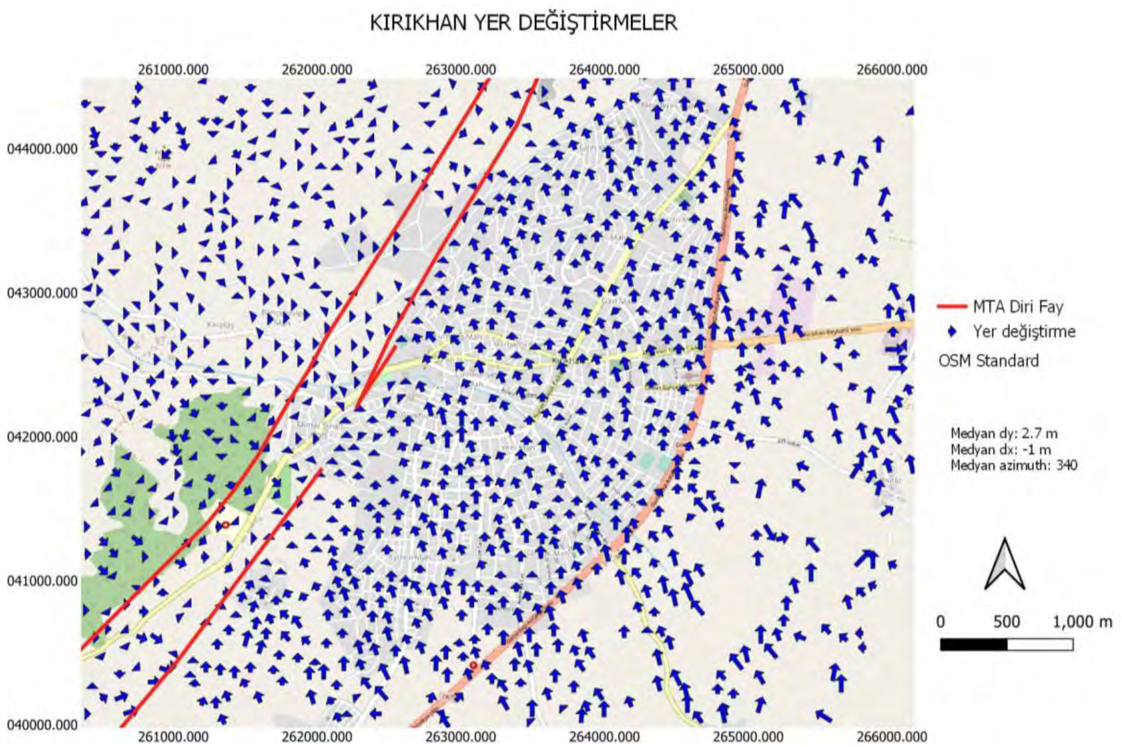

Figure 5.275. Local surface changes obtained from Sentinel-2 images: Kırıkhan, Hatay (median values were obtained from the points located in the east of the fault line in the image)

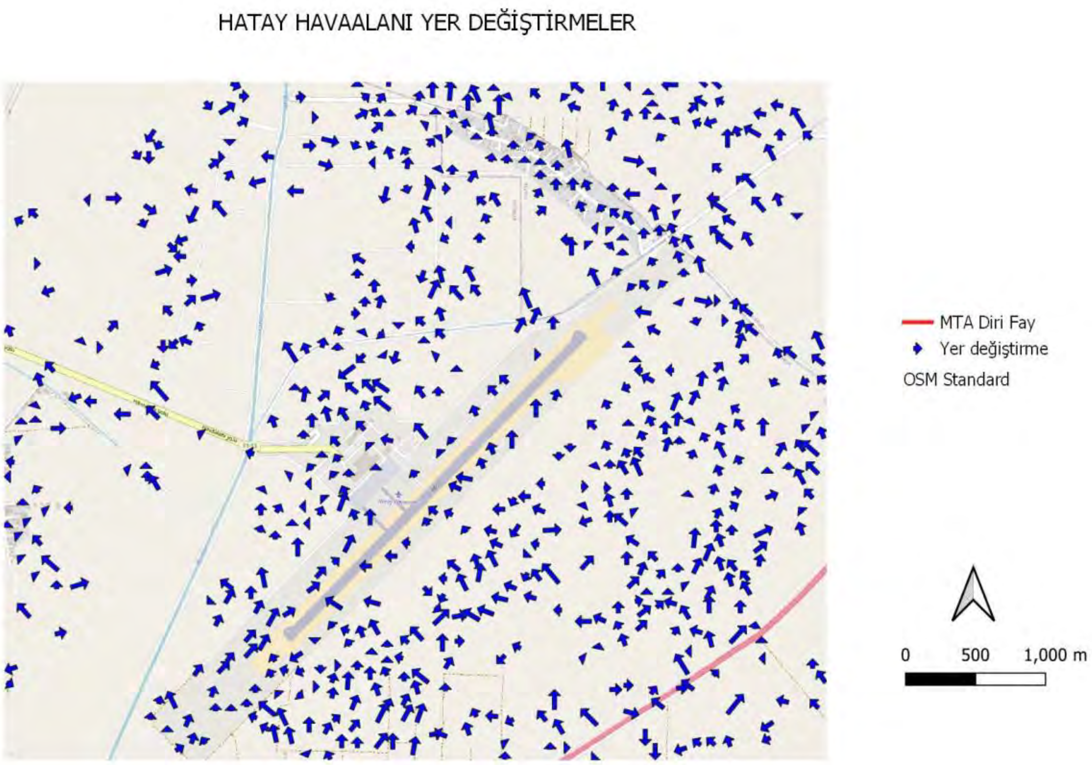

Figure 5.276. Local surface changes obtained from Sentinel-2 images: Hatay airport.

References

Akıl B., Akpınar K., Üçkardeşler C., Araz H., Sağlam M., Ecemiş B., Uran Ş. B., 2008, Evaluation of Settlement Suitability of Gölbaşı (Adıyaman) Town, located on the East Anatolian Fault Zone, Geological Bulletin of Türkiye, Vol 51 No 1.

Brew, G., Barazangi, M., Al-Maleh, A. K., & Sawaf, T. (2001). Tectonic and Geologic Evolution of Syria. GeoArabia, 6(4), 573–616.

Balakani LM, Moskvina AG (2004). Seismogenic zones of Eastern Anatolian and the Dead Sea rift: Probable locations of future large earthquakes. Izvestiya-Physics of the Solid Earth, 40 (12): 972-990.

Coskun B, Coskun B (2000). The Dead Sea Fault and Related Subsurface Structures, Gaziantep Basin, Southeast Turkey. Geological Magazine, 137 (2): 175-192.

Directorate General of Monuments and Museums, Syria.

Bikce M, Over S, Durukal E, Genes M C (2009) Antakya Havzasi kuvvetli deprem yer hareketi izleme sisteminin kurulmasi ve havza icindeki dalga yayilmalarinin arastirilmasi. TUBITAK Project (Project Code: 108M170)

Cilsar and Temiz, 2020. Probabilistic Seismic Hazard Assessment of City Center of Kayseri, Erciyes Üniversitesi Fen Bilimleri Enstitüsü Dergisi, Cilt: 36 Sayı: 2 Sayfa Aralığı: 286 – 298.

Elsaid, A. (2022). The Assessment of Seismic Site Effects during the 24 January 2020 Elazig-Sivrice Mw: 6.8 Earthquake (Master's thesis, Middle East Technical University).

Gül, M. A., 2000, Geology of Kahramanmaraş Region. Hacettepe University, Graduate School of Natural and Applied Sciences, Ph.D. Dissertation, 304 s.

Kelam, A.A., Karimzadeh, S., Yousefibavil, K., Akgün, H., Askan, A. Erberik, M.A., Koçkar, M.K., Pekcan, O., Ciftci, H., 2022, "An evaluation of seismic hazard and potential damage in Gaziantep, Turkey using site-specific models for sources, velocity structure and building stock," Soil Dynamics and Earthquake Engineering, Vol. 154, Article Number 107129.

Koçyiğit, A, Beyhan, A., 1998. A new intracontinental transcurrent structure: the Central Anatolian Fault Zone, Turkey, Tectonophysics. 284(3-4),317-336.

Koçyiğit, A, Erol, O., 2001. A tectonic escape structure: Erciyes pull-apart basin, Kayseri, central Anatolia, Turkey. Geodinamica Acta, 14(1-3), 133-145.

https://www.canligaste.com/son-dakika-depremin-ardindan-kayseri-de-yikilacak-bina-sayisi-belli-oldu/307798/).

Over S, Buyuksarac A, Bektas O and Filazi A 2011. Assessment of potential seismic hazard and site effect in Antakya (Hatay Province), SE Turkey; Environ. Earth Sci. 62, 313–326.
Piper, J.D.A. (Eds.), Tectonics and Magmatism of Turkey and Surrounding Area. Geological Society of London, Special Publication No. 173: 97-138.,

Rigo de Righi M, Cortesini A (1964). Gravity Tectonics in Foothill Structure Belt of Southeast Turkey. Bulletin of the American Association of Petroleum Geologist, 48: 1596-1611.

Robertson AHF (2000). Mesozoic- Tertiary Tectonic- Sedimentary Evolution of a South Tethyan Oceanic Basin and Its Margins in Southern Turkey. In Bozkurt, E. Winchester, J.A.,

Sümengen, M., 2014. 1/100.000 scale Turkish Geological Map, Gaziantep-M38 map section, General Directorate of MTA, Department of Geological Studies, No: 216 ANKARA.

Terlemez HCI, Senturk K, Ates S, Sumengen M, Oral A (1992). Geology of Gaziantep region and Pazarcık-Sakcagoz-Kilis-Elbeyli-Oguzeli Area. Ankara: General Directorate of Mineral Research and Exploration of Turkey (MTA). Report no: 9526.

Westaway R (2003). Kinematics of the Middle East and Eastern Mediterranean updated. Turkish Journal of Earth Sciences, 12: 5- 46.

Acknowledgements

We would like to acknowledge the funding provided for the fieldwork by The Scientific and Technological Research Institution of Turkiye (TÜBİTAK) “1002-C Natural Disasters-Focused Fieldwork Emergency Support Program (Doğal Afetler Odaklı Saha Çalışması Acil Destek Programı)”.

Chapter 6. Performance of Earth Dams

By:

Faik Cuceoglu[(a)], Seçkin Aydın[(a)], Sefa Yıldırım[(a)], Bilal Umut Ayhan[(b)], Kemal Önder Çetin[(c)], Robb E.S. Moss[(d)], and Mehmet Sagnak[(a)]

(a) The General Directorate of State Hydraulic Works, Ankara, Türkiye
(b) İstanbul Bilgi University, Department of Civil Engineering, İstanbul, Türkiye
(c) Middle East Technical University, Civil Engineering Department, Ankara, Türkiye
(d) California Polytechnic State University, Civil and Environmental Engineering, San Luis Obispo, California, U.S.A.

6. 1. Performance of Earth Dams

Immediately after February 6, 2023, Kahramanmaraş Earthquakes, reconnaissance teams assembled by the State of Hydraulics (DSI) and several researchers from various Universities visited the dam sites to conduct a preliminary investigation on the dams induced by the events. DSI has identified 140 dams for irrigation, drinking water, flood control and electricity generation in the region close to the earthquake epicenter and fault ruptures. Within a few days after the events, DSI reconnaissance teams completed the inspection of 140 dams by performing a visual inspection of crests, abutments, upstream-downstream slopes, and the hydraulic structures (inlet, spillway, etc.), and all teams reported that there was no situation requiring urgent action.

Türkiye Minister of Agriculture and Forestry Prof. Dr. Vahit Kirişçi announced to the public that there is no situation threatens the safety of dams in any of our facilities. Dr. Kirisci affirmed that DSI engineers daily check the safety of the dams and for security reasons, the reservoirs of Sultansuyu and Ariklikas dams were commenced to be evacuated.

In general, these dams showed outstanding performance against intense shaking, even though they were exposed to two separate significant earthquakes. Most of the dams are in the high seismicity zone (more than 50% g exposed to the structures), with extreme intensity. Although some dams experienced minor to major permanent deformations under severe seismic conditions, they did not fail to retain water and resulted in no uncontrolled release of water from the reservoir.

The examination was later elaborated with instrumental methods, including aerial pictures and 3D mapping via unmanned aerial vehicle, measurement of cracks, and failure mode detection. Besides, samples were collected from some areas for further analysis. Table 6.1 summarizes the full list of dams inspected by reconnaissance teams, their main characteristics, and preliminary findings. Some important cases among 140 dams will be shortly discussed here.

Table 6.1 List of dams inspected by reconnaissance teams.

Dam Name	Location	Purpose *	Construction Completion (year)	Dam Type**	Dam Volume (10^3 m^3)	Crest Elevation (m)	Crest Length (m)	Height from Foundation (m)	Active Storage (hm^3)	Damage***
Seyhan	Adana	I + E + F	1956	ZED	7500	72.70	1,955.00	77.00	1,063.00	No Reported Damage
Mehmetli	Osmaniye	I + E	1971	ECRD	5347	220.00	609.79	79.00	106.24	No Reported Damage
Kozan	Adana	I + E	1972	CFRD	1740	280.50	290.09	82.50	147.97	No Reported Damage
Tahtaköprü	Hatay	I + F	1975	CFSGD	2142	407.50	401.03	46.50	350.27	No Reported Damage
Aslantaş	Osmaniye	I + E + F	1984	ZED	8493	160.00	566.00	95.00	1,928.00	Minor crest cracks: max 10 cm width and 40-45 cm depth
Kalecik	Osmaniye	I	1985	ECRD	843	537.00	194.59	80.00	32.75	Moderate crest cracks: 40 – 50 cm width and 30-150 cm depth
Yarseli	Hatay	I	1989	ECSGD	3000	138.50	960.00	43.50	49.80	Moderate crest cracks: 5 – 30 cm width and 60-125 cm depth
Nergizlik	Adana	I	1995	ECSGD	1474	331.25	351.32	54.00	21.80	No Reported Damage
Çatalan	Adana	I + E + D + F	1996	ECSGD	14500	130.00	894.00	82.00	2,126.00	No Reported Damage
Yayladağ	Hatay	I + D	1998	ECRD	360	486.00	191.11	47.40	6.50	No Reported Damage
Sarıçam Hakkıbeyli	Adana	I	1999	ZED	250	205.20	206.50	33.00	5.75	No Reported Damage
Bahçe Arıklıkaş	Osmaniye	I	2000	ED	615	580.50	355.00	25.00	1.87	Major crest cracks: 80-120 cm lateral displacements

Samandağ Karamanlı	Hatay	I	2005	ED	359	186.00	406.00	26.00	2.00	Minor crest cracks: 2-10 cm width and 10-70 cm depth
Yüreğir Kılıçlı	Adana	I	2006	ED	604	146.00	510.00	37.50	7.54	No Reported Damage
Hassa Demrek	Hatay	I	2006	ED	358	286.00	503.00	26.00	2.00	Minor crest cracks: 6-8 cm width and 40-60 cm depth
Pozantı Yağlıtaş	Adana	I	2014	ED	334	1,341.82	191.66	32.82	0.92	No Reported Damage
Sarıçam Baklalı	Adana	I	2014	ED	465	122.55	307.00	32.95	2.26	No Reported Damage
Sarıçam Karlık	Adana	I	2014	ECRD	74	301.00	110.47	20.78	0.26	No Reported Damage
Kozan Bağtepe	Adana	I	2015	ZED	330	359.00	310.00	31.90	1.02	No Reported Damage
Kozan Postkabasakal	Adana	I	2015	ZED	188	431.50	210.00	34.32	0.63	No Reported Damage
Kozan Zerdali	Adana	I	2015	ZED	269	392.50	329.00	30.80	0.60	No Reported Damage
İskenderun Pirinçlik	Hatay	I	2015	ZED	113	350.80	85.00	30.60	0.49	No Reported Damage
Samandağ Çökek	Hatay	I	2015	ECRD	275	195.00	250.00	34.15	1.82	No Reported Damage
Merkez Bahçeköy	Osmaniye	I	2015	ECRD	73	191.00	128.50	22.00	0.46	No Reported Damage
Merkez Köyyeri	Osmaniye	I	2015	ED	144	177.85	165.00	24.85	0.75	No Reported Damage
Aladağ Dölekli	Adana	I	2016	ZED	385	849.65	234.50	30.00	1.49	No Reported Damage

Karaisalı Demirçit	Adana	I	2016	ECSGD	890	255.50	598.07	34.00	4.50	No Reported Damage
Kozan Meletmez	Adana	I	2016	ECRD	534	227.50	270.55	46.00	4.33	No Reported Damage
Merkez Tanışma	Hatay	I	2016	ZED	235	268.70	200.00	26.70	0.92	No Reported Damage
Düziçi Karacaören	Osmaniye	I	2016	ECSGD	320	614.20	186.74	39.00	0.50	No Reported Damage
Büyük Karaçay	Hatay	I + E + D + F	2017	CFRD	2500	352.00	415.07	105.00	53.67	Minor crest cracks: 2-6 cm width and 14-32 cm depth
Kırıkhan Kurtlusoğuks u	Hatay	I	2017	ECRD	362	195.00	419.09	40.00	0.75	Major crest cracks: 1-1.2 m lateral displacements
Aladağ Kasımlı	Adana	I	2019	ECRD	414	915.50	367.50	45.00	5.86	No Reported Damage
Reyhanlı	Hatay	I	2020	ED	20730	118.00	9,271.00	28.20	460.00	Major crest cracks: 10 – 120 cm width and max. 2.8 m depth
Merkez Mustafa Kemalpaşa	Hatay	I	2021	ED	71	161.40	175.00	15.90	0.07	No Reported Damage
Berke Dam and HEPP	Osmaniye	E	2002	AD	735	346.00	270.00	201.00	427.00	No Reported Damage
Feke 2 Dam and HEPP	Adana	E	2010	RCC	227	545.00	135.00	70.00	63.07	No Reported Damage
Yedigöze Dam and HEPP	Adana	E	2010	CFRD	3700	240.00	400.00	130.00	642.82	No Reported Damage
Menge Dam and HEPP	Adana	E	2011	RCC	349	483.00	303.00	68.00	50.80	No Reported Damage
Gökkaya Dam and HEPP	Adana	E	2012	RCC	700	762.00	115.13	69.00	18.25	No Reported Damage

Kavşak Bendi Dam and HEPP	Adana	E	2013	CFRD	1000	323.00	170.00	95.40	30.19	No Reported Damage
Köprü Dam and HEPP	Adana	E	2013	RCC	975	418.00	413.00	109.00	98.41	No Reported Damage
Karakuz Dam and HEPP	Adana	E	2015	RCC	400	834.00	161.75	45.00	5.11	No Reported Damage
Göktaş 1 Dam and HEPP	Adana	E	2016	RCC	749	632.50	211.75	132.50	109.33	No Reported Damage
Sürgü	Malatya	I	1969	ECRD	1220	1,311.60	736.00	57.00	70.93	Moderate crest cracks: 14 – 20 cm width and 46-55 cm depth
Medik	Malatya	I	1975	ECRD	1030	779.00	100.00	43.00	22.00	No Reported Damage
Polat	Malatya	I	1989	ZED	1850	1,434.00	538.00	53.80	11.50	No Reported Damage
Sultansuyu	Malatya	I	1992	ECSGD	3205	906.00	721.25	60.00	53.30	Major crest cracks: ~ 1.5 m lateral displacements
Çat	Malatya	I	1997	ZED	2500	1,419.50	267.00	78.00	240.00	No Reported Damage
Hekimhan Güzelyurt	Malatya	I	2005	ZED	630	1,652.40	325.00	36.40	1.44	No Reported Damage
Arapgir	Malatya	I	2009	MFSGD	150	1,209.65	195.00	25.65	0.31	No Reported Damage
Darende Sofular	Malatya	I	2009	ZED	360	1,626.00	178.44	36.00	2.43	No Reported Damage
Kapıkaya Turgut ÖZAL	Malatya	I	2012	ECRD	4720	868.00	514.50	89.50	71.10	No Reported Damage
Boztepe Recai KUTAN	Malatya	I	2013	ECSGD	7580	902.00	852.00	82.00	132.50	No Reported Damage

Doğanşehir Söğüt	Malatya	I	2014	ZED	150	1,703.95	142.56	35.00	0.51	No Reported Damage
Kuluncak Bicir	Malatya	I	2016	MFSGD	160	1,560.00	158.54	33.00	0.91	No Reported Damage
Akçadağ Taşevler	Malatya	I	2017	MFRD	610	1,342.00	232.80	50.50	5.12	No Reported Damage
Darende Ayvalı	Malatya	I	2017	ECRD	420	1,720.00	287.00	33.60	0.87	No Reported Damage
Güzelyurt Karamahmut	Malatya	I	2020	ECSGD	540	1,165.00	266.55	43.00	1.12	No Reported Damage
Hekimhan Budaklı	Malatya	I	2020	ECSGD	650	1,288.00	305.00	46.00	1.38	No Reported Damage
Hekimhan Kurşunlu	Malatya	I	2020	ECRD	190	1,575.00	121.00	38.00	1.14	No Reported Damage
Merkez Yaygın	Malatya	I	2020	ECRD	510	1,112.00	227.03	50.00	2.09	No Reported Damage
Yeşil Vadi (Beyler Deresi)	Malatya	I	2020	RCC	170	909.25	249.00	39.00	4.95	No Reported Damage
Hekimhan Karadere	Malatya	I	2021	ZED	370	1,206.50	186.81	38.50	2.28	No Reported Damage
Merkez Gözegöl	Diyarbakır	I	1964	ZED	48	752.00	255.00	13.32	16.10	No Reported Damage
Devegeçidi	Diyarbakır	I	1972	ECRD	2930	759.00	7,000.00	34.80	202.32	No Reported Damage
Çermik Halilan	Diyarbakır	I	1982	ZED	230	771.00	440.00	26.80	7.45	No Reported Damage
Karakaya	Diyarbakır	E	1987	AD	2000	698.00	462.00	173.00	9,580.00	No Reported Damage

Göksu	Diyarbakır	I	1991	ECRD	1860	702.00	673.50	53.00	62.00	No Reported Damage
Dicle	Diyarbakır	I + E + D	1997	ECRD	3100	718.00	307.00	87.00	595.00	No Reported Damage
Kralkızı	Diyarbakır	I + E	1997	ECRD	15170	820.00	1,037.00	126.00	1,919.00	No Reported Damage
Pamukçay	Diyarbakır	I	2013	ZED	1400	683.50	540.19	37.50	45.00	No Reported Damage
Ergani	Diyarbakır	I	2018	RCC	127	919.00	229.30	54.00	14.51	No Reported Damage
Başlar	Diyarbakır	I	2019	ZED	944	683.00	856.50	30.00	28.87	No Reported Damage
Kuruçay	Diyarbakır	I	2020	ECSGD	900	681.75	738.00	34.70	41.38	No Reported Damage
Ambar	Diyarbakır	I	2021	ECSGD	3811	715.00	1,184.88	45.00	131.97	No Reported Damage
Birecik Mezra	Şanlıurfa	I	2022	CFSGD	111	422.15	330.00	39.15	3.13	No Reported Damage
Siverek Ericek	Şanlıurfa	I	2022	MFRD	111	987.50	509.69	17.50	0.97	No Reported Damage
Hacıhıdır	Şanlıurfa	I	1989	ECRD	1600	634.60	737.00	42.00	67.60	No Reported Damage
Atatürk	Şanlıurfa	I + E	1992	ECRD	84500	549.00	2,000.00	169.00	48,700.00	No Reported Damage
Taşbasan Depolaması	Şanlıurfa	I	2014	ZED	398	574.50	721.00	22.50	5.36	No Reported Damage
Siverek Çamurlu	Şanlıurfa	I	2015	MFRD	442	669.00	595.70	22.50	9.92	No Reported Damage

Siverek Külhan	Şanlıurfa	I	2015	ECRD	380	775.50	282.19	37.44	2.50	No Reported Damage
Viranşehir Nohutlu	Şanlıurfa	I	2015	CFRD	406	711.50	1,048.00	32.00	6.15	No Reported Damage
Siverek Narlıkaya	Şanlıurfa	I	2018	ECRD	430	731.00	313.85	35.50	0.73	No Reported Damage
Siverek Taşıkara	Şanlıurfa	I	2021	ECRD	398	690.75	216.15	36.77	3.14	No Reported Damage
Birecik-Nizip Dam and HEPP	Şanlıurfa	E	2000	ECRD	9400	389.50	2,510.00	63.00	1,220.20	No Reported Damage
Çetintepe	Adıyaman	I	2022	ECRD	12700	910.50	780.00	116.00	460.00	Moderate crest cracks: 30–40 cm width and 100-120 cm depth
Merkez Akçalı 1	Adıyaman	I	2022	RCC	120	1,042.00	291.00	43.00	3.02	No Reported Damage
Kartalkaya	Kahramanmaraş	I + D + F	1972	ZED	1452	722.00	205.00	57.00	195.00	Major crest cracks: 20-30 cm lateral displacements
Hancağız	Gaziantep	I	1988	ZED	3300	435.00	1,955.00	48.00	100.00	No Reported Damage
Merkez Kınık	Adıyaman	I	1989	ZED	172	717.00	215.00	23.30	1.78	No Reported Damage
Menzelet	Kahramanmaraş	I + E + F	1989	ZED	8700	614.50	340.00	150.50	1,950.00	No Reported Damage
Merkez Zülfikar	Gaziantep	I	1991	ED	59	901.00	140.00	19.30	0.77	No Reported Damage
Merkez Hasancık	Adıyaman	I	1993	ZED	260	682.00	340.00	25.00	0.77	No Reported Damage
Gözebaşı	Adıyaman	I	1994	ZED	182	692.20	228.00	27.00	0.91	No Reported Damage

Merkez İncesu	Adıyaman	I	1995	ZED	253	665.50	322.00	35.00	1.88	No Reported Damage
Türkoğlu Kızıliniş	Kahramanmaraş	I	1995	ZED	404	576.90	335.00	31.90	3.95	No Reported Damage
Elbistan İncecik	Kahramanmaraş	I	1996	ED	109	1,474.90	325.00	21.90	0.42	No Reported Damage
Merkez Karahöyük	Adıyaman	I	1997	ZED	301	635.50	297.00	25.50	3.00	No Reported Damage
Çamgazi	Adıyaman	I	1998	ZED	5100	651.00	4,852.00	45.00	56.17	No Reported Damage
Karkamış	Gaziantep	I	1999	ZED	2100	344.00	1,607.79	29.00	157.00	No Reported Damage
Musabeyli Balıklı	Kilis	I	1999	ZED	338	643.70	355.62	31.00	3.94	No Reported Damage
Seve	Kilis	I + D	2005	ECRD	1340	590.00	789.00	41.00	20.86	No Reported Damage
Kayacık	Gaziantep	I	2006	ZED	1900	603.00	791.00	49.50	103.00	No Reported Damage
Şahinbey Alleben	Gaziantep	I	2006	ZED	350	945.30	430.00	26.00	2.54	No Reported Damage
Şehitkamil Yamaçoba	Gaziantep	I	2007	ZED	980	1,227.00	123.50	24.00	0.60	No Reported Damage
Ayvalı	Kahramanmaraş	I + D + F	2007	ZED	6600	841.50	613.00	103.00	80.00	No Reported Damage
Onikişubat Yenicekale (Meydan)	Kahramanmaraş	I	2008	ECRD	170	1,196.50	292.00	22.50	0.55	No Reported Damage
Musabeyli Üçpınar	Kilis	I	2008	ZED	200	548.00	380.00	28.00	4.57	No Reported Damage

Çağlayancerit Merk	Kahramanmaraş	I	2009	ZED	560	1,447.50	271.50	38.50	1.75	No Reported Damage
Kahta Menzil	Adıyaman	I	2011	ZED	320	623.20	362.00	33.50	1.58	No Reported Damage
Çağlayancerit Zorkun	Kahramanmaraş	I	2012	ECRD	380	1,160.00	263.00	36.00	1.55	No Reported Damage
Adatepe	Kahramanmaraş	I	2013	ECRD	4580	1,315.00	651.00	95.00	500.00	No Reported Damage
Elbistan Sarsap	Kahramanmaraş	I	2013	ECRD	700	1,292.00	1,263.00	26.00	4.23	No Reported Damage
Onikişubat Püren	Kahramanmaraş	I	2013	ZED	68	1,514.90	3,700.00	7.50	1.18	No Reported Damage
Sapkanlı	Kilis	I	2013	ZED	240	600.60	302.50	28.00	2.50	No Reported Damage
Kılavuzlu	Kahramanmaraş	E	2014	ECSGD	3800	489.00	556.00	61.00	74.00	Moderate crest cracks: 30-50 cm width
Ardıl	Gaziantep	I	2016	RCC	140	681.00	246.50	54.00	10.97	No Reported Damage
İslahiye Bayraktepe	Gaziantep	I	2017	ECSGD	690	656.40	233.45	41.00	2.81	Minor crest cracks: 3-5 cm width and 15-20 cm depth
Nurdağı Kuzoluk	Gaziantep	I	2017	ECRD	320	988.00	318.00	36.50	0.87	No Reported Damage
Doğanpınar	Gaziantep	I	2018	ECRD	4852	603.00	3,622.00	55.50	153.00	No Reported Damage
Nurdağı Hamidiye	Gaziantep	I	2018	ECRD	150	811.00	182.00	29.00	1.86	Moderate crest cracks: 15-18 cm width
Merkez Demirciler	Kilis	I	2018	ECRD	130	701.05	318.75	22.00	0.58	No Reported Damage

Yukarı Afrin	Kilis	D	2015	ECSGD	3167	686.00	720.16	60.00	37.77	Minor crest cracks: 3-4 cm width and 30-35 cm depth
Gerger Çifthisar	Adıyaman	I	2019	ECSGD	120	629.50	116.84	31.00	1.09	No Reported Damage
İslahiye Güneş	Gaziantep	I	2019	ZED	760	468.10	243.32	39.10	2.40	No Reported Damage
Akçalı 2	Adıyaman	I	2020	SSB	70	1,042.00	148.00	40.00	0.82	No Reported Damage
Çelikhan Yeşiltepe	Adıyaman	I	2020	ECRD	220	1,151.60	196.68	30.00	0.75	No Reported Damage
Sincik Arıkonak	Adıyaman	I	2020	MFSGD	94	1,661.00	107.00	28.50	0.53	No Reported Damage
Çağlayancerit Düzbağ	Kahramanmaraş	I	2020	ZED	400	1,082.00	300.00	30.00	0.80	No Reported Damage
Merkez Başderviş	Kahramanmaraş	I	2020	ZED	150	1,418.20	163.40	25.00	1.01	No Reported Damage
Çağlayancerit Zeynepuşağı	Kahramanmaraş	I	2021	ZED	310	1,270.50	259.00	33.00	1.00	No Reported Damage
Göksun Büyükkızılcık	Kahramanmaraş	I	2021	ECRD	282	1,455.50	224.90	32.50	1.10	No Reported Damage
Merkez Ağabeyli	Kahramanmaraş	I	2021	MFSGD	290	1,482.00	252.00	32.00	1.49	No Reported Damage
Sır Dam and HEPP	Kahramanmaraş	E	1991	AD	494	445.00	325.00	116.00	1,120.00	No Reported Damage
Suçatı Dam and HEPP	Kahramanmaraş	E	1999	RCC	60	647.00	191.00	36.00	11.34	No Reported Damage
Sırımtaş Dam and HEPP	Adıyaman	E	2013	GD	1600	863.50	205.56	97.50	33.86	No Reported Damage

Kandil Dam and HEPP	Kahramanmaraş	E	2013	CFRD	2210	1,101.00	347.41	104.00	438.68	No Reported Damage
Sarıgüzel Dam and HEPP	Kahramanmaraş	E	2013	ECSGD	3140	872.00	463.50	94.00	59.40	No Reported Damage

***Purpose:** I = Irrigation, F = Flood Control, D = Drinking water, E = Power Generation

****Dam Type:** ECRD = Earth Core Rockfill Dam, ECSGD = Earth Core Sand-Gravel Dam, ZED = Zoned Earthfill Dam, ED = Earthfill Dam, RCC = Roller Compacted Concrete, CFRD = Concrete Face Rockfill Dam, CFSGD = Concrete Face Sand-Gravel Dam, MFRD = Membrane Face Rockfill Dam, MFSGD = Membrane Face Sand Gravel Dam, AD = Arch Dam, GD = Gravity Dam

*****Damage:** In some cases, the values given for crack width represent the summed crack widths.

6. 2. Sultansuyu Dam

Sultansuyu Dam is a clay core sand-gravel dam constructed between 1986-1992 in Malatya for irrigation purposes. The crest height from the foundation level is about 60 meters. After the earthquake, cracks formed with varying depths, and earthquake-induced permanent deformation occurred on the crest and upstream side of dam body (see Figure 6.1a-c). All permanent lateral displacements are towards upstream side.

a) 38.31884° N, 38.05164° E

b) 38.31991° N, 38.09159° E

c) 38.31908° N, 38.05036° E

Figure 6.1. Earthquake-induced permanent deformations on the crest, a) illustration of depth, b) general overview, c) lateral movement on the dam body (1st failure, transitional slide)

On the dam body nearby the water level at the reservoir, liquefaction manifestation (soil ejecta) was observed (see Figure 6.2). Findings at the site reveal the suspicion of a composite failure mechanism. First, a transitional slide took place due to liquefaction on the dam body near the water level (see Figure 6.1c). Then, a rotational slide occurred starting from the crest due to loss of strength at the point where cracks formed due to the first mechanism (see Figure 6.1b). On the other hand, no damage was detected on hydraulic structures (spillways, bottom outlets, gates, etc., see Figure 6.3).

a) 38.31860° N, 38.05129° E b) 38.31770° N, 38.05549° E c) 38.34652° N, 38.0593° E

Figure 6.2. a, b) Sand boils on dam surface, c) lateral movements on reservoir area

38.31763° N, 38.05549° E

Figure 6.3. Gates and spillway of Sultansuyu Dam

6. 3. Arıklıkaş Dam

Arıklıkaş Dam is another critical zoned earth-fill dam constructed between 1994-1998 in Osmaniye for irrigation purposes. The crest height from the foundation level is 25 meters. The earthquake-induced permanent lateral displacement was observed at the crest and the upstream side of dam body similar to Sultansuyu Dam (see Figures 6.4a and b). Besides, the failure mode is similar. The surface manifestation of liquefaction was observed on the dam body near the water level and reservoir area.

The earthquake-induced lateral deformation towards upstream side was observed as 1.95 m at most at the crest whereas the maximum lateral deformation was 1.2 m on the dam body toward upstream (see Figures 6.4c and 6.4d). No damage was detected on the hydraulic structures except for minor cracks on the wing walls at the spillway outlet. The downstream dam body performed great against leakage since no water leakage was detected on the surface (see Figures 6.4e and 6.4f). No manifestation regarding the liquefaction at downstream side was noted. The ground water level was about 6 m below the talweg level which confirms the positive cut-off of Arıklıkaş dam is still functioning well.

a) 37.15491° N, 36.50593° E

b) 37.15510° N, 36.51782° E

c) 37.15491° N, 36.50593° E

d) 37.15510° N, 36.51782° E

e) 37.15857° N, 36.51358° E

f) 37.15510° N, 36.51782° E

Figure 6.4. Sand boils on a) dam body, b) on reservoir near dam body; Permanent lateral displacement c) at crest, d) at upstream dam surface; e) earth-dam view from downstream, f) wings at the outlet of spillway

6. 4. Yarseli Dam

Yarseli Dam is a clay sand-gravel dam constructed between 1985-1991 in Antakya for irrigation purposes. The crest height from the foundation level is almost 43.5 meters. A typical cross-section of Yarseli Dam is given in Figure 6.5. Unlike the previous earth dams, the lateral movement was toward downstream (see Figure 6.6a). The hydraulic structures seemed functional because they experienced no damage (see Figure 6.6b).

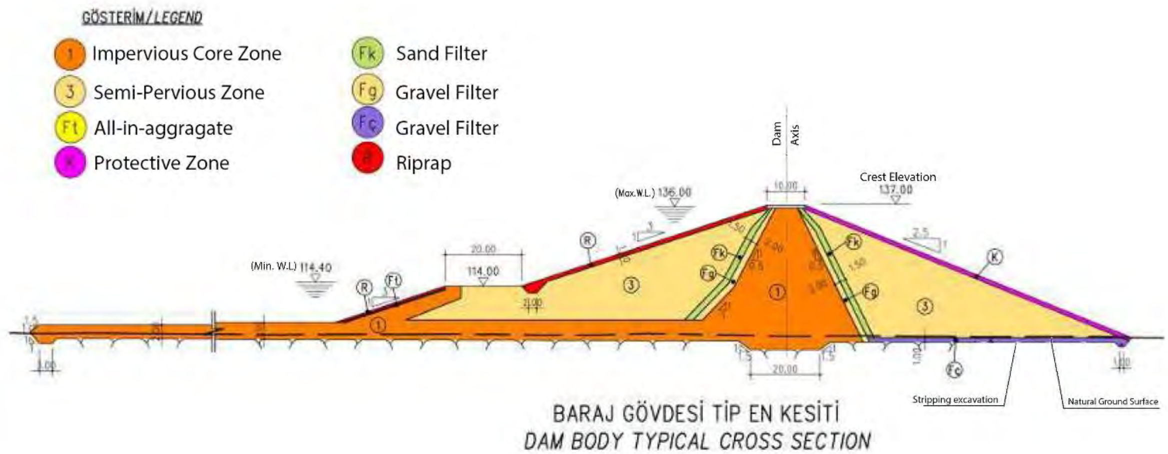

Figure 6.5. A typical cross-section of Yarseli Dam (courtesy of DSI)

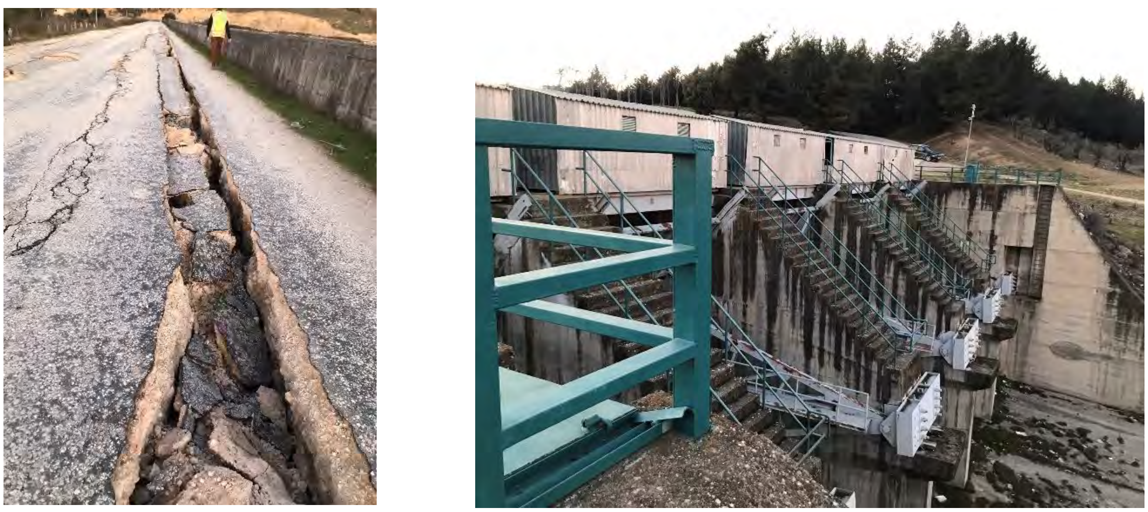

a) 36.19436° N, 36.32891° E b) 36.19497° N, 36.32190° E

Figure 6.6. a) Cracks on the crest of Yarseli Dam, b) gates and spillways (courtesy of DSI)

The seismic compression during earthquakes resulted in the crest cracks. The permanent lateral displacements vary between 5-30 cm. There was no sand boil on the earth-dam body, but at the edge of the dam body on the downstream side, where the projection of the crest with the broader lateral deformation lay on this location, sand boils, and liquefaction-induced lateral spreading was detected. (see Figure 6.7).

Figure 6.7. Demonstration of Yarseli Dam regarding findings obtained site visit

6. 5. Kartalkaya Dam

The Kartalkaya Dam is another one constructed between 1965-1972 in Kahramanmaraş for irrigation, drinking water supply and flood control purposes. The crest height from the foundation level is about 57 meters. An inclined clay core sand-gravel dam was constructed between the valley, so it sits on the bedrock. Due to seismic compression during the earthquake, the crest got damaged (see Figure 6.8a). The slight bulges formed on both downstream and upstream slopes close to the crest level, but no water leakage was detected on the dam surface.

Since the reservoir has already been almost empty due to the present climate conditions, leakage through the spillway gates has not been controlled, yet (see Figure 6.8b). Wings located at the water inlet through the gates have damage due to intense shaking because the dam is too close to the epicenter of Mw=7.7 Pazarcık Earthquake (see Figure 6.8c). One segment moved toward the earth dam, where seismic compression occurred. Besides, there are no connections between segments on the wings so that damaged segments easily move apart. Surface manifestation of liquefaction was not detected neither on the dam surface, nor nearby the dam body.

a) 37.46811° N, 37.23947° E   b) 37.46838° N, 37.23856° E   c) 37.46811° N, 37.23947° E

Figure 6.8. a) Cracks on crest, b) radial gates and spillway, c) wings on the inlet of gates

6. 6. Sürgü Dam

The Sürgü Dam is an earth-fill dam constructed between 1965-1969 in Malatya for irrigation purposes. The crest height from the stream level is almost 57 meters. Dam's location is critical since the nearby faults ruptured during the 7.7 M_w and 7.6 M_w events according to the spatial distribution of aftershocks, except for the one passing through the dam (see Figure 6.9a). For this reason, no significant damage was detected on the crest and the earth-dam body. Cracks on the crest seem like seismic landslide stability problem with 14-20 cm crack width (see Figure 6.9b). Hydraulic structures got no damage except for the small cracks on the wings of the spillway at the outlet.

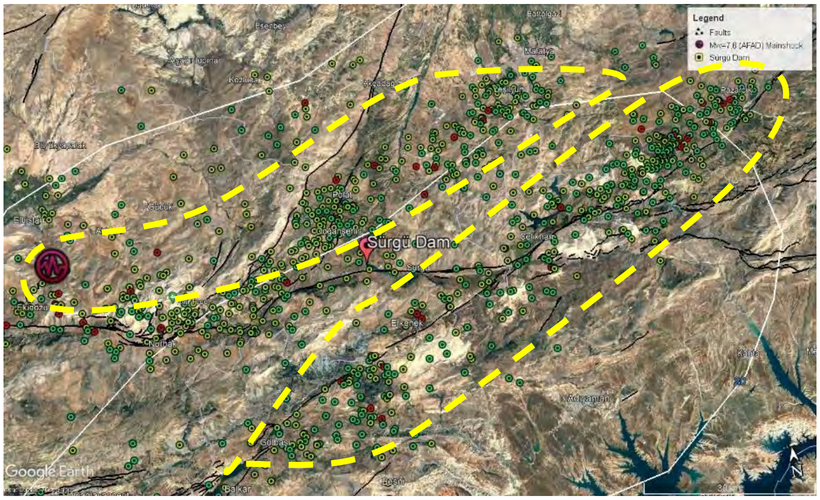

(a) (b) 38.03519° N, 37.8795° E

Figure 6.9. Sürgü Dam, a) spatial distribution of aftershocks, b) cracks on the crest

6. 7. Reyhanlı Dam

Reyhanlı dam was constructed between 2013-2020 with a 30 meters crest height from the foundation level. The crest length is 9271 meters, which is too long compared to the other dams. Similar to the previous ones, the dam is serving for irrigation purpose. The dam comprises two different dam types such as zoned earth-fill (Km: 0+000-6+000) and clay core sand-gravel (Km: 6+000-9+200). The dam starts with 3H:1V downstream and 3.5H:1V upstream slopes then, the upstream slope flattens to 9H:1V. In the second part, the slope for the downstream and upstream sides becomes 2.25H:1V and 2.75H:1V, respectively.

Figure 6.10 depicts the spatial distribution of the cracks on the crest roughly regarding the dam position. The red line code emphasizes the most critical part, where the dam cross-section is the second one shown in Figure 6.11b. The cracks extended to 1-1.2 meters with 2.8 meters depth, whereas the settlement at the crest reaches 50-80 cm according to the site observations (see Figure 6.11). The earthquake-induced permanent lateral deformation is toward the upstream side. The surface manifestation of liquefaction was not observed at the dam body and the ground nearby the dam.

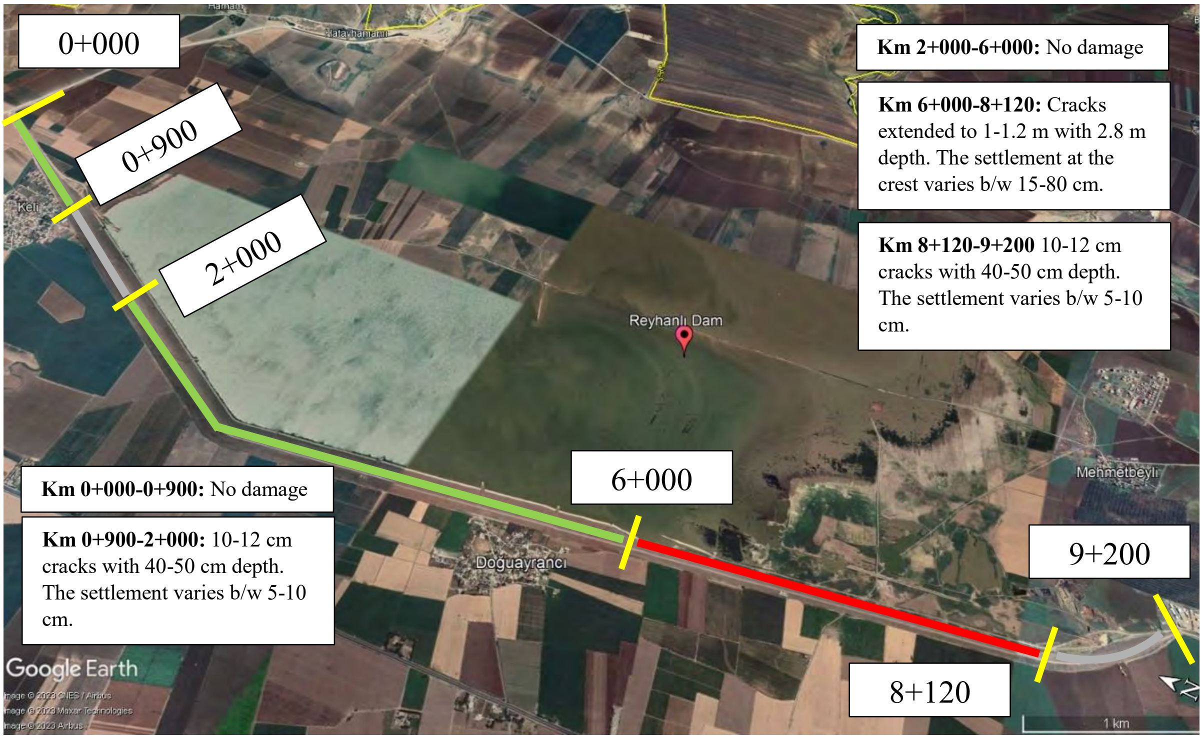

Figure 6.10. Spatial distribution of cracks and settlements on the crest in Reyhanlı Dam

a) 36.37758° N, 36.56494° E b) 36.55659° N, 36.55659° E b) 36.32988° N, 36.55695° E

Figure 6.11. a, b) Cracks on the crest and c) dam body view from upstream (courtesy of DSI)

6. 8. Kalecik Dam

The Kalecik Dam is a clay core rockfill dam constructed between 1983-1985 in Osmaniye for irrigation purposes. The crest height from the foundation level is 80 meters. Earthquake-induced lateral deformations and settlements were observed at the crest. The deformation direction is upstream and downstream, but the failure mechanism has not been clearly understood yet. The settlement values vary 10-40 cm along with the crest, and the maximum lateral deformation was measured as 40-50 cm towards both upstream and downstream separately. Bulges formed on the dam surface in both directions around 5-8 m away from the crest level. The hydraulic structures seem functional, and no liquefaction manifestation was detected (see Figure 6.12).

a) 37.14988° N, 36.46066° E

b) 37.14819° N, 36.45919° E

c) 37.14707° N, 36.45852° E

Figure 6.12. a) Hydraulic strucres in Kalecik Dam, b) cracks observed at the crest and c) slope at upstream (courtesy of DSI)

References

Republic of Türkiye Ministry of Agriculture and Forestry, the General Directorate of State Hydraulic Works, Action Report between 06.02.2023 and 24.02.2023 after the Earthquake

Chapter 7. Performance of Residential Structures

By:

Barış Binici[(a)], Ahmet Yakut[(a)], Erdem Canbay[(a)], İsmail Ozan Demirel[(a)], Mevlüt Kahraman[(b)], Altuğ Erberik[(a)], İsmail Özgür Yaman[(a)], Eray Baran[(a)], Afşin Canbolat[(c)], Koray Kadaş[(c)], Orkun Öztaşkın[(c)], Selin Aktaş[(a)], Erkut Sayın[(d)], Mesut Gör[(d)], Özgür Yıldız[(e)], Alper Özmen[(f)], Kübra Sertkaya[(d)], Ömer Faruk Taş[(d)], Taha Taşkıran[(g)], M. Salih Keskin[(h)], Moutasem Zarzour[(a)], Abd Alhamed Arif[(i)]

(a) Middle East Technical University, Civil Engineering Department, Ankara, Türkiye
(b) Bilkent University, Construction works, Ankara, Türkiye
(c) Middle East Technical University, Office of Revolving Funds (DSIM), Ankara, Türkiye
(d) Fırat University, Civil Engineering Department Elazığ, Türkiye
(e) Malatya Turgut Özal University, Civil Engineering Department, Malatya, Türkiye
(f) Inönü University, Civil Engineering Department, Malatya, Türkiye
(g) Ankara Yıldırım Beyazıt University, Civil Engineering Department, Ankara, Türkiye
(h) Dicle University, Civil Engineering Department, Diyarbakır, Türkiye
(i) Civil Engineer Aleppo, Syria

7. 1. Performance of Buildings

Pazarcık and Elbistan-Kahramanmaraş earthquakes were one of the most destructive earthquakes, if not the most, experienced in Türkiye in the last century. Unlike previous earthquakes for which the damage has usually concentrated in a certain city, the building damage spread to eleven cities. The building damage inventory collected as of February 16, 2023, is given in Table 7.1. Based on this inventory, Hatay, Kahramanmaraş, Gaziantep, Adıyaman and Malatya experienced extensive damage due to the proximity of these cities to the faults, whereas the number of buildings collapsed in Kilis, Adana, Diyarbakır, Osmaniye, Şanlıurfa and Elazığ is smaller.

The intensity of the ground motion, the structural system, design, and construction quality were decisive in the building performance. The acceleration response spectra for the recorded motions in Göksun, Kahramanmaraş, Narlı, Hatay, Fevzipaşa, Malatya are presented in Chapter 4. It can be observed that design response spectra for residential buildings (i.e. maximum design earthquake with a return period of 475 years) are exceeded for a wide period range, whereas the maximum credible earthquake level (return period of 2475 years) response spectra is generally exceeded for long periods especially in soft soils, in certain regions. This implies that in Gaziantep (İslahiye and Nurdağı districts), Hatay, Kahramanmaraş, and Adıyaman the buildings were subjected to seismic actions larger than Turkish Earthquake Code design levels.

The building damage inventory in the region can be divided into two, based on their construction periods. A significant change is believed to occur in Türkiye between 1998 and 2001 due to the following four factors:

- A modern earthquake code was put into effect on September 2, 1998,
- Two destructive earthquakes occurred on August 17, and November 12, 1999, in Kocaeli and Düzce awakening awareness for seismic resistance,
- A modern reinforced concrete design guideline (TS-500) come to force on October 12, 2000, making ready mix concrete and ductile low carbon content steel as reinforcement,
- Building Inspection Law enacted on July 13, 2001, for 19 pilot cities including Gaziantep and Hatay. This law was extended to the whole country in 2010.

We divided our reconnaissance into two groups: reinforced concrete (RC) buildings constructed before and after 2002, based on the information collected at the building sites.

Table 7.1 Identified Building Damage Distribution (Ministry of Environment, Urbanization and Climate Change)

Damage State	Hatay	K.maraş	Adıyaman	Malatya	Gaziantep	Kilis	Adana	Diyarbakır	Osmaniye	Ş.urfa	Elazığ
None	29188	25420	21365	7463	89092	2849	1688	18039	22041	19585	9503
Light	17212	20556	38823	8960	29471	2208	5314	6725	8034	13507	15532
Moderate	2827	1058	2613	945	4361	137	304	713	266	550	138
Heavy/Collapse Urgent Demolish	15248	12980	6990	8365	12964	812	59	643	2531	466	664

7. 1. 1. Performance of RC Buildings Before 2000

Typical deficiencies of the frame buildings constructed before 2000 were the use of smooth reinforcing bars, insufficient steel reinforcement detailing and possibly low concrete strength resulting in heavy damage and collapse (Figure 7.1). The presence of soft story in the ground level or above the plinth was one of the key reasons of collapse in many buildings. The use of the ground floors as commercial stores with little or no infill walls were responsible for plastic hinging in columns occurred resulting in pancake type collapse as observed in previous earthquakes (Kocaeli 1999, Van 2011). This is displayed in Figure 7.2. Several buildings have experienced beam-column joint failures. Another interesting type of failure was the overturning of the building from its base due the inability of transferring lateral forces to the foundation (Figure 7.3).

Figure 7.1. Building Collapse in Antakya and Kahramanmaraş

Figure 7.2. Building Collapse in Malatya

Figure 7.3. Overturning due to soil liquefaction and insufficient joint reinforcement detailing

7. 1. 2. Performance of RC Buildings After 2000

These buildings presumed to be designed and constructed according to the codes performed better than the older buildings. However, more than 1000 buildings constructed after 2000 were heavily damaged or collapsed violating the code given performance objective. This appears to be an important observation demanding further investigations on the design and construction quality of those buildings. Some examples of these heavily damaged buildings are shown in Figure 7.4. The possible reasons for these damages can be attributed to i) the use of flexible joist slabs as diaphragms, ii) insufficient engineering design to distribute lateral forces to vertical load bearing elements perhaps due to the blind use of building design softwares, iii) possible detailing errors on building construction site, iv) underestimation of seismic demands, iv) insufficient investigations geotechnical site investigations prior to building construction and poor foundation design especially in Hatay and Gölbaşı regions. Such heavy damage observed in new buildings bring concerns about the target seismic performance of residential buildings nearly in compliant with the current seismic code. The significant disruption of city life, heavy monetary loss, and long recovery times may require reassessing the performance targets of buildings.

Tunnel form buildings in the region performed in an outstanding manner (Figure 7.5) with some damage in the coupling beams and infill walls due to the following key reasons: i) the use of more shear wall area more than usually 2.5% of the floor area, ii) siting at stiff soil or rock sites, iii) mid-rise construction ranging from (4 to 8 stories). This performance provided further confidence in the use of significant shear wall area for the buildings constructed in high seismic zones.

Figure 7.4. Heavily damaged new buildings in Adıyaman and İslahiye

Figure 7.5. Performance of a tunnel form building

7. 1. 3. Performance of Precast Buildings

Industrial Regions in Kahramanmaraş and Gaziantep have many precast concrete buildings with one or two stories. Typical main direction of the buildings has a span of about 20 m, and the other direction has a span of 7.5 m. The story heights vary between 7 to 10 m. The building frame columns are fixed at the base with a socket connection, whereas the prestressed (for long spans) roof girders are pinned to the column corbels usually with two grouted anchors embedded into the corbels. Typical buildings are shown in Figure 7.6. Two buildings that were under construction collapsed due to overturning of the girders. The failure is assumed to be initiated at the pin connections under the lateral force demands. Interestingly no indication of column base hinging was observed. In Gaziantep, most of the prefabricated buildings showed satisfactory performance.

In a few lightly damaged buildings, the typical damage was observed in column corbels due to the girder rotations causing local crushing of concrete, which is repairable (Figure 7.7).

Figure 7.6. Overview of precast industrial building connection damage in Kahramanmaraş

Figure 7.7. Corbel damages in Gaziantep

7. 1. 4. Performance of Non-Structural Elements

One of the most important non-structural damage in the region was observed in the infill walls. Several levels of damage events were observed depending on the strong ground motion levels (Figure 7.8). At low ground motion levels (< 0.1 g), the infill wall-column/beam interfaces cracked. At moderate levels, the infill walls sustained inclined cracks with varying widths (0.5-2 mm).

Under such damage, despite the absence of any structural damage, the occupants safely left the building and were reluctant to occupy the building after the earthquake. Similar to our past observations after 2011 Van earthquake, the infill walls are observed to be the key components to establish the damage state of a building affecting the psychology of the occupants. The infill wall construction technique suggested in the latest seismic code in 2019 did not seem to be applied in any of the recent buildings. For regions that have experienced accelerations well over the design values, the infill walls were severely damaged and failed under combined in and out of plane. Infill wall damage was observed in buildings constructed both before and after year 2002 exhibiting no significant difference in their performance. Furthermore, the damage was similar in all the infill walls made of hollow clay brick, autoclaved aerated concrete or bims blocks, indicating that none of the block materials showed superior seismic performance.

Figure 7.8. Infill wall damage examples

7. 1. 5. Performance of Masonry Buildings

Masonry construction constitutes the second largest type in Turkish building inventory. Although the percentage of masonry buildings in urban areas is low, it is more common in rural areas. Similar to the other buildings, non-engineered masonry building stock in the region either suffered significant damage or collapsed under the two earthquake motions (Figure 7.9). However, the collapse of masonry buildings constructed with relatively better materials having 1-3 stories was less compared to 8-10 story RC buildings. It appears that the height and rigidity of the buildings played an important role. Besides, many historical masonry buildings suffered heavy damage or collapse due to strong shakings that they experienced.

Figure 7.9. Damage in masonry structures

7. 1. 6. Performance of Strengthened Buildings

One building strengthened in 2008 by the METU team with the addition of shear walls, fiber reinforced polymers was visited in Hatay. None of the strengthened buildings collapsed while some damage was observed, as shown in Figure 7.10. These observations that will be extended in further site visits seem to encourage the wider spread application of building strengthening.

Figure 7.10. Performance of the strengthened building in Hatay

7. 1. 7. Performance of Electrical Substation Buildings

Service buildings (typically 1-2 stories) in twenty-three substations were visited to check the damage levels. The locations of the substations are shown in Figure 7.11. It can be observed that some of the substations are located in close proximity to strong ground shaking. However, none of the switch yard or control buildings were heavily damaged to disrupt the operation of the substations. It can be stated that the successful building performance of the substation buildings allowed continuous electricity transmission in the earthquake region.

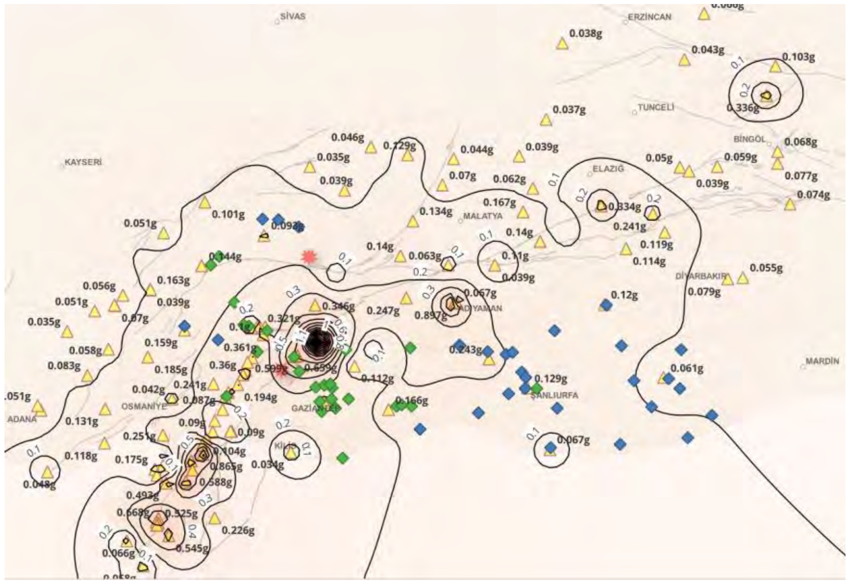

Figure 7.11. PGA distribution and substation locations (Yellow: Strong motion instruments, Blue and Green: Substation Locations)

7. 1. 8. Performance of Buildings in Malatya

The results of the field survey conducted in the center of Malatya reveal that there are numerous collapsed structures. The old building stock is typically to blame for these collapses. Also, new buildings were collapsed in the Bostanbaşı District, Malatya. Due to aftershocks, the exact number of the collapsed buildings increase. According to observations, structural design, material defects are the main causes of collapses. The first notable factors are inadequate reinforcement, design mistakes in structural system, use of unribbed reinforcement, low concrete strength and inappropriate aggregate gradation (Figure 7.12-17).

Figure 7.12. Structural collapses in Malatya city center-1

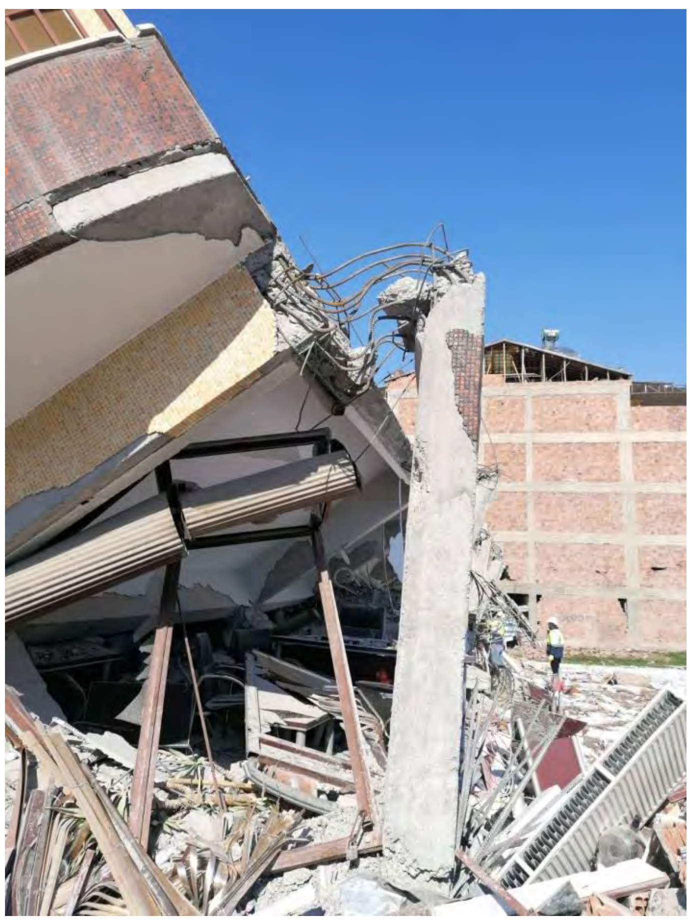

Figure 7.13. Structural collapses in Malatya center-2

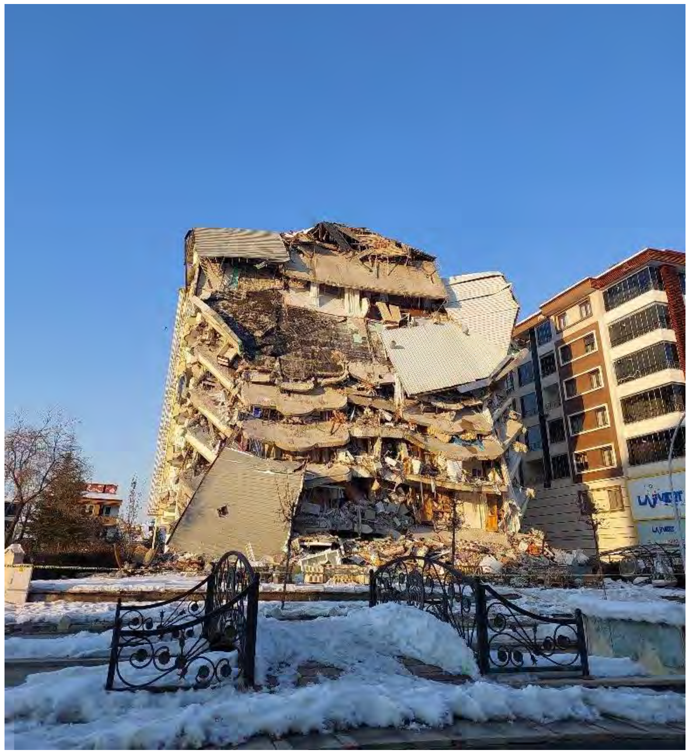

Figure 7.14. Structural collapses in Malatya center-3

Figure 7.15. Unribbed reinforcement in Malatya Center

Figure 7.16. Structural collapses in Malatya center-4

Figure 7.17. Inappropriate aggregate gradation in Malatya

7. 1. 9. Performance of Buildings in Elaziğ

Structural damages were not observed related to soil, liquefaction, lateral spread in the preliminary field surveys conducted in Elazığ. Also, no damage was seen at the retaining structures. One building was collapsed, and about 3309 buildings have been severely damaged so far. In the field studies, it was observed that collapse and damage were caused by structural design, building ages, material, and design defects (Figure 7.18-23). Short columns, improper beam-column connections, corrosion, and infill wall damage are the most common damages and deficiencies. The soil-based phenomena like liquefaction or settlement were not noted in building collapse.

Figure 7.18. Heavy damaged minaret in Elazığ

Figure 7.19. An example of short column in Elazığ

Figure 7.20. Structural damages in Elazığ

Figure 7.21. Concrete cover and corrosion in Elazığ

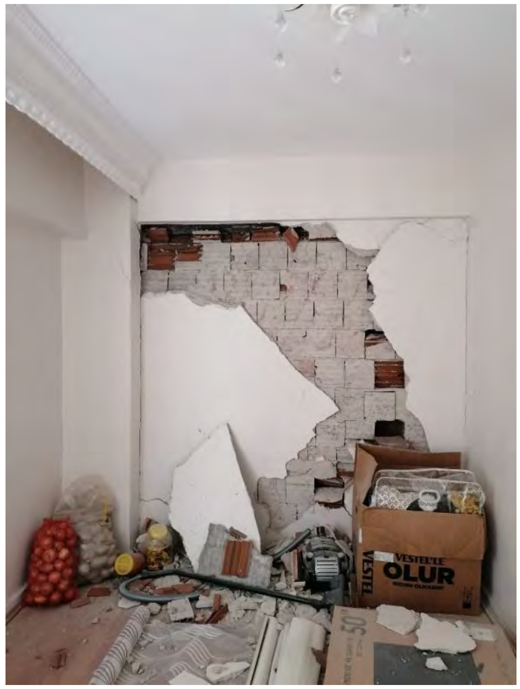

Figure 7.22. Infill wall damage in Elazığ

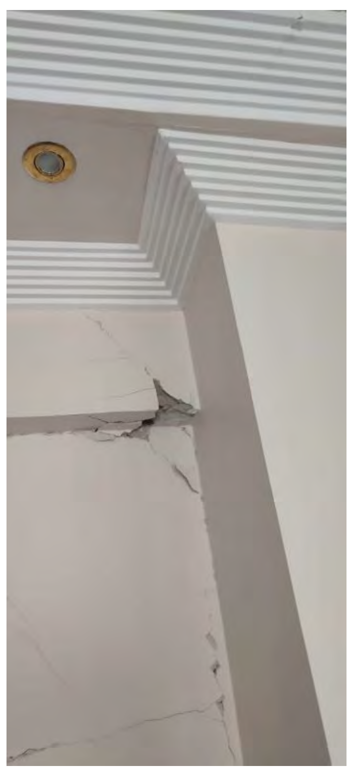

Figure 7.23. Beam damage in Elazığ

7. 1. 10. Performance of Buildings in Diyarbakir

During the Diyarbakır field surveys, no structural damage was not observed caused by soil issues (liquefaction, settlement, etc.). It is believed that the collapses are the result of material defects and improper structural design (Figure 7.24-27) since the city's terrain is typically rock. 194 severely damaged buildings and 7 completely collapsed buildings were observed. The retaining walls in the city center did not have any damage, and there were no issues with slope stability. In the field investigations, there was no evidence of liquefaction.

Figure 7.24. Structural damages (Buckling) at column in Diyarbakır

Figure 7.25. Structural damages at column in Diyarbakır

Figure 7.26. Structural collapses in Diyarbakır

Figure 7.27. Infill wall damages in Diyarbakır

7. 1. 11. Performance of Buildings in Syria

Syria is located to the southeast of Türkiye on the north of the Arabian plate and bordered by the Dead Sea fault to the west, the East Anatolian fault to the north, and the Eurasian plate to the northeast and east, Figure 7.28.

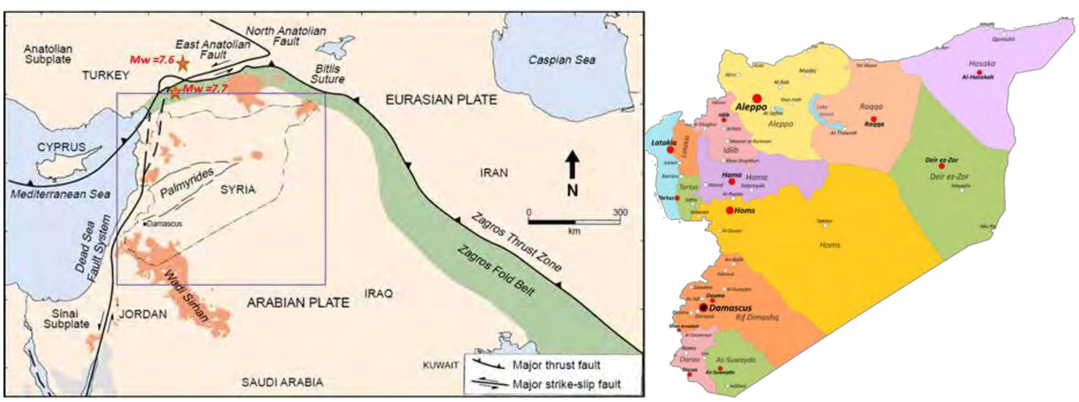

Figure 7.28. Syria and its location in correspondence to tectonic plates, showing the epicenters of the earthquake events, (After Brew et al., 2001, ontheworldmap.com).

Syria was greatly affected by the earthquake events that occurred in Türkiye, especially, in the northwestern region of the country resulting during the date of writing this report, more than 8.8

million people affected, more than 6000 deaths, and 12000 injuries. Regarding structures, more than 1700 were destroyed and 5700 were partially damaged buildings according to United Nation Humanitarians Affairs.

The affected cities in Syria are Aleppo, Idlib, Latakia, and Hama, respectively, along with relatively less damage in the other cities of the country. The severity of the damage was gradually decreasing with increased distance to Türkiye’s border and in turn the earthquake's epicenter proximity.

The greatest damage was in the city of Aleppo and its northwestern suburbs (Mostly in Jindires, Afrin, A’zaz, and Sawran). Figure 7.29 shows an example of the destruction in Jindires, where most of the buildings have been totally collapsed or damaged severely.

Figure 7.29. Destruction in Jindires – Afrin, Aleppo, approximate location (36°23'46.76"N, 36°41'14.26"E)

Nevertheless, in Idlib North suburban (Mostly in Harem, Sarmada, Aldana, Salqin, and Armanaz). Figure 7.30 shows the destruction in Harem due to the earthquake.

Figure 7.30. Destruction in Harem, Idlib, approximate location (36°12'45.01"N, 36°31'13.72"E)

Regarding affected service structures, it was spoken of 17th April or Medanki dam in Afrin as being damaged due to the earthquake. But, as per reported by a committee of civil engineers who inspected the dam, there is no visible damage in the body of the dam and there is no water leakage observed. The seen cracks at the top road constructed over it are just in the asphalt layer of the road with a 4cm width and 40cm depth, Figure 7.31.

It is an earth-fill dam with 980 x 10 / 325 x 75 m and has a capacity of 190 million m^3.

Figure 7.31. Medanki dam showing the cracks in the road at the crest, (36°37'18.56"N, 36°52'17.19"E), (syria.tv).

In the Tloul village in the subdistrict Salqin, Idlib, a flood occurred due to an increase in the AlAsi river water level due to the winter season and damage to the constructed mud shoulders on the sides of the river in the mentioned village and its neighborhood resulting in approximately 1000 home affected and evacuation of 7000 people, Figure 7.32.

Figure 7.32. Flooded village of Tloul in Salqin, Idlib, (36°12'42.82"N, 36°23'40.89"E), (nasnews.com).

In the subdistrict of Afrin, collapsed electricity supply tower as a result of a stability problem in the foundation soil, Figure 7.33.

Figure 7.33. Slope failure in the proximity of the Afrin subdistrict.

Also, due to the earthquake historical buildings sustained limited damage. In the case of Aleppo castle, some parts of the ottoman mill, and the northeastern defensive walls. Also, historical buildings in Hama and Banias have sustained similar light to moderate damage, (Directorate General of Monuments and Museums, Syria).

As a reminder, the damage due to the earthquake is not limited to the above-mentioned, many other areas were stroked by the earthquake and sustained different levels of damage in a country worn out by 12 years of civil war. Even before the earthquake events, the living conditions were harsh and now many families are still under the rubble due to the earthquake, waiting for help and the local capabilities are lacking to machinery tools to be able to rescue these people, especially in the north and northwestern parts of the country.

References

Brew, G., Barazangi, M., Al-Maleh, A. K., & Sawaf, T. (2001). Tectonic and Geologic Evolution of Syria. *GeoArabia*, *6*(4), 573–616.

Directorate General of Monuments and Museums, Syria.

Chapter 8. Industrial Structures

By:

Altuğ Bayram, Cemal İçel, İzzet Mert Özdemir, Aras Kalyoncuoğlu, Merve Çiftçi, Maral Sağbazar, İrem Evcen Yapıcı[a]

[a]Promer Müşavirlik Mühendislik A.Ş.

8. 1. Introduction

Türkiye is a country located in a seismically active region where several tectonic plates converge, making it prone to earthquakes. Over the years, Türkiye has experienced several devastating earthquakes that have caused significant loss of life and property damage.

(a)

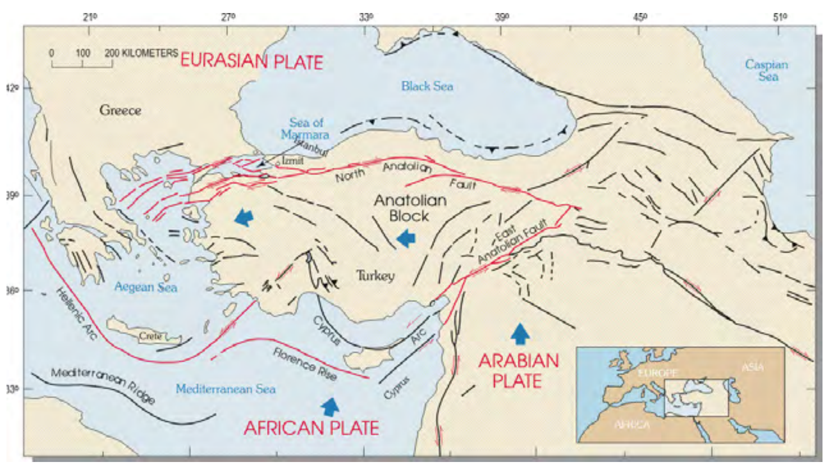

(b)

Figure 8.1. a) Seismic Map of Türkiye, b) Tectonic Faults in Türkiye

Like most coastal countries that import raw materials for production, raw materials come by ports in Türkiye. As seen in Figure 8.1, this causes the concentration of settlements and heavy industry facilities in coastal areas with intense earthquake activity. Most industrial facilities face middle-high size earthquakes during their service lives in Türkiye.

Industrial buildings are generally exposed to high equipment loads, high span / axes lengths and story heights. Therefore, their structrural member sizes are considerably large compared to the residential buildings. That is why, industrial building weights and their seismic loads are generally highly significiant.

This report includes first site inspections of the engineering team at some industrial structures after the earthquake. And the aim of the report is to share the effects of the earthquake forces on the structures and maybe guide engineers to visualize the effects during designing of the industrial buildings. The photos included in this report are intentially blurred to protect the owners rights, however other than the aim of the document, it is not permitted to use the photos for any other reason.

In the following, the effects on industrial buildings/structures are catagorized and presented.

8. 2. Shear Wall – Beam Connection In-Plane Mechanism Under Earthquakes

Shear walls are structural elements designed to resist lateral loads, such as those caused by earthquakes. They transfer the lateral loads to the foundation through their stiffness and strength.

During an earthquake, the ground shakes back and forth, causing the building to move laterally. The shear walls resist this lateral movement and transfer the forces to the foundation. However, in some cases considering the selected lateral structural system, these forces may be too great for the shear walls alone to handle, which is where the shear wall-beam mechanism comes into play.

The shear wall-beam mechanism involves the interaction between the shear walls and the beams that connect them. When lateral loads affect the structural system, cracks may occur due to exceeded capacity or ductile behaviour of structural members.

During an earthquake, beams and shear walls may experience various types of cracking due to the levels of lateral forces and shear stresses that they are subjected to. Below, it can be seen structure behaviour during earthquake. The cracks and behaviour are the expected behaviours during eathquake. Some of the common types of cracks that can be observed on beams and shear wall connections are listed as follows.:

- Flexural cracking: This type of cracking is caused by bending stresses that occur when the beam or shear wall is subjected to lateral or gravitational forces. Flexural cracks are generally localized at mid span of the beam due to gravitational forces, at support connection due to cyclic forces of earthquake. These cracks run across the depth of the beam.

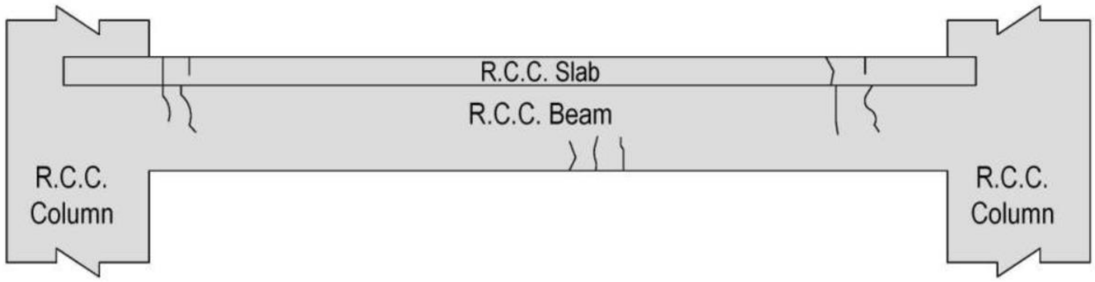

See photographs below:

- Shear cracking: Shear cracks occur when the beams are subjected to shear stresses transferred from shear walls. Shear cracks are typically inclined at 45 degrees with the horizontal and runs parallel to the direction of the shear force. When properly designed shear reinforced beams, some microcracks will occur where shear reinforcements are located through the beam length.

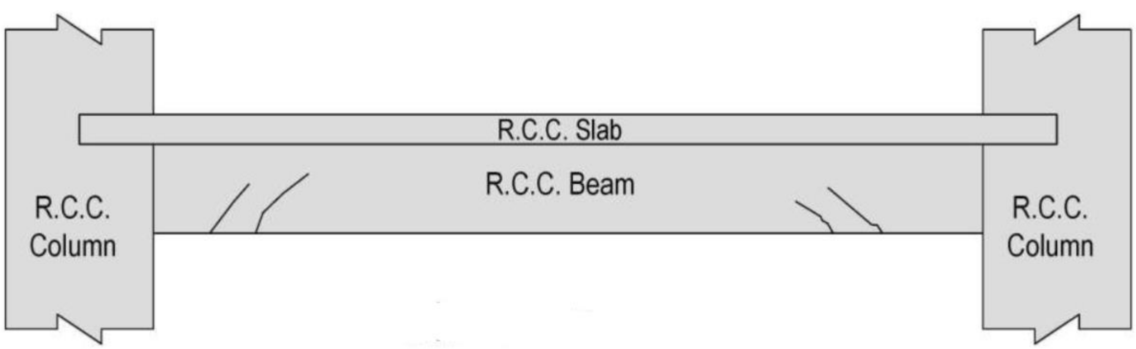

- Spalling: Spalling occurs when the surface layer of the beam or shear wall peels away due to the high stresses that occur during an earthquake. High concrete cover thickness and concrete segregation may lead to spalling cracks on beams or shear walls.

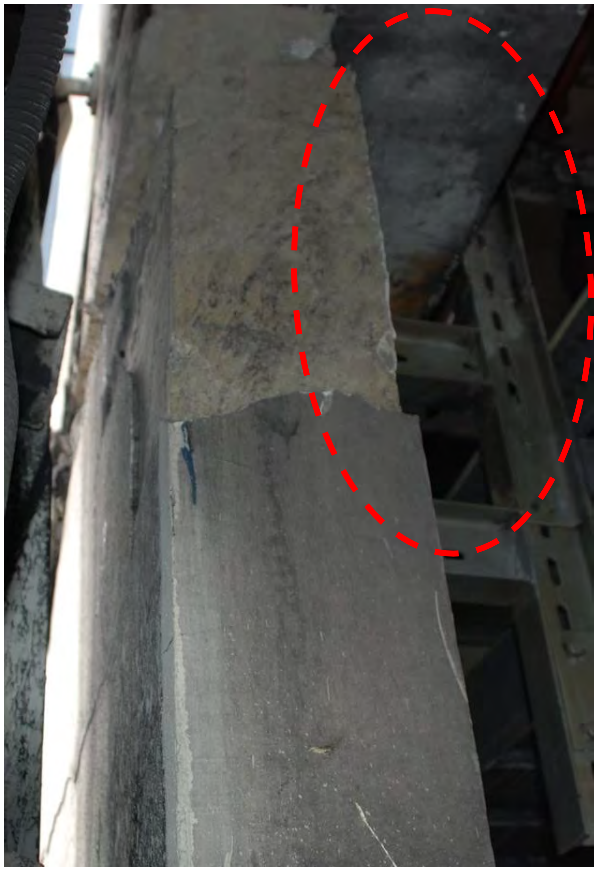

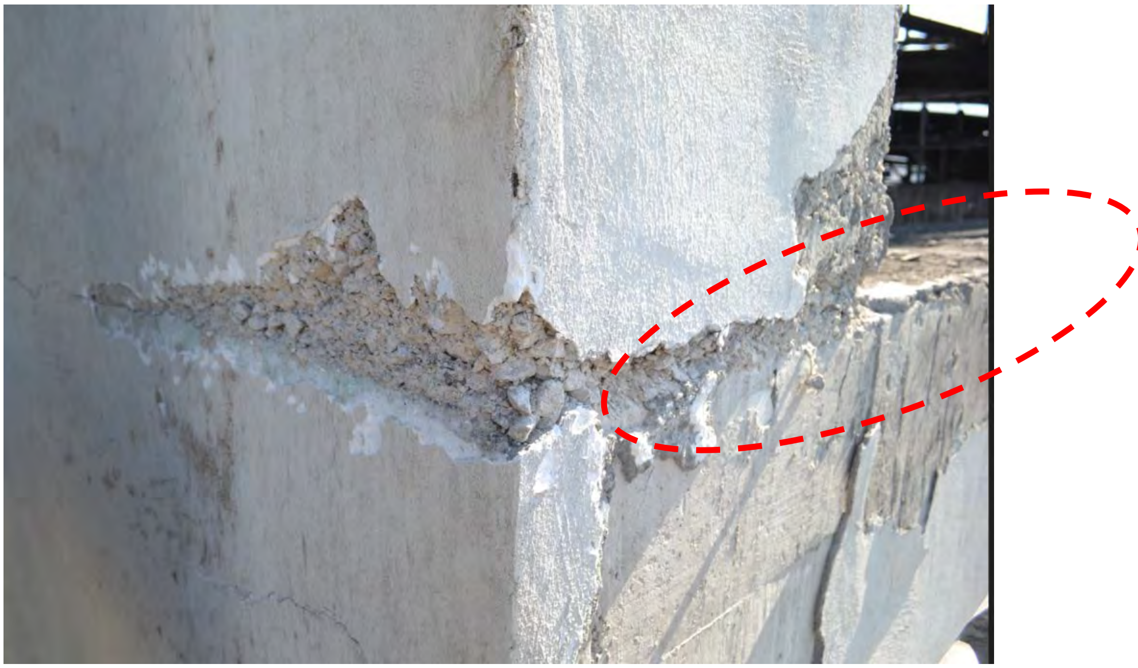

- Shear Flow Cracking: Flexure flow cracking occurs at the body of the shear wall starting from beam connection joints and spreading through the beam body. This type of cracking is caused by shear stress flow through the shear wall cross section. Typically diagonally cracks are observed

As a conclusion, the type and severity of cracking observed on beams and shear walls will depend on a variety of factors, such as the magnitude and duration of the earthquake, the design and construction of the structure, and the properties of the materials used. From the structural point of view, ductile behaviour is crucial for R/C structures. This means that the cracks will occur under the earthquake loads in order to provide ductility demand of the system as long as the designed hinge mechanism is achieved. After the structure subjected to the design earthquake loads, it is mandatory to make a site inspection to detect and categorize the cracks to calculate the performance of the structure and determine its structural requirements for further service life.

8. 3. Shear Wall – Beam Connection Out-Of-Plane Mechanism Under Earthquakes

Out-of-plane beam connections on shear walls can be an important consideration for seismic design, particularly in regions with high seismicity. The connections must be able to resist the forces induced by the earthquake and ensure the integrity of the entire shear wall cross section.

Beams transfer highly localized forces on shear walls under the earthquake. Therefore, out-of-plane beam connections on shear walls play a critical role in structural systems to ensure these localized forces are safely transferred or resisted.

An engineer should design these connections under these localized loads on shear walls (e.g. two way shear controls, localized internal moment strength controls etc.) and ensure that the out-of-plane beam connections are properly designed and detailed for adequate seismic resistance. This often requires, additional transverse & flexural reinforcement at connection areas or adding a column head at shear walls where very high loads are transferred to the shear walls.

8. 4. Effect of Constructive Non-Structural Beams Between R/C Columns or Shear Walls Under Earthquake

Industrial buildings generallly have high span / axes lengths and story heights. Therefore non-structural constrictive beams (stiffeners) are usually added to a building to provide additional support and stability to non-structural elements such as masonry walls and utility mechanical systems. However, during an earthquake, these members can have both positive and negative effects on the overall performance of the building structure.

Positive Effects:

- Increased lateral stiffness: As long as they are considered in the first design calculation step and detailed accordingly, the role of these members can be changed from non-structural stiffener beams to structural beams and provide additional lateral stiffness to a building, which can help reduce the building's displacement during an earthquake.
- Improved load distribution and overall performance: As long as they are considered in the first design calculation step and detailed accordingly, these stiffener beams can help distribute the seismic loads more evenly throughout the structure and improve the overall performance of the structure during an earthquake.
- Non-structural stiffener beams can help distribute the loads from non-structural elements to the structural members, which can reduce the damage to these non-structural elements. They can also help to reduce the forces of non-structural elements during an earthquake, which can prevent them from becoming dislodged or falling off.

Negative Effects:

- Non-structural stiffener beams can increase the overall stiffness of the building, which can lead to increased seismic forces on the structural members during an earthquake. This can result in higher stresses and deformations in the structural members, potentially leading to damage or collapse.
- Concentration of forces: In some cases, non-structural stiffener beams can concentrate forces on main structural elements of the structure and leading to localized damage.They can also create local stress concentrations and can cause additional structural irregularities that can affect the overall seismic performance of the building.

In general, the engineer should carefully design and provide detail about these non-structural stiffener beams to minimize their negative effects or maximize their positive effects during an earthquake. This can be achieved by either considering these members in structural calculations and designing accordingly or, classifying these members are non-structural and provide special details in order to not contribute their effect under seismic movements of the structure.

8. 5. Effect of Mechanically Connected Masonry Brick Walls in R/C Structures Under Earthquake

In industrial buildings, structures generally require wide openings due to maintenance and erection of big mechanical equipments. Therefore, it is possible to see high span / axes lengths and story heights in these type of structures. In order to cover the inner and outer part of these openings, there are several methods. Providing a non-structural masonry infill wall is one of the option. These infill walls are connected to the main structural member with mechanical connections.

These non-structural walls are designed only for archtitectural reasons. Therefore, at the design stage of the structural members effects of these walls are not considered. Therefore, during an earthquake, these members have some negative effects to the structure. These effects are as follows:

- These non-structural infill walls have an additional contribution to the lateral stiffness and energy dissipation of the building. Overall stiffness of the building can increase which causes an increase in the seismic forces on the structural members during an earthquake. Due to increased lateral stiffness irregularities such as "Soft Story" irregularity is encountered in the structure. Thus, due to increased stress and deformations, even the main structural member can be damaged.
- If the connections in between masonry infill wall and the main structural member are insufficient, the masonry wall will show a weak out-of-plane behaviour under earthquake loads. Such a situation will endanger both human life and the seismic performance of the building.

Below figures shows the poorly designed / constructed non-structural walls. As a result of the earthquake loads infill walls are collapsed and reinforced non-structural walls showed a weak contribution to the seismic performance of the building.

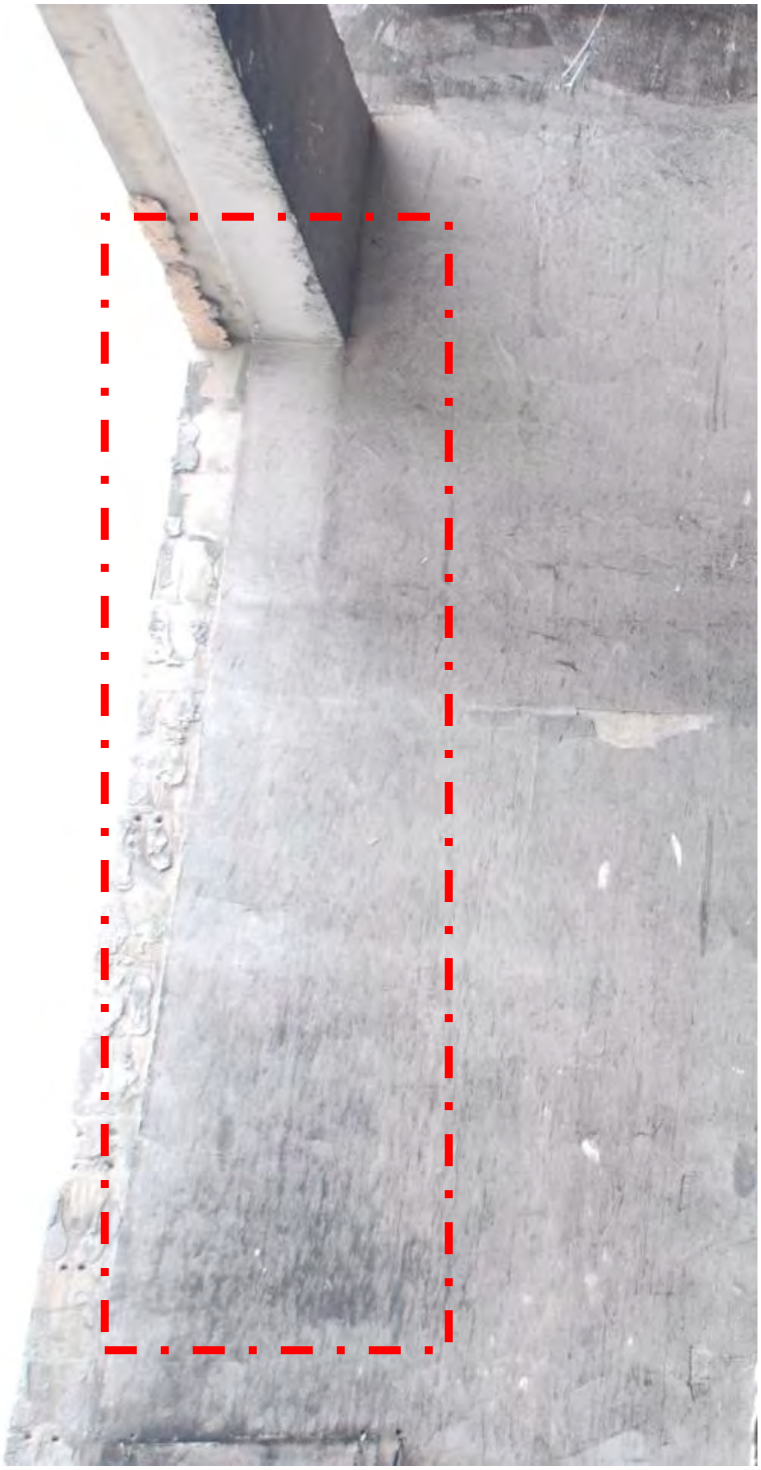

8. 6. Observed Damages at Dilatations Between Structures Under Earthquake

Dilatation gaps can be seen in such areas as given below,

- Structures which have irregular plan geometry,
- Structures with different mechanical purposes,
- Structures with different material / element compositions.

These structures can face with many different structural damages. Especially in R/C structures dilatation failures under earthquake loads could lead to irreversible damages. In order to minimize these damages, proper dilatation gaps are required in buildings in order to prevent plan irregularlirites on structural systems.

Dilatations are the gaps which are required in between two or more adjacent buildings as explained in above cases.

In case of poor engineering or construction, it is possible for buildings to clash under earthquake load at dilatation locations and cause greater damage with hammering effect.

As a result of this severe earthquake there are dilatation failures occured in the facility as shown in below figures:

As shown in photos above, two adjacent buildings touched each other as a result of the earthquake load. It shows the gap in between these two buildings is insufficient which causes sequential damages. It can be seen from first figure that the structure is seperated. However, in the second one which is an another view of the same structure, the structure touched due to the torsional effect.

Additionally, another improper case is the application of reinforced ground slab. In order to ensure the architectural integrity of these two buildings, contractor had poured the ground slab together for the two buildings. Thus, when the dilatation failure occured, there were cracks encountered on ground slab. In next photo, cracks on ground slab are shown.

Figures below show when the construction joint is not designed or constructed properly, such cracks occur due to displacement caused by earthquake.

8. 7. Spherical Storage Tanks and Bracing Behavior Under Earthquake

The spherical storage tanks are widely used to store LNG-LPG storage.

According to recent seismic design codes all over the world, the bracing member shall be designed under both compressive and tensile force. 'Tension member only' design is not suitable for these kinds of structures if the buckling of compressive members not acceptable. The figure below, basically represents the compressive and tensile forces on bracing members under horizontal loading.

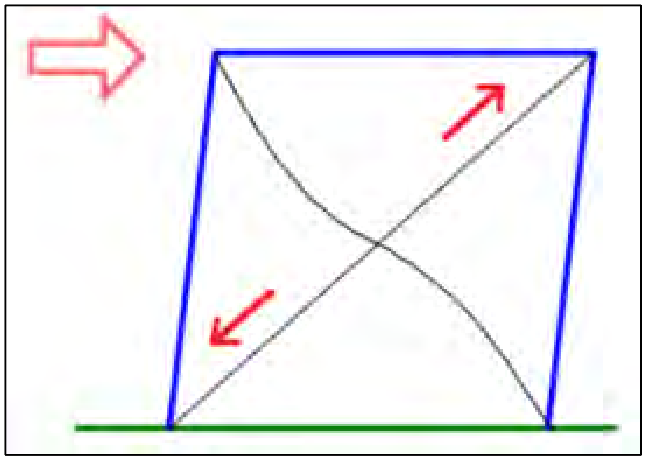

During the investigations after earthquake, the compression brace failures (buckling) are detected. Please see following figures for buckling cases.

The figure above clearly shows that the bracing members should be designed under both compressive and tensile force.

Another major issue about the braces is the unbraced lengths and out plane behavior of the members. As seen in the figures below, the intersection points of X bracing are free to displace in out of plane individually. This case is not an effective way for the buckling design of cross-section.

Two increase the buckling capacity of compressive members, additional connection plates shall be used in the mid portion of bracings.During earthquake, horrible sound was heart coming from the clash of the bracing members.

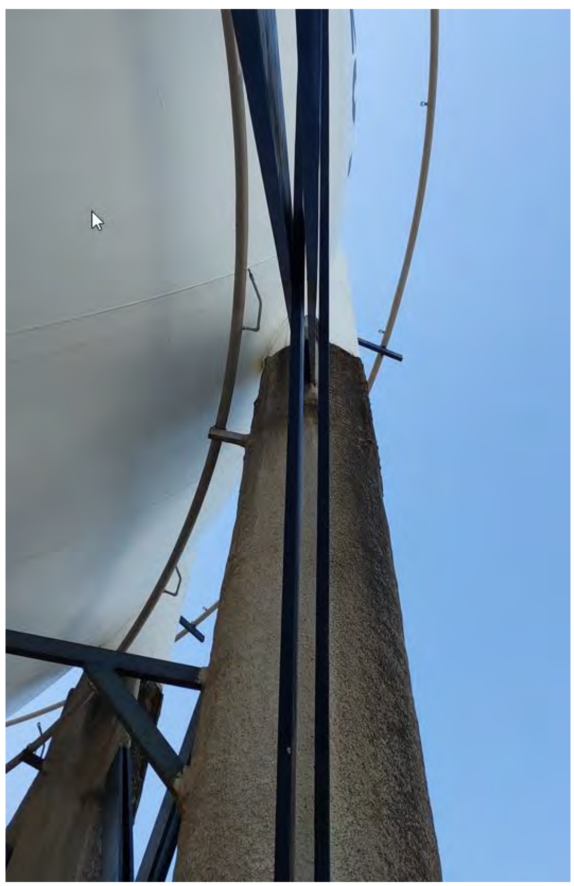

8. 8. Importance of Second Phase Concrete Pouring for Anchorage Lugs

For the pocket type of anchorage, the procedure is like followings:

- First phase concrete pouring
- Placing the anchorage in pockets
- Second phase concrete poring

Please see following figure for the arrangement of pocket type of anchorages.

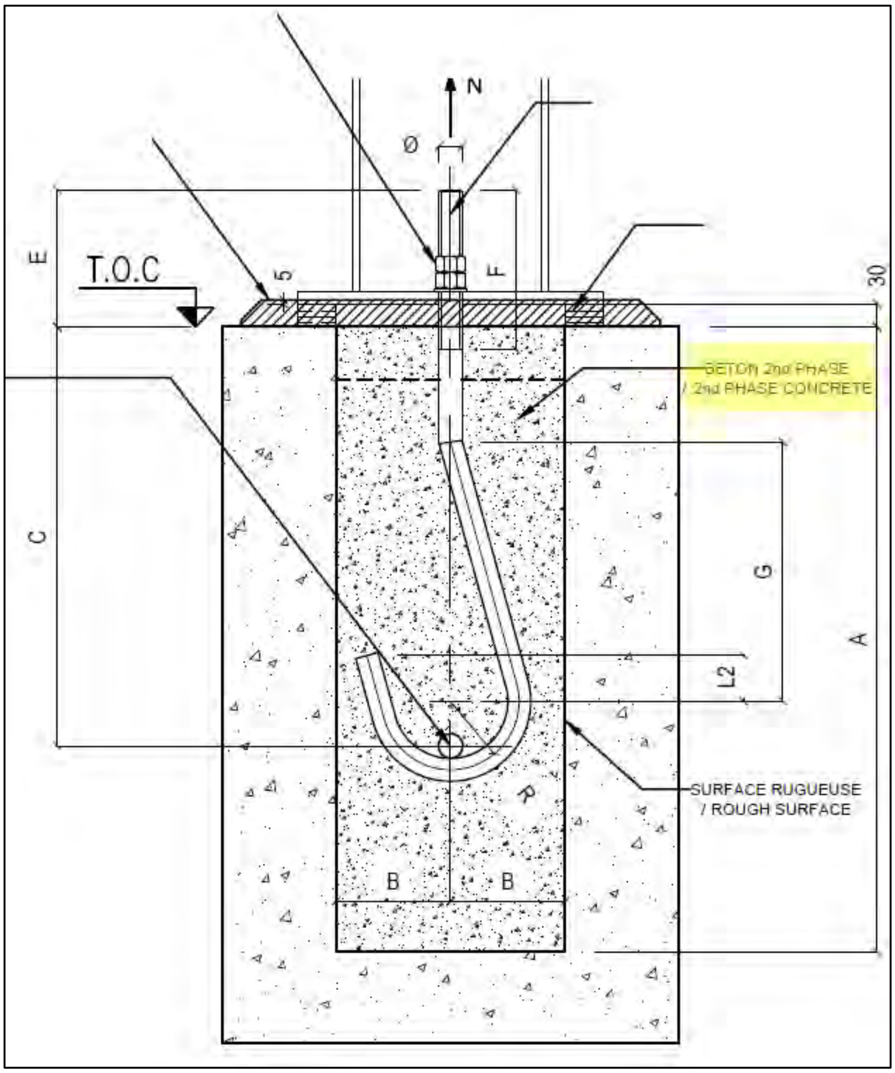

During the investigations after earthquake, a pocket is detected where the second pouring is missing. The columns base was free to move under horizontal load during earthquake. Please see following figures for empty pocket. The column deformed the concrete pier due to horizontal movement of steel column.

As a result, the second phase concrete pouring is very important for earthquake behavior of structure. The pocket shall be filled after the placing the anchorages.

8. 9. Conveyor Bridges Sliding Joint Effects Under Earthquake

The philosophy of the conveyor bridge design is represented below. The first part of the conveyor is connected on braced steel pier with axially sliding connection to reduce the effect of thermal effects. In this case the connection detail is designed to let the axial movement. The dimension of movement is determined by considering the seismic loads and thermal loads.

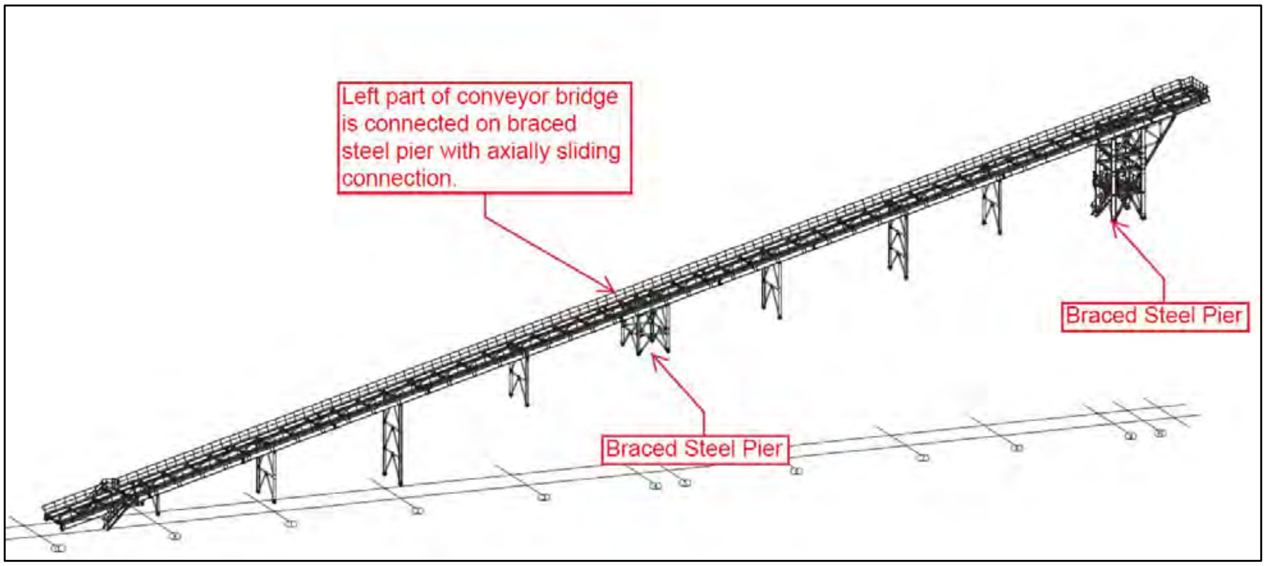

Please see following figure for the sliding connection detail. The movement space in this detail is calculated by considering the deflection of adjacent structures, like dilatation calculation. The free movement space is limited by stoppers.

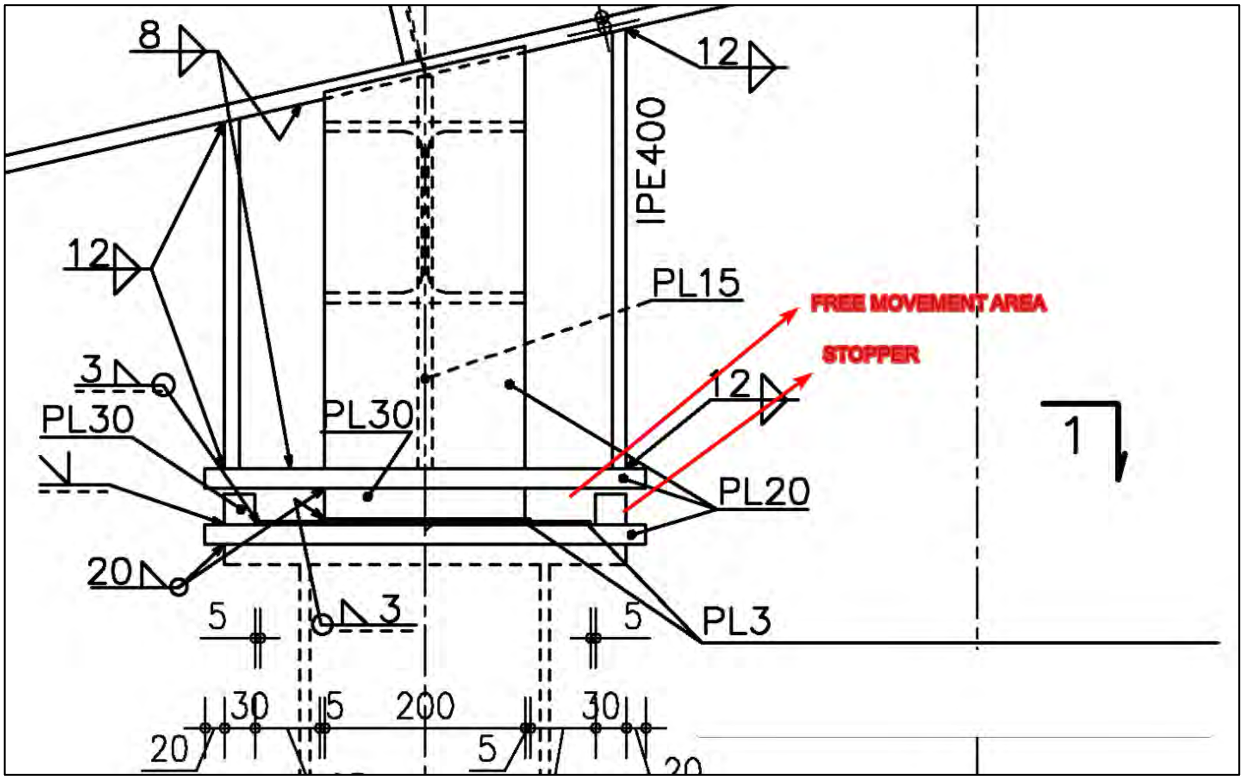
8
12
IPE400
12
PL15
FREE MOVEMENT AREA
STOPPER
3
12
PL30
PL30
1
PL20
20
5
3
5
PL3
30
5
200
30
20
5
20

However, during the investigations after earthquake, it is detected that the movement during earthquake is absolutely more than predicted, so the sliding connection dimension is not sufficient. There are several reasons for this issue, for example tilt of foundations, unexpected mechanism cases and plastic hinges. Please see following figures to see the insufficient sliding connection details after earthquake. The stoppers are clashed with members and deformation occurred.

8. 10. Soil Liquefaction and Jet-Grout Applications

Liquefaction is the loss of strength of water-saturated and not well-compacted cohesionless soils under an earthquake or similar cyclical dynamic load. The pore water pressure of cohesionless soils increases enough to lift the above during liquefaction. The soil loses its strength and induces large deformation and huge settlements. For this reason, liquefaction beneath buildings and other structures may cause significant damage during earthquakes. Water-saturated rivers, skirt and wind sediments, alluvial fans, alluvial plains, beaches, terraces, playa, and estuary sediments have high liquefaction vulnerability.

The jet grouting technique is a soil improvement method based on forming a rigid column by injecting a water-cement mixture into the soil under high pressure, with the soil by kneading, fragmentation, erosion, and penetration mechanisms. This technique is widely used all over the world against liquefaction risks. The injected water-cement mixture hydrates over time in the ground, creating a solidified mass of ground & cement. The immediate applicability of the method, being economical, and the possibility of working in narrow areas are considered the main advantages.

Unlike conventional grouting, the jet grouting method cuts the soil and thus can improve a broad spectrum of soil types regardless of the grain size of the soil. The expected results from the soil improvement made with the jet grouting method are mainly an increase in the improved soil strength and a decrease in permeability.

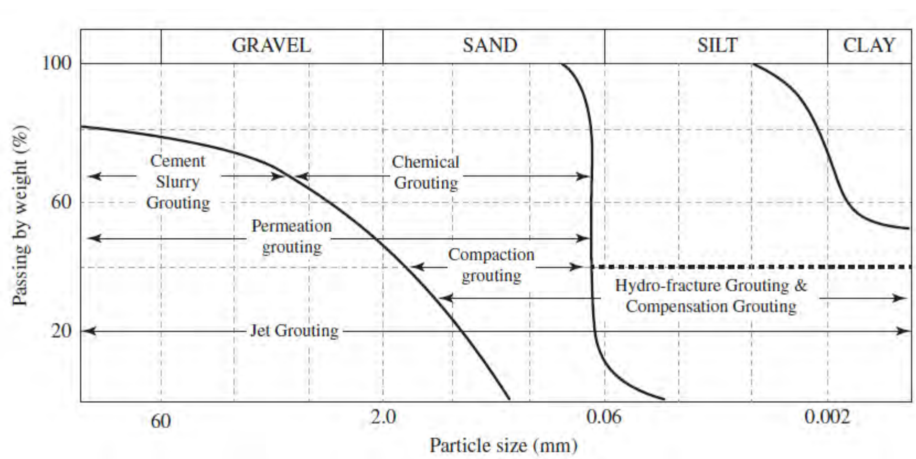

It was stated in research that in risky soils with liquefaction potential triggered during earthquakes, the excess pore water pressure increases during liquefaction and post-liquefaction deformations can be minimized with jet injection columns produced in densely liquefied soil layer thickness.

It is determined by a investigation team in an industrial project on-site that the areas with jet grout retrofitted soil parts showed excellent protection against earthquakes during the 6 February Pazarcık and Elbistan earthquakes.

As can be seen from the photographs given below, a liquefaction area formed in the area where the spherical tanks were located during the earthquake and this liquefaction continued along the line and progressed along the facility. During this progress, the liquefaction zone continued around the spherical tank area due to the jet grout improvement made at the location of the spherical tanks. This determined situation shows how successful the jet grout soil improvement method is against soil liquefaction. The jet grout application stands out as a proven ground improvement method for areas with such liquefaction risk.

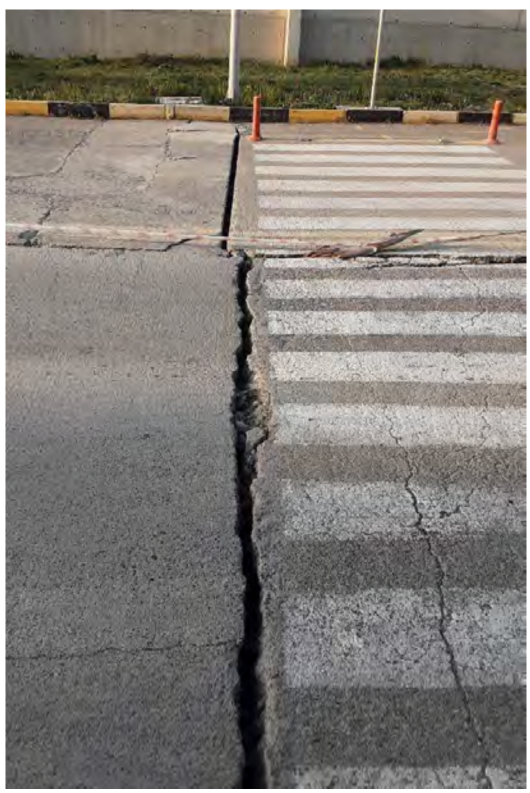

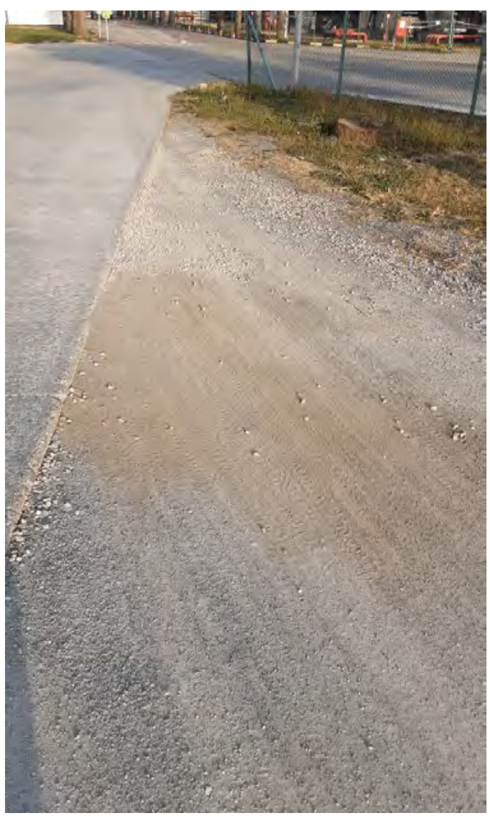

Chapter 9. Performance of Bridges and Tunnels

By:
Alp Caner[(a)], Kemal Önder Çetin[(a)], Candan Gökçeoğlu[(b)]

[(a)] Middle East Technical University, Civil Engineering Department, Ankara, Türkiye
[(b)] Hacettepe University, Geological Engineering Department, Ankara, Türkiye

9. 1. Bridge and Tunnel Condition Assessment

In the successive major earthquakes, no collapse or loss of lives was observed or reported associated with poor bridge and tunnel performances. In the disaster region, there are more than 1000 bridges. Only 15 bridges were affected by these events, and about 50% were opened to traffic within a day after the shakings. One railway tunnel, near Ozan village, Gölbaşı was severely damaged by the earthquakes. This tunnel was constructed in the 1940s, and it is a stone-lining tunnel. Except this tunnel, the remaining tunnels performed well with some minor damages. Linings experienced some concrete spalling, and some minor portal damages were observed.

More specifically, no serious damages were observed in the tunnels constructed in the last three decades. The Nurdağı Portal of the Bahçe-Nurdağı Tunnel twin tunnels, the longest railway tunnels of Türkiye with a length of approximately 10 km, is near the active fault. The portals and the segments experienced no damage. However, some rockfalls were observed in the Nurdağı Portal of this tunnel. Additionally, the Tarsus-Gaziantep Motorway Tunnels between Bahçe and Nurdağı showed a good performance. Visible signs of damage were not observed, and they were open to traffic. It can always be expected that damaged structures in the region may collapse under subsequent earthquakes in the future. For example, it has been observed several times that some of the damaged structures after the first earthquake collapsed in the second earthquake.
The typical observed engineering problems are:

- Bearing and joints movements
- Expansion joint movements
- Abutment approach fill settlement
- Pounding at expansion joints
- Shear key damage
- Soil liquefaction
- Column concrete spalling and start of plastic hinges.

Examples of bridges and tunnels can be seen in the following figures.

Figure 9.1. Abutment rotation due to seismic soil liquefaction induced foundation failure

Figure 9.2. Joint movements

Figure 9.3. Concrete spalling

Figure 9.4. Bearing dislocation and movement

Figure 9.5. Rail misalignment

Figure 9.6. Shear key damage

Figure 9.7. Abutment wall concrete spalling

Figure 9.8. Bridge typical have no damage

Figure 9.9. Tunnel portal movement and concrete spalling

Figure 9.10. Nurdağı portal of Bahçe-Nurdağı railway tunnels

Chapter 10. Preliminary Reconnaissance Observations on Lifelines After 6 February 2023 Earthquakes in Türkiye

By:

Nejan Huvaj[a], Volkan Kalpakcı[b], Şevki Öztürk[c], Tamer Y. Duman[d], Eray Baran[a], Burak Talha Kılıç[a], Ali Serdar Uysal[d], Suat Dalkılıç[e], Emre Dalkılıç[e], Onur Pekcan[a]

(a) Middle East Technical University, Civil Engineering Department, Ankara, Türkiye
(b) GEOCE, Ankara, Türkiye
(c) Çankaya University, Civil Engineering Department, Ankara, Türkiye
(d) Fugro Sial, Ankara, Türkiye
(e) EMAD Enerji Harita, Ankara, Türkiye

10. 1. Introduction

Lifelines provide flow of resources and services that sustain communities, and they are typically composed of linear, connected networks such as transportation corridors (highways, roads, railways, tunnels), water distribution pipelines, electric power transmission systems, gas and liquid fuel, communication networks/systems as well as other critical infrastructure such as airports, ports, and harbors. Lifeline systems have different, and perhaps more complex, vulnerabilities to earthquakes as compared to individual buildings and industrial structures. Disruptions in lifelines can lead to regional, national social, and economic impacts. Lifelines are constructed over broad geographical areas, and they are interdependent, i.e., the disruption of one lifeline system may affect the performance of another. For example, water pumping stations or equipment control in liquid fuel and natural gas pipeline systems may use the energy provided by electric power networks. When multiple different lifelines gather or pass through the same area, all are vulnerable to disruption from a single cause, such as an earthquake.

In this section, we briefly describe the preliminary observations on the performance of lifeline system infrastructure in the region after the 6 February 2023 earthquakes in Türkiye. The preliminary fieldwork was conducted on 10-12 February 2023 (during 13-14 February 2023 some members of the team continued the field survey) in Kahramanmaraş and Gaziantep by a team composed of Nejan Huvaj, Volkan Kalpakcı, Şevki Öztürk, Eray Baran, Tamer Y. Duman, Burak Talha Kılıç, Ali Serdar Uysal, Suat Dalkılıç, and Emre Dalkılıç. We would like to acknowledge the funding provided for the fieldwork by The Scientific and Technological Research Institution of Türkiye (TÜBİTAK) "1002-C Natural Disasters-Focused Fieldwork Emergency Support Program (Doğal Afetler Odaklı Saha Çalışması Acil Destek Programı)". The preliminary objective of the reconnaissance efforts was to document the effects of the earthquakes on lifelines including the performances of railway systems, highways, water, and gas pipelines as well as electric transmission systems, and to collect and document perishable data.

10. 2. Brief Information about the Critical Infrastructure in The Region

The lifelines in the study area support eleven cities with a total population of 14,013,196 people, constituting 16.4% of the 2022 population of Türkiye, which is 85,279,553 (data from Turkish Statistical Institute, https://data.tuik.gov.tr/Bulten/Index?p=Adrese-Dayali-Nufus-Kayit-Sistemi-

Sonuclari-2022-49685, accessed on 17.02.2023). Some of the biggest cities (in terms of their 2022 population) that are significantly impacted by the earthquakes in the region are: Adana 2,274,106 population; Gaziantep 2,154,051; Hatay 1,686,043, Kahramanmaraş 1,177,436; Adıyaman 635,169; Malatya 812,580.

In order to demonstrate the size and distribution of the lifeline networks in the region, few examples of critical infrastructure maps (highways and railways) are provided (Figure 10.1). State Highway Agency, KGM, and State Railway Agency (TCDD) are the national authorities responsible for highways and railways, respectively. These maps, when considered together with their proximity to the epicenters of both earthquakes (approximately placed as star symbols in Figure 10.1), as well as the active fault lines in the region, can help visualize the scale of the possible impact on the lifelines over a large geographic area.

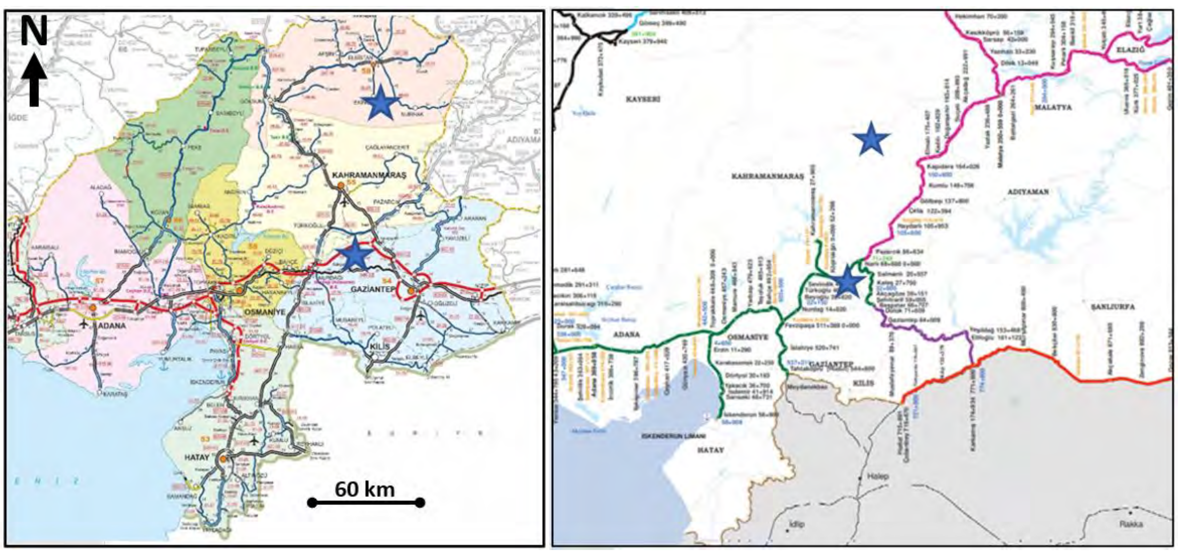

(a) (b)

Figure 10.1. a) Parts of the state highway network in the region (source: State Highway Agency, KGM website, https://www.kgm.gov.tr/SiteCollectionImages/KGMimages/Haritalar/b5.jpg), b) Parts of the state railway network in the region (source: Turkish State Railway Agency website: https://static.tcdd.gov.tr/webfiles/userfiles/files/genel/tcddharita.pdf)

As for the state of damage and serviceability of the airports, railways and roads as well as gas and electricity services in the region after the two earthquakes, the information from National Disaster Agency (AFAD), provided on 06.02.2023, at 15:35 local time (few hours after the 2nd earthquake), published at The Press Bulletin No. 6 (https://www.afad.gov.tr/Kahramanmaraş -pazarcikta-meydana-gelen-deprem-hk-basin-bulteni6) noted that Kahramanmaraş, Gaziantep, Hatay airports were closed to operation due to damages caused by the earthquakes and electricity could not be provided to 27 communities/neighborhoods in the region (including Kahramanmaraş city, Osmaniye Bahçe-Düziçi, and some parts of Malatya city) due to earthquake-caused damages. Emergency repair works were carried out and alternative electricity resources were put into service and electricity was provided to Kahramanmaraş city within twenty-four hours after the 1st earthquake. As time went by, further checks were carried out by relevant state and local agencies and updates were given by AFAD on the state of lifelines. Information from National Disaster Agency (AFAD), on 07.02.2023, at 12:10 local time, published at The Press Bulletin No.10 of AFAD (https://www.afad.gov.tr/Kahramanmaraş -pazarcikta-meydana-gelen-deprem-hk-basin-bulteni10) noted that Kahramanmaraş and Hatay airports were closed to service due to damages caused by the earthquakes; Gaziantep and Şanlıurfa airports were open to aid flights; and Malatya, Adana, Diyarbakır, Adıyaman airports were open to service. Railway service through Fevzipaşa-Narlı, Narlı-Gaziantep, Narlı-Malatya railway lines were closed to service; Malatya-Çetinkaya, Malatya-Yolçatı railway lines were open to emergency use, and Ulukışla-Adana, Adana-Mersin, Adana-Toprakkale, Yolçatı-Diyarbakır, Yolçatı-Elazığ, Elazığ-Tatvan railway lines were open to rail traffic. In terms of roads, Adıyaman-Çelikhan road, Osmaniye-Gaziantep direction, Hatay-Reyhanlı state highway, Hatay Kırıkhan-Topboğaz roads were closed to traffic; Adıyaman-Çelikhan-Sürgü Road Balık Burnu bridge has collapsed; Adıyaman Gölbaşı-Malatya Sürgü road was closed due to landslides and Şanlıurfa-Gaziantep Road was open to traffic. Soon after, emergency repair and recovery operations were carried out by all relevant state agencies.

BOTAŞ Petroleum Pipeline Corporation is the state-owned crude oil and natural gas pipelines and trading company in Türkiye, which provides natural gas service in the region. TEİAŞ, Turkish Electricity Transmission Corporation, a government-owned corporation, is the transmission system operator for electricity in Türkiye. According to the State National Television TRT's press quotes of the Ministry of Energy and Natural Resources of Türkiye, Mr. Fatih Dönmez, published on 06.02.2023, there were some damages and disruptions in the electricity and natural gas infrastructure on the day of the earthquakes (https://www.trthaber.com/haber/gundem/bakan-donmez-deprem-bolgesinde-enerji-hatlarinda-hasarlar-var-743813.html, accessed on 17.02.2023), however, immediate repair efforts and utilization of alternative solutions helped a quick recovery in the infrastructure system. For example, electricity was brought to the city of Kahramanmaraş within 24 hours of the first earthquake.

One of the significant damages was observed in the main natural gas transmission line, in Türkoğlu county, which is located near the epicenter of the one of the earthquakes, and serves the cities of Kahramanmaraş, Gaziantep, Hatay according to the Ministry of Energy's TRT news quote. According to the Information Note released by BOTAŞ, the gas supply was remotely cut-off right after the earthquakes. Critical facilities in the region were immediately supplied with CNG and LNG while repair works were ongoing. According to the press quotes of the Ministry of Energy and Natural Resources of Türkiye published on 11.02.2023, this natural gas transmission line was repaired and put back into service on 11.02.2023 (https://www.dunya.com/gundem/bakan-donmez-acikladi-deprem-bolgesindeki-evlere-elektrik-verilecek-mi-haberi-685515, accessed on 17.02.2023). However, in areas where building damages were significant, gas supply is not connected to buildings unless the building safety level and the safety of the gas transmission system are confirmed. Finally, as part of precautionary measures, controls on the pipelines designed according to ASME Standart B31.8 continue uninterruptedly in the fault approach regions or inevitable crossings due to the faults.

10. 3. Field Observations on Lifelines

The region has been particularly affected by ground rupturing (left-lateral slip motion) of the faults and intense seismic shaking, demonstrated by typically observed damages such as:

- Surface fault rupture-induced deformations, offset, buckling, uplift and subsidence on asphalt roads, highways, railway tracks as well as on unpaved roads and farmlands.
- Landslides and rockfalls triggered by the earthquakes disrupting the road and railway networks.
- Ground deformation-triggered damage and partial disruption of the water pipeline systems
- Cracks, tilt, lateral displacement, and damages on retaining walls.
- Damages caused by ground deformations on airport pavements and access roads.
- Tilt and damages on electric poles, buried utilities, broken underground pipelines.

Examples of such damages can be seen in the following figures.

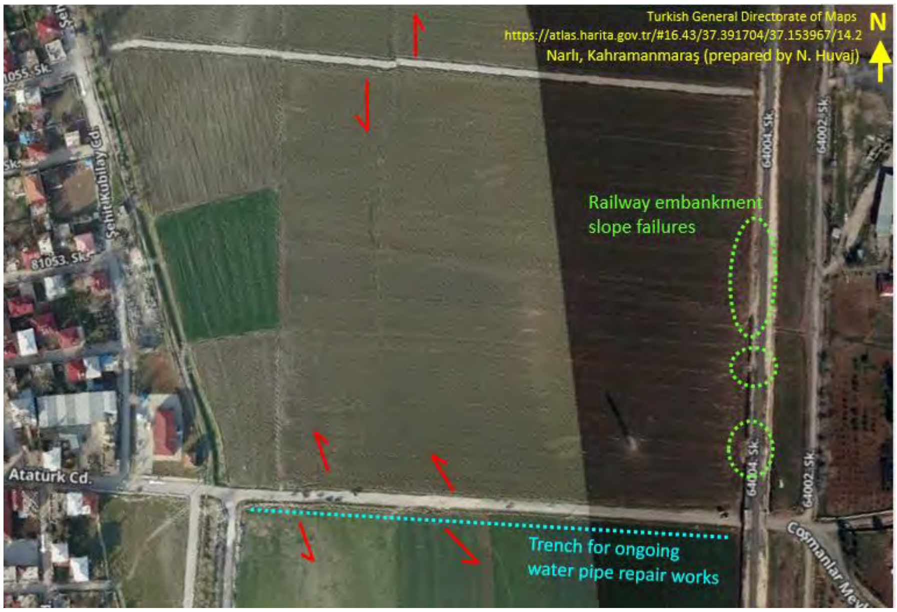

Figure 10.2. Aerial view of the surface fault rupture and examples of damages caused by the two earthquakes on some of the lifelines: railway line, roads and water distribution network, near Narlı, Kahramanmaraş (Satellite images are provided by Turkish General Directorate of Maps via atlas.harita.gov.tr website)

Figure 10.3. Referring to Figure 10.2 for locations of the photos: offset on the road due to surface fault rupture, railway embankment slope instability, water pipeline repair works, and a tilted electric pole can be seen, near Narlı, Kahramanmaraş. (Active fault data is taken from Emre et al. (2013) published by the General Directorate of Mineral Research and Exploration, MTA (Maden Tetkik ve Arama Genel Müdürlüğü)).

Figure 10.4. Surface rupture, offset, cracks and damages on railway tracks and roads, as well as a damaged electric tower, near the surface rupture (Narlı, Kahramanmaraş). (Active fault data is taken from Emre et al. (2013)).

Figure 10.5. A landslide and crack/damages on the road next to a water canal, causing significant lateral displacement of a concrete retaining wall (pushed towards the water canal), a tilt on an electric pole, in southern part of the city of Kahramanmaraş (active fault data from Emre et al. (2013)).

Figure 10.6. Surface rupture observations causing a 3.6 m offset on Gaziantep-Kahramanmaraş Road, cracks on the asphalt road at several locations, road embankment instability and more than 250 m-long longitudinal cracks at the top of the road embankment as well as on the asphalt road, near Kapıçam, Kahramanmaraş (Satellite images are provided by Turkish General Directorate of Maps via atlas.harita.gov.tr website)

Figure 10.7. Referring to Figure 10.6 for the location: surface rupture observations and 3.6 m offset on Gaziantep-Kahramanmaraş Road (active fault data from Emre et al. (2013)).

Figure 10.8. Landslides and surface cracks on the roads, near Kartal and Yarbaşı, Kahramanmaraş (Active fault data from Emre et al. (2013)).

Figure 10.9. Landslides, rockfalls and surface cracks on the roads, near Fevzipaşa, Gaziantep causing disruption in the service (Active fault data from Emre et al. (2013)).

Acknowledgments

We would like to acknowledge the funding provided for the fieldwork by The Scientific and Technological Research Institution of Turkey (TÜBİTAK) “1002-C Natural Disasters-Focused Fieldwork Emergency Support Program (Doğal Afetler Odaklı Saha Çalışması Acil Destek Programı)”.

References

Emre, Ö., Duman, T.Y., Özalp, S., Elmacı, H., Olgun, Ş. ve Şaroğlu, F., 2013, Açıklamalı Türkiye Diri Fay Haritası. Ölçek 1:1.250.000, Maden Tetkik ve Arama Genel Müdürlüğü, Özel Yayın Serisi-30, Ankara-Türkiye. ISBN: 978-605-5310-56-1), published by the General Directorate of Mineral Research and Exploration, MTA (Maden Tetkik ve Arama Genel Müdürlüğü)).

ASME Standart B31.8 (Gas Transmission and Distribution Piping Systems)

Chapter 11. Preliminary Structural Performance Summary of Historic Structures

By:

Ahmet Türer [a]

[a] Middle East Technical University (METU, Ankara)

11. 1. Introduction

Structural evaluation of historic structures which are part of architectural heritage in Türkiye is important with regards to i) restoration maintenance related issues from conservation of architectural heritage point of view and ii) earthquake performance of historic masonry structures as a part of civil engineering practice. A site visit to Malatya and Elazığ cities was carried out as a team effort together with T.R. Directorate General of Foundations - Republic of Türkiye Ministry of Culture and Tourism. Some of the mosques and mausoleums were visited after the earthquake; this chapter summarizes the preliminary performance evaluation of visited sites (historic mosques, minarets, and mausoleums) as well as gathered information on Gaziantep Castle and a church performance from Hatay.

11. 2. Visual Inspection of the Historic Structures

Southeastern Türkiye has a rich cultural heritage structure stock that are in the form of houses, bridges, earliest churches, synagogues, mosques, castles, and listed UNESCO World Heritage Sites (Figure 11.1)[5]. The eleven cities that are affected by the recent earthquakes (Figure 11.2)[6] are listed as Kahramanmaraş (520), Gaziantep (906), Malatya (685), Diyarbakır (1113), Kilis (420), Şanlıurfa (1764), Adıyaman (144), Hatay (1099), Osmaniye (161), Adana (874), Elazığ (301) [7] and contains about 8 thousand registered cultural heritage. Malatya and Elazığ cities were selected for evaluation of historic structures since cities closer to the epicenter were more difficult to access since the survivor rescue missions were given the priority. About a dozen structures in Malatya and about 20 sites in Elazığ were visually investigated on site. Additional few historic structures were also evaluated based on visual information obtained from the internet using satellite imaging and photos on the news. These are the Gaziantep Castle, Antakya Rum Orthodox Church, and Antakya Protestant Church. Damage patterns are investigated and briefly reported.

[5] https://globalheritagefund.org/places/mena/
[6] https://www.google.com/maps/@37.4892096,35.1985455,7z/data=!4m2!21m1!1s%2Fg%2F11shww_tpt
[7] Republic of Türkiye Ministry of Culture and Tourism data, gathered by Assoc. Prof. Dr. Nurdan Kuban, Kocaeli Univ.

Figure 11.1. World heritage sites in and around Türkiye

Figure 11.2. Cities affected by the Kahramanmaraş Earthquakes including Malatya and Elazığ.

The first earthquake's epicenter distance to Malatya and Elazığ cities is about 165 km and 250 km, respectively; while the second earthquake epicenter to Malatya and Elazığ are about 100 km and 190 km, respectively (Figure 11.3) and has been more damaging for these two cities than the first one. Malatya being about half distance closer to both earthquakes with respect to Elazığ, the damage is expected to be larger in Malatya. Most devastating damage was observed at central Malatya, a relatively large mosque with the name Yeni Cami (new mosque, about 100 years old) suffered significant damage and major collapse. Before and after earthquake pictures (Figure 11.4) of Yeni Cami show the level of damage, which raised concerns since the mosque was recently renovated and strengthened. Although a thorough investigation is necessary before any conclusions can be drawn, the collapsed newly added buttress and insufficient anchorage to the existing walls seems to be one of the factors that went wrong.

Other historic structures in Malatya region were investigated in the Eski (old) Malatya part of the city, which resided most of the historic structures. About 12 mosques and mausoleums were observed in this area with minor to medium damage, but total collapse was not observed. The common damage and failure types may be listed as:

a) Minaret top cracked and slightly moved,
b) Minaret body had a horizontal crack towards the bottom but remained in position,
c) Perpendicular wall connection had a slight crack which is minor and may be fixed with paint,
d) Vaults were cracked at the top crest indicating compression levels exceeding material capacity,
e) Some newly constructed buttresses failed because of insufficient anchorage length and lack of interlocking between wall and buttress stones.

In addition to these mentioned damage mechanisms, some of the walls have been noticed to crack diagonally and compression failure by dislocated stones and cracking at the mortar level were observed. However, only one mosque had total collapse (relatively new and stone masonry), but older historic structures have proved to be worthy to survive centuries and still in good condition.

The historic structures in Elazığ region showed lesser amount of structural damage from the recent earthquakes. Minor cracking (if any) in the historic masonry mosques and masonry buildings such as hamam (Turkish bath) indicated that the buildings remained in linear elastic range. If properly maintained and water damage is prevented, the historic structures have proven themselves to survive centuries without any significant earthquake damage. It was observed that tension rods were added in some of the smaller mosques at the arch level and may have some positive impact on the overall earthquake performance of masonry buildings, which are sturdy in general with relatively small rooms and thick walls. Two reinforced concrete mosques in Elazığ city had minor cracks in the 2020 Elazığ Earthquake and the same cracks remained intact with small amount of cement dust on the carpets but no major or minor damage. Corners of the mosques that suffered humidity from the roof had also some flakes on the ground, which was told to be a regular cleaning task with or without earthquakes.

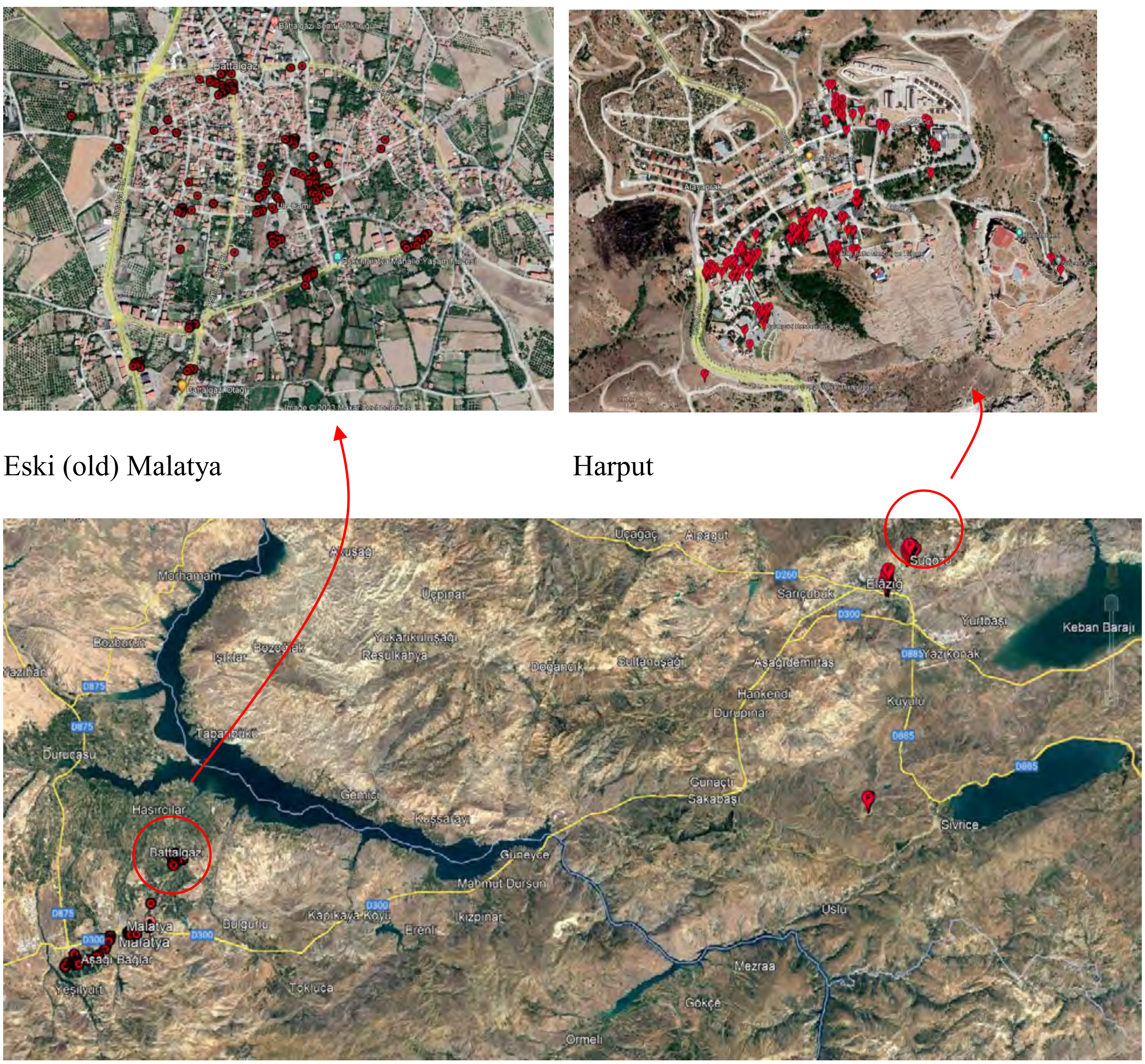

Figure 11.3. Geographic location of the historic structures evaluated in Malatya and Elazığ.

Figure 11.4. Yeni Cami (new mosque) before and after pictures and short anchorage.

An important historic heritage located in southeastern Türkiye is Gaziantep Castle (Figure 11.5). Unfortunately, Gaziantep to the epicenter of the first earthquake is only about 32 km and the second earthquake is about 115 km distance. The orientation of the castle walls to the earthquake epicenter may be the reason of south-west castle walls to suffer the largest damage when the first impact must have pushed these walls and sending wall stones towards the slope towards the city. It is fortunate that the castle wall stones did not cause major damage to people, houses, businesses at the skirts of the castle. The castle being located at the top of a hill may also had lens action amplifying the pga and damaging effects of the earthquakes.

Figure 11.5. Gaziantep Castle before and after the earthquakes.

Last examples of historic structures were selected from Hatay region. The Antakya Rum Orthodox Church (Antioch Greek Orthodox Church) and Antakya Protestant Church are located very close to each other within 150 meters, and both suffered significant damage during the earthquakes. The distances between the churches and the first and second earthquakes are about 135 km and 225 km respectively. Satellite images before and after the earthquakes (Figure 11.6) [8] indicate that both structures suffered immense damage. The after-earthquake picture of the Antakya Rum Orthodox Church (Figure 11.7) shows total roof collapse while only west wall and partial south cylindrical walls are standing. The collapsed picture of the Antakya Rum Orthodox Church also shows roof collapse with probably south wall collapse. The epicenter to the historic structures' distances are comparable between Malatya and Hatay, both cities with significant damage to their historic buildings. Majority of the mosques showed acceptable performance in Malatya (exception of Yeni Cami) while both studied churches suffered major damage in Hatay.

The level of damage to historic structures depends on many parameters other than the distance to the epicenter as many times discussed here. Some of the other significant parameters controlling damage to historic structures may be listed as a) poor ground conditions, groundwater level, soil-structure interaction, foundation type and properties, earlier relative settlement of the structure, tilt of columns and walls, b) presence of tension-shear elements such as wooden lintels inside and corner of the walls and tension rings around the domes, c) discontinuous (before the edge wall) arches and vaults, d) buttresses that are not fully integrated with the wall, e) poor or weakened material and workmanship quality, frequency of maintenance of the structure and water damage – excessive moisture, f) interlocking mesh at walls connections and free (unsupported out of plane) spacing between orthogonal walls, g) past war, earthquakes damages; quality of repair and restorations; adding or removing sections from the walls, h) the symmetry of the building, i) the minaret being inside the wall or independent of the building, j) the bell towers and minarets being too slender and the whipping effect for the bell and minaret balcony, k) the presence of tension rods on the arches and vaults, their quality to column and wall connection, l) slenderness of walls and columns, m) spacing and dimensions of window and door openings in walls, minarets, and domes, n) ratio of wall thickness to height and unsupported length perpendicular to the plane, o)

[8] Google Earth images.

dimensions of cut stone, quality of rubble masonry, p) the match between the earthquake response spectrum and the natural modal frequencies of the structure, q) the earthquake magnitude, the distance to the earthquake epicenter, the movement type of the fault, the presence of mountains that will reflect earthquake waves, r) the presence and quality (rusting and expansion) of horizontal and vertical locking metal braces between stones, s) the stair overlap ratios and the number of overlaps in a minaret, t) vertical joints between stones in a wall being aligned (not staggered), u) vandalism and treasure hunting etc should be mentioned. Existing historical building performance and damage observations have been made in the form of rapid preliminary assessment. Some of the structures that require a comprehensive examination must be re-evaluated with a closer and more detailed look considering most of the items listed above.

Acknowledgements

The author acknowledges kind help and collaboration received from the T.R. Directorate General of Foundations - Republic of Türkiye Ministry of Culture and Tourism regarding this work.

Figure 11.6. The Antakya Rum Orthodox and Protestant Churches Before and After Earthquakes

Figure 11.7. The Antakya Rum Orthodox Church after the earthquake [9]

Figure 11.8. The Antakya Rum Protestant Church after the earthquake [10]

---

[9] https://www.ntv.com.tr/galeri/turkiye/deprem-antakyadaki-tarihi-kiliseleri-yikti,MFWsAiJ73UqDkzS2avW3_A/XTLZYWkAQkKjGWjO0SLVCw
[10] https://haberortakoy.com/deprem-antakyadaki-tarihi-kiliseleri-yikti/

Chapter 12. Coastal Structures in the Gulf of Iskenderun and Tsunami in the Eastern Mediterranean

By:

Ahmet Cevdet Yalciner[a], Gozde Guney Dogan[a], Isikhan Guler[a], Bilge Karakutuk[a], Furkan Demir[a], Didem Cambaz[b], Vassilios Skanavis[c], Costas Synolakis[c,d]

[a] Middle East Technical University, Department of Civil Engineering, Ocean Engineering Research Center, Turkiye
[b] Bogazici University, Kandilli Observatory and Earthquake Research Insitute, Turkiye
[c] Academy of Athens, Greece
[d] University of Southern California, USA and Academy of Athens, Greece

12. 1. Coastal Structures in The Gulf of Iskenderun and Tsunami in the Eastern Mediterranean

A strong earthquake (M_W=7.7) of strike-slip faulting with epicenter (37.1123N, 37.1195E) at a shallow depth striking about NE-SW on the East Anatolian fault zone occurred on 06th February 2023 (01:17 UTC) in Pazarcik, Kahramanmaras (southeastern Türkiye). As one of the UNESCO IOC NEAMTWS (UNESCO, Intergovernmental Oceanographic Commission, Northeast Atlantic, Mediterranean and the connected seas Tsunami Warning System) Tsunami Service Provider, Bogazici University Kandilli Observatory and Earthquake Research Institute (KOERI) issued four tsunami messages according to the decision matrix based on earthquake magnitude, with a tsunami warning 15 min (after the earthquake) with expected tsunami amplitudes above 0.5 m along the southern coast of Türkiye. Although the epicenter is ~90 km inland, the earthquake generated a tsunami, which is measured at four tide gauge stations, (Iskenderun-Arsuz, Erdemli, Gazimagusa (Famagusta), and Girne (Kerinya) in the Eastern Mediterranean. The recorded water motions have been analyzed after detiding to distinguish the arrival time of the wave and the profile of the water level fluctuations. The tide gauge record in Arsuz shows a ~14 cm positive and ~10 cm negative tsunami amplitude with approximately a 10 min wave period. The arrival times of the first and maximum waves are around 25 min and 33 min after the earthquake, respectively. The first wave arrivals are around 36 min at Gazimagusa(Famagusta) and 48 min at Erdemli and Girne(Kerinya) stations. The maximum tsunami amplitudes were measured as 13 cm at Erdemli (54 min), and 17 cm at Gazimagusa (Famagusta) (65 min).

Although the tsunami event is small-scale, scientific investigation and understanding the source location and the generation mechanism are important for possible future tsunami events and preparedness. The tsunami has also been a test for the effective working and communication of the early warning system in the area. For the assessment of the 06 February 2023 small amplitude tsunami, numerical simulations are performed using the tsunami numerical model NAMI DANCE. For topography and bathymetry EMODnet (https://emodnet.ec.europa.eu/en/bathymetry, ~105 m resolution) and ASTER (https://asterweb.jpl.nasa.gov/gdem.asp, ~30 m resolution) data are used. The modeling database is established as a 100 m grid size covering the Eastern Mediterranean. The arrival times of the waves at the four tide gauges indicate a possible tsunami origin North of Samandag near Kale cape with a source of bipolar elliptical subsidence and uplift shape (Figure

1.1a). Mass movements are possible atypical (nonseismic) tsunami sources but those hypotheses regarding this event definitely need more data and further analysis. The distribution of the maximum water elevations computed by 120-minute simulations of the possible source considered in the North of Cevlik is given in Figure 12.1b.

The 06 February 2023 tsunami needs to be well understood in terms of the source areas and generation mechanisms. A field survey is performed on 11-13 February 2023 to investigate the tsunami traces, conduct eyewitness interviews, identify the types and locations of the possible sources, and investigate the damage to the coastal structures. The field survey covered the coast of the Gulf of Iskenderun from Karatas (West) to Samandag-Cevlik (East).

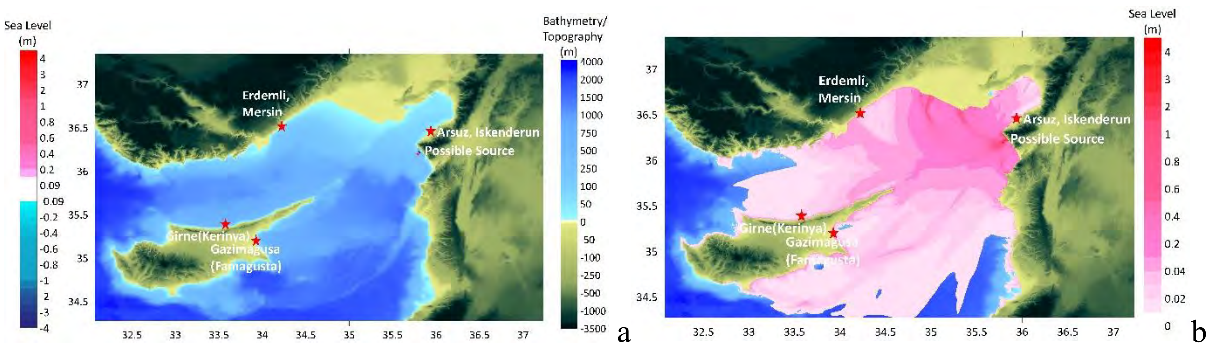

Figure 12.1. a) The location of the possible source of small amplitude tsunami and the tide gauge stations, and b) distribution of maximum water elevations computed from the possible source, North of Cevlik

Simulations are performed using the survey findings and the numerical results are compared with the tide gauge measurements. Sample figures showing the tsunami wave propagation at different times after the earthquake are shown in Figure 12.2.

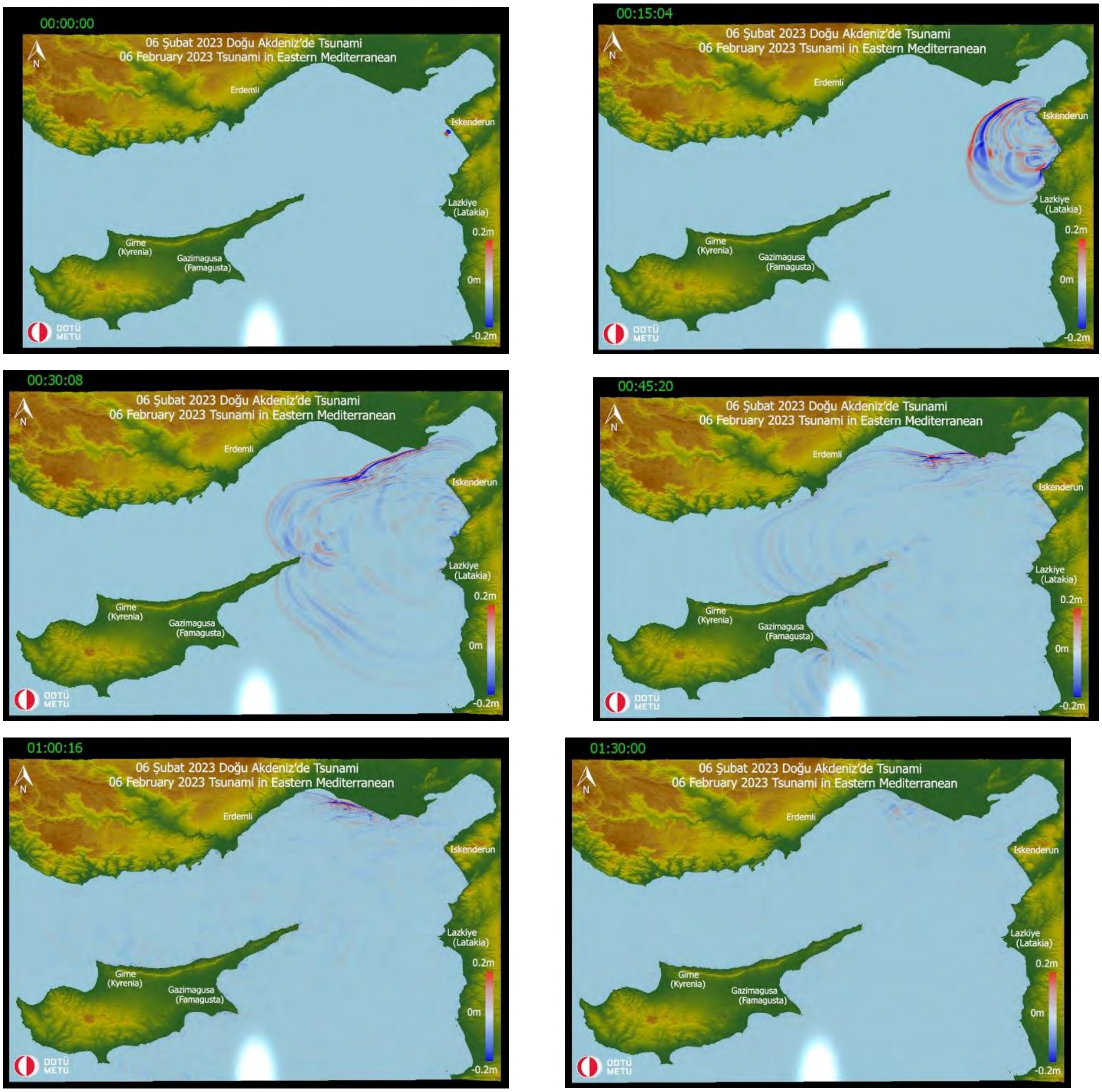

Figure 12.2. Figures showing the tsunami wave propagation at different times (0, 15, 30, 45, 60, 90 minutes) after the earthquake.

Figure 12.3 shows the comparison of the measured (black) and computed (blue) time histories at four tide gauge stations. The additional time histories of modeling results are presented for the localities near Karatas, Yumurtalik and Cevlik fishery ports, where the eyewitness observations are collected from the fishermen or coast guard staff. The arrival times of the first wave nearly fit with the measured data. However, more detailed modeling studies are required to determine the location and type of the source when new data is collected by new field studies.

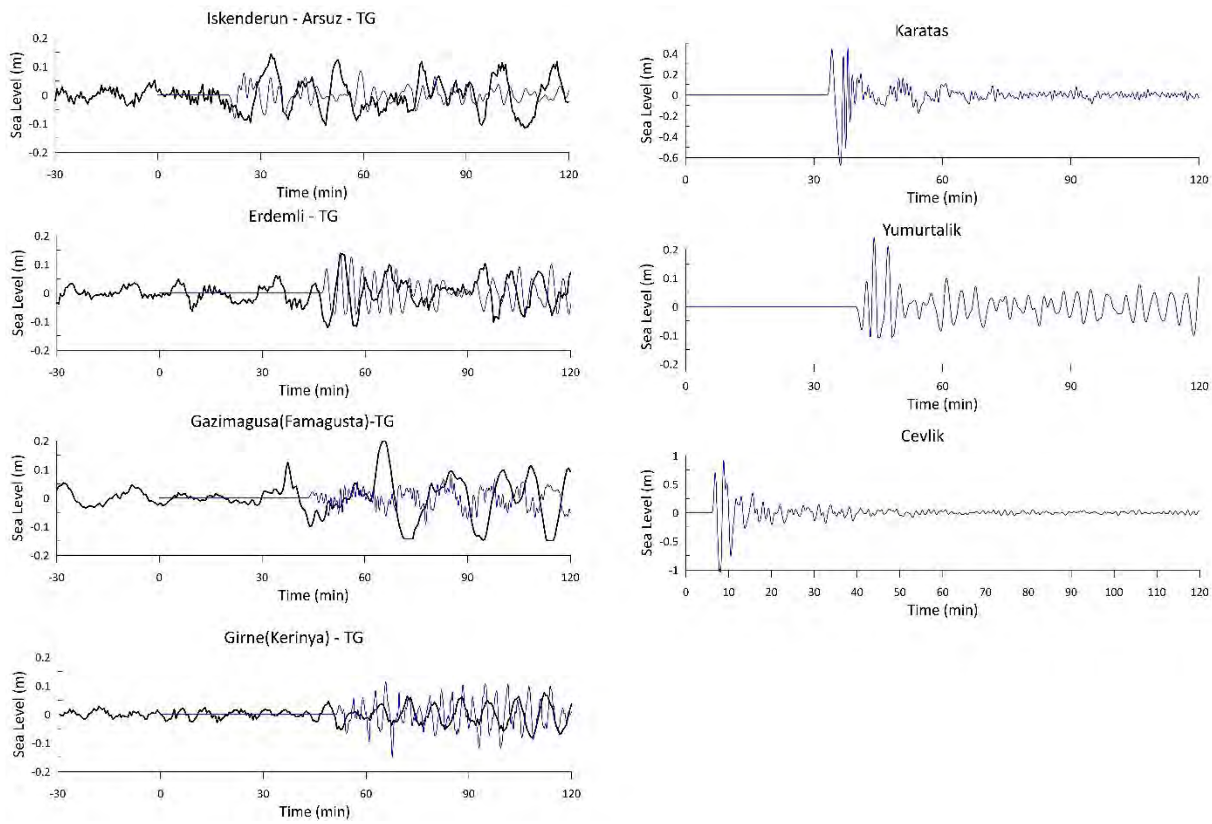

Figure 12.3. The comparison of the measured (black) and computed (blue) time histories of water surface fluctuations at four tide gauge stations (first column) and computed time histories near Karatas, Yumurtalik and Cevlik fishery ports, where only eyewitness observations (second column) could be obtained.

Some of the pictures taken during the field survey are also presented in Figures 11.4, 11.5 and 11.6. Figure 12.4 shows the traces of the coastal inundation observed in the morning after the earthquake near the Samandag fishery port at Cevlik village. Figure 12.5 shows the damages to the coastal structure and the pier of Iskenderun fishery port, which are the results of the coastal subsidence at the reclamation area, backside of the fishery port and nearby coastal region. Figure 12.6 shows the damages to the coastal structure in Dortyol fishery port.

Figure 12.4. Coastal Inundation and traces, South of Samandag-Cevlik Fishery Port

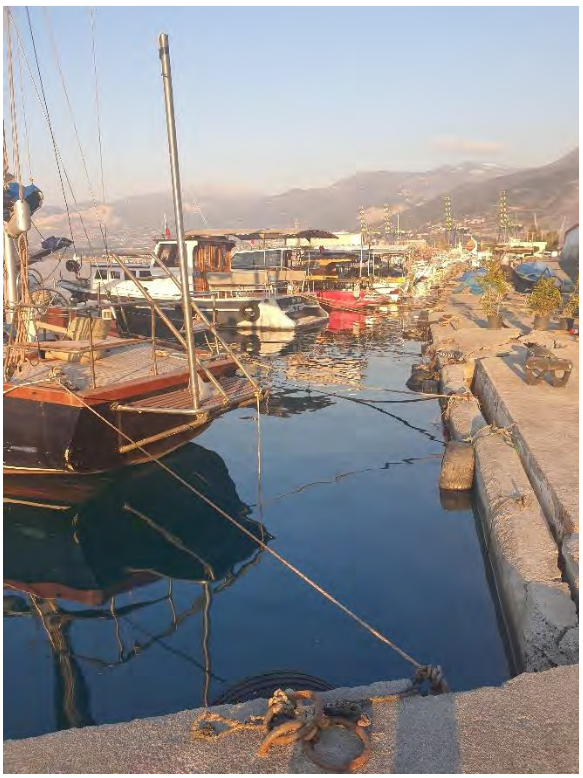

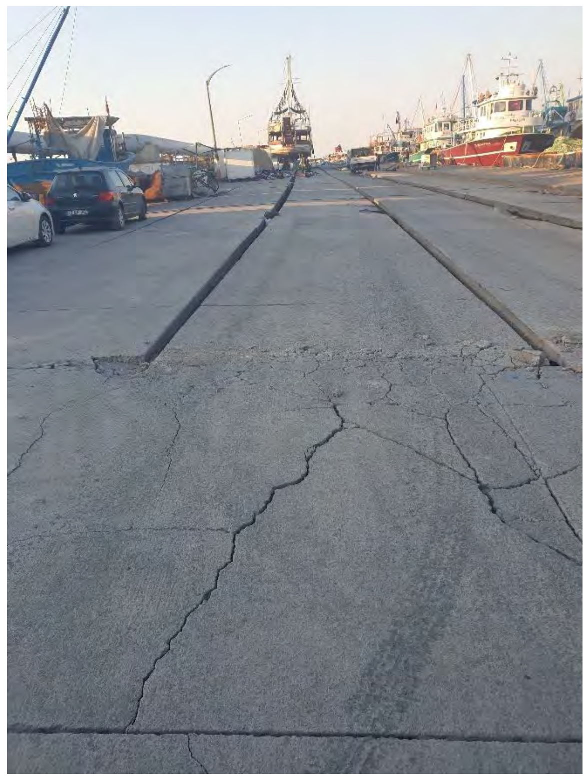

Figure 12.5. Structural damage at Iskenderun Fishery Port

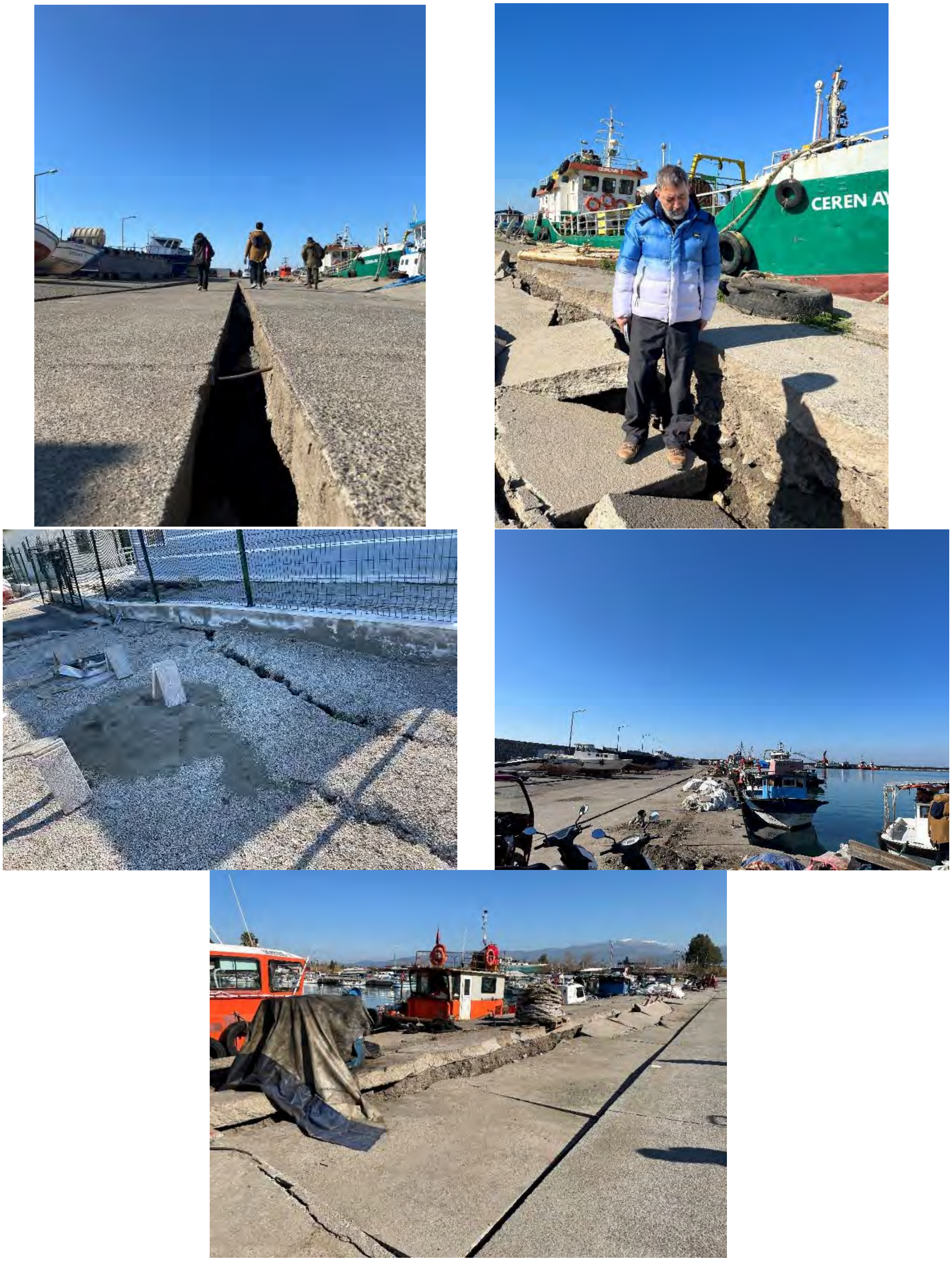

Figure 12.6. Structural damage at Dörtyol Fishery Port (Photos by METU DMAM Geotechnical Investigation Team, Prof. Dr. Kemal Önder Çetin)

12. 2. Coastal Subsidence at Iskenderun Fishery Port

Days after the earthquake, considerable water inundation has been observed behind and on the eastern side of the Iskenderun Fishery port, which has drawn the attention of the general public to consider the tsunami as a reason. However, the observations and evidence obtained during the field survey clearly identified that the reason was the subsidence of the coastal area behind the fishery port during the earthquake shaking most probably due to the liquefaction or similar means. During high tide (because of full moon days), seawater gradually invaded the subsided area and could not be drained because of collapsed surface water drainage system. Therefore, the phenomenon that occurred in the area is the gradual invasion of seawater by the high tide during the full moon phase to the area, where the ground subsided considerably.

The report will be updated with new data from the field and with new simulations using a higher-resolution database and other possible source alternatives.

Acknowledgements

This study is supported by TUBITAK 1002 C Rapid Support Grant, METU, Bogazici University and European Commission European Civil Protection and Humanitarian Aid Operations DG-ECHO funded UNESCO-CoastWAVE Project. Headquarter of General Command of Turkish Coast Guard and commanders of Coast Guard in the bases of Iskenderun Bay facilitated the survey significantly. Navigation, Hydrography and Oceanography Department of Turkish Navy and General Directorate of Mapping are acknowledged for providing on time valuable data and information. Zülfikar İnönü Tümer, Saffet Aslan, Erdinç Altıok, Emin Bilen Tümer are acknowledged for their valuable support and logistics. Taylan Sağlamtaş, Semih Taş, Ömür Küçükkör, Mustafa Ünlü and Ali Hoca are also acknowledged for their collaboration and valuable eyewitness information.

Chapter 13. Emergency Response, Recovery and Community Impact

By:

Meltem Şenol Balaban[(a)], Ali Fırat Çabalar[(b)], A. Nuray Karancı[(c)], Canay Doğulu[(d)], Gözde İkizer[(e)], Haldun Akoğlu[(f)], Müge Akın[(g)], Nil Akdede[(h)], Onur Karakayalı[(i)], Özlem Özdemir[(j)], Sarper Yılmaz[(k)], Selin Güzel[(l)], Serkan Yılmaz[(m)], Sıdıka Tekeli Yeşil[(n)], Tolulope Ajobiewe[(o)], Yeşim Ünal[(p)]

(a) Middle East Technical University, Department of City and Regional Planning, Ankara, Türkiye
(b) University of Gaziantep, Geotechnical Engineering, Gaziantep, Türkiye
(c) TOBB University of Economics and Technology, Department of Psychology, Ankara, Türkiye
(d) TED University, Department of Psychology, Ankara, Türkiye
(e) TOBB University of Economics and Technology, Department of Psychology, Ankara, Türkiye
(f) Marmara University, Faculty of Medicine, Department of Emergency Medicine, İstanbul, Türkiye
(g) Abdullah Gül University, Department of Civil Engineering, Kayseri, Türkiye
(h) Atılım University, Department of Architecture, Ankara, Türkiye
(i) Sakarya University, Faculty of Medicine, Department of Emergency Medicine, Sakarya, Türkiye
(j) Middle East Technical University, Department of Business Administration, Ankara, Türkiye
(k) University of Health Sciences Dr Lutfi Kirdar Kartal Education and Research Hospital, Department of Emerging Medicine, İstanbul, Türkiye
(l) Middle East Technical University, Graduate School of Natural and Applied Sciences, Geodetic and Geographic Information Technologies, Ankara, Türkiye
(m) Kocaeli University, Faculty of Medicine, Department of Emergency Medicine, Kocaeli, Türkiye
(n) Fraunarzt Praxis Rheinfelden, Rheinfelden, Switzerland
(o) Middle East Technical University, Graduate School of Social Sciences, Urban Policy Planning and Local Governments, Ankara, Türkiye
(p) Haliç University, Department of Psychology, İstanbul, Türkiye

13. 1. Introduction

This section of the Reconnaissance Report will be prepared as a preliminary compilation of first and secondary data regarding the efforts on "Emergency Response and Community Impact". Since the extent of the whole destroyed area is enormous, the data about the actual situation of the current state of the stricken area will be gathered and presented as much as possible within a limited time. According to the literature, the necessary activities of this period start with just after the earthquake event, so that the time for each activity should be realized in a timely manner.

On February 6, 2023 on 4:17 am, a major earthquake (M_w=7.4, later corrected as 7.7) occurred in Pazarcık district of the city of Kahramanmaraş and strongly felt by many surrounding cities by Kahramanmaraş, Hatay, Osmaniye, Gaziantep, Şanlıurfa, Diyarbakır, Malatya, and Adana (Adıyaman, Kilis cities followingly added to the list as of 10:00 and 14:20) according to the first official declaration issued by AFAD. Based on the initial information many search and rescue teams were declared to dispatch the stricken area. However, on 5:45 am within the scope of the Turkey Disaster Response Plan (TAMP), the level of the earthquake was declared as Level 4. In meetings with the Ministry of Foreign Affairs, international assistance was called for in the field of urban search and rescue through the Emergency Response Coordination Center (ERCC).

After 9 hours on the same day, consecutively, Kahramanmaraş Elbistan district was struck with another earthquake of M_w=7.6, causing additional extensive damages.

This report has been prepared based on the preliminary data collected from the initial earthquake on February 6 until February 14. However, we have added and extended some parts of this report like temporary shelter activities, which have been observed following days. The main purpose of this chapter of the report is to understand ongoing situation after major destructive earthquakes to get necessary lessons for further preparation activities. We all are thankful for the first responders and supporters at the field during those hard times and conditions.

13. 2. Emergency Response

Emergency response activities will be presented according to major categories. The preliminary evaluations of the possible impacts show the extension of the damages across the affected area covering 11 cities, affecting approximately 14 million people. Together with the Syrian population living in the devastated area, the total affected population reached 15.8 million (TÜİK, 2022, see Table 13.1).

Table 13.1 Highly affected population and demographic structure by cities

City	Population	Household Size	Population Density	Syrian Population	Other Foreign Population	Total Number of Collapsed buildings
Adana	2.274.106	3.40	163	250.679	15.899	18
Adıyaman	635.169	4.00	90	22.267	1.625	2742
Diyarbakır	1.804.880	4.43	120	21.727	1.657	174
Elazığ	591.497	3.10	70	13.255	4.238	1
Gaziantep	2.154.051	3.97	316	459.751	18.020	2665
Hatay	1.686.043	3.65	289	354.549	5.093	5885
K.Maraş	1.177.436	3.68	82	94.888	4.260	3746
Kilis	147.919	3.46	104	87.408	2.009	289
Malatya	812.580	3.40	69	38.650	4.766	2335
Osmaniye	559.405	3.46	179	31.427	840	232
Şanlıurfa	2.170.110	5.12	116	369.145	10.616	63
TOTAL	14.013.196	-	-	1.743.746	69.023	18150

Source: (TÜİK, 2022, TC. Çevre, Şehircilik ve İklim Değişikliği Bk, 23.2.2023)

Although highly affected cities are mentioned as listed on Table 13.1, there were other cities mentioned that have several life and property damages. Ministry of Environment, Urbanization and Climate Change has already started damage surveys in 11 cities including Elazığ (Figure 13.1).

As you can see the map (Figure 13.1) earthquakes with epicenters in Pazarcık and Elbistan, and ruptures along "East Anatolian Fault Zone" have destructed settlements causing simultaneous collapses of residential blocks, damages on commercial areas, highways, roads, bridges, ports, airports, state hospitals, natural gas pipelines, potable water systems. According to Türkiye's Emergency Response Plan (TAMP) which has been activated by the Turkish authorities at central and provincial level, while search and rescue teams have been deployed to the region. A Level-4 emergency has been declared in the country, which entails a call for international assistance, initially focused on search and rescue support.

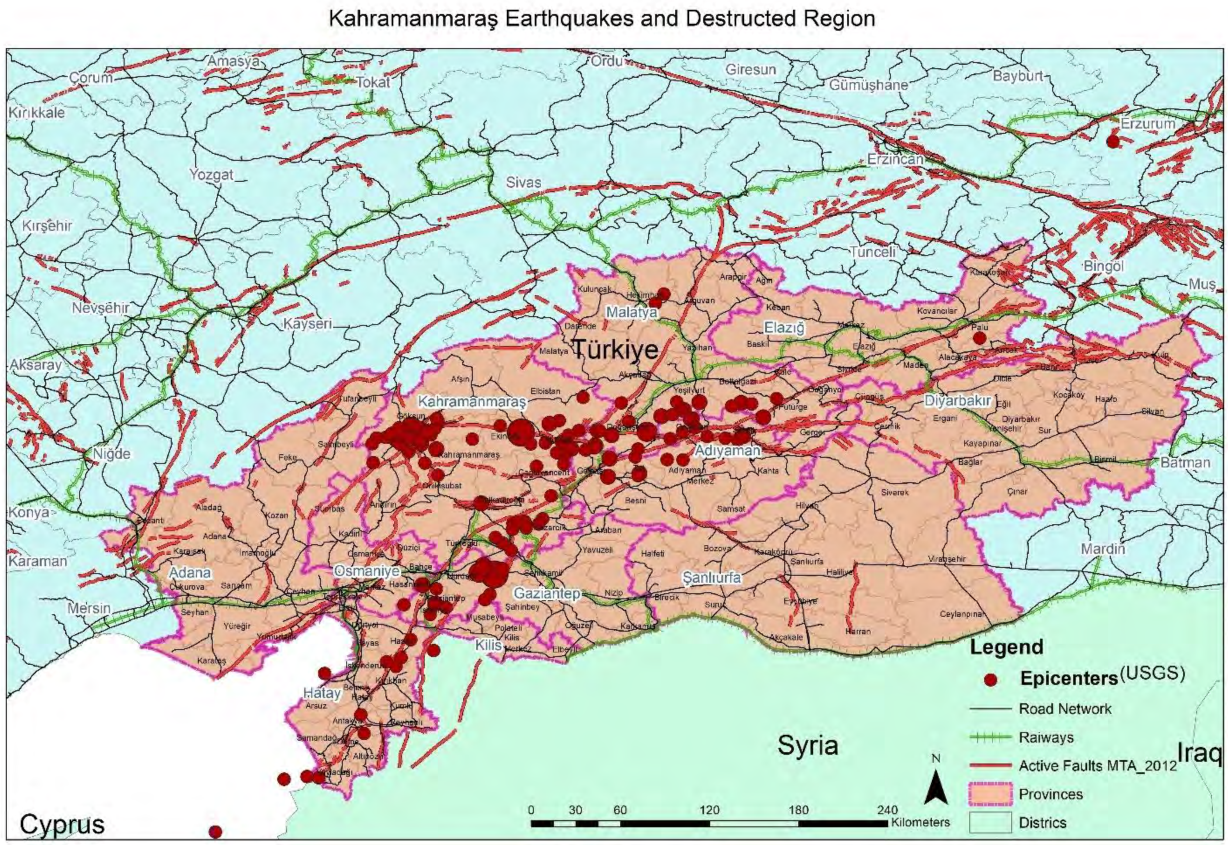

Figure 13.1. Affected Areas after Kahramanmaraş Earthquakes on Feb 6, 2023 (prepared by authors)

13. 2. 1. Coordination

Türkiye Disaster Response Plan (TAMP) was updated and issued in 2022. According to TAMP 2022, coordination activities should be prepared based on degree of levels, which is decided by the extension of the damages. Table 13.2 shows the levels and details for the support groups.

A Level-4 emergency has been declared in the country, which entails a call for international assistance, initially focused on search and rescue support. The Turkish President announced a 3-month state of emergency on February 7 for the 10 provinces affected by the earthquake.

Table 13.2 Level – Impact Scale Table

Severity Scale	**Levels**	**Impact**	**Event Type and Support Scale**
Slightly	Level-1	Local capacity is adequate.	Provincial AFAD Directorate
Moderately	Level-2	Backup needed from supporting provinces	Provincial AFAD Directorate + 1st Group Supporting Provinces
Very	Level-3	National support required	1st and 2nd Group Supporting Provinces + National Capacity
Extremely	Level-4	International support required	1st and 2nd Group Supporting Provinces + National Capacity + International Capacity

Source: TAMP 2022 (prepared by authors)

As shown in Table 13.2 level 4 requires 1st and 2nd group supporting provinces as well as national and international capacities. However, supporting groups have substantive damages too as can be seen from the Table 13.3. Hence, it was very complicated and difficult to help those provinces by 1st and 2nd groups as planned in TAMP. Since most of the transportation possibilities were too limited due to the extensive damages on highways, roads, air and seaports, railways, accessibility deficiencies created difficulties on transferring supportive search and rescue groups from other parts of Türkiye as well as foreign countries.

Table 13.3 Supporting Provinces Table (Damaged Provinces in red)

Name of Province (if disaster hits)	1st Group Supporting Provinces (Regional and Neighboring Provinces)	2nd Group Supporting Provinces
ADANA	Mersin-Osmaniye-Kahramanmaraş Gaziantep- Kilis- Hatay - Niğde	Kayseri Konya Malatya
ADIYAMAN	Erzincan – Bingöl Malatya – Elazığ Kahramanmaraş-Gaziantep-Şanlıurfa Diyarbakır	Tunceli Kilis Kayseri
DIYARBAKIR	Şanlıurfa – Mardin - Siirt – Şırnak - Batman Adıyaman- Malatya Elazığ – Bingöl - Muş	Bitlis Erzurum Tunceli
ELAZIĞ	Erzincan - Tunceli Bingöl - Malatya Adıyaman - Diyarbakır	Sivas Erzurum Şanlıurfa
GAZIANTEP	Mersin -Osmaniye- K.Maraş – Kilis- Hatay Adıyaman - Şanlıurfa	Kayseri Malatya Adana
HATAY	Adana – Osmaniye- K.Maraş – Gaziantep - Kilis	Şanlıurfa – Kayseri Mersin
KAHRAMANMARAŞ	Mersin-Adana-Osmaniye-Gaziantep-Kilis -Hatay -Adıyaman Sivas -Malatya - Kayseri	Şanlıurfa -Niğde- Diyarbakır
KILIS	Adana-Osmaniye-K.Maraş Gaziantep- Hatay	Şanlıurfa-Malatya -Mersin
OSMANIYE	Mersin-Adana-K.Maraş-Gaziantep-Kilis-Hatay	Kayseri-Adıyaman-Şanlıurfa
MALATYA	Erzincan –Tunceli Elazığ - Adıyaman Diyarbakır -K.Maraş-Sivas	Gaziantep Kayseri-Bingöl
ŞANLIURFA	Diyarbakır-Mardin-Siirt-Şırnak-Batman Gaziantep-Adıyaman	Elazığ-Kahramanmaraş Malatya

Source: TAMP (2022), p.59 (prepared by authors)

On February 13th, Minister of Interior declared that "the total number of AFAD staff is 7300. It is not possible to manage such a great disaster or any disaster in Türkiye with such a limited number of staffs. AFAD is a coordination institution. The working groups have many stakeholders including search and rescue, subsistence, communication, shelter, health." There are approximately 300 thousand employees in the field as a total number of people who work for immediate rescue and response activities as Minister highlighted.

13. 2. 2. Immediate Rescue and Response

Immediate rescue and response teams tried to reach disaster-stricken region. However, time lags occurred due to abovementioned reasons like accessibility. Another issue on the site of collapsed buildings, the necessary equipment for rescue operations, cranes, trucks were scarce. During night times electricity blackouts slowed down the S&R activities.

The graph below (Figure 13.2) indicates the trends of activities and casualties during the emergency response stage. It can be observed that emergency services including search and rescue teams, subsistence and medical aid were provided to the disaster-stricken region within the first 24 hours but not for all cities simultaneously. On the other hand, evacuation of earthquake survivors did not start within the first 72 hours. Disaster survivors could be transferred to dormitories and accommodation facilities on the fourth day in the predetermined cities outside of the disaster region. From the first day of the earthquakes until today the regional sums of emergency response services and casualties have been declared in official announcements so that it was hard to find provincial statistics which is necessary to analyze local deficiencies in a timely manner.

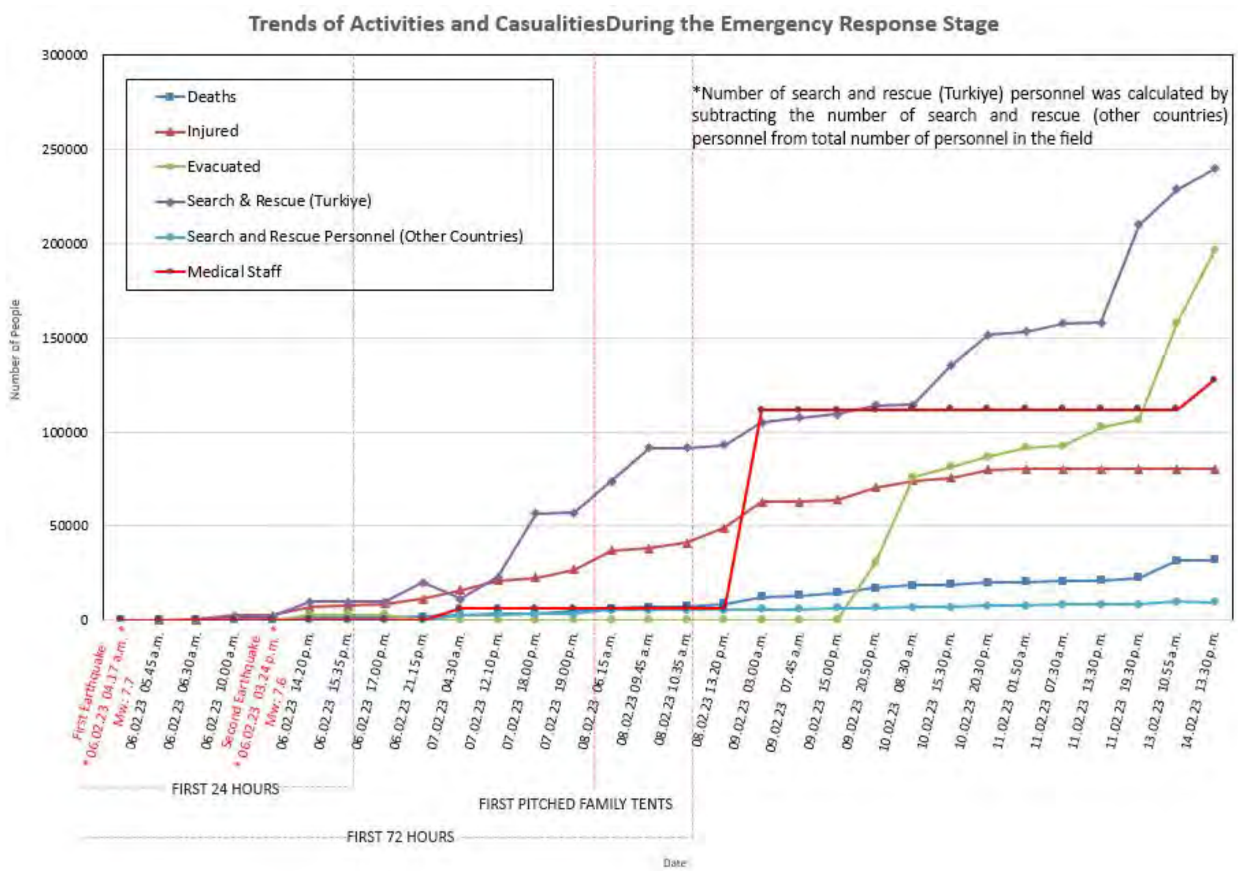

Figure 13.2. Map Trends of activities and casualties btw February 6 to 14 2023. Source: AFAD and Min. of Health as of 14.02.2023 13:30 (GMT+3) (drawn by the authors)

13. 2. 3. Infrastructure

On February 6 at 10:00 am, according to the first information received from disaster energy sources, natural gas cannot be supplied to Hatay/Hassa and Kırıkhan regions. BOTAŞ crude oil has been stopped as a precaution. As another precautionary measure, gas is cut from the entrance natural gas power plants of Gaziantep Nurdağı and Islahiye districts. 27 centers cannot be supplied with electricity. Electricity cannot be supplied to Osmaniye Bahçe-Düziçi, Kahramanmaraş city center, Malatya; Akçadağ, Doğanşehir and Doğanyol regions. Since winter conditions are freezing cold for that area for about 3 to 4 days heating options were not possible. Following days partial provision of electricity for some local areas has been possible but still heating problem is critical, most of the people set fires for heating outside.

Currently it is not possible to sure about the actual reasons and effects of earthquakes on critical infrastructure some scientists say those power shortages could be disruption by fault rupture (Figure 13.3).

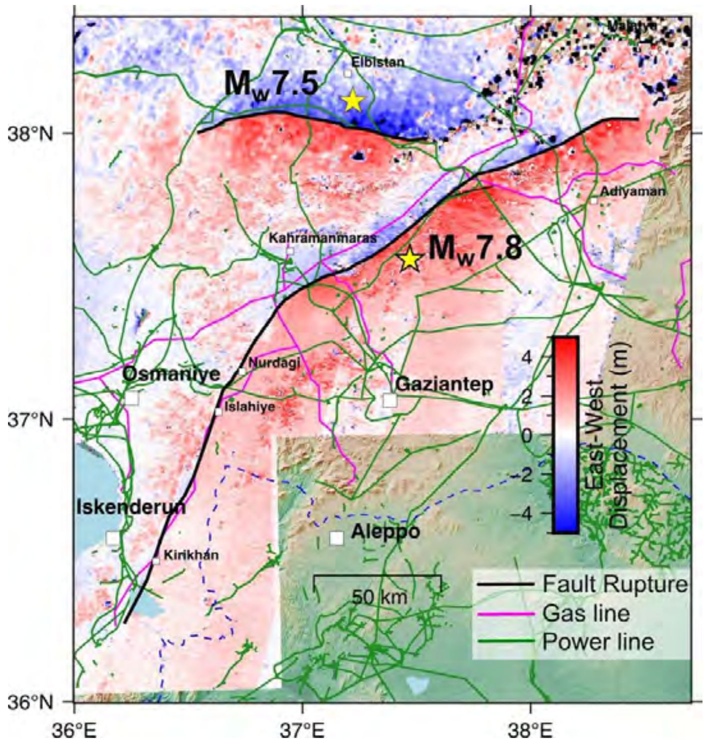

Figure 13.3. Effects on critical infrastructure might be because of fault rupture (Milliner 2023)

Another critical infrastructure is potable water system. Disaster-stricken area has no water supply for drinking and cleaning purposes due to damages on lines of potable water infrastructure. Water tankers have supported those cities, but hygiene and epidemic possibility is getting quite high day by day. Portable toilets are the most necessary need for the region.

13. 2. 4. Health Services

Health services during emergency response stage after Kahramanmaraş earthquakes have been observed from the field and presented in this part by the help of official announcements of Ministry of Health since the first hit on February 6, 2023. Just after the initial earthquake Hatay Education and Research Hospital suffered severe damage, while Hatay Antakya State Hospital, the A Block of the İskenderun State Hospital collapsed, and the Kahramanmaraş State Hospital became unusable. The injured patients in these hospitals were transferred to the city hospitals in Mersin and Adana, which survived the earthquake without any damage. The Malatya Women and

Children's Hospital, Malatya Battalgazi State Hospital, Gaziantep Inayet Topçu Hospital, Kahramanmaraş Necip Fazıl City Hospital, Kahramanmaraş Sütçü İmam University Medical Faculty Hospital, Kahramanmaraş Elbistan State Hospital, Hatay Dörtyol State Hospital, Elazığ Fethi Sekin City Hospital, and Hatay Samandağ State Hospital, which had just opened four days before the earthquake, were not affected and could continue their services.

The failure of electric and internet-dependent systems such as registration, identification, and legal notification, and the lack of alternative systems prepared for such situations caused problems in the identification of the injured, the recording of those transferred, the follow-up of unaccompanied children, and the identification of the dead. While patient examination and care were accelerated in emergency services equipped with ultrasound (USG) machines, the need to transport patients for imaging in emergencies without USG devices was a negative factor complicating the overcrowding. At the end of the second day, it was observed that the newly assigned healthcare workers had reached their stations, but most of them faced problems in finding shelter, heating, toilet, clean water, and food. The majority of the national health teams arriving in the disaster area were unable to operate autonomously without external equipment, medical and personal materials, and rations. It was observed that the equipment and resources brought by the teams were exhausted early due to intense demand.

After the earthquake, immediate concerns centered on the lack of electricity, lighting, heating, communication, and transportation. Healthcare workers were unable to provide adequate services due to overwhelming demand, shortages of materials, equipment, personnel, and poor coordination. Hospital disaster plans were not implemented, officials were unfamiliar with their duties, and there was no inventory of necessary equipment and materials. Harsh winter conditions compounded these issues. The inability to refill depleted medical resources due to transportation problems brought patient care problems to the forefront on the second day. Electricity, lighting, heating, communication, and transportation problems could still not be solved. Voluntary and assigned healthcare personnel could only start to provide support to the region at the end of the second day. Identification of injured patients, recording of transfers and referrals, legal documentations, follow-up of unaccompanied children, and the identification of the dead were hampered by the failure of electric and internet-dependent systems, and lack of alternative paper-based standard systems prepared for such situations. While patient examination and care were accelerated in emergency services equipped with ultrasound (USG) machines, the need to transport patients for imaging in emergencies without USG devices was a negative factor complicating the overcrowding. At the end of the second day, most of the newly assigned healthcare workers had reached their stations, but they faced problems finding shelter, heating, toilet facilities, clean water, and food. The majority of the national health teams arriving in the disaster area were unable to operate autonomously without external backup, equipment, medical and personal materials, and rations. Equipment and resources brought by the teams were exhausted early due to intense demand.

Starting from the second day of the earthquake, problems such as diabetic ketoacidosis, seizures, or hypertension developed due to chronic patients' inability to access their routine treatment and medications. Oral medications that those patients use was not available in the inventory of the EDs, hopefully, the Turkish Pharmacists Association began establishing pharmacies and distributing those drugs for free starting from the 43rd hour.

By the third day, a total of 2,101 ambulances, 296 UMKE vehicles, 5 air ambulances, 7 helicopter ambulances, and 14,429 emergency health personnel, including local and dispatched teams, were serving in the disaster area. The number of field hospitals and emergency response units in the region had reached 77, and significant amounts of medical supplies and drugs were delivered via 3 planes, 1 helicopter, 15 ambulances, and 200 vehicle loads. From the third day, most systems started to function, transportation and referral options diversified, and communication and transportation problems were mostly resolved, although occasional issues persisted. Therefore, it is logical to recommend that the health system deposit enough resources to serve independently for at least 48 hours.

As of February 12, 2023, a total of 21,631 patients rescued from the rubble were transferred to cities outside the region, 1,174 by air vehicles, 20,130 by land ambulances, and 327 by sea vehicles. As of February 14, 2023, 105,505 earthquake victims were rescued from the rubble as injured, and the number of casualties was announced as 35,418. It was reported that the number of public and private search and rescue personnel working in the region was 35,249, and 9,456 of them were international aid teams' personnel.

13. 2. 5. Accommodation Response: Emergency and Temporary Shelter

The 2023 earthquakes in Kahramanmaraş affected and have been affecting 11 densely populated cities in Southeast Türkiye. By March 1, 2023, approximately 202,000 buildings had heavily damaged or collapsed buildings in these 11 cities (T.C. Çevre, Şehircilik ve İklim Değişikliği Bakanlığı, 2023c); as a result, there is a need for widespread housing for the earthquake victims. By March 1, 2023, 1,971,589 people had to abandon their residences and leave their hometowns temporarily or permanently (AFAD, 2023a). Of these, thousands of people have been accommodated either in governmental buildings, public buildings, or houses of a friend or a family member. Besides sports halls, educational buildings, and other governmental buildings, dormitories had opened their doors to the earthquake victims with the capacity of 850,000 beds in 81 cities (AFAD, 2023b).

Considering the need for widespread housing and the harsh climatic conditions, approximately 10 hours after the first earthquake, AFAD (2023a) indicated that 19,772 living tents had been sent to the earthquake region. Almost 24 hours after the first jolt, AFAD announced that 41,504 family tents, 557 containers, and 747 tents (with an area of 112m2) had been sent to the earthquake-affected region (AFAD, 2023a). On 8 February 2023, AFAD (2023a) reported the establishment of 50.818 family tents to accommodate earthquake victims in 10 densely populated cities. On 13 February 13, 2023, AFAD (2023a) announced that the number of established family tents reached 155,379. The latest updates as of 1 March 2023 by AFAD (2023a) show that the number of established tents reached 358,037. One of the types of emergency sheltering settlements, 'tent cities', have been established in 332 different locations of these 11 cities (AFAD, 2023a). In addition, the construction of container settlements has been continuing in 162 different locations of 10 cities (AFAD, 2023a). As a result, 1,915,687 people have been accommodated in the above-mentioned emergency or temporary sheltering or housing areas (AFAD, 2023a).

To illustrate the pace of the establishment of emergency shelters, Figure 13.4. summarizes the data obtained from the AFAD Press Bulletin (AFAD, 2023a).

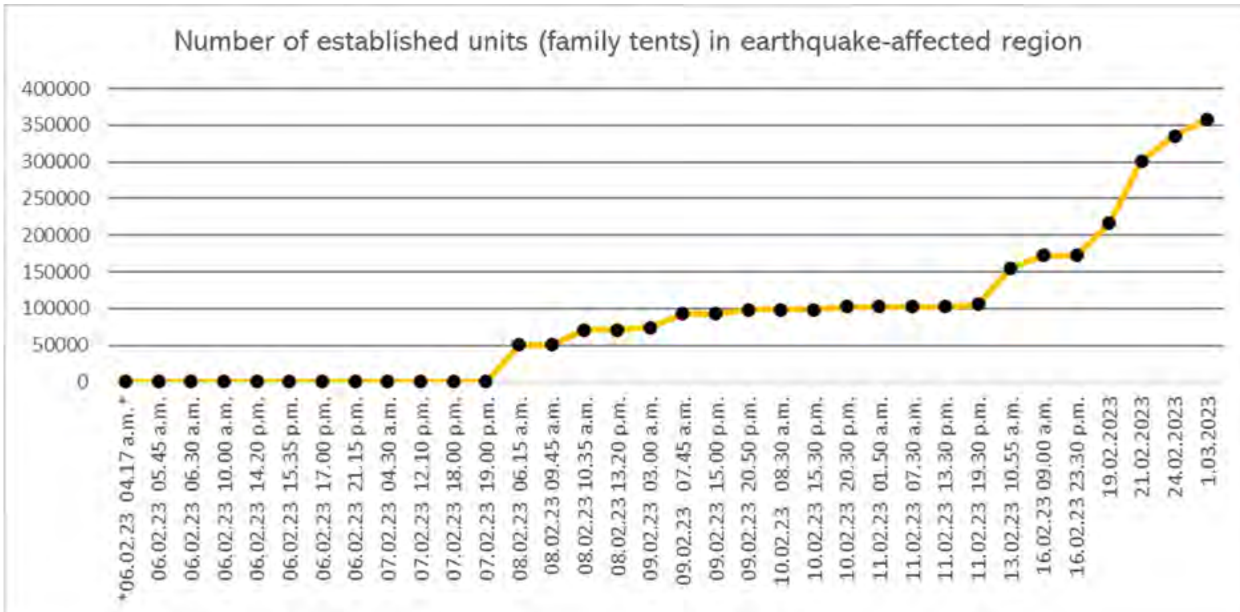

Figure 13.4. Number of established units (family tents) in earthquake region. Drawn by the authors, source: AFAD (2023a)

President Erdoğan announced that the Ministry of Environment, Urbanization, and Climate Change of the Republic of Türkiye will construct permanent housing with a maximum of 5 stories within a year (T.C. Çevre, Şehircilik ve İklim Değişikliği Bakanlığı, 2023b; En Son Haber, 2023). In addition to the provided emergency and temporary units, although an official announcement by the government could not be reached, several media sources (Anadolu Ajansı, 2023a; Haberler, 2023) published that 21 settlements provided for Syrians under temporary protection in 10 cities had opened their doors for the victims of Kahramanmaraş earthquakes. However, the authors observed, during the site visit to Sarıçam Container Settlement, that only Syrian earthquake-affected people who are currently living in Türkiye preferred to accommodate in these settlements.

To provide detailed information on emergency and temporary housing, the data obtained from AFAD's Twitter account (AFAD, 2023b) were examined. On 8 February 2023, AFAD (2023b) established tents on the field of 12 Şubat Stadium in Kahramanmaraş. However, the video published by AFAD (2023b) on Twitter and HGM Atlas (2023) shows that tents were located without a settlement plan, which indicates a planning problem (Figure 13.5). On the site visit done by the authors on 25 February 2023 to the 12 Şubat Stadium, it is observed that people who are responsible for the settlements were trying to change the settlement plan according to the minimum dimension between the tents to avoid fire.

As an urgent accommodation response for one of the most affected cities, Hatay, AFAD (2023b) established a tent settlement on the carparks of Hatay Stadium and Sports Hall of Hatay Centre by February 9th, 2023. On 11 February 2023, AFAD, together with several institutions, NGOs, and organizations, established tent settlements in İskenderun, Hatay (AFAD, 2023b). Besides these swiftly established emergency settlements, during the site visit, authors observed that by February 20, 2023, cruise ships, such as the ship of Mediterranean Shipping Company, have started to welcome earthquake-affected people for temporary accommodation at İskenderun Harbour.

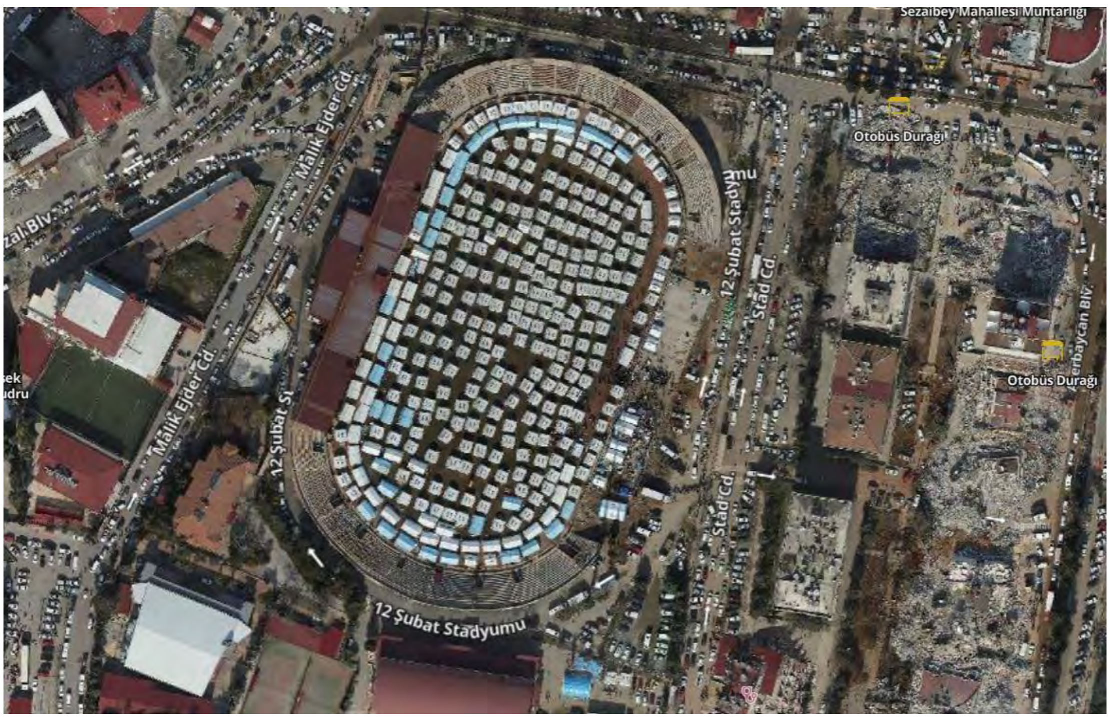

Figure 13.5. Established tents on the field of 12 Şubat Stadium in Kahramanmaraş (HGM Atlas, 2023)

In addition to tent settlements, a container settlement started to be constructed in the Malatya Technopark, İnönü University, Malatya (AFAD, 2023b; Anadolu Ajansı, 2023b). In addition to the newly-established or ongoing construction of emergency and temporary sheltering settlements in city centers, AFAD coordinates the tent supply for rural areas in earthquake-affected regions (AFAD, 2023b). Besides shelter supplies by AFAD for vulnerable people, numerous NGOs, companies, and foreign countries announced that they would establish or transfer tents and/or containers for the earthquake victims of the Kahramanmaraş earthquakes (T.C. Çevre, Şehircilik ve İklim Değişikliği Bakanlığı, 2023b).

During the site visit between 20-26 February 2023, in addition to the tens of emergency and temporary settlements established by AFAD, authors also observed that many different municipalities all around Türkiye (İstanbul Metropolitan Municipality, İzmir Metropolitan Municipality, Kocaeli Metropolitan Municipality, Gemlik Municipality, Beylikdüzü Municipality), government agencies (TOKİ - Toplu Konut İdaresi Başkanlığı (*Housing Development Administration of the Republic of Türkiy*e) (Figure 13.6 Left)), companies (Aselsan, Rönesans Holding), and non-profit organizations (Better Shelter (Figure 13.6 Right)) have already established or have been establishing tent or container settlements for earthquake victims with the approval of AFAD and the responsible governors. In addition to these, as a foreign country shelter supply, Qatar started to ship container houses which have been specially configured for the World Cup 2022 Organization to Türkiye for earthquake victims (Yeni Şafak, 2023).

Figure 13.6. Left: Temporary houses constructed by TOKİ in Nurdağı; Gaziantep; Right: Better Shelter Settlement in Hassa, Hatay, photographed by Nil Akdede and Özay Özaydın

To summarize, based on AFAD reports (2023) indicating that tents were provided almost 50 hours after the first earthquake, it can be concluded that earthquake victims spent the first two nights either in their cars, on the streets, in assembly areas, or on open-air marketplaces. Furthermore, several sources including TMMOB (2023) underline that the number of tents is insufficient considering the size of the affected group and the established tents are inadequate to protect against the sub-zero temperatures. Consequently, during the first two weeks, the lack of shelter is one of the most pressing issues following the 2023 earthquakes in Kahramanmaraş.

By considering the problems of emergency and temporary shelter settlements, Şehir Plancıları Odası (*Chamber of City Planners*) (2023) and Türk Tabipleri Birliği (*Turkish Medical Association*) (2023) published the reports underlining the guidelines emphasizing their own area of the profession for these settlements. Hence, these guidelines can be recommended to be used for the configuration of emergency and temporary settlements in the accommodation response after Kahramanmaraş earthquakes.

13. 2. 6. Psychosocial Support

Immediately following the two earthquakes, the Ministry of Family and Social Services dispatched psychosocial support personnel to affected provinces. A mobile social service center truck and service vehicles were sent to Hatay, Kahramanmaraş, Osmaniye, and Malatya (Railly News, 2023). In the AFAD Press Bulletin released on February 13th, it has been stated that, as of February 11th 19:30 (GMT+3), 2,174 officers and 327 vehicles were sent to the region to provide psychosocial support (AFAD, 2023c). Support was provided to a total of 110,650 people (99,916 in the earthquake-hit zone and 10,734 outside the affected provinces).

The Ministry of National Education (MEB, 2023a) has announced a Psychosocial Support Action Plan on February 10th, 2023. The plan includes presentations, booklets, and brochures for children, families, and teachers about the psychological impact of earthquakes, grief, psychological first aid, and psychosocial support in addition to psychoeducational programs for teachers and employee support programs.

On February 13th, 2023, the Turkish Red Crescent (2023) released a statement that 53 psychosocial support teams (including psychologists, psychological counselors, social workers, and guidance specialists) have begun providing psychological first aid to earthquake survivors. Over 5,000 mental health professionals volunteered to provide psychological support to survivors in affected provinces. In addition, The Turkish Red Crescent will set up psychosocial support tents in coordination with the Ministry of Family and Social Services and the Ministry of Health.

In the earthquake-hit zones, the need for psychosocial support services is huge and immediate (World Health Organization [WHO], 2023). Nevertheless, despite intensive efforts, since ten provinces were heavily affected by the quakes and the coverage area is quite extensive, planning psychosocial support services in those provinces continue to pose challenges for support teams and coordinators.

13. 2. 7. Community Impact

On February 6th, 2023, immediately after Kahramanmaraş earthquakes, the cities affected by the quakes were declared as state of emergency areas for three months (BBC, 2032a). The impact of the devastating earthquakes on the community following the first week can be addressed mainly with respect to earthquake response in relation to various decisions and activities bearing on education, rescue and relief efforts, and communication. This impact is elaborated with its main highlights in the following parts as they have implications for supporting the psychosocial needs of people affected in the region.

Concerning education, initially “suspension until further notice” decision was announced by the Ministry of National Education (MEB; 2023a) and Council of Higher Education (YÖK; 2023a, 2023b) in the immediate aftermath of the earthquakes. Later a press release by YÖK on February 11th (YÖK, 2023c; preceded by the Presidency statement on a live TV broadcast) announced that the 2022-2023 spring semester was to be completed with distance education in all higher education institutions and that the residence halls were to be used for accommodation of earthquake survivors. On the same day MEB (2023b) announced that education for primary, secondary, and high schools in the affected cities would be suspended until March 1st (to be followed by specific decisions for each district and school) and that education in other cities would continue on February 20th, 2023. However, the distance education decision for universities was objected by many education stakeholders, asking for starting face-to-face education for university students as soon as possible (e.g., Bianet, 2023; NTV, 2023; TMMOB, 2023c). The main reasons for this objection focused on views that distance education would hamper psychosocial recovery and that alternatives other than residence halls (such as hotels and guest houses) should be considered for accommodating earthquake survivors.

Concerning rescue and relief efforts, field observations based on official evaluation reports (TMMOB, 2023b; 2023c) as well as media (including both individual social media accounts and news platforms of press channels) have revealed that the affected areas were reached late, with search and rescue teams and aid starting to arrive only after about two days after the earthquakes and that lack of coordination hampered rescue and relief efforts. Particularly, there have been many reports that teams in the field were not able to start their search and rescue activities upon their arrival to their assigned areas, as they had to wait for official permission from AFAD (TMMOB, 2023c). This indicated that a timely and efficient decision-making was lacking in the field (TMMOB, 2023c). Within this post-quake immediate context where people in the affected areas were experiencing lack of and/or late arrival of aid, the statements of officials on the success of immediate earthquake response (e.g., president of the Turkish Red Crescent said that there was no place that the rescuers could not reach; Al-Monitor, 2023; T24, 2023) contradicted with the observed lack of timely and efficient decision-making. Unfortunately, this contradiction created frustration and anger among those in the affected areas waiting for the rescue teams to save their families in the rubbles of their homes. Their frustration and anger increased as they were waiting in the extremely cold weather outside their homes and the probability of reaching their family members alive decreased as time passed by, waiting for the rescuers to come. Furthermore, lack of coordination seemed to have negatively affected the involvement of non-governmental organizations (NGOs) and other solidarity networks in rescue and aid efforts (TMMOB, 2023c).

This was accompanied by various negative discourses of politicians that compared and criticized different institutions (local vs. central government bodies; government vs. NGOs, etc.) in terms of their earthquake response for rescue and aid efforts. For instance, the president of the far-right nationalist political party in Turkey (Nationalist Movement Party) criticized some NGOs and social media platforms (BBC, 2023b), which worked rigorously for aid organization as well as confirmation and communication of denunciations of people trapped in debris. Such discourses observed in post-quake communication of public officials were viewed as weakening the efficiency of efforts to unite in solidarity in the face of the massive devastating earthquakes.

As further related to communication, earthquake response was observed to be negatively affected by the restriction of social media use for dissemination and organization of rescue and relief activities. After the earthquake there were interruptions and disruptions in infrastructure, and this hampered the streaming of communication of both affected citizens and field workers in the earthquake region during the critical time for rescue and aid operation. The government's restriction of access to Twitter (Netblocks, 2023; Reuters, 2023) was criticized because Twitter served as the primary source for communication needs of people during the immediate post-quake response phase for those under the rubble to share their locations with relevant bodies. This restriction thus limited communication required for saving people from the rubble and identifying their needs in the affected area. Another point related to communication concerned post-quake discourses of officials and media that portray the devastating event as the catastrophe of the century due to its high magnitude and that it was not possible to be prepared for this kind of an inevitable and powerful earthquake (e.g., Teyit, 2023) and attributing it to fate (e.g., BirGün, 2023). Such discourse seemed to undervalue the importance of risk mitigation efforts especially for regulation and implementation of seismic building codes in the affected region where a great majority of the buildings collapsed or were seriously damaged. Communication in the immediate post-quake period was further challenged for the religious practice that took place on the night of the earthquake day. Specifically, at a time when many people were still under the rubble waiting to be rescued, absentee funeral prayer was offered in all the mosques all over the country for all the people who died in the earthquakes (Habertürk, 2023; TGRT Haber, 2023). Though religion overall could be considered as a source of social support for many, the timing of this funeral prayer was questioned as it can hamper psychological efforts at instilling hope among earthquake victims for staying alive and being rescued in the post-quake period.

Overall, it can be said that the emergency response decisions and activities following the Kahramanmaraş earthquakes did not consider the psychosocial needs of the affected people in the region at a desired level and that seemed to have worsened the negative impact of the earthquakes on the community, which would thus require future work to be invested in.

13. 3. Overview of International Media Response

This part of the chapter discusses the widespread criticisms that have been levied against the emergency response activities and efforts of the Turkish authorities in the wake of the February 6 earthquake that rocked about 10 cities in Türkiye. The criticisms summarized in this part were curated from published news reports and articles by international news agencies such as the BBC, CNN, Aljazeera, and the Financial Times to mention only a few. The issues for which the criticisms were based upon as this section of the report shows changes, so much so that it is has a new and different theme daily. In the early days of the response and recovery efforts/activities, the criticisms were specifically on the "Delayed Search and Rescue' efforts of the concerned agencies/departments. Following that, the criticisms dwelled on issues such as regional politics, polarized politics, rhetoric from the state and the presidency, security, and unrest in some parts of the affected cities.

Table 13.4. Major reported highlights on Emergency Response Activities

Day	Response Activity	Details
February 6-7	**Searching for Survivors**	AFAD said it had requested international help through the Emergency Response Coordination Centre (ERCC), the European Union's humanitarian program
		Nearly 1,000 search and rescue volunteers have been deployed from Turkey's largest city, Istanbul, along with dogs, trucks, and aid.
	Relief and Rescue	"People revolted [on Tuesday] morning. The police had to intervene," said **Celal Deniz**, 61, whose brother and nephews remain trapped.
		It took time for the response to build, and some villages could not be reached for days.
		With the military left out of the planning it had to wait for an order from the government, "this created a delay in the start of rescue and search operations."
	Government Efforts/Rhetoric/Statements	President Recep Tayyip Erdoğan declared a disaster zone in the 10 provinces affected by the earthquakes, imposing a state of emergency in the region for three months.
		The initial hours were critical, but roads were damaged, and search and rescue teams struggled to get through until day two or day three.
		Among the government's first actions in response to the earthquake was temporarily blocking Twitter, which was being used in Turkey to help rescuers locate survivors.
		The government said it was being used to spread disinformation and police detained a political scientist for posting criticism of the emergency response.

February 8	**Risk Mapping**	Mapping damage to the extent possible from satellites
	NASA Earth Observatory	Use of satellites to track increased landslide risks, power outages, and weather that could pose challenges to response efforts.
	Searching for Survivors	More than 8,000 people so far have been pulled from the debris in Turkey, said the Turkish vice-president, **Fuat Oktay**.
		Turkey deployed more than 24,400 search and rescue personnel to the quake area.
	Relief and Rescue	About 380,000 people have taken refuge in government shelters or hotels, with others huddling in shopping malls, stadiums, mosques and community centres.
		The ministry of transport and infrastructure said that overnight 3,400 people took shelter in trains being used as emergency accommodation.
		Anger mounted over what was described as a slow and inadequate response by authorities, the Guardian's **Ruth Michaelson and Sam Jones** reported.
		Dozens of survivors are taking refuge at an airport in Turkey's Gaziantep. About 100 people wrapped in blankets slept in one lounge of the terminal normally used to welcome Turkish politicians and celebrities, the AFP news agency reported.
February 9	**Relief and Rescue**	The International Federation of Red Cross and Red Crescent Societies launched "immediate cash assistance" from its Disaster Response Emergency Fund to help relief efforts in both countries.
		Some 95 nations and 16 international organizations have pledged aid to Turkey following this week's devastating earthquake, Foreign Minister **Mevlut Cavusoglu** said Thursday.
		At least 28,044 people have been evacuated out of Kahramanmaraş, the southern Turkish province near the epicenter of Monday's deadly earthquake. As of Thursday, at 11:38am local time, at least 23,437 people have been evacuated by air and 4,607 by road and rail, according to Turkey's disaster management agency, AFAD.

February 10	**Aid Efforts**	More than 141,000 rescue personnel are working on the ground in 10 earthquake-struck provinces in Turkey.
		President Erdogan said that Turkish institutions and organizations are providing hot meals to relief teams for the survivors of the earthquake through mobile kitchens and soup kitchens.
		"We have allocated an initial fund of 100 billion Turkish Liras ($5,309,405.33) for all this work," he said, adding that from "the AFAD (Turkey's Disaster and Emergency Management) emergency fund, we are starting to offer 15,000 Turkish Liras ($796.51) per household in relocation aid to citizens whose homes have collapsed or moderately or severely damaged."
February 11	**Relief and Rescue**	Germany has also suspended rescue and relief work at the site of a deadly earthquake in Turkey due to security concerns.
		The Austrian Army has suspended rescue operations in Turkey due to an "increasingly difficult security situation," according to the Austrian Forces Disaster Relief Unit (AFDRU).
		“In the last few hours, the security situation in the Hatay region has apparently changed. There are increasing reports of clashes between different groups. The search and rescue teams of ISAR Germany and THW will therefore remain in the joint base camp for the time being. ISAR and THW will resume their work as soon as AFAD deems the situation to be safe,” read the statement.
	Relief and Recovery	In Istanbul’s Yenikapı Port, a midnight transformation was underway Friday night, as city authorities raced to transform one of two ferryboats into a floating village, with enough showers, kitchens, and even school teachers to temporarily house 1,200 people left homeless by this week’s deadly earthquake.
	Aid (Relief and Recovery)	The border crossing between long-feuding Armenia and Turkey reopened on Saturday for the first time in 35 years to allow aid through.
February 12	**Recovery**	More than 2,000 people have been discharged from hospitals in the Turkish city of Istanbul following treatment for injuries suffered in Monday’s powerful earthquake, Turkish state broadcaster TRT Haber reported on Sunday.

	Relief	Turkey has more experience of earthquakes than almost any other country, but the founder of the main volunteer rescue group believes this time, politics got in the way. After the last major earthquake in August 1999, it was the armed forces who led the operation, but the **Erdogan government** has sought to curb their power in Turkish society.
February 13	**Recovery**	At least 19,300 earthquake victims are under treatment in hospitals in Turkey, according to Turkey's Health Ministry.
		They include 3,636 people who are in intensive care units, the ministry reported Monday. At least 8,851 patients had to have surgery, according to the ministry, and some of them are already discharged.

Prepared by authors, Sources: CNN; TheGuardian; Reliefweb; Aljazeera; BBC

13. 4. Conclusion

Emergency response activities as a part of relief activities and initial recovery services are covered in this section as much as the data available. Some of the parts might be missing since the limited number of authors went to disaster region. It is planned to go to region in following weeks and months based on the research topics. However, there is still time to observe rehabilitation and reconstruction practices, although the President of Türkiye announced that 30 thousand units of temporary houses will be started to be constructed in March. Topics like immediate macroeconomic impact, socioeconomic resilience might also be covered in more comprehensive and updated versions of this report.

References

AFAD. (2023a). *Duyurular*. T.C. İçişleri Bakanlığı Afet ve Acil Durum Yönetimi Başkanlığı. https://www.afad.gov.tr/duyurular

AFAD. (2023b, February 6-14). AFAD. https://twitter.com/AFADBaskanlik

AFAD. (2023c, February 13). *AFAD press bulletin about the earthquake in Kahramanmaraş - 28*. https://en.afad.gov.tr/press-bulletin-28-about-the-earthquake-in-Kahramanmaraş

Al-Monitor. (2023, February 7). *'Waiting for our dead': Anger builds at Turkey's earthquake response.* https://www.al-monitor.com/originals/2023/02/waiting-our-dead-anger-builds-turkeys-earthquake-response

Anadolu Ajansı. (2023a, February 6). *Geçici Barınma Merkezleri*. Retrieved February 14, 2023, from https://www.aa.com.tr/tr/info/infografik/32142

Anadolu Ajansı. (2023b, February 12). *Malatya'da 10 bin 500 kişilik konteyner kent kurulması için çalışmalar başladı*. Retrieved February 14, 2023, from https://www.aa.com.tr/tr/asrin-felaketi/malatyada-10-bin-500-kisilik-konteyner-kent-kurulmasi-icin-calismalar-basladi/2816807

BBC. (2023a, February 7). *Turkey earthquake: Erdogan announces three-month state of emergency in quake area.* https://www.bbc.com/news/world-europe-64548985

BBC. (2023b, February 14). *Bahçeli, Ahbap Derneği'ni ve Babala'yı hedef aldı.* https://www.bbc.com/turkce/live/64533110/page/2

Bianet. (2023, February 13). *Education union objects to closing of universities until summer after earthquakes.* https://m.bianet.org/english/print/274180-education-union-objects-to-closing-of-universities-until-summer-after-earthquakes

BirGün. (2023, February 8). *Erdoğan bu kez deprem için söyledi: Bunlar kader planının içerisinde olan şeyler.* https://www.birgun.net/haber/erdogan-bu-kez-deprem-icin-soyledi-bunlar-kader-planinin-icerisinde-olan-seyler-420668

Council of Higher Education [YÖK]. (2023a, February 6). *Press release.* https://www.yok.gov.tr/en/Sayfalar/news/2023/statement-from-the-council-of-higher-education-regarding-the-earthquake-centered-in-Kahramanmaraş .aspx

Council of Higher Education [YÖK]. (2023b, February 9). *Opening of spring term temporarily postponed at universities until further notice.* *https://www.yok.gov.tr/en/Sayfalar/news/2023/openning-of-spring-term-temporarily-postponed-at-universities-until-further-notice.aspx*

Council of Higher Education [YÖK]. (2023c, February 11). *Press release.* https://www.yok.gov.tr/en/Sayfalar/news/2023/announcement-term-of-the-2022-2023-academic-year-distance-education.aspx

En Son Haber. (2023, February 9). *Cumhurbaşkanı Erdoğan: 10 ilimizde konutları sahiplerine teslim edeceğiz*. Retrieved February 14, 2023, from https://www.ensonhaber.com/gundem/cumhurbaskani-erdogan-10-ilimizde-konutlari-sahiplerine-teslim-edecegiz

Haberler. (2023, February 6). *Deprem bölgelerindeki geçici barınma merkezleri açıklandı!* Retrieved February 14, 2023, from https://www.haberler.com/teknoloji/deprem-bolgelerindeki-gecici-barinma-merkezleri-15612822-haberi/

Habertürk (2023, February 6). *Depremde hayatını kaybedenler için camilerde sela ve Kur'an tilaveti okundu.* https://www.haberturk.com/depremde-hayatini-kaybedenler-icin-camilerde-sela-ve-kur-an-tilaveti-okundu-3562986

HGM Atlas. (2023, February). *HGM Atlas*. Retrieved February 15, 2023, from https://atlas.harita.gov.tr/mobile/#17.12/37.574224/36.923679

Milliner C. (2023).
https://twitter.com/Geo_GIF/status/1625925235819282432?s=20

Netblocks. (2023, February 8). *Twitter restricted in Turkey in aftermath of earthquake.* https://netblocks.org/reports/twitter-restricted-in-turkey-in-aftermath-of-earthquake-oy9LJ9B3

NTV. (2023, February 13). *"Uzaktan eğitim"' tartışması: İlk akla gelen bu oldu.* https://www.ntv.com.tr/turkiye/uzaktan-egitim-tartismasi-ilk-akla-gelen-bu-oldu,EjSGw-ztPUWwE9-Pmf_IHg

Railly News. (2023, February 7). *Psychosocial support personnel were dispatched to 10 provinces affected by the earthquake.* https://www.raillynews.com/2023/02/Psychosocial-support-personnel-were-dispatched-to-10-provinces-affected-by-the-earthquake./

Reuters. (2023, February 8). *Twitter restricted in Turkey two days after quake, says NetBlocks.* https://www.reuters.com/business/media-telecom/twitter-restricted-turkey-netblocks-2023-02-08/

Şehir Plancıları Odası. (2023). *ŞPO: Geçici barınma alanları rehberi*. Retrieved February 14, 2023, from https://www.tmmob.org.tr/icerik/spo-gecici-barinma-alanlari-rehberi

T24. (2023, February 7). *Kızılay Başkanı Kınık'ın "Deprem bölgelerinin tamamına ulaşıldı" sözlerine Kübra Par: Bize öyle bilgiler gelmiyor.* https://t24.com.tr/video/kizilay-baskani-kinik-in-deprem-bolgelerinin-tamamina-ulasildi-sozlerine-kubra-par-bize-oyle-bilgiler-gelmiyor,52050

The Türkiye Emergency Response Plan (TAMP). (2022). Retrieved February 14, from https://www.afad.gov.tr/kurumlar/afad.gov.tr/e_Kutuphane/Planlar/TAMP.pdf#page=18&zoom=100,80,876

T.C. Çevre, Şehircilik ve İklim Değişikliği Bakanlığı. (2023a, February 10). *Bakan Kurum:"10 ilimizde Cumhuriyet tarihinin en büyük afet konut seferberliğini başlatmış olacağız"*. Retrieved

February 14, 2023, from https://csb.gov.tr/bakan-kurum-10-ilimizde-cumhuriyet-tarihinin-en-buyuk-afet-konut-seferberligini-baslatmis-olacagiz-bakanlik-faaliyetleri-38419

T.C. Çevre, Şehircilik ve İklim Değişikliği Bakanlığı. (2023b, February 11). *Gaziantep'te 532 köyün tamamindaki depremzedelere yardim malzemesi gönderildi*. Retrieved February 14, 2023, from https://www.csb.gov.tr/gaziantep-te-532-koyun-tamamindaki-depremzedelere-yardim-malzemesi-gonderildi-bakanlik-faaliyetleri-38421

T.C. Çevre, Şehircilik ve İklim Değişikliği Bakanlığı. (2023c, March 1). Bakan Kurum: "582 bin bağımsız bölüm ve 202 bin binanın acil yıkılacak, ağır hasarlı veya yıkık olduğu tespitini yaptık". Retrieved March 1, 2023, from https://csb.gov.tr/bakan-kurum-582-bin-bagimsiz-bolum-ve-202-bin-binanin-acil-yikilacak-agir-hasarli-veya-yikik-oldugu-tespitini-yaptik-bakanlik-faaliyetleri-38458

Teyit. (2023, February 12). *"Böylesi büyük felakete hazırlıklı olabilmek mümkün değildir" iddiası.* https://teyit.org/demec-kontrolu-boylesi-buyuk-felakete-hazirlikli-olabilmek-mumkun-degildir-iddiasi

TGRT Haber (2023, February 6). *Depremde hayatını kaybedenler için ülke genelindeki camilerde sela okundu.* https://www.tgrthaber.com.tr/gundem/depremde-hayatini-kaybedenler-icin-ulke-genelindeki-camilerde-sela-okundu-2873393

The Ministry of National Education [MEB]. (2023, February 10). *Psikososyal destek eylem planı ve psikososyal destek programları yayımlandı*. https://www.meb.gov.tr/psikososyal-destek-eylem-plani-ve-psikososyal-destek-programlari-yayimlandi/haber/29014/tr

The Ministry of National Education [MEB]. (2023b, February 6). *Education is suspended until 13 February in Türkiye.* https://www.meb.gov.tr/education-is-suspended-until-13-february-in-turkiye/haber/28950/en

The Ministry of National Education [MEB]. (2023c, February 14). *Depremden etkilenen 10 ilde eğitim öğretime 1 Mart'a kadar ara verildi. https://www.meb.gov.tr/depremden-etkilenen-10-ilde-egitim-ogretime-1-marta-kadar-ara-verildi/haber/29029/tr*

Turkish Red Crescent. (2023, February 13). *Kızılay'ın psikososyal destek ekipleri deprem bölgesinde psikolojik ilk yardım veriyor*. https://www.kizilay.org.tr/Haber/KurumsalHaberDetay/7202

TURKSTAT. (2022). https://www.tuik.gov.tr/

Türk Mühendis ve Mimar Odaları Birliği [TMMOB]. (2023a, February 9). *TMMOB ön değerlendirme raporu yayımlandı.* https://www.tmmob.org.tr/icerik/tmmob-degerlendirme-raporu-yayimlandi

Türk Mühendis ve Mimar Odaları Birliği [TMMOB]. (2023b, February 14). *TMMOB Kahramanmaraş Depremi Güncel Durum Tespiti -2- (14 Şubat 2023).* http://www.tmmob.org.tr/icerik/tmmob-Kahramanmaraş -depremi-guncel-durum-tespiti-2-14-subat-2023

Türk Mühendis ve Mimar Odaları Birliği [TMMOB]. (2023c, February 14). *Uzaktan değil, güvenli ortamlarda yüz yüze eğitim istiyoruz!* http://www.tmmob.org.tr/icerik/uzaktan-degil-guvenli-ortamlarda-yuz-yuze-egitim-istiyoruz

Türk Tabipleri Birliği. (2023, February 11). *6 şubat 2023 Depremi Bilgi Notu - 9: Geçici Barınma Yerlerinin şematik Yerleşim Biçimi*. Retrieved February 14, 2023, from https://www.ttb.org.tr/haber_goster.php?Guid=706d3bfa-aa11-11ed-b4b5-486b41055497

World Health Organization [WHO]. (2023, February 10). *WHO flash appeal: Earthquake response in Türkiye and whole of Syria*. https://cdn.who.int/media/docs/default-source/documents/emergencies/2023/who_flashappeal_earthquakeresponse_11-feb-2023.pdf?sfvrsn=94d4de2a_1

Yeni Şafak. (2023, February 13). *Dünya Kupası konteynerleri Katar'dan yola çıktı*. Retrieved February 14, 2023, from https://www.yenisafak.com/gundem/dunya-kupasi-konteynerleri-katardan-yola-cikti-4507254

Acknowledgements

We would like to acknowledge the funding provided for the fieldwork by The Scientific and Technological Research Institution of Turkiye (TÜBİTAK) "1002-C Natural Disasters-Focused Fieldwork Emergency Support Program (Doğal Afetler Odaklı Saha Çalışması Acil Destek Programı)".